Exact Convex Modeling of the Optimal Power Flow for the Operation and Planning of Active Distribution Networks with Energy Storage Systems

THÈSE N^{O} 7008 (2016)

PRÉSENTÉE LE 17 JUIN 2016

À LA FACULTÉ DES SCIENCES ET TECHNIQUES DE L'INGÉNIEUR
LABORATOIRE DES SYSTÈMES ÉLECTRIQUES DISTRIBUÉS - CHAIRE EOS HOLDING
PROGRAMME DOCTORAL EN GÉNIE ÉLECTRIQUE

ÉCOLE POLYTECHNIQUE FÉDÉRALE DE LAUSANNE

POUR L'OBTENTION DU GRADE DE DOCTEUR ÈS SCIENCES

PAR

Mostafa NICK

acceptée sur proposition du jury:

Prof. P. Frossard, président du jury
Prof. M. Paolone, Dr S.-R. Cherkaoui, directeurs de thèse
Prof. J. A. Peças Lopes, rapporteur
Prof. F. Pilo, rapporteur
Prof. J.-Y. Le Boudec , rapporteur

ÉCOLE POLYTECHNIQUE
FÉDÉRALE DE LAUSANNE
Suisse
2016

To my family

Acknowledgements

I would never have been able to finish my dissertation without the help and support of many kind people, to only some of whom it is possible to give particular mention here.

First of all, I would like to express my deepest gratitude to my supervisors, Prof. Mario Paolone and Dr. Rachid Cherkaoui for giving me the opportunity to pursue my PhD thesis under their supervision. Their invaluable guidance, scientific enthusiasm, and intimacy made my PhD period a delightful period and also have allowed my personal and professional growth in a friendly environment.

I would also like to express my gratitude to the jury members, Prof. João Peças Lopes, Prof. Fabrizio Pilo, Prof. Jean-Yves Le Boudec, and Prof. Pascal Frossard for their valuable comments and discussions during and after the PhD exam. My special thanks goes to Prof. Jean-Yves Le Boudec who helped me a lot with his deep knowledge of mathematics.

My sincere thanks goes to, Prof. Farhad Rachidi for his generosity and friendship. It was a great pleasure for me to be with Farhad in the ELL offices of EPFL.

I would like also to gratefully acknowledge the EOS Holding for funding this dissertation. The activities of this work has been carried out within the frame-work of the research project entitled “Advanced control of distribution networks with the integration of dispersed energy storage systems”.

I am deeply grateful to Mrs. Andrée Moinat and Mrs. Sophie Flynn secretaries of the Laboratory, for all their constant availability, sympathy, and kindness.

My time at EPFL was made enjoyable by an amicable environment in the laboratory. Many thanks to all the members of ELL building for the friendly atmosphere and the priceless moments: Jean-Michel Buemi, Dr. Lazar Bizumic, Dr. Carlos Alberto Romero, Dr. Alexander Smorgonskiy, Dr. Felix Vega, Dr. Nicolas Mora, Dr. Gaspar Lugrin, Dr. Paolo Romano, Dr. Stela Sarri, Dr. Konstantina Christakou, Dr. Dimitri Torregrossa, Marco Pignati, Lorenzo Reyes, Lorenzo Zanni, Georgios Sarantakos, Dr. Fabrizio Sossan, Mathilde Brocard, Asja Derviskadic, Emil Namor, Dr. Daniele Colangelo, Zhaoyang Wang, Enrica Scolari, Andreas Kettner, Asia Codino, and Diego Nicorta. My special thanks goes to my Iranian friends in ELL: Dr. Ali Ahmadi-Khatir, Dr. Omid Alizadeh Mousavi, Dr. Mokhtar Bozorg, Dr. Reza Razzaghi, Maryam Bahramipanah, Mohammad Azadifar, and Hossein Mahmoudimanesh,

I would like to thank all my friends in Lausanne, with whom I have shared incredible moments. In particular, many thanks goes to Mohssen, Masoumeh, Elham, Samira, Mahbube, Christina, Mohsen, Hamed, Reza, Majid, Arizu, Elahe, Farhang, Saba, Mina, Sina, and Mehdi.

Last but not least, my deepest and forever thanks to my beloved parents for their dedication, many years of support, for their endless love and infinite patience and compassion. I wish to express my heartfelt thanks to my brothers Mohammad and Morteza, my sister in law, Noushin, and my sister and her family Narges, Jafar and Viana. This thesis is dedicated to them.

Lausanne, May 06, 2016

Mostafa Nick

Abstract

In the last decade, the power systems are experiencing important changes driven by the massive integration of renewable energy conversion systems. Although these changes are experienced by both transmission and distribution grids, the largest impact is definitely on the planning and operation processes of the latter. In this respect, the power systems research community has defined the term 'Active Distribution Networks' to identify distribution systems for which embedded generation is actively controlled by suitably-defined Energy Management System (EMS) in order to achieve specific operational objectives. However, the lack of direct controllability of the Distributed Generation (DG) supplying ADNs represents a major obstacle to the increase of the penetration of DG and, more specifically, of renewable energy resources characterized by a non-negligible volatility. The successful development of ADNs depends on the combination of i) specific control tools and ii) availability of new technologies and controllable resources. Within this context, this thesis focuses on developing practical and scalable methodologies for the ADN planning and operation with particular reference to the integration of Energy Storage Systems (ESSs) owned, and directly controlled, by the DNOs.

In this respect, an exact convex formulation of Optimal Power Flow (OPF) problem, called AR-OPF, is first proposed for the case of radial power networks. The proposed formulation takes into account the correct model of the lines (two-port Π model). Moreover, the security constraints related to the nodal voltage magnitudes, as well as, the lines ampacity limits are suitably incorporated into the AR-OPF using a set of more conservative constraints. Therefore, the AR-OPF is characterized by a slightly reduced space of feasible solutions where the removed space is in correspondence of the one that is close to the technical limits of the grid. Sufficient

conditions are provided to guarantee that the solution of the AR-OPF formulation is feasible and optimal (i.e., the relaxation used in the formulation is exact). Moreover, by analyzing the exactness conditions, it is revealed that they are mild and hold for real distribution networks operating in feasible region. The so-called linear DistFlow model for OPF problem is also improved by adding the shunt elements of the lines to the load flow equations. Another linear OPF model, based on voltage sensitivity coefficients, is also developed as an alternative to the AR-OPF and DistFlow including the transverse parameters.

Next, the AR-OPF is further augmented by suitably incorporating radiality constraints in order to develop an optimization model for optimal reconfiguration of ADNs. Similar to the AR-OPF, this new formulation properly takes into account the exact lines model and security constraints. The optimality and the exactness of the proposed ADN reconfiguration, as well as its scalability are demonstrated using standard benchmark networks.

Then, in order to address the variations and uncertainties of the parameters (PV and load), the developed linear OPF model based on DistFlow formulation is employed to formulate a two-stage optimization problem for day-ahead resource scheduling in ADNs accounting for the uncertainties of nodal injections. The Adaptive Robust Optimization (ARO) and stochastic optimization techniques are successfully adapted to solve this two-stage optimization problem. The solutions of ARO and stochastic optimization problems are discussed and, as expected, they reveal that the ARO provides feasible solutions for any realization of the uncertain parameters even if its solutions are optimal only for the worst case realization (in other words, it is a conservative and risk averse approach). On the other hand, the stochastic optimization provides a solution taking into account the probability of the considered scenarios.

Finally, the problem of optimal resource planning in ADNs is investigated with particular reference to the ESSs. It is assumed that the ESSs are owned, and directly controlled, by the DNOs. In this respect, a dedicated optimization model is first proposed for optimal siting of ESS units in ADNs aiming at providing local voltage support to the grid. The linearized OPF model, based on the voltage sensitivity coefficients, is used to assess the advantages and performances of the ESS units. In view of the large size of the problem, its solution relies on the so-called Benders decomposition technique. The capability of this methodology to find the best locations for providing local voltage control is demonstrated using standard IEEE test case networks. Further, it is shown that employing the Benders decomposition could possibly decrease the computation time up to 10 times with respect to solving the original problem. Afterwards, the AR-OPF jointly with the proposed ADN reconfiguration model are employed to develop optimization models for the optimal siting and sizing of ESSs in ADNs. The objective function is further augmented

aiming at finding the optimal trade-off between technical and economical goals. In particular, the proposed procedures accounts for (i) network voltage deviations, (ii) feeders/lines congestions, (iii) network losses, (iv) cost of supplying loads (from external grid or local producers) together with the cost of ESS investment/maintenance, (v) load curtailment and (vi) stochasticity of loads and renewables production. Similar to the case of optimal ESS siting, the use of decomposition methods for solving the targeted optimization problems with discrete variables and probable large size is investigated. More specifically, Benders decomposition and Alternative Direction Method of Multipliers (ADMM) techniques are successfully applied to the targeted problems. Various numerical analysis with respect to the standard and real networks are performed to demonstrate the capabilities of the proposed methodologies for providing optimal and feasible solutions as well as their computational efficiency and scalability. In particular, it is shown that the ESSs could possibly prevent load and generation curtailment, reduce the voltage deviations and lines congestions, and do the peak shaving. Further, it is shown that the Benders decomposition potentially could be the best solution methodology for large-scale problems with presence of binary variables.

Keywords- optimal power flow, energy storage systems, active distribution networks, convex optimization, convex relaxation, robust optimization, stochastic optimization, distribution networks reconfiguration, Benders decomposition, alternative direction method of multipliers, distributed generation, renewable energy, photo voltaic, voltage sensitivity coefficients, smart grid.

Résumé

De nos jours, les réseaux électriques connaissent des changements importants de par l'intégration massive de systèmes de conversion d'énergie renouvelable. Bien que ces changements soient vécus par les deux réseaux de transport et de distribution, le plus grand impact est sans aucun doute sur les processus de planification et de fonctionnement de ces derniers. À cet égard, la communauté de recherche sur les systèmes d'énergie a défini le terme «réseau de distribution actif» (ADN) pour identifier les réseaux de distribution pour lesquels la production distribuée est activement contrôlée par un EMS (Energy Management System) dans le but d'atteindre des objectifs d'exploitations spécifiques. Cependant, le manque de contrôlabilité directe de la production distribuée (DG) constitue un obstacle majeur à l'augmentation de la pénétration de ces sources et en particulier celles de nature renouvelable caractérisées par une volatilité non négligeable. Le succès de l'expansion des ADNs dépend i) des outils de contrôle spécifiques et ii) de la disponibilité de nouvelles technologies et de ressources contrôlables. Dans ce contexte, cette thèse se concentre sur le développement de méthodologies pratiques et extensibles pour la planification et l'exploitation des ADNs en accordant une attention particulière à l'intégration des systèmes de stockage d'énergie (ESSs).

A cet égard, une formulation convexe exacte du problème de l'Optimal Power Flow (OPF), appelé AR-OPF, est d'abord proposée pour le cas des réseaux de distribution radiaux. La formulation proposée prend en compte le modèle en pi des lignes. En outre, les contraintes de sécurité liées aux tensions nodales, ainsi que les limites des courants admissibles dans les lignes sont judicieusement intégrées dans l'AR-OPF moyennant un ensemble de contraintes conservatrices. Par conséquent, l'AR-OPF se caractérise par un espace de solutions légèrement réduit mais dont les limites traduisent assez fidèlement les limites techniques de l'exploitation du réseau.

Malgré tout, des conditions suffisantes sont prévues pour garantir que la solution de l'AR-OPF est réalisable et optimale. En outre, en analysant l'exactitude de ces conditions, il s'est révélé qu'elles sont « mild » et peuvent être considérées dans le cas des réseaux de distribution réels lorsque l'exploitation est dans les limites admissibles. Le modèle DistFlow linéaire pour les problèmes OPF est utilisé et également améliorée par la prise en considération des éléments shunts des lignes dans les équations des flux de charge dans celles-ci. Un autre modèle OPF linéaire, basé sur l'utilisation des coefficients de sensibilité de tension, a également été mis au point en tant qu'alternative à l'AR-OPF et au DistFlow mais tout en tenant compte des éléments shunts précités.

Par la suite, l'AR-OPF a été renforcé par l'incorporation appropriée de contraintes d'arborescence afin de développer un modèle d'optimisation pour la reconfiguration optimale des ADNs. Semblable à l'AR-OPF, cette nouvelle formulation prend correctement en compte le modèle exact des lignes et les contraintes de sécurité. L'optimalité et l'exactitude de la méthode proposée, notamment dans le cas de réseaux de grande taille, sont démontrées en utilisant des réseaux de référence.

Afin de répondre aux variations et aux incertitudes des paramètres (PV et charge), le modèle OPF linéaire basé sur la formulation du DistFlow est utilisé pour formuler un problème d'optimisation en deux étapes pour la planification des ressources tout en considérant les incertitudes sur les injections nodales. Des techniques d'optimisation robustes (ARO) et stochastique sont adaptées pour résoudre avec succès ce problème d'optimisation en deux étapes. Les solutions selon ces deux approches sont discutées et, comme prévu, l'ARO fournit des solutions réalisables pour toute réalisation de paramètres incertains, même si ses solutions ne sont optimales que pour le cas des réalisations les plus défavorables. Autrement, l'optimisation stochastique quant à elle, fournit une solution tout en tenant compte des probabilités associées aux scénarios envisagés.

Enfin, le problème de la planification optimale des ressources est étudié tout en considérant la présence d'unités ESS. À cet égard, un modèle d'optimisation dédié est d'abord proposé pour déterminer l'emplacement optimal d'unités ESS visant à fournir un soutien de tension au réseau. Dans ce but, le modèle OPF linéarisé, sur la base des coefficients de sensibilité de tension, est utilisée pour évaluer les avantages et les performances des unités ESS. Compte tenu de l'éventuelle grande taille des problèmes à traiter, la solution repose sur la technique de décomposition de Benders. La capacité de cette méthode pour trouver les meilleurs emplacements pour assurer le contrôle de la tension est démontrée en utilisant les réseaux tests standard IEEE. En outre, il est démontré que l'utilisation de la décomposition de Benders pourrait diminuer le temps de calcul jusqu'à 10 fois par rapport au cas de la résolution directe du problème original. Ensuite, l'AR-OPF conjointement avec le modèle de reconfiguration des ADNs proposé est utilisé pour formuler des modèles

d'optimisation pour l'emplacement et le dimensionnement optimaux des ESSs. A ce sujet, la fonction objectif est définie de sorte à trouver le meilleur compromis entre les objectifs techniques et économiques. En particulier, les critères suivant sont pris en considération : (i) les écarts de tension du réseau, (ii) les congestions de ligne, (iii) les pertes ohmiques du réseau, (iv) les coûts d'approvisionnement (à partir du réseau externe ou des producteurs locaux) ainsi que les coûts d'investissement / maintenance des unités ESSs, (v) le délestage de charge et (vi) la nature stochastique des charges et des productions intermittentes. Comme dans le cas de l'emplacement optimal d'unités, les méthodes de décomposition pour résoudre le problème d'optimisation précité sont étudiées. Plus précisément, la décomposition de Benders et la méthode ADMM sont appliquées avec succès à ce problème. Diverses applications à des réseaux standards et réels ont été effectuées pour démontrer l'aptitude des méthodes proposées à fournir des solutions optimales et réalisables notamment pour des problèmes de grande taille et leur performance en temps de calcul. En particulier, il est démontré que la présence d'unités ESS pourrait prévenir le délestage de charge, réduire les écarts de tension et la congestion des lignes, et permettre l'écrêtage des pointes de consommation. En outre, il est démontré que potentiellement la décomposition de Benders se prêterait le mieux pour résoudre les problèmes à grande échelle.

Mots clés : répartition des puissances optimale (OPF), système de stockage d'énergie, réseau de distribution actif, optimisation convexe, optimisation robuste, optimisation stochastique, reconfiguration des réseaux de distribution, décomposition de Benders, méthode ADMM, énergie renouvelable, coefficients de sensibilité pour la tension, smart grid

Contents

1 Introduction 1
1.1 Motivation of the Thesis 1
1.2 Objectives and Contributions of the Thesis 2
1.2.1 Optimal operation and control of ADNs 3
1.2.2 Uncertainty management in optimal operation and scheduling of ADNs 3
1.2.3 Optimal planning of ESSs in ADNs 4
1.3 Thesis Outline 5
2 Optimal Operation and Control of Active Distribution Networks 7
2.1 Chapter Organization 8
2.2 Optimal Power Flow in Active Distribution Networks 8
2.2.1 State-of-the-art of the Optimal Power Flow (OPF) problem in radial power grids 8
2.2.2 Notations and definitions 10
2.2.3 Power flow equations in radial distribution networks 13
2.2.4 Proposed optimal power flow in radial distribution networks 14
2.2.5 Exactness of augmented relaxed OPF 18
2.2.6 Proof of exactness of AR-OPF 20
2.2.7 Numerical analysis of AR-OPF 38
2.2.8 Comparison of AR-OPF with existing OPF formulation 41
2.3 Topology Changes in Optimal Operation of Radial Power Grids 46
2.3.1 State-of-the-art of optimal ADN reconfiguration 46
2.3.2 Proposed optimization model for distribution network reconfiguration 47

2.3.3 Computational Examples 52
2.4 Voltage Control of Active Distribution Networks Using Sensitivity Coefficients 57
2.4.1 Introduction and state-of-the-art 57
2.4.2 Voltage control using sensitivity coefficients 57
2.4.3 Simulation results 59
2.5 Summary and Conclusion 61
3 Optimal Operation and Scheduling of Active Distribution Networks under Uncertainty 63
3.1 Chapter Organization 64
3.2 Load and PV forecasting methods 64
3.2.1 The ARIMA forecasting tool 65
3.2.2 Load and PV forecasting using the ARIMA model 67
3.3 Two-stage Optimization Problem for Day-ahead Scheduling of Active Distribution Networks 69
3.3.1 First stage formulation 69
3.3.2 Second stage formulation 70
3.4 Adaptive Robust Optimization for Day-ahead Scheduling of Active Distribution Networks 71
3.4.1 State-of-the-art of robust optimization in power system optimization problems 72
3.4.2 Dynamic uncertainty set for ARO 73
3.4.3 ARO problem formulation 76
3.4.4 Numerical analyses 84
3.5 Day-ahead Scheduling of Active Distribution Networks using Scenario-based Stochastic Optimization 87
3.5.1 Stochastic optimization formulation 88
3.5.2 Uncertainty modeling 89
3.5.3 Simulation results 91
3.6 Adaptive Robust Approach vs. Stochastic Approach 94
3.7 Summary and Conclusion 96
4 Optimal Planning of Energy Storage Systems in Active Distribution Networks 99

4.1 Chapter Organization....100
4.2 State-of-the-art of the optimal ESSs planning in ADNs....100
4.3 Energy Storage Modeling....102
4.4 Treatment of Uncertainties for Long-term Planning....104
4.4.1 Scenario generation for load consumption, photovoltaic production and energy price....104
4.4.2 Scenario reduction technique....106
4.5 Optimal Siting of ESSs in ADNs to Achieve Voltage Control Using a Linearized OPF Model....107
4.5.1 Solution methodologies....108
4.5.2 Simulation results....111
4.6 Optimal Planning of ESSs in ADNs for energy balance and local grid support....112
4.7 Solution Approaches....118
4.7.1 Alternative Direction Method of Multipliers (ADMM) applied to ESSs optimal planning....119
4.7.2 Bender decomposition approach applied to the optimal siting and sizing of ESSs in ADNs....121
4.7.3 Comparisons of solution approaches....124
4.8 Summary and Conclusion....127
5 Application Examples of the developed methodologies for ESS siting and sizing using benchmark and real power grids....129
5.1 Chapter Organization....130
5.2 Optimal ESS Siting and Sizing....130
5.3 Optimal ESS Planning in a Real Distribution Network Using the ADMM....137
5.4 Optimal ESS Siting and Sizing Taking into Account Network Reconfiguration Using Benders Decomposition....142
5.5 Summary and Conclusion....147
6 Conclusion....149
7 Appendices....153
8 Bibliography....159

List of Figures

Fig. 2-1: Classical two-port Π model of a transmission line adopted for the formulation of the OPF relaxed constraints.....11

Fig. 2-2: Feasible solution spaces of O-OPF, R-OPF, and AR-OPF under the provided sufficient conditions.....38

Fig. 2-3: Distribution networks adapted to verify conditions *C1-C7* of AR-OPF. a) IEEE 34 buses distribution test feeder [25], b) CIGRE benchmark distribution grid for integrating distributed energy resources [26] 40

Fig. 2-4: Schematic of the 4 bus case study.....42

Fig. 2-5: Current flow magnitude of the lines vs. cables length. a) AR-OPF, b) R-OPF, and c) AR-OPF without transverse parameters (nominal voltage 24.9 kV)) ..44

Fig. 2-6: Current flow magnitude of the lines vs. nominal voltage level a) AR-OPF, b) R-OPF, and c) AR-OPF without transverse parameters (line factor 1) 45

Fig. 2-7: Classical two-port Π model of a transmission line adopted for the formulation of the optimal ADN reconfiguration.....48

Fig. 2-8: Simple network for verifying radiality constraints 52

Fig. 2-9: Schematic of the standard 33 buses network [43] (dashed lines are the default open switches). 53

Fig. 2-10: IEEE 123 buses test case network.....54

Fig. 2-11: IEEE 123 buses network with obtained switches status 56

Fig. 2-12: Topology of the IEEE 13 bus test feeder. Adapted from [18]. 60

Fig. 2-13: Load and PV time series: a) PV profile b) load profile (base MVA = 2 MW) 60

Fig. 2-14: Nodal voltages CDF with and without control action 61

Fig. 3-1: Load forecast using ARIMA a) load profiles used to train the ARIMA , 1. commercial 2. Residential, b) forecasted and actual day-ahead load profiles, 1. commercial 2. Residential (**Uf** and **Lf** are upper and lower bounds of confidence interval with $\pm$**7**% **and** $\pm$ **10**% error intervals for commercial and residential loads, respectively) 68

Fig. 3-2: PV forecast using ARIMA in p.u. of total capacity: a. PV profiles used to train the ARIMA (1. partially cloudy sky, 2. clear sky) b. forecasted and actual day-ahead PV profiles (1. partially cloudy sky, 2. clear sky) 68

Fig. 3-3: Approximated confidence intervals of PV forecast 75

Fig. 3-4: Estimated level of errors for hourly and 15 minutes forecast intervals .. 75

Fig. 3-5: Linearized model of square of active and reactive power flows 83

Fig. 3-6: Linearized capability curve of ESS 84

Fig. 3-7: Daily energy price..... 85

Fig. 3-8: Energy import/export scheduling in day-ahead for two cases i) base case without considering the forecast errors and ii) the ARO scheduling (base value of energy is 2.5 MWh) 85

Fig. 3-9: ESSs scheduling in day-ahead a) ARO scheduling, b) base case (base value of power is 2.5 MW) 86

Fig. 3-10: The convergence of Benders decomposition approach used to solve the ARO 87

Fig. 3-11: Euclidean distance aligns the ith point in one sequence with the ith point in the other, DTW alignment allows a more intuitive distance measure to be calculated [100]. 91

Fig. 3-12: Final residential load scenarios (base value of active power is 2.5 MW) 93

Fig. 3-13: Final commercial load scenarios (base value of active power is 2.5 MW) 93

Fig. 3-14: Final PV production scenarios (base value of power is 2.5 MW)..... 93

Fig. 3-15: Hourly scheduling of energy import/export from the external grid 93

Fig. 3-16: The nodal voltage magnitudes boxplot with presence of ESSs (a). First half of the day, b). Second half of the day) 94

Fig. 3-17: The nodal voltage magnitudes boxplot without presence of ESSs (a). First half of the day, b). Second half of the day) 95

Fig. 4-1: Load, energy price and PV data clustering a) load and energy price b) PV data 105

Fig. 4-2: QQ-plots of zero-mean load data (recorded data in the southern east part of Switzerland) for a specific time interval during a) fall-spring b) summer 106

Fig. 4-3: QQ-plots of zero-mean PV data (recorded data in the southern east part of Switzerland) for a specific time interval during a) partially cloudy sky b) clear sky 106

Fig. 4-4: Flowchart of the proposed methodology using Benders decomposition ..109

Fig. 4-5: Scenarios for a) active power consumption b) PV active power production (base value is 5 MW).....113

Fig. 4-6: Distribution of nodal voltage magnitudes in the network (for 100 days with 15 minutes discretization; a) without ESSs b) with optimally placed ESSs 113

Fig. 4-7: Bender decomposition convergence.....112

Fig. 4-8: ADMM procedure applied to the problem of ESS optimal planning.....121

Fig. 4-9: The Benders decomposition procedure adapted for optimal siting and sizing of ESSs considering network reconfiguration 124

Fig. 4-10: a) the aggregated active power load scenarios (base vale for power is 2.5 MW), b) the energy price scenarios 126

Fig. 5-1: The modified IEEE 34 bus test feeder. 130

Fig. 5-2: The linearized dispatchable DG capability curve.....131

Fig. 5-3: Initial yearly load profile (base power Sb=2.5 MW). 132

Fig. 5-4: Initial yearly PV production profile (base power Sb=2.5 MW).....133

Fig. 5-5: Initial yearly wind production profile (base power Sb=2.5 MW).....133

Fig. 5-6: Bus voltage CDFs for the case with and without optimally-planned ESSs. 135

Fig. 5-7: ESSs state-of-charge during one summer (a) and one winter (b) day (base energy Eb=2.5 MWh). 136

Fig. 5-8: Active power profiles of load, PV, wind, and two dispatchable DGs during one summer (a) and one winter (b) day (base power Sb=2.5 MW). 136

Fig. 5-9: The schematic of the real test case study (total number of buses: 287, number of feeder: 9).....138

Fig. 5-10: Aggregated network loads: active-power profiles for the four considered weeks. a) winter, b) summer, c) fall, and d) spring (base value of power is 1 MW) 138

Fig. 5-11: Profiles of the electricity prices in the four considered weeks.....139

Fig. 5-12: The CDF of nodal voltage magnitudes for the cases with and without optimal ESS siting and sizing 140

Fig. 5-13: *SoC* profiles of the ESSs in summer period (Base value of energy is 5 MWh)..... 141

Fig. 5-14: . *SoC* profiles of the ESSs in winter period (Base value of energy is 5 MWh). 141

Fig. 5-15: Norm of the primal residual versus iteration 142

Fig. 5-16: Norm of the dual residual versus iteration..... 142

Fig. 5-17: Identified ADN topology and ESS sites (the buses with PV are shown with blue color) 145

Fig. 5-18: Nodal voltage magnitudes CDF, i) with optimal placement of ESSs ii) without ESSs..... 146

Fig. 5-19: Convergence of the Benders decomposition procedure..... 146

List of Tables

Table 2-1: The solution of AR-OPF and a-posteriori load flow analysis in very high loading condition for the IEEE 34 buses network depicted in Fig. 2-3.b 39

Table 2-2: The solution of AR-OPF and a-posteriori load flow analysis in very high loading condition for the CIGRE network depicted in Fig. 2-3.b.....41

Table 2-3: 4 buses test network parameters. 42

Table 2-4: Voltage magnitude obtained with the AR-OPF (line factor: 3, nominal voltage: 24.9 Kv) 43

Table 2-5: Voltage magnitudes obtained using the AR-OPF without the transverse parameters (line factor 3, nominal voltage value 24.9 KV) 43

Table 2-6: Voltage magnitude comparison obtained with the R-OPF (line factor 5, nominal voltage value 24.9 kV) 43

Table 2-7: Identified optimal switches status 54

Table 2-8: PV capacities in the IEEE 123 buses test network 54

Table 2-9: Voltage magnitude comparison: load flow vs. optimal solution 55

Table 2-10: ESSs sites and sizes.....60

Table 3-1: Installed PV capacities in the IEEE 34 buses 85

Table 3-2: Total upward and downward deviations for two cases i) with ESS ii) without ESS 92

Table 3-3: Hourly OLTC tap position 93

Table 3-4: Comparison between ARO and stochastic optimization 96

Table 4-1: Identified ESSs sites and numbers (each unit of ESS has 10kW power rating capacity and 100kWh energy reservoir capacity) 113

Table 4-2: Comparison between the solutions of the original problem and the decomposed one using Benders decomposition (each unit of ESS has 125 kVA and 125 kWh capacity)..... 126

Table 4-3: Comparison between the solutions of the original problem and the decomposed one using ADMM..... 126

Table 5-1: Simulation parameters..... 132

Table 5-2: Pairwise comparisons of the objective terms 133

Table 5-3: Obtained optimal ESSs location and size (base power Sb=2.5 MW, base energy Eb=2.5 MWh). 135

Table 5-4: Changes in each term of the objective function 136

Table 5-5: Average feeder loading with respect to the primary substation aggregated power in the four considered weeks 139

Table 5-6: Optimal ESS sites and sizes..... 139

Table 5-7: Changes in each term of the objective function 139

Table 5-8: Changes in the objective function with optimal planning of ESS units 144

Table 5-9: Candidate buses for installing ESSs..... 144

Table 5-10: Simulation parameters..... 144

Table 5-11: Identified optimal ESS sites and sizes..... 144

Notation

The notations used in this dissertation are listed below. For the sake of clarity, they are provided separately for each section of the Thesis. They are in [p.u.].

Abbreviations:

ADMM	Alternative Direction Method of Multipliers
ADN	Active Distribution Network
ARO	Adaptive Robust Optimization
A-OPF	Augmented OPF
AR-OPF	Augmented Relaxed OPF
DG	Distributed Generation
DNO	Distribution Network Operator
DTW	Dynamic Time Wrapping
ED	Economic Dispatch
ESS	Energy Storage System
GA	Genetic Algorithm
KKT	Karush–Kuhn–Tucker
LP	Linear Programming
MILP	Mixed Integer Liner Programming
MINLP	Mixed Integer Non Linear Programming
MISOCP	Mixed Integer Second Order Cone Programming
MIQCP	Mixed Integer Quadratically Constrained Programming
MIQCQP	Mixed Integer Quadratically Constrained Quadratic Programming
MIQP	Mixed Integer Quadratic Programming
OLTC	On Load Tap Changer
OPF	Optimal Power Flow
RO	Robust Optimization
SCUC	Security Constrained Unit Commitment
SOC	State of Charge
SOCP	Second Order Cone Programming

Notation:

$\Re(.)$, $\Im(.)$	Real and imaginary parts of a complex number
$j \coloneqq \sqrt{-1}$	Imaginary unit
$\max\{a, b\}$	Maximum value of a and b

Section 2.2: Optimal Power Flow in Radial Power Grids

Parameters:

b_l (b)	Susceptance of line l (corresponding vector of all lines)
B_l (B)	Sum of the susceptance of the lines connected to bus l (corresponding vector of all buses)
$\mathbf{G}$	The adjacency matrix of the oriented graph of the grid
$\mathbf{H}$	Closure of $\mathbf{G}$
$\mathbf{I}$	Identity matrix
$I_l^{\max}$ $(I^{\max})$	Upper limit of line l current flow square (corresponding vector of all lines)
$p_l^{\max}/p_l^{\min}$ $(p^{\max}/p^{\min})$	Upper and lower bounds of bus l active power consumption (corresponding vector of all buses)
$q_l^{\max}/q_l^{\min}$ $(q^{\max}/q^{\min})$	Upper and lower bounds of bus l reactive power consumption (corresponding vector of all buses)
$P_l^{\max}/Q_l^{\max}$	Upper bounds associated with the maximum active and reactive power flows of line l
$v_l^{\max}/v_l^{\min}$ $(v^{\max}/v^{\min})$	Upper and lower bounds associated with the bus l voltage magnitude square (corresponding vector of all buses)
$z_l = r_l + jx_l$ $(z = r + jx)$	Longitudinal impedance of line l (corresponding vector of all lines)

Variables:

f_l (f)	Square of current producing losses in line l
$\bar{f}$ $(\bar{f})$	Auxiliary variables associated with the square of current producing losses in line l
$s_l = p_l + jq_l$ $s = p + jq$	Complex load at bus l (corresponding vector)
$S_l^b = P_l^b + jQ_l^b$	Complex power flow entering bus l from the bottom part of line l
$\hat{S}_l^b = \hat{P}_l^b + j\hat{Q}_l^b$	Auxiliary variable for the complex power flow entering bus l from the bottom part of line l (lower bound for S_l^b)
$\bar{S}_l^b = \bar{P}_l^b + j\bar{Q}_l^b$	Auxiliary variable for the complex power flow entering bus l from the bottom part of line l (upper bound for S_l^b)
$S_l^c = P^t + Q_l^c$	Complex power flow entering the central element of line l (from top))
$S_l^t = P_l^t + jQ_l^t$, $(S = P + jQ)$	Complex power flow entering line l from the top (corresponding vector of all buses)
$\hat{S}_l^t = \hat{P}_l^t + j\hat{Q}_l^t$, $(\hat{S} = \hat{P} + j\hat{Q})$	Auxiliary variable (lower bound for S_l^t) for the complex power flow entering line l from the top (corresponding vector of all buses)

$\bar{S}_l^t = \bar{P}_l^t + j\bar{Q}_l^t$, $(\bar{S} = \bar{P} + j\bar{Q})$	Auxiliary variable (upper bound for S_l^t) for the complex power flow entering line l from the top (corresponding vector of all buses)
v_l, (v)	Square of voltage magnitude of bus l (corresponding vector of all buses)
$\hat{v}_l$ $(\hat{v})$	Auxiliary variable for the square of voltage magnitude of bus l (corresponding vector of all buses)

Indices and sets:

l	Index of the lines and buses other than slack bus
L	Number of the lines
$\mathcal{L}$	Set of the lines and buses other than slack bus
$\mathcal{L}^m$	Set of the buses that are upstream of bus m
$\mathcal{L}_m$	Set of the buses that are non-upstream of bus m
$\underline{\mathcal{L}}$	Set of the buses that are leaves of the oriented graph of the grid

Section 2.3: Topology Changes in Optimal Operation of Radial Power Grids

Parameters:

b_{kl}	Shunt susceptance of the lines between buses k and l
P_{kl}^{max},Q_{kl}^{max},I_{kl}^{max}	Upper limits of active power, reactive power, and current flow of the line between buses k and l
r_{kl}	Resistance of the line between buses k and l
$v^{\max}$	Upper limit of nodal voltage magnitudes' square
$v^{\min}$	Lower limit of nodal voltage magnitudes' square
x_{kl}	Reactance of the line between buses k and l
z_{kl} (z_{kl}^*)	Impedance (conjugate of impedance) of the line between buses k and l
$\mathfrak{B}$	A big number

Variables:

$d_{kl}(d_{lk})$	The direction of the line between buses k and l ($d_{kl} = 1$ means the direction is from k to l, $d_{lk} = 1$ means the direction is from l to k)
$f_{kl}(f_{lk})$	The square of current flow producing losses in the line between buses k and l (from l to k)
$\bar{f}_{kl}(\bar{f}_{lk})$	Auxiliary variable for the square of current flow producing losses in the line between buses k and l (from l to k)
$P_{kl}(P_{lk})$	Active power flow from bus k to l (from l to k)
$\hat{P}_{kl}, \bar{P}_{kl}(\hat{P}_{lk}, \bar{P}_{lk})$	Auxiliary variables for the active power flow from bus k to l (from l to k)
$Q_{kl}(Q_{lk})$	Reactive power flow from bus k to l (from l to k)
$\hat{Q}_{kl}, \bar{Q}_{kl}$ $(\hat{Q}_{lk}, \bar{Q}_{lk})$	Auxiliary variables for the reactive power flow from bus k to l (from l to k)
Q_l^{sh}	Reactive power injection associated with the shunt capacitance of the lines connected to bus l

$\hat{Q}_l^{sh}$	Auxiliary variable for the reactive power injection associated with the shunt capacitance of the lines connected to bus l
$S_{kl}(S_{lk})$	Complex power flow from bus k to l (from l to k)
$\hat{S}_{kl}, \bar{S}_{kl}(\hat{S}_{lk}, \bar{S}_{lk}$	Auxiliary variables for the complex power flow from bus k to l (from l to k)
v_l	Voltage magnitude square at bus l
$\hat{v}_l, v_l', v_l^{"}, \hat{v}_l', \hat{v}_l^{"}$	Auxiliary variables for the voltage magnitude square at bus l
κ_{kl}	State of the switch between buses k and l (1 is open, 0 is colesd)

Indices and sets:

$\mathcal{L}$	Set of the lines
$\mathcal{L}_s$	Set of the lines with switch
$\mathcal{L}\backslash\mathcal{L}_s$	Set of the lines without switch
$\mathcal{L}_l$	Set of the lines connected to bus l
N	Set of the buses
N_G	Set of substation buses
$N\backslash N_G$	Set of the buses that are not substation

Section 2.4: Voltage Control of Active Distribution Networks Using Sensitivity Coefficients

Parameters:

$\mathbf{A}_l^P(t)$	Matrix that relates the voltage magnitude changes at bus l to the change of active power injection (absorption) in all network buses (at time step t)
$\mathbf{A}_l^Q(t)$	Matrix that relates the voltage change at bus l to the changes of reactive power injection (absorption) in all network buses (at time step t)
C_l	Power rating of the ESS located at bus l
$E_l^{\max}, E_l^{\min}$	Maximum and minimum allowed SOC level of the ESS located at bus l
$V_l(t)$	Voltage magnitude of bus l at time step t
V^r	Reference voltage magnitude
$\bar{V}_l(t)$, $\underline{V}_k(t)$	Voltage phasors of bus l, and its relevant conjugate at time step t
η_l^d, η_l^{ch}	Charging and discharging efficiencies of the ESS located at bus l

Variables

$E_l(t)$	Level of energy stored in the ESS located at bus l at time step t
$P_l^{ch}(t)(P_l^d(t))$	Active power production (discharge)/consumption (charge) of the ESS located at bus l at time step t
$Q_l\ (t)$	Reactive power output of the ESS located at bus l at time step t

$u_l^{ch}(t)$, $u_l^d(t)$	Binary variables associated with the charging/discharging state of the ESS located at bus l at time step t
$\Delta P_k(t)$	Adjustment in active power injection (absorption) of bus k at time step t
$\Delta Q_k(t)$	Adjustment in reactive power injection (absorption) of bus k at time step t
$\Delta V_l(t)$	Amount of change in the voltage magnitude of bus k at time step t

Sets and indices:

l, k	Index of network buses (without slack bus)
$\mathcal{L}, \mathcal{L}_{ess}, \mathcal{L}/\mathcal{L}_{ess}$	Sets of network buses, buses with ESS, and buses without ESS, respectively
t	Index of time steps
T	Set of time steps

Section 3.4: Adaptive Robust Optimization for Scheduling of Active Distribution Networks

The notation for the second stage minimization in ARO:

Parameters:

$a_l^{p,r}$	Coefficient representing the amount of residential active load at bus l with respect to the total residential apparent power
$a_l^{p,c}$	Coefficient representing the amount of commercial active load at bus l with respect to the total commercial apparent power
a_l^{pv}	Coefficient representing the amount of active power production of PV located at bus l with respect to total active power production of PVs
$a_l^{q,r}$	Coefficient representing the amount of residential reactive load at bus l with respect to the total residential apparent power
$a_l^{q,c}$	Coefficient representing the amount of commercial reactive load at bus l with respect to the total commercial apparent power
b_l	Shunt susceptance of the line l
C_l	Power rating of the ESS located at bus l
$E_l^{\max}, E_l^{\min}$	Maximum and minimum allowed SOC level of the ESS located at bus l
$I_l^{\max}$	Upper limit associated with the square of line l current flow
$s^{r,f}(t)$	Forecasted value of the aggregated residential load apparent power at time step t
$s^{c,f}(t)$	Forecasted value of the aggregated commercial load apparent power at time step t
$s^{pv,f}(t)$	Forecasted value of the aggregated PVs active power production at time step t
U^r/L^r	Upper and lower bounds of uncertainty budget for the residential load

U^c/L^c	Upper and lower bounds of uncertainty budget for the commercial load
$v^{\max}$	Upper limit of the square of nodal voltage magnitudes
$v^{\min}$	Lower limit of the square of nodal voltage magnitudes
$v_{thr}^{\max}, v_{thr}^{\min}$	Maximum and minimum voltage magnitudes' square beyond which voltage deviations will be minimized
$V^{\min}$	Lower bound of nodal voltage magnitudes
W_v	Weighting coefficient of the voltage deviation minimization in the objective function
z_l (z_l^*)	Impedance (conjugate of impedance) of the line l
$\bar{\zeta}^c(t), \underline{\zeta}^c(t)$	Upper and lower bounds of the forecast confidence interval associated with the aggregated commercial load at time t
$\bar{\zeta}^r(t), \underline{\zeta}^r(t)$	Upper and lower bounds of the forecast confidence interval associated with the aggregated residential load at time t
$\bar{\zeta}^{pv}(t), \underline{\zeta}^{pv}(t)$	Upper and lower bounds of the forecast confidence interval associated with the aggregated PV production at time t
$\bar{\zeta}_h^c(t)$, $\underline{\zeta}_h^c(t)$	Upper and lower bounds of the aggregated PV production variation at hour h
η^{ch}, η^d	ESS charging and discharging efficiencies
$\pi^-(t), \pi^+(t)$	Downward and upward deviations price
Δt	Time step

Set and indices:

$F_n(x)$	Set of the lines for modeling an upper bound for x^2
h	Index of hours
H_t	Set of time steps (t) inside hour h
l	Index of the lines (and the buses without slack bus)
n	Index of the lines for modeling an upper bound for the square of a variable
t	index of time step
T	Set of the time steps
up(l)	Index of the bus that is connected to bus l through line l
$\mathcal{L}$, $\mathcal{L}_{ess}$	Set of the lines (buses without slack bus), set of the buses with ESS
$\mathcal{N}$	Set of the lines used for modeling an upper bound for the square of a variable

Variables:

$d^G(t), u^G(t)$	Downward and upward deviations (from day-ahead energy scheduling) at time step t
$d_l^{p,ch}(t), d_l^{p,d}(t)$	Downward deviation of ESS l active power (charge/discharge) output at time step t with respect to its day-ahead scheduling
$d_l^{q,p}(t), d_l^{q,n}(t)$	Downward deviation of the ESS l reactive power (charge/discharge) output at time step t with respect to its day-ahead scheduling

$E_l(t), (\hat{E}_l(t))$	Level of energy stored in the ESS l (its auxiliary variable) at time step t
$I_l^{P,t}(t), I_l^{P,b}(t)$	Active current flows at both ends of the line l at time step t
$I_l^{Q,t}(t), I_l^{Q,b}(t)$	Reactive current flows at both ends of the line l at time step t
$\hat{I}_l^{P,t}(t), \hat{I}_l^{P,b}(t)$	Upper bounds for the square of active power flows at both ends of the line l at time step t
$\hat{I}_l^{Q,t}(t), \hat{I}_l^{Q,b}(t)$	Upper bounds for the square of reactive powers flow at both ends of the line l at time step t
$p_l^{ch}(t), p_l^{d}(t)$	ESS l active power output (charge/discharge) at time step t
$q_l^{p}(t), q_l^{n}(t)$	ESS l reactive power output (positive/negative) at time step t
$s_l(t)$	Net consumption associated with the bus l at time step t
$s^c(t)$	Residential apparent power at time t
$s^{pv}(t)$	PV power production at time t
$s^r(t)$	Commercial apparent power at time t
$S_l(t)$ $= P_l(t) + Q_l(t)$	Complex power flow of line l at time step t
$u_l^{p,ch}(t), u_l^{p,d}(t)$	Upward deviation of ESS l active power output (charge/discharge) at time step t with respect to its day-ahead scheduling
$u_l^{q,p}(t), u_l^{q,n}(t)$	Upward deviation of ESS l reactive power output (charge/discharge) at time step t with respect to its day-ahead scheduling
$v_l(t)$	Square of voltage magnitude of bus l at time step t
x	Vector of variables related to the first stage minimization in ARO (day-ahead scheduling)
$x_l^{p,ch}(t), x_l^{q,ch}(t)$	Active power output scheduling (in day-ahead) of the ESS l (charging and discharging) at time step t
$x_l^{p,p}(t), x_l^{q,n}(t)$	Reactive power output scheduling (in day-ahead) of the ESS l (charging and discharging) at time step t
$x^{scd}(t)$	Energy import scheduling (in day-ahead) from external grid at time step t
y	Vector of variables in the second stage minimization of ARO (intra-day operation)
$\Delta s^c(t)$	Forecast error related to the residential apparent power at time t
$\Delta s^{pv}(t)$	Forecast error related to the PV power production at time t
$\Delta s^r(t)$	Forecast error related to the commercial apparent power at time t
$\Delta\Psi$	Vector of variables of the second stage maximization in ARO (variation in the uncertain parameters)

Section 3.5: Day-ahead Scheduling of Active Distribution Networks using Scenario-based Stochastic Optimization

Parameters

v_0	Voltage magnitude square at substation
$v_{thr}^{\max}, v_{thr}^{\min}$	Maximum and minimum voltage magnitudes' square beyond which voltage deviations will be minimized
W_v	Weighting coefficient of voltage deviation minimization in the objective function

Δv^c	Step change in the voltage magnitude associated with the change of OLTC tap
$\pi(t)$	Energy price at time t
$\pi^+(t), \pi^-(t)$	Upward and downward deviations' prices
ρ_φ	Probability of scenario χ
ϑ_φ	Set of parameters associated with the models of linearized DistFlow and ESS constraints

Sets and indices

l	Index of the lines and the buses other than substation
t	Index of time steps
T	Set of time steps
φ	Index of scenarios
Φ	Set of scenarios

Variables

$P_{1,\varphi}$	Energy imported from the external grid at time step t in scenario φ
$T^c(t)$	OLTC tap position
u_φ^G, d_φ^G	Upward and downward deviations at time step t, scenario χ
$v_{l,\varphi}$	Nodal voltage magnitude square of bus l at scenario χ
$\alpha(t)$	Cost of changing OLTC tap position
δ^{DA}	Energy import scheduling in day-ahead at time step t
τ_φ	Set of variables for modeling the constraints related to the linearized DistFlow and ESSs

Section 4.3: Energy Storage Modeling

C	Capacity of the ESS reservoir
E^u, E^l	Maximum and minimum allowed SoC levels of ESSs
$E(t), (\hat{E}(t))$	Energy stored level in the reservoir at time t (corresponding auxiliary variable)
$P^c(t), P^d(t)$	Discharging and charging powers of ESS at time t
$Q^e(t)$	Reactive power output of the ESS at time t
r^{ess}	Internal equivalent resistance of the ESS
R^{up}, R^{dn}	Ramp-up and ramp-down of the ESS
$\mathcal{R}$	Power rating of ESS
Δt	Time step discretization
η^d, η^c	Discharging and charging efficiencies of ESSs
Λ	Resistive losses of ESS

Section 4.5: Optimal Siting of ESSs in ADNs to Achieve Voltage Control Using a Linearized OPF Model

Parameters

$\mathbf{A}_l^P$	Matrix that relates the voltage magnitude changes at bus l to the change of active power injection (absorption) in all network buses
$\mathbf{A}_l^Q$	Matrix that relates the voltage changes at bus l to the change of reactive power injection (absorption) in all network buses
a, b	Power rating and energy reservoir capacity of one ESS unit
$\mathcal{U}$	Total number of ESS units that can be installed
V^r	Reference voltage magnitude
$\beta_{l,\varphi}$	Set of parameters corresponding to ESS models
θ_φ	Probability of scenario φ
$\lambda_{l,\varphi}^{(n)}$	Dual multipliers associated with the fixed ESS capacity located at bus l in scenario φ in the iteration n of Benders decomposing subproblems

Sets and indices

l	Index of the lines and the buses other than substations
$\mathcal{L}(\mathcal{L}_{ess})$	Set of the buses (set of the buses with ESS)
t	Index of time steps
T	Set of time steps
φ	Index of scenarios
Φ	Set of scenarios
$\Psi(\alpha, \beta)$	Set of equations for modeling ESSs constraints

Variables

C_l	Energy reservoir capacity of ESS located at bus l
$P_{l,\varphi}^{ch}(t)/P_{l,\varphi}^{d}(t)$	Active power production (discharge)/consumption (charge) of the ESS located at bus l at time t, and scenario φ
$Q_{l,\varphi}^{e}$	Reactive power output of the ESS located at bus l at time t, and scenario φ
$\mathcal{R}_l$	Power rating of the ESS located at bus l
u_l	Integer variable representing the number of ESSs allocated at bus l
$\alpha_{l,\varphi}$	Set of variables for modeling ESS located at bus l
$\Delta P_{l,\varphi}(t)$	Adjustment in the active power injection (absorption) of bus l, at time t, and scenario φ
$\Delta Q_{l,\varphi}(t)$	Adjustment in the reactive power injection (absorption) of bus l, at time t, and scenario φ
$\Delta V_{l,\varphi}(t)$	Amount of change in bus l voltage magnitude at time t, and scenario φ

Section 4.6: Optimal Siting and sizing of ESSs in ADNs

Parameters

a	Positive number representing the constant power factor of loads
$\mathcal{B}^T$	Total budget for installing ESS units
$C_l^{\max}, C_l^{\min}$	Maximum and minimum ESS energy reservoir capacity that can be installed at bus l
$\hat{C}_{y,\varphi}^{o(n)}$	Vector of ESSs energy reservoir capacity obtained in the second stage of ADMM procedure in iteration n, scenario φ
$\hat{C}^{i(n)}$	Vector of ESSs energy reservoir capacity obtained in the first stage of ADMM procedure in iteration n
I^+	square of lines current magnitude beyond which the lines current flow is minimized
$\mathcal{I}_c, \mathcal{I}_p, \mathcal{I}_e$	Unit costs associated with the ESSs fixed installation, power rating, and energy reservoir capacity respectively.
$p_{l,y,\varphi,t}^{pv}$	Active power production of PV located at bus l at time t, scenario φ, and year y
$p_{l,y,\varphi,t}^{l}/q_{l,y,\varphi,t}^{l}$	Active and reactive power consumptions of bus l at time t, scenario φ, and year y
r_{kl} (r_l)	Resistance of the line between buses k and l (resistance of the line l)
$\mathcal{R}_l^{\max}, \mathcal{R}_l^{\min}$	Maximum and minimum ESS power rating capacity that can be installed at bus l
$\hat{\mathcal{R}}^{i(n)}$	Vector of ESSs power rating obtained in the first stage of ADMM procedure in iteration n
$\hat{\mathcal{R}}_{y,\varphi}^{o(n)}$	Vector of ESSs power rating obtained in the second stage of ADMM procedure in iteration n
v^+, v^-	upper and lower bounds for nodal voltage square magnitudes beyond which the nodal voltage deviations are minimized
$W_v, W_I,$ W_l, W_E, W_S	Weighting coefficients associated with various objectives (voltage, deviation, lines congestion, resistive losses, energy import from external grid, and load curtailment)
$z_l = r_l + jx_l$	longitudinal impedance of line l
$z_{kl} = r_{kl} + jx_{kl}$	longitudinal impedance of the line between buses l and k
$\beta_{l,y,\varphi,t}$	Set of parameters associated with the model of the ESS located at bus l, at time t, scenario φ, and year y
$\theta_{y,\varphi}$	Probability of scenario φ in year y
ξ^E	Energy price
$\lambda_{y,\varphi}^{(n)}$	Dual multipliers of the constraints that link the first and second stages of ADMM at time t, scenario φ and iteration n
$\mu_{l,y,\varphi}^{(n)}/\vartheta_{l,y,\varphi}^{(n)}$	Dual of constraints related to the fixed ESS capacities in the subproblems of Benders decomposition
ρ	ADMM penalty parameter
$\tau_{y,\varphi,t}$	Parameters associated with the power flow and auxiliary power flow equations at time t, scenario φ, and year y
$\varsigma_{y,\varphi,t}$	Parameters associated with the ADN reconfiguration constraints at time t, scenario φ, and year y

$\varsigma'_{\varphi_m,t}$	Parameters associated with the ADN reconfiguration constraints using DistFlow equations
ω	Annual interest rate

Sets and indices

l	Index of the lines
$\mathcal{L}$	Set of the lines and the buses other than slack bus
$\mathcal{L}_{ess}/N_{ess}$	Set of the buses with ESS
N	Set of the buses
t	Index of time steps
T	Set of time steps
Y	Set of yeas
y	Index of years
$\mathrm{B}(\sigma,\varsigma)$	Set of equations for modeling ADN reconfiguration constraints
$\mathrm{B}'(\sigma',\varsigma')$	Set of equations for modeling ADN reconfiguration constraints using DistFLow equations
$\Theta(\gamma,\tau)$	Set of equations for modeling AR-OPF constraints
Φ	Set of scenarios
φ_m	Index of scenarios in the master problem of Benders decomposition
Φ_m	Set of the scenarios in the master problem of Benders decomposition
φ	Index of scenarios
$\Psi(\alpha,\beta)$	Set of equations for modeling ESSs constraints

Variables

C_l	Energy reservoir capacity of the ESS located at bus l
$C^i_{y,\varphi}$	Vector of the variables related to the energy reservoir capacity of the ESSs in the first stage of ADMM
$C^o_{y,\varphi}$	Vector of the variables related to the energy reservoir capacity of the ESSs in the second stage of ADMM
$f_{l,y,\varphi,t}$	Square of current flow magnitude producing losses in line l (line
$(f_{kl,y,\varphi,t}, f_{lk,y,\varphi,t})$	between buses l and k) at time step t, scenario φ, and year y
$I^t_{l,y,\varphi,t}/I^t_{l,y,\varphi,t}$	Square of current flow at both ends of line l (line from k to l), at
$I^b_{lk,y,\varphi,t}/I^b_{kl,y,\varphi,t}$	time step t, scenario φ, and year y
$\mathcal{M}_{l,y}$	Maintenance cost of ESSs
$P^c_{l,y,\varphi,t}$	Active power consumption (charging) of the ESS located at bus l, time step t, scenario φ, and year y
$P^d_{l,y,\varphi,t}$	Active power production (discharging) of the ESS located at bus l, time step t, scenario φ, and year y
$P_{lk,\varphi_m}(t)$,	Active power flow between buses k and l at time step t, scenario φ_m
$P_{kl,\varphi_m}(t)$	

$P_{1,y,\varphi,t}$	Active power import from the external grid at time step t, scenario φ, and year y
$Q^{e}_{l,y,\varphi,t}$	Reactive power output of the ESS located at bus l, time step t, scenario φ, and year y
$Q_{lk,\varphi_m}(t)$, $Q_{kl,\varphi_m}(t)$	Reactive power flow in the central part of the line between buses k and l at time step t, scenario φ_m
$\mathcal{R}_l$	Power rating of the ESS located at bus l
$\mathcal{R}^{i}_{y,\varphi}$	Vector of variables associated with the power rating of the ESSs in the first stage of ADMM
$\mathcal{R}^{o}_{y,\varphi}$	Vector of variables associated with the power rating of the ESSs in the second stage of ADMM
$s_{l,y,\varphi,t}$	Complex load at bus l, time step t, scenario φ, and year y
u_l	Binary variable associated with the presence of an ESS at bus l
$v_{k,\varphi_m}(t)$	Square of voltage magnitude at time step t, scenario φ_m
$v_{l,y,\varphi,t}$	Square of voltage magnitude of bus l, at time step t, scenario φ, and year y
$\hat{v}_{l,y,\varphi,t}$	Auxiliary variable for the square of voltage magnitude of bus l, at time step t, scenario φ, and year y
$\alpha_{l,y,\varphi,t}$	Set of variables for modeling ESS l at time step t, scenario φ, and year y
$\gamma_{l,y,\varphi,t}$	Set of variables for modeling power flow and auxiliary power flow equations (AR-OPF) at time step t, scenario φ, and year y
$\zeta_{l,y,\varphi,t}$	Amount of load curtailment at bus l, time step t, scenario φ, and year y
$\sigma_{\ l,y,\varphi,t}$	Set of variables for modeling ADN reconfiguration equations at time step t, scenario φ, and year y
$\sigma'_{l,y,\varphi,t}$	Set of variables for modeling ADN reconfiguration equations using DistFlow equations at time step t, scenario φ, and year y

1 Introduction

1.1 Motivation of the Thesis

The level of penetration of Renewable Energy Resources (RERs) is progressively and massively increasing at low and medium voltage levels. In this regard, the distribution networks are no longer passive networks and non-negligible changes in their operational practices are imminent. The Distribution Network Operators (DNOs) have to face increasing challenges introduced by the high volatility of the RERs. In this context, the term Active Distribution Networks (ADNs) has been introduced to define power networks that [1, 2]

"[...] have systems in place to control a combination of distributed energy resources, defined as generators, loads and storage. Distribution system operators (DSOs) have the possibility of managing the electricity flows using a flexible network topology. DERs take some degree of responsibility for system support, which will depend on a suitable regulatory environment and connection agreement."

On the other hand, the lack of direct controllability of distributed generation (DG) by DNOs represents the main obstacles in operating ADNs. The difficulties associated with the near-term deployment of dedicated telecommunication infrastructures, as well as the availability of advanced SCADA implementing active control functions, are contributing to the delay in the deployment of the ADN concept. The level of successful RERs penetration into existing grids depends on the combination of i) specific control tools and ii) availability of new technologies and resources.

The former element is motivating the emergence of new optimization tools to efficiently manage and operate the ADNs in normal and contingency states.

Particularly proficient tools are indispensable to control the power flows in the grid as well as other fundamental state variables like bus voltages. In this respect, the well-known Optimal Power Flow (OPF) problem is expected to be the core of emerging Energy Management Systems (EMS) in ADNs. The OPF has been the main building block for the formulation of optimal controls as well as operation and planning problems in power systems. Nevertheless, the OPF is inherently a non-convex *NP*-hard problem and, consequently, its solution is challenging. As a consequence, it is necessary to define computationally efficient OPF to be integrated into EMS in order to be able to manage these network in short time periods (in scale of seconds)[1].

Regarding the later point (availability of new technologies and resources) one of the most promising near-term solutions allowing the postpone of infrastructure investments, is the possibility to indirectly control the DG by means of dispersed Energy Storage Systems (ESSs) owned by the DNOs. Indeed, the availability of distributed storage systems allows, in principle, to: (i) actively control the power flows into the grid, (ii) indirectly control the voltage profiles along the network feeders and (iii) locally balance the hour/daily and weekly load variations.

Another important issue needed to be addressed in ADNs is related to the inclusion of uncertainties of the RERs and loads in the grid operation. The uncertainties of their day-ahead and intra-day forecast impact the ADN operation, particularly when the RERs penetration level is high. This could cause financial and technical problems to DNOs. In this respect DNO need controllable resources as well as appropriate models to optimally and safely steer the grid and its resources.

In addition to the previous approaches, several research efforts have been performed on the use of knowledge-based fault location methods. Expert systems identify the most probable fault location by means of available information regarding the network status (e.g., the state of switches, unpowered user complaints, etc.) (e.g., [38], [39]). artificial neural networks (ANN) and fuzzy logic have been widely studied for the fault location problem. (e.g., [40], [41]). Nevertheless, the extensive training of such methods limits their application to real systems.

1.2 Objectives and Contributions of the Thesis

The aim of this thesis is to address the above-mentioned challenges regarding the control, operation and planning of controllable resources in ADNs with particular reference to ESSs. In this respect, first an exact convex model is proposed for the formulation and solution of the OPF in radial power networks. Further, the proposed OPF is used to develop appropriate models for optimal reconfiguration of ADNs as well as o find the optimal site and size of ESSs in ADNs. Moreover, stochastic optimization

[1] This reduced time-scale might be associated with the need of solving the OPF problem to chase the fast volatility of RERs.

and Adaptive Robust Optimization (ARO) are suitably employed to manage the uncertainties of parameters in operation and control of ADNs. In what follows, the main contributions of the thesis are summarized by making reference to three main issues mentioned above. It should be noted that in this thesis the ESSs are owned and directly controlled by DNOs.

1.2.1 Optimal operation and control of ADNs

A) Propose of an exact convex formulation for OPF in radial power networks

The thesis first proposes an exact convex formulation for the OPF in ADNs. It is capable to include the correct model of transmission lines (two-port Π equivalent) as well as the network security constraints (nodal voltages and lines ampacity limits). We have augment the original OPF formulation with a new set of more conservative constraints to limit the line current flows together with the nodal voltage magnitudes. Sufficient conditions are provided to ensure the feasibility and optimality of the proposed OPF solution.

B) Development of an optimal ADN reconfiguration model based on the proposed convex OPF

The proposed OPF model is augmented with radiality constraints and inclusion of tie-line switches to develop an optimization programming for optimal reconfiguration of ADNs. It takes into account the two-port Π equivalent model of lines and network security constraints. In order to formulate the radiality constraints, binary variables are only introduced to model tie-line switches. This approach reduces the number of binary variables and, consequently, decreases the computation time. The developed model belongs to the category of Mixed Integer Second Order Cone Programming (MISOCP) problems and could be solved efficiently by the state of the art commercial solvers for convex optimization and as a consequence is applicable to real large-scale networks.

C) Voltage control in ADNs using ESSs based on voltage sensitivity coefficient

The thesis also proposes an optimal voltage control scheme based on nodal voltage sensitivity coefficients and using ESSs as controllable resources. The developed model is linear and could be used as an alternative to the proposed OPF one.

1.2.2 Uncertainty management in optimal operation and scheduling of ADNs

A) Development of an Adaptive Robust Optimization model for ADN uncertainty management

The day-ahead optimal scheduling of ADNs is suitably modeled as a two stage optimization model. The decisions of the first stage (or *here- and- now*) decisions, are

made when the random parameters are unknown. In context of our targeted problem, they deal with the day-ahead decision variables (the amount of import/export energy from the external grid at each hour to the day-ahead market, and ESSs set points). Given the first stage decisions, the second stage (or *wait and see*) decisions are made based on the realization of the random parameters. In case of our specific problem, the second stage decision variables are the 15 minutes ESSs set points. An adaptive robust optimization technique, considering the spatial and temporal correlations, is proposed to solve this two stage optimization programming.

B) Development of a stochastic optimization model for ADN uncertainty management

A stochastic optimization technique is proposed to solve the above-mentioned two-stage programming. Further, On Load Tap Changer (OLTC) transformers are properly modeled and incorporated into the optimization problem.

1.2.3 Optimal planning of ESSs in ADNs

A) Development of an optimization programming for siting ESSs for voltage control

The above-mentioned optimization model that relies on voltage sensitivity coefficients for voltage control, is further augmented for optimal siting of ESS units in ADNs. In particular, an optimal planning procedure is proposed that accounts specifically for the minimization of the network voltage deviations based on the formulation of a mixed-integer linear programing problem. In view of the large size of the problem, its solution relies on the so-called benders decomposition technique.

B) Development of an optimization programming for optimal siting and sizing of ESSs with a multi-objective for energy balance and grid support

A multi-objective optimization problem is developed for optimal siting and sizing of ESSs in ADNs aiming at finding the optimal trade-off between technical and economical goals. In particular, the proposed procedure accounts for (i) network voltage deviations, (ii) feeders/lines congestions, (iii) network losses, (iv) cost of supplying loads (from external grid or local producers) together with the cost of ESS investment/maintenance, (v) load curtailment and (vi) stochasticity of loads and renewables production. The ESSs are suitably modeled to consider their ability to support the network by both active and reactive powers. The proposed OPF is used as the core of the model.

C) Inclusion of ADN reconfiguration model into ESSs planning problem

The above-mentioned model (section 1.2.1.C) for optimal ESSs siting and sizing is further developed by including the developed AND reconfiguration model into the optimization problem.

D) Successful application of decomposition methods for targeted long-term planning problems

The long-term planning problems are normally large-scale ones since they should include a reasonable number of scenarios to address the variations and uncertainties of various parameters. In case of our targeted problems, their size increase drastically with the increase of both network size and number of scenarios. As a consequence, a dedicated decomposition method might be required. In this thesis we proposed the proper application of Alternative Direction Method of Multipliers (ADMM) and Bender decomposition to break down the optimization problems.

1.3 Thesis Outline

The structure of the rest of this thesis dissertation is as follows.

Chapter 2 presents a literature review of the existing models and solution approaches for OPF problem in ADN. Then, the proposed OPF, along with the sufficient conditions for its exactness, are described. Various numerical analysis are also provided to demonstrate the effectiveness of the proposed OPF and showing the infeasible behavior of the existing convex OPF models. Further in this chapter, the proposed ADN optimal reconfiguration model, along with a relevant literature review of distribution networks reconfiguration, are presented.

In the last part of this chapter, we present a linearized OPF model for voltage control in ADN based on voltage sensitivity coefficients as an alternative to the relaxed OPF formulation.

Chapter 3 presents first a literature review dedicated to uncertainty management in power system optimization problem. Then, the inclusion of uncertainties into optimal operation of ADNs is investigated. In this respect, first based on standard forecasting processes of renewables production (in particular PV) and load consumption, a dedicated two-stage optimization problem for the day-ahead multi period optimal scheduling of ADNs with presence of ESSs is presented. In this optimization problem, the daily forecast curves of demand consumption and RERs composed by PV production are subject to uncertainty. Finally, adaptive robust optimization and stochastic optimization techniques are suitably casted to solve the developed optimization problems. The IEEE 34 buses test case network is used to demonstrate the effectiveness of the proposed robust and stochastic methods.

Chapter 4 presents first a literature review describing the state of the art in optimal siting and sizing of controllable resources in ADNs. Then, a dedicated optimization problem using voltage sensitivity coefficients is developed for siting of ESSs aiming to decrease the total voltage deviations. The proposed approach uses the concept of voltage sensitivity coefficients. Further, the proposed OPF model in chapter 2, is used to formulate the problem of optimal siting and sizing of ESSs in ADNs with multi-objective

function for energy balance and grid support. The topology changes of ADNs is also incorporated in the optimization problem using the proposed ADN optimal reconfiguration model. In order to account for the variations of different parameters (load, PV and energy price) during the life-time of ESS units, an appropriate scenario generation method is developed relying on multivariate Gaussian distribution of uncertain parameters. In the last part of this chapter different solution approach adapted to solve this large-scale Mixed Integer Second Cone Programming (MISOCP) problem are presented. In particular, Alternative Direction Method of Multipliers (ADMM) and Benders decomposition are suitably casted to decompose the targeted large-scale problem.

Chapter 5 presents various numerical analysis with reference to standard IEEE distribution networks as well as real distribution grids. In particular, this chapter presents three case study each one solved by one of the solution approaches described in chapter 4.

Chapter 6 summarizes the main contributions of this research and provides an outlook on the potential future works.

2 Optimal Operation and Control of Active Distribution Networks

Chapter Highlights:

We first introduce a relaxed convex OPF formulation, called AR-OPF, for radial power networks. Its features are i) convex formulation ii) inclusion of lines transverse parameters iii) inclusion of lines ampacity limits. Further, we provide sufficient conditions under which the relaxation in the proposed formulation is exact.

The AR-OPF is then used to develop a Mixed Integer Second Order Cone Programming (MISOCP) model for the ADN optimal reconfiguration problem. The radiality constraints are incorporated into the AR-OPF by using binary variables only for the lines equipped with switches. The proposed MISOCP model is tractable and can be solved efficiently with state-of-the-art optimization solvers.

Finally, in the last part of this chapter, we present a linearized OPF model for voltage control in ADN based on voltage sensitivity coefficients as an alternative to the relaxed OPF formulation.

2.1 Chapter Organization

The first part of the chapter is devoted to the literature review about the OPF problem. Afterwards, in section 2.2.3, the power flow equations in radial distribution networks are described. The OPF problem and the proposed Augmented Relaxed OPF (AR-OPF) formulations are described in sub-section 2.2.4. The required conditions for exactness of AR-OPF and the corresponding proofs are provided in sections 2.2.5 and 2.2.6, respectively.

Section 2.3 proposes a model to include the grid reconfiguration feature into the AR-OPF. In this respect, first a dedicated literature review is provided regarding the optimal ADN reconfiguration. Afterwards, an optimization programming based on the AR-OPF formulation is proposed for this specific problem. This section is concluded with numerical results to demonstrate the effectiveness of the proposed model.

The voltage control problem using a linearized OPF model based on voltage sensitivity coefficients is presented in section 2.4. First a literature review is presented, then the developed model is described in sub-section 2.4.2. The last part of this section provides numerical simulation results carried out using IEEE standard networks. The conclusion of this chapter is provided in section 2.5.

2.2 Optimal Power Flow in Active Distribution Networks

Optimal Power Flow is a known challenging optimization problem. It has been the main building block for the formulation of optimal controls as well as operation and planning problems in power systems. Typical examples refer, but not limited to: unit commitment, grid planning and reactive power dispatch problems [3-6].

Power distribution networks are designed in a meshed structure but are normally operated in radial topology due to several reasons essentially related to: limit short circuit current levels, selectivity of directional protections, etc. Therefore, in what follows we make reference to the power flow equations for radial distribution networks.

2.2.1 State-of-the-art of the Optimal Power Flow (OPF) problem in radial power grids

The OPF is inherently a non-convex NP-hard problem and, consequently, its solution is challenging. Several methods have been proposed to solve this optimization problem. They can be clustered in four general categories: (i) approximated methods that modify the physical description of the power flows equations [7-9], (ii) non-linear optimization methods [10-12], (iii) heuristic methods [13], [14] and (iv) convexification approaches [15-23]. Here below we briefly recall the main characteristics of each of the above-listed categories.

Approximations of the OPF constraints – This category of OPF solution methods relies on the approximations of the power flow constraints. The first and well known one, is the DC load flow. It is based on the following three main assumptions: a) voltage magnitudes are constant, b) line longitudinal resistances are assumed null and c) the angle differences between nodal voltages are small. It has been extensively used for the OPF in transmission networks (e.g. [3-7]). This approximation might be reasonable for most of OPF problems applied to transmission networks since the resistance/inductance ratio of high-voltage transmission lines is small and reactive power flows might be supplied locally. However, the DC OPF has several shortcomings like, for instance, the inability to optimize the reactive power dispatch. Additionally, its main drawback is that it always provides a solution even when it is physically meaningless (i.e., line power flows above the static transmission line limit).

Another approach is the so-called DistFlow formulation [8], [9]. It applies to power flow equations in radial systems. It should be noted that the DistFlow formulation, unlike DC OPF, does not neglect the resistance of the lines. It does not consider the voltage magnitude to be constant, and does not neglect the flow of the reactive power.

Solution of the non-convex OPF – These techniques seek to find a local optimum solution of the OPF. They cannot guarantee the identification of the global optimal solution as well as the sub-optimality gap. Typical examples of these techniques refer to interior point methods (e.g.,[10]), trust-region based methods (e.g.,[11]), and Lagrangian Newton methods [12].

Heuristic methods applied to OPF –Heuristic methods are widely used to solve the OPF. Typical application examples refer to Genetic Algorithm [13] and Particle Swarm Optimization[14]. Similarly to the previous category, they cannot guarantee the identification of the global solution and, additionally, they are generally characterized by a high computation time.

Convexification of the OPF – Several relaxations have been applied to convexify the AC-OPF problem (see the survey discussed in [15]). The Authors of [16] have proposed a linearized-relaxed model to approximate and solve the AC-OPF problem. A semidefinite relaxation method is proposed in [17]. A distributed optimization based on Alternative Direction Method of Multipliers (ADMM) and semidefinite relaxation is proposed in [18] to solve OPF in the case of unbalanced distribution networks. The Authors in [19] and [20] have investigated the application of moment-based relaxation to OPF problem. The Second Order Cone Programming (SOCP) relaxation is proposed in [21-23] to solve the OPF in radial power networks.

In this thesis the focus is on this last category of OPF solution methods. The reason of making reference to these specific category is justified by the increasing needs of Distribution Network Operators (DNOs) to actively control their grids in an optimal fashion due to increasing connection of the distributed generation (mainly from

renewable energy resources) and potentially controllable devices such as distributed storage and demand response.

Based on our best of knowledge, the latest contribution published on this subject is [23]. The Authors have shown that the SOCP relaxation is computationally more efficient than the semidefinite relaxation. In [21] the Authors have shown that the SOCP relaxation is tight when there is no upper bound on the nodal load consumptions. In [22] it is shown that the relaxation is exact with no upper bound on the nodal voltages together with specific conditions that can be checked a-priori and are a function of the network parameters. In [23] the Authors have improved the work of [22] by introducing a more conservative constraint on the upper bound for the nodal voltages.

Although the model proposed in [23] works properly in many operating conditions, it has a few deficiencies. In particular, it does not take into account the shunt capacitors of the equivalent two-port Π line model as well as the line ampacity constraints (which is an important limit, for instance, in grids with coaxial underground cables). Regarding the line shunt capacitors, even if these elements might be aggregated to nodal loads, their absence leads to an incorrect computation of the line current flows and, as a consequence, to the violation of line ampacity constraints.

In [24] it is proposed a methodology based on the augmented Lagrangian method to solve the original non-convex OPF problem considering the shunt impedances and the capacity limits of the feeders. However, this method is iterative and, as a consequence, computationally expensive. The positive aspect of it is that it can be easily formulated in a distributed manner.

In order to overcome the above limitations, in this first part of the chapter we propose a convex relaxed formulation of the OPF problem applied to radial power grids capable to include both shunt impedances of the classic two-port Π line model together with the line ampacity constraints. The formulation is augmented with a set of more conservative constraints for upper nodal voltage magnitudes and feeders current flows to preserve the exactness of the relaxed power flow model. The proposed formulation is characterized by a slightly reduced space of feasible solutions. The removed space is in correspondence of the one that is close to the technical limits of the grid being, from the grid operation view point, technically sound. Further, specific sufficient conditions are derived under which the AR-OPF is exact. The proof of exactness of the proposed AR-OPF is also provided.

2.2.2 Notations and definitions

The network is radial. Index 0 is for the slack bus and its voltage is fixed (v_0). Without loss of generality, we can assume that only bus 1 is connected to the slack bus (otherwise the problem separates into several independent problems). Buses other than the slack bus are denoted with $1, \dots, L$; $\mathcal{L}$ denotes the set $\mathcal{L} = \{1,\dots,L\}$ and up(l) is the label of the bus that is upstream of bus l. We also label with l the line whose downstream bus is

bus l; its upstream bus is therefore up(l). $\mathcal{L}_m$ denotes the set of the buses that are non-upstream of bus m ($\mathbf{H}_{lm} = 0$) and $\mathcal{L}^m$ denotes the set of the lines that are upstream of bus m ($\mathbf{H}_{lm} = 0$) ($\mathbf{H}$ is defined in (2.1)). Finally, $\underline{\mathcal{L}}$ denotes the set of the buses that are leaves of the grid.

Let: $S_l^t = P_l^t + jQ_l^t$ be the complex power flow entering line l from the top, i.e. from bus up(l); $S_l^c = P^t + Q_l^c$ the complex power flow entering the central element of line l (it is equal to S_l^t minus the reactive power associated with the shunt admittance connected to bus up(l), see Fig. 2-1); $S_l^b = P_l^b + jQ_l^b$ the complex power flow entering bus l from the bottom part of line l and f_l the square of the current in the central element of line l (Fig. 2-1). Let $z_l = r_l + jx_l$ and b_l be the longitudinal and shunt impedances of line l. We denote with z_l^* the complex conjugate of z_l.

Let v_l be the square of voltage magnitude and $s_l = p_l + jq_l$ the power absorption at bus l ($p_l \geq 0$ and $q_l \geq 0$ denote power consumptions, $p_l \leq 0$ and $q_l \leq 0$ denote powers injections). Let B_l denote the sum of the susceptances of the lines connected to bus l.

$v^{\max}$ and $v^{\min}$ are the square of maximum and minimum magnitude of nodal voltages. $I_l^{\max}$ is the square of maximum current flow limit of line l ($l \in \mathcal{L}$). $\Re(.)$ and $\Im(.)$ denote the real and imaginary parts of complex numbers and $j := \sqrt{-1}$ is the imaginary unit; $\max\{a, b\}$ returns the maximum of a and b.

A notation without subscript such as v denotes a column vector with L rows as in

$$v = \begin{pmatrix} v_1 \\ \vdots \\ v_L \end{pmatrix}, S = \begin{pmatrix} S_1^t \\ \vdots \\ S_L^t \end{pmatrix}, P = \begin{pmatrix} P_1^t \\ \vdots \\ P_L^t \end{pmatrix}, I^{\max} = \begin{pmatrix} I_1^{\max} \\ \vdots \\ I_L^{\max} \end{pmatrix}, \text{etc.}$$

Note that for S, P, Q and their related auxiliary variables ($\bar{S}, \hat{S}, \ldots$) the vectors S, P, Q represent the relevant values at upper side of line l (S_l^t). The notation $|P|$ represents the column vector with L rows whose l^{th} element is the absolute value of P_l. Comparison of vectors is entry-wise, i.e. $P \leq P'$ means $P_l \leq P_l'$ for every $l \in \mathcal{L}$. The transpose of P is denoted with P^T.

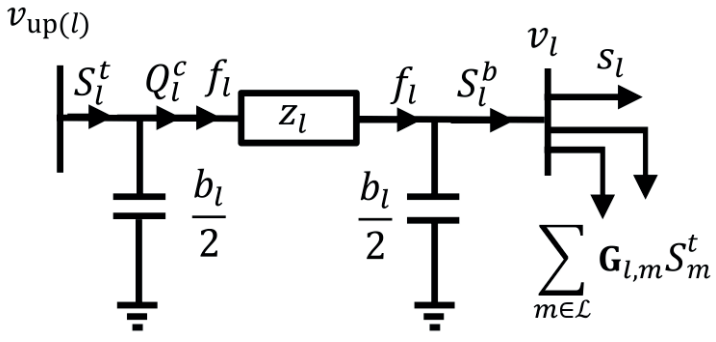

Fig. 2-1: Classical two-port Π model of a transmission line adopted for the formulation of the OPF relaxed constraints.

Matrices are shown with bold non-italic capital letters such as $\mathbf{A}$. We use the l_1–norm for vectors $\|v\| = \sum_{l=1}^{L}|v_l|$ and the induced l_1–norm for matrices $\|\mathbf{A}\| = \max_{l=1\ldots L}\sum_{k=1}^{L}|A_{k,l}|$. For two matrices $\mathbf{A},\mathbf{B}$ of equal dimensions, the notation $\mathbf{A}\circ\mathbf{B}$ denotes their Hadamard product, defined by $(\mathbf{A}\circ\mathbf{B})_{k,l} = \mathbf{A}_{k,l}\mathbf{B}_{k,l}$ for all k,l.

For the reader's convenience, the matrices defined are listed below.

- $\mathbf{I}$ is the $L \times L$ identity matrix.
- For a vector such as r, $\mathrm{diag}(r)$ denotes the diagonal matrix whose l^{th} element is r_l.
- $\mathbf{G}$ is the adjacency matrix of the oriented graph of the network, i.e. $\mathbf{G}_{k,l}$ is defined for $k,l \in \mathcal{L}$ and $\mathbf{G}_{k,l} = 1$ if $k = \mathrm{up}(l)$ and 0 otherwise.
- $\mathbf{H}$ is the closure of $\mathbf{G}$, i.e. $\mathbf{H}_{k,l} = 1$ if bus k is on the path from the slack bus to bus l or $k = l$, and $\mathbf{H}_{k,l} = 0$ otherwise. Because the network is radial, $\mathbf{G}^L = 0$ and

$$\mathbf{H} = \mathbf{I} + \mathbf{G} + \mathbf{G}^2 + \ldots + \mathbf{G}^{L-1} = (\mathbf{I} - \mathbf{G})^{-1} \tag{2.1}$$

$$\mathbf{M} = \mathrm{diag}(x)\mathbf{H}\mathrm{diag}(B) \tag{2.2}$$

$\mathbf{C} = (\mathbf{I} - \mathbf{G}^T - \mathbf{M})^{-\mathbf{1}}$. ($\mathbf{C}$ is well-defined and is nonnegative (entry-wise) when Condition C1 (later defined in sub-section 2.2.5.1) holds).

- $\mathbf{D}$ is the entry-wise positive matrix defined by

$$\mathbf{D} = \mathbf{C}\left[2\mathrm{diag}(r)\left((\mathbf{H}-\mathbf{I})\mathrm{diag}(r)\right) + 2\mathrm{diag}(x)\left((\mathbf{H}-\mathbf{I})\mathrm{diag}(x)\right) + \mathrm{diag}\left(|z|^2\right)\right] \tag{2.3}$$

- π, ϱ and ϑ are the vectors defined by

$$\pi_l = \frac{\max\left\{P_l^{\max}, \left|\mathbf{H}p^{\min}\right|_l\right\}}{v_l^{\min}} \tag{2.4}$$

$$\varrho_l = \frac{\max\left\{Q_l^{\max}, \left|\mathbf{H}q^{\min} - \frac{1}{2}\mathbf{H}\mathrm{diag}(b)\left(\mathbf{I}+\mathbf{G}^{\mathbf{T}}\right)\left(v^{\max}\right)\right|_l\right\}}{v_l^{\min}} \tag{2.5}$$

$$\vartheta_l = (\pi_l)^2 + (\varrho_l)^2 \tag{2.6}$$

where $p^{\min}$ and $q^{\min}$ are the vectors of minimum loads level on the buses of system.

- $\mathbf{E}$ and $\mathbf{F}$ are the entry-wise positive matrix defined by

$$\mathbf{F} = \left(\mathbf{H}\mathrm{diag}(x) + \frac{1}{2}\mathbf{H}\mathrm{diag}(B)(\mathbf{G}^T)\mathbf{D} \right) \tag{2.7}$$

$$\mathbf{E} = 2\mathrm{diag}(\pi)\mathbf{H}\mathrm{diag}(r) + 2\mathrm{diag}(\varrho)\mathbf{F} + \mathrm{diag}(\vartheta)\mathbf{D} \tag{2.8}$$

2.2.3 Power flow equations in radial distribution networks

For a given radial power network, the power flow equations without considering the lines shunt impedances are given in (2.9.a)-(2.9.c).

$$S_l^t = s_l + \sum_{m \in \mathcal{L}} (\mathbf{G}_{l,m} S_m^t) + z_l f_l, \quad \forall l \in \mathcal{L} \tag{2.9.a}$$

$$v_l = v_{\mathrm{up}(l)} - 2\Re\left(z_l^* S_l^t\right) + |z_l|^2 f_l, \ \ \forall l \in \mathcal{L} \tag{2.9.b}$$

$$f_l = \frac{\left|S_l^t\right|^2}{v_{\mathrm{up}(l)}}, \quad \forall l \in \mathcal{L} \tag{2.9.c}$$

The equation (2.9.a) represents the complex flow on the line between buses up(l) and l. The voltages between the two ends of the feeders are linked with the equation (2.9.b) and the equation (2.9.c) represents the square of the current flow from bus up(l) to l.

The DistFlow equations for the given radial network are given in (2.10.a)-(2.10.b). In these equations f is neglected and consequently they are linear.

$$\hat{S}_l^t = s_l + \sum_{m \in \mathcal{L}} (\mathbf{G}_{l,m} \hat{S}_m^t), \quad \forall l \in \mathcal{L} \tag{2.10.a}$$

$$\hat{v}_l = v_{\mathrm{up}(l)} - 2\Re\left(z_l^* \hat{S}_l^t\right), \ \ \forall l \in \mathcal{L} \tag{2.10.b}$$

These equations have been extensively used in the literature. However, they don't consider the transverse parameters of the transmission lines. For instance, these parameters are not negligible in the networks characterized by underground coaxial cables and, therefore, have to be taken into accounts for network studies, operation and control. In the followings, the transverse parameters are appropriately incorporated into power flow equations and the new power flow equations considering transverse parameters are presented.

For sake of clarity, the complete transmission line two-port Π model is shown in Fig. 2-1. For a given radial power network, the correct power flow equations are given by (2.11).

$$S_l^t = s_l + \sum_{m \in \mathcal{L}} \mathbf{G}_{l,m} S_m^t + z_l f_l - j\left(v_{\mathrm{up}(l)} + v_l\right)\frac{b_l}{2}, \ \ \forall l \in \mathcal{L} \tag{2.11.a}$$

$$v_l = v_{\mathrm{up}(l)} - 2\Re\left(\mathrm{z}_l^*\left(S_l^t + j\frac{v_{\mathrm{up}(l)}b_l}{2}\right)\right) + \left|z_l\right|^2 f_l, \forall l \in \mathcal{L} \tag{2.11.b}$$

$$f_l = \frac{\left|S_l^t + j\frac{v_{\mathrm{up}(l)}b_l}{2}\right|^2}{v_{\mathrm{up}(l)}} = \frac{\left|S_l^b - j\frac{v_l b_l}{2}\right|^2}{v_l}, \quad \forall l \in \mathcal{L} \tag{2.11.c}$$

$$S_l^b = s_l + \sum_{m\in\mathcal{L}} \mathbf{G}_{l,m} S_m^t, \quad \forall l \in \mathcal{L} \tag{2.11.d}$$

Equations (2.11.a), (2.11.b) and, (2.11.c) directly derived by the application of the Kirchhoff's law to Fig. 2-1 represent the power and voltage equilibriums in the line. Equation (2.11.d) represents complex power flow of line l at its l side (see Fig. 2-1). It is a derived variable, which is introduced here for notational convenience.

It should be noted that (2.11.c) represents the physically correct value of the internal current of the two-port Π model. It is worth noting that the term f_l does not represent the square of the current that one can measure at the line terminals; it is an internal state variable of the two-port Π model.

The corresponding DistFlow equations including transverse parameters are as followings:

$$\hat{S}_l^t = s_l + \sum_{m\in\mathcal{L}} \mathbf{G}_{l,m}\hat{S}_m^t - j\left(\hat{v}_{\mathrm{up}(l)} + \hat{v}_l\right)\frac{b_l}{2}, \quad \forall l \in \mathcal{L} \tag{2.12.a}$$

$$\hat{v}_l = \hat{v}_{\mathrm{up}(l)} - 2\Re\left(\mathrm{z}_l^*\left(\hat{S}_l^t + j\frac{\hat{v}_{\mathrm{up}(l)}b_l}{2}\right)\right), \forall l \in \mathcal{L} \tag{2.12.b}.$$

2.2.4 Proposed optimal power flow in radial distribution networks

One can formulate an optimization problem, called OPF, with the power flow equations shown in (2.11.a)-(2.11.d). The objective function is generally represented by a convex one and practical examples refers to minimization of: (i) nodal voltage magnitude deviations with respect to the rated value, (ii) network resistive losses, (iii) line congestion, (iv) cost of supplied energy, etc. Here we consider that the objective function is the minimization of the generation cost of dispatchable units available in the network and energy imported from the transmission network (or maximization of the energy exported to the grid). It should be noted that the minimization (resp. maximization) of energy import (resp. export) from the grid and the total resistive losses minimization are the same objectives. Therefore, the objective function shown in (11.a) is strictly increasing in total resistive losses or energy import from the gird. The general optimization problem is shown in (2.13.a)-(2.13.g).

Original Optimal Power Flow (O-OPF)

$$\underset{s,S,v,f}{\text{minimize}} \sum_{l \in \mathcal{L}} \left(\mathcal{C}\left(\Re\left(s_l\right), \Im\left(s_l\right)\right)\right) + \mathcal{C}^e\left(P_1^t\right) \tag{2.13.a}$$

subject to:

(2.11.a)-(2.11.d)

$$v_l \le v^{\max}, \ \forall l \in \mathcal{L} \tag{2.13.b}$$

$$v^{\min} \le v_l, \ \forall l \in \mathcal{L} \tag{2.13.c}$$

$$\frac{\left|S_l^t\right|^2}{v_{\text{up}(l)}} \le I_l^{\max}, \ \forall l \in \mathcal{L} \tag{2.13.d}$$

$$\frac{\left|S_l^b\right|^2}{v_l} \le I_l^{\max}, \ \forall l \in \mathcal{L} \tag{2.13.e}$$

$$p_l^{\min} \le \Re\left(s_l\right) \le p_l^{\max}, \ \forall l \in \mathcal{L} \tag{2.13.f}$$

$$q_l^{\min} \le \Im\left(s_l\right) \le q_l^{\max}, \ \forall l \in \mathcal{L} \tag{2.13.g}$$

where $\mathcal{C}(.)$ is the cost function of nodal absorption (injection), $\mathcal{C}^e(P_1^t)$ is the cost function related to energy import from the grid. Both $\mathcal{C}(.)$ and $\mathcal{C}^e(.)$ are assumed to be convex, and as mentioned above, $\mathcal{C}^e(.)$ is strictly increasing. $I_l^{\max}$ and $v^{\max}/v^{\min}$ represent the maximum square current flow limit of the lines and maximum/minimum nodal square voltage magnitudes. $I_l^{\max}$ and $v^{\max}/v^{\min}$ represent the maximum square current flow limit of the lines and maximum/minimum nodal square voltage magnitudes. In order to account for the voltage and line current operational constraints, equations (2.13.b)-(2.13.e) are added to the optimization problem. It is worth noting that line ampacity limits must not be applied to f_l since, as stated before; it does not represent the exact value of the current at its terminals. Additionally, it has to be applied to both ends of the feeder since the current flow at both ends are not equal. The constraints (2.13.g) and (2.13.f) represent the upper and lower limits of nodal loads (it worth to mention that $p_l^{\min}$ and $p_l^{\min}$ correspond to the maximum generation capacity of active and reactive power on bus l.).

This optimization problem is non-convex due to equation (2.11.c). However, as shown in [21]), it becomes convex if we replace (2.11.c) by (2.14):

$$f_l \ge \frac{\left|S_l^t + j\frac{v_{\text{up}(l)} b_l}{2}\right|^2}{v_{\text{up}(l)}}, \ \forall l \in \mathcal{L} \tag{2.14}$$

The problem obtained when we replace (2.11.c) by (2.14) in O-OPF is called the Relaxed Optimal Power Flow (R-OPF).

Relaxed Optimal Power Flow (R-OPF)

$$\underset{s,S,v,f}{\text{minimize}} \sum_{l \in \mathcal{L}} \mathcal{C}\left(\Re(s_l), \Im(s_l)\right) + \mathcal{C}^e\left(P_1\right) \tag{2.15.a}$$

subject to:

(2.11.a), (2.11.b), (2.11.d), (2.14),(2.13.b)-(2.13.g)

It can easily be shown that R-OPF is a convex problem, however, it may often occur that the optimal solution does not satisfy the original constraint (2.11.c), i.e. is not a physical solution [24].

In the next section, we present an augmented formulation of R-OPF which does not have this problem, as we prove in the following.

2.2.4.1 Proposed OPF model for ADN

In order to ensure the feasibility of the proposed OPF formulation, we first introduce the following sets of auxiliary variables $\bar{f}$, $\hat{S}$, $\bar{S}$ for the lines of the grid and $\hat{v}$ for the buses of the network as defined in (2.15.b) - (2.15.h). It should be noted that $\hat{S}$ and $\hat{v}$ represent lower bound and upper bound on S and v, respectively and are adapted from DistFlow equations [8]. $\bar{S}$ and $\bar{f}$ are upper bounds on S and f, respectively (The proof of these statements is in *2.2.6.1*).

$$\hat{S}_l^t = s_l + \sum_{l \in \mathcal{L}} \mathbf{G}_{l,m} \hat{S}_l^t - j\left(\hat{v}_{\text{up}(l)} + \hat{v}_l\right)\frac{b_l}{2}, \quad \forall l \in \mathcal{L} \tag{2.15.b}$$

$$\hat{v}_l = \hat{v}_{\text{up}(l)} - 2\Re\left(\mathrm{z}_l^*\left(\hat{S}_l^t + j\frac{\hat{v}_{\text{up}(l)} b_l}{2}\right)\right), \quad \forall l \in \mathcal{L} \tag{2.15.c}$$

$$\bar{S}_l^t = s_l + \sum_{m \in \mathcal{L}} \mathbf{G}_{l,m} \bar{S}_m^t + z_l \bar{f}_l - j\left(v_{\text{up}(l)} + v_l\right)\frac{b_l}{2}, \quad \forall l \in \mathcal{L} \tag{2.15.d}$$

$$\bar{S}_l^b = s_l + \sum_{m \in \mathcal{L}} \mathbf{G}_{l,m} \bar{S}_l^t, \quad \forall l \in \mathcal{L} \tag{2.15.e}$$

$$\hat{S}_l^b = s_l + \sum_{l \in \mathcal{L}} \mathbf{G}_{l,m} \hat{S}_l^t, \quad \forall l \in \mathcal{L} \tag{2.15.f}$$

$$\bar{f}_l \geq \frac{\left|\max\left\{\left|\hat{P}_l^b\right|, \left|\bar{P}_l^b\right|\right\}\right|^2}{v_l} + \frac{\left(\max\left\{\left|\hat{Q}_l^b - j\frac{\hat{v}_l b_l}{2}\right|, \left|\bar{Q}_l^b - \frac{v_l b_l}{2}\right|\right\}\right)^2}{v_l}, \quad \forall l \in \mathcal{L} \tag{2.15.g}$$

$$\bar{f}_l \geq \frac{\left|\max\left\{\left|\hat{P}_l^t\right|,\left|\bar{P}_l^t\right|\right\}\right|^2}{v_{\mathrm{up}(l)}} + \frac{\left(\max\left\{\left|\hat{Q}_l^t + j\frac{\hat{v}_{\mathrm{up}(l)}b_l}{2}\right|,\left|\bar{Q}_l^t + \frac{v_{\mathrm{up}(l)}b_l}{2}\right|\right\}\right)^2}{v_{\mathrm{up}(l)}},\ \forall l \in \mathcal{L} \qquad (2.15.h)$$

In in *2.2.6.1* we will show that for any set of $(s, S, v, f, \hat{S}, \hat{v}, \bar{f}, \bar{S})$ that satisfies (2.11.a) -(2.11.d) and (2.15.b)-(2.15.h) we have (recall that a notation such as S represents the vector S_l^t):

$$\hat{P} \leq P \leq \bar{P} \qquad (2.16.a)$$

$$\hat{Q} \leq Q \leq \bar{Q} \qquad (2.16.b)$$

$$v \leq \hat{v} \qquad (2.16.c).$$

2.2.4.2 Proposed Augmented Relaxed OPF model

The following Augmented OPF (A-OPF) formulation is obtained by adding new variables $(\hat{S}, \bar{S}, \bar{f}, \hat{v})$ to (2.13) and modifying security constraints as shown in (2.17).

Augmented Optimal Power Flow (A-OPF)

$$\underset{s,S,v,f,\hat{S},\hat{v},\bar{S},\bar{f}}{\text{minimize}} \sum_{l\in\mathcal{L}}\left(\mathcal{C}\left(\Re(s_l),\Im(s_l)\right)\right) + \mathcal{C}^e\left(P_1^t\right)) \qquad (2.17.a)$$

subject to:

(2.11.a)-(2.11.c)

(2.13.f),(2.13.g)

(2.15.b)-(2.15.h)

$$v^{\min} \leq v_l, \quad \forall l \in \mathcal{L} \qquad (2.17.b)$$

$$\hat{v}_l \leq v^{max},\ \forall l \in \mathcal{L} \qquad (2.17.c)$$

$$\left\|\max\left\{\left|\hat{P}_l^b\right|,\left|\bar{P}_l^b\right|\right\}\right| + j\max\left\{\left|\hat{Q}_l^b\right|,\left|\bar{Q}_l^b\right|\right\}\Big|^2 \leq v_l I_l^{\max},\ \forall l \in \mathcal{L} \qquad (2.17.d)$$

$$\left|\max\left\{\left|\hat{P}_l^t\right|,\left|\bar{P}_l^t\right|\right\} + j(\max\left\{\left|\hat{Q}_l^t\right|,\left|\bar{Q}_l^t\right|\right\}\Big|^2 \leq v_{\mathrm{up}(l)} I_l^{\max}, \forall l \in \mathcal{L} \qquad (2.17.e)$$

$$\bar{P}_l^t \leq P_l^{\max},\ \forall l \in \mathcal{L} \qquad (2.17.f)$$

$$\bar{Q}_l^t \leq Q_l^{\max},\ \forall l \in \mathcal{L} \qquad (2.17.g)$$

$$P_l^t \leq P_l^{\max},\ \forall l \in \mathcal{L} \qquad (2.17.h)$$

$$Q_l^t \leq Q_l^{\max},\ \forall l \in \mathcal{L} \qquad (2.17.i)$$

In the A-OPF formulation, the nodal voltage magnitudes upper limit is imposed on $\hat{v}$, an upper bound of v). This is shown in equation (2.17.c). Similarly, the lines current flow limit is modeled using the maximum of absolute values of $\bar{P}$(resp. Q) and $\hat{P}$(resp. $\hat{Q}$) as shown in (2.17.d)-(2.17.e). As it is shown in equations (2.16.a) and (2.16.b) $\bar{P}$(resp. Q) and $\hat{P}$(resp. $\hat{Q}$) are upper and lower bounds of P (resp. Q) respectively. We have also added constraints (2.17.f) -(2.17.i) to the optimization problem. It should be noted that they are not a physical constraint of the system. We have added these constraints to derive the exactness conditions (later presented in section 2.2.5.1) more straightforward. The values of $P_l^{\max}$, and $Q_l^{\max}$ are chosen so that this constraints don't affect the feasible solution space of A-OPF (by performing a load flow with maximum injection and absorption levels of the system and obtain the maximum possible values of P_l^t ($\bar{P}_l^t$) and Q_l^t ($\bar{Q}_l^t$)).

It should be noted that the new set of constraints (2.17.b)-(2.17.i) is a bit more conservative and slightly shrinks the feasible solution space. However, the removed space covers an operation zone close to nodal voltages and line ampacity limits that is not a desirable operating region for the network operators.

The A-OPF is non convex due to equation (2.11.c). The proposed OPF formulation is obtained by replacing (2.11.c) with (2.14) in A-OPF, which gives the following convex model, called AR-OPF:

Augmented Relaxed Optimal Power Flow (AR-OPF)

$$\underset{s,S,v,f,\hat{S},\hat{v},\bar{S},\bar{f}}{\text{minimize}} \sum_{l\in\mathcal{L}} \left(\mathcal{C}\left(\Re(s_l),\Im(s_l)\right)\right) + \mathcal{C}^e\left(P_1^t\right) \tag{2.18.a}$$

subject to:

(2.11.a),(2.11.b), (2.11.d)(2.14)(2.13.f),(2.13.g),

(2.15.b)-(2.15.h),

(2.17.b)-(2.17.i).

In the next section, we provide conditions for exactness of AR-OPF.

2.2.5 Exactness of augmented relaxed OPF

In this section, we provide seven conditions under which the relaxation (2.14) in (AR-OPF) is guaranteed to be exact. These conditions can be easily verified using the static parameters.

2.2.5.1 Statement of the Conditions for exactness of AR-OPF

The seven conditions are as follows (matrices **D**, **E** and **H** are defined in (2.3), (2.8) and (2.1)).

Condition C1:

$$\left(\max_{l\in\mathcal{L}} x_l\right)\left(\max_{l\in\mathcal{L}} B_l\right) < \frac{1}{\left\|\mathbf{H}^{\mathrm{T}}\right\|\left\|\mathbf{H}\right\|} \tag{2.19.a}$$

or

$$\left(\max_{l\in\mathcal{L}} x_l\right)\left(\max_{l\in\mathcal{L}} B_l\right) < \frac{1}{L^2} \tag{2.19.b}$$

Condition C2:

$$\left\|\mathbf{E}\right\| \le 1 \tag{2.20}$$

Condition C3: there exists a $\eta_1 < 0.5$ such that:

$$\left(\mathbf{H}\mathrm{diag}(r)\mathbf{E}\right)\circ\mathbf{H} \le \eta_1\mathbf{H}\mathrm{diag}(r) \tag{2.21}$$

Condition C4: there exists a $\eta_2 < 0.5$ such that:

$$\mathbf{H}\mathrm{diag}(r)\mathbf{E}^2 \le \eta_2\mathbf{H}\mathrm{diag}(r)\mathbf{E} \tag{2.22}$$

Condition C5: there exists a $\eta_4 < 0.5$ such that:

$$\left(\mathbf{H}\mathrm{diag}(x)\mathbf{E}\right)\circ\mathbf{H} \le \eta_4\mathbf{H}\mathrm{diag}(x) \tag{2.23}$$

Condition C6: there exists a $\eta_5 < 0.5$ such that:

$$\mathbf{H}\mathrm{diag}(x)\mathbf{E}^2 \le \eta_5\mathbf{H}\mathrm{diag}(x)\mathbf{E} \tag{2.24}$$

Condition C7: there exists a $\eta_3 < 0.5$ such that:

$$\mathbf{D}\mathbf{E} \le \eta_3\mathbf{D} \tag{2.25}$$

The following Theorem is defined to show the exactness of AR-OPF.

Theorem I: Under conditions *C1-C7*:

1) For every feasible solution $(s, S, v, \bar{f}, \hat{S}, \hat{v}, f, \bar{S})$ of AR-OPF there exist a feasible solution $(s, S^*, v^*, f^*, \hat{S}, \hat{v}, \bar{f}^*, \bar{S}^*)$ of A-OPF with the same power injection vector s.

2) Every optimal solution $(s, S, v, \bar{f}, \hat{S}, \hat{v}, f, \bar{S})$ of AR-OPF satisfies (2.11.c), and is thus an optimal solution of A-OPF.

Part 1) of *Theorem I* implies that the vector of absorptions (s) of any feasible solution of the proposed OPF formulation belongs to the region where the nodal voltages upper and lower limits and the lines ampacity limit are satisfied. Part 2) of *Theorem I* is the exactness of the relaxation.

The main idea of the proof of *Theorem I* is as follows. If $(s, S, v, \bar{f}, \hat{S}, \hat{v}, f, \bar{S})$ is feasible for AR-OPF, then (S, v, f) is in general not a load flow solution for the power injections s (as (2.14) replaces (2.11.c)) but it is always possible to replace (S, v, f) by (S^*, v^*, f^*) obtained by a performing a load flow on s. The technical difficulty is to find the good load flow solution (as there are multiple solutions), namely one that satisfies the voltage and ampacity constraints. This "good" load flow solution is obtained using an ad-hoc iterative scheme (later described in this section). Further, we show that an optimal solution of AR-OPF is also a load flow solution.

In case of direct power flow operating condition the following Theorem is introduced.

Theorem II: Under conditions *C1* and when $\mathbf{H}p^{\min} \geq 0$ and $\mathbf{H}q^{\min} - \frac{1}{2}\mathbf{H}\mathrm{diag}(b)\left(\mathbf{I}+\mathbf{G}^{\mathbf{T}}\right)\left(v^{\max}\right) \geq 0$:

1) Every optimal solution $(s, S, v, \bar{f}, \hat{S}, \hat{v}, f, \bar{S})$ of AR-OPF satisfies (2.11.c), and is thus an optimal solution of A-OPF.

Theorem II implies that, under condition *C1*, for a network operating in direct power flow, the relaxation shown in (2.11.c) is exact. The proof of *Theorem II* is provided in 2.2.6.

2.2.6 Proof of exactness of AR-OPF

In this sub-section, first we derive the matrix form of power flow equations. Then, we prove that under condition *C1* matrix $\mathbf{C} = \mathbf{I} - \mathbf{G}^T - \mathbf{M}$ is invertible. Finally, the proofs of *Theorems I* and *II* are provided.

2.2.6.1 Formulation of constraints in matrix form

For $l \neq 1$, the upstream bus of l, up(l), is the unique $j \in \{1, \dots, L\}$ such that $\mathbf{G}_{j,l} = 1$ and thus the voltage $v_{\mathrm{up}(l)}$ at the upstream bus of l is given by $v_{\mathrm{up}(l)} = \sum_j \mathbf{G}_{j,l} v_j$, namely $v_{\mathrm{up}(l)} = (\mathbf{G}^T v)_l$.

Using equations (2.11.b) we can rewrite the nodal voltage equation for $l = 1, \dots, L$ as follows:

$$v = \mathbf{G}^T v + v_0 e - 2\mathrm{diag}(r)P - 2\mathrm{diag}(x)Q - \mathrm{diag}(x)\mathrm{diag}(b)\mathbf{G}^T v + \mathrm{diag}(|z|^2)f \qquad (2.26)$$

where $e = (1,0,\dots 0)^T$. Similarly, (2.11.a) gives:

$$P = p + \mathbf{G}P + \mathrm{diag}(r)f \qquad (2.27)$$

$$Q = q + \mathbf{G}Q + \mathrm{diag}(x)f - \frac{1}{2}\mathrm{diag}(b)\left(\mathbf{I}+\mathbf{G}^{\mathbf{T}}\right)v \qquad (2.28).$$

Using (2.1) we can rewrite (2.27) and (2.28) as:

$$P = \mathbf{H}p + \mathbf{H}\mathrm{diag}(r)f \tag{2.29}$$

$$Q = \mathbf{H}q + \mathbf{H}\mathrm{diag}(x)f - \frac{1}{2}\mathbf{H}\mathrm{diag}(b)\left(\mathbf{I} + \mathbf{G}^{\mathbf{T}}\right)v \tag{2.30}.$$

Similarly we have:

$$\overline{P} = \mathbf{H}p + \mathbf{H}\mathrm{diag}(r)\overline{f} \tag{2.31}$$

$$\overline{Q} = \mathbf{H}q + \mathbf{H}\mathrm{diag}(x)\overline{f} - \frac{1}{2}\mathbf{H}\mathrm{diag}(b)\left(\mathbf{I} + \mathbf{G}^{\mathbf{T}}\right)(v) \tag{2.32}.$$

We can eliminate P, Q from (2.26), using (2.29), (2.30) and obtain:

$$\begin{aligned}&\left(\mathbf{I} - \mathbf{G}^{T} + \mathrm{diag}(x)\mathrm{diag}(b)\mathbf{G}^{T} - \mathrm{diag}(x)\mathbf{H}\mathrm{diag}(b)\left(\mathbf{I} + \mathbf{G}^{T}\right)\right)v = \\ &v_0 e - 2\mathrm{diag}(r)\mathbf{H}p - 2\mathrm{diag}(x)\mathbf{H}q + \left(-2\mathrm{diag}(r)\mathbf{H}\mathrm{diag}(r) - 2\mathrm{diag}(x)\mathbf{H}\mathrm{diag}(x) + \mathrm{diag}\left(|z|^2\right)\right)f\end{aligned} \tag{2.33}$$

now using (2.1) and the following equation

$$\mathbf{G}\mathrm{diag}(b)\mathbf{G}^{T} = \mathrm{diag}(B) - \mathrm{diag}(b) \tag{2.34}$$

this gives:

$$\begin{aligned}\left[\mathbf{I} - \mathbf{G}^{\mathbf{T}} - \mathbf{M}\right]v = v_0 e - 2\mathrm{diag}(r)\left(\mathbf{H}p + (\mathbf{H} - \mathbf{I})\mathrm{diag}(r)f\right) - \\ 2\mathrm{diag}(x)\left(\mathbf{H}q + (\mathbf{H} - \mathbf{I})\mathrm{diag}(x)f\right) - \mathrm{diag}\left(|z|^2\right)f\end{aligned} \tag{2.35}$$

where $\mathbf{M} = \mathrm{diag}(x)\mathbf{H}\mathrm{diag}(B)$.

Under condition *C1* (given in the sub-section 2.2.5.1), we prove that $\mathbf{C} = [\mathbf{I} - \mathbf{G}^{\mathbf{T}} - \mathbf{M}]^{-1}$ exists and has non-negative entries. It follows that we can solve for v in equation (2.35) as follows:

$$v = v_0\mathbf{C}e - 2\mathbf{C}\mathrm{diag}(r)(\mathbf{H}p) - 2\mathbf{C}\mathrm{diag}(x)(\mathbf{H}q) - \mathbf{D}f \tag{2.36}$$

where $\mathbf{D}$ is defined in (2.3). Note that $\mathbf{D}_{k,l} \geq \mathbf{C}_{k,l}|z|_l^2 > 0$ for all k, l i.e. $D > 0$ entrywise. Further, $\mathbf{D}$ is "small" when z is small. Next, we can write (2.15.c) as follows:

$$\hat{v} = v_0\mathbf{C}e - 2\mathbf{C}\mathrm{diag}(r)(\mathbf{H}p) - 2\mathbf{C}\mathrm{diag}(x)(\mathbf{H}q) \tag{2.37}$$

thus:

$$v = \hat{v} - \mathbf{D}f \tag{2.38}.$$

Since $\mathbf{D}$ and f are non-negative matrices, thus:

$$v \le \hat{v} \tag{2.39}.$$

Further the equation (2.11.a) and (2.15.b) can be rewritten in matrix form as:

$$\hat{P} = \mathbf{H}p \tag{2.40}$$

$$\hat{Q} = \mathbf{H}q - \frac{1}{2}\mathbf{H}\mathrm{diag}(b)\left(\left(\mathbf{I}+\mathbf{G}^{\mathbf{T}}\right)\hat{v}\right) \tag{2.41}$$

$$P = \mathbf{H}p + \mathbf{H}\mathrm{diag}(r)f = \hat{P} + \mathbf{H}\mathrm{diag}(r)f \tag{2.42}$$

$$\begin{aligned} Q = \mathbf{H}q + \mathbf{H}\mathrm{diag}(x)f - \frac{1}{2}\mathbf{H}\mathrm{diag}(b)\left(\mathbf{I}+\mathbf{G}^{\mathbf{T}}\right)(v) = \\ \hat{Q} + \mathbf{H}\mathrm{diag}(x)f + \frac{1}{2}\mathbf{H}\mathrm{diag}(b)\left(\mathbf{I}+\mathbf{G}^{\mathbf{T}}\right)(\mathbf{D}f) \end{aligned} \tag{2.43}.$$

Since r, b, x **D** and f are all non-negative thus:

$$\hat{P} \le P \tag{2.44}$$

$$\hat{Q} \le Q \tag{2.45}.$$

We are also interested in $Q_l^t + \frac{v_{\mathrm{up}(l)} b_l}{2}$ and $\widehat{Q}_l^t + \frac{\hat{v}_{\mathrm{up}(l)} b_l}{2}$ namely the power flows inside the longitudinal components, which we call Q_l^c and $\hat{Q}_l^c$. Using (2.41) and (2.43) we have:

$$\hat{Q}^c = \hat{Q} + \frac{1}{2}\mathrm{diag}(b)\mathbf{G}^{\mathbf{T}}\hat{v} = \mathbf{H}q - \frac{1}{2}\mathbf{H}\mathrm{diag}(B)\hat{v} \tag{2.46}$$

$$Q^c = Q + \frac{1}{2}\mathrm{diag}(b)\mathbf{G}^{\mathbf{T}}v = \mathbf{H}q + \mathbf{H}\mathrm{diag}(x)f - \frac{1}{2}\mathbf{H}\mathrm{diag}(B)v = \hat{Q}^c + \mathbf{F}f \tag{2.47}$$

where **F** is defined in (2.7).

Similar to (2.45) we have:

$$\hat{Q} \le \hat{Q}' \le Q' \tag{2.48}.$$

Lemma I: If $(s, S, v, f, \hat{S}, \hat{v}, \bar{f}, \bar{S})$ satisfies (2.11.a)-(2.11.d) and (2.15.b)-(2.15.h) then:

1- $f \le \bar{f}$ and $S \le \bar{S}$
2- If $\left(s, S', f', v', \hat{S}, \hat{v}, \bar{f}', \bar{S}'\right)$ satisfies (2.11.a), (2.11.b), (2.11.d), (2.14), (2.15.b)-(2.15.h) and $0 < v' \le v$ then it is always possible to construct $\bar{S}''$ and $\bar{f}''$ such that $(s, S, v, f, \hat{S}, \hat{v}, \bar{f}'', \bar{S}'')$ satisfies (2.11.a)-(2.11.d) and (2.15.b)-(2.15.h) and $\bar{f}'' \le \bar{f}'$ and $\bar{S}'' \le \bar{S}'$.

We prove this lemma by mathematical induction starting from the leaves of the grid. Formally, for a bus l, let height(l) denote its height in the tree, defined by height(l) = 0 when l is a leaf and height(l) = $1 + \max_{k:\,\mathrm{up}(k)=l} \mathrm{height}(k)$ otherwise.

1- Base case (height =0)

For the base case we show that *Lemma I* holds for leaves of the system.

a) Suppose bus l is a leaf of the network ($l \in \underline{\mathcal{L}}$) with $s_l = p_l + jq_l$ as its total load (see Fig. 2-1) ($(s, S, v, f, \hat{S}, \hat{v}, \bar{f}, \bar{S})$ satisfies (2.11.a)-(2.11.d) and (2.15.b)-(2.15.h)). From (2.11.c) we have:

$$f_l = \frac{(p_l)^2 + \left(q_l - \frac{v_l b_l}{2}\right)^2}{v_l}, \forall l \in \underline{\mathcal{L}} \qquad (2.49).$$

Noting that $0 < v_l \le \hat{v}_l$ from (2.15.g) we have:

$$0 \le f_l \le \frac{\left(\max\left\{\left|(p_l)\right|, |p_l|\right\}\right)^2}{v_l} + \frac{\left(\max\left\{\left|q_l - \frac{v_l b_l}{2}\right|, \left|q_l - \frac{\hat{v}_l b_l}{2}\right|\right\}\right)^2}{v_l} \le \bar{f}_l, \forall l \in \underline{\mathcal{L}} \qquad (2.50)$$

combining with (2.29)-(2.32) it comes that:

$$\hat{S}_l^t \le S_l^t \le \bar{S}_l^t, \forall l \in \underline{\mathcal{L}} \qquad (2.51)$$

this shows item 1 of *Lemma I*.

b) One can choose $\bar{f}_l^{''}$ as followings so that $\bar{f}_l^{''} \le \bar{f}_l'$ and $\bar{f}_l^{''}$ satisfies (2.15.g) and (2.15.h) (note that $v' \le v$)

$$\bar{f}_l^{'} \ge \bar{f}_l^{''} = \max\left\{\begin{array}{l}\left(\frac{\left(\max\left\{\left|(p_l)\right|, |p_l|\right\}\right)^2}{v_l^{'}} + \frac{\left(\max\left\{\left|q_l - \frac{v_l^{'} b_l}{2}\right|, \left|q_l - \frac{\hat{v}_l b_l}{2}\right|\right\}\right)^2}{v_l^{'}}\right), \\ \left(\frac{\left(\max\left\{\left|(p_l + r_l \bar{f}_l^{'})\right|, |p_l|\right\}\right)^2}{v_{\mathrm{up}(l)}^{'}} + \frac{\left(\max\left\{\left|q_l + x_l \bar{f}_l^{'} - \frac{v_l^{'} b_l}{2}\right|, \left|q_l - \frac{\hat{v}_l b_l}{2}\right|\right\}\right)^2}{v_{\mathrm{up}(l)}^{'}}\right)\end{array}\right\} \qquad (2.52)$$

Thus we have:

$$\bar{f}_l' \geq \bar{f}_l'' \geq \max\left\{\begin{array}{l}\left(\frac{\left(\max\left\{\left|\left(p_l\right)\right|,\left|p_l\right|\right\}\right)^2}{v_l}+\frac{\left(\max\left\{\left|q_l-\frac{v_l b_l}{2}\right|,\left|q_l-\frac{\hat{v}_l b_l}{2}\right|\right\}\right)^2}{v_l}\right),\\ \left(\frac{\left(\max\left\{\left|\left(p_l+r_l\bar{f}_l''\right)\right|,\left|p_l\right|\right\}\right)^2}{v_{\mathrm{up}(l)}}+\frac{\left(\max\left\{\left|q_l+x_l\bar{f}_l''-\frac{v_l b_l}{2}\right|,\left|q_l-\frac{\hat{v}_l b_l}{2}\right|\right\}\right)^2}{v_{\mathrm{up}(l)}}\right)\end{array}\right\} \tag{2.52.b}$$

thus $\bar{f}_l'' \leq \bar{f}_l'$ and it satisfies (2.15.g) and (2.15.h). Consequently from (2.31) and (2.32) we have $(\bar{S}_l^t)'' \leq (\bar{S}_l^t)'$.

This shows item 2 of *Lemma I*.

2- Induction step

Assume the statements in *Lemma I* are true for all buses of height $\leq n$, for some $n \geq 0$. We now want to show that is also holds for all buses of height $\leq n+1$. Let k be a bus with height$(k) = n+1$.

a) For all downstream buses l of k, we have height$(l) \leq n$ thus $S_l^t \leq \bar{S}_l^t$ and from equations (2.11.d), (2.15.e) and (2.15.f)

$$\hat{S}_k^b \leq S_k^b \leq \bar{S}_k^b \tag{2.53}$$

thus (recall that $0 < v \leq \hat{v}$):

$$f_k = \frac{\left|P_k^b\right|^2+\left|Q_k^b-\frac{v_k b_k}{2}\right|^2}{v_k} \leq \frac{\left|\max\left\{\left|\hat{P}_k^b\right|,\left|\bar{P}_k^b\right|\right\}\right|^2}{v_k}+\frac{\left(\max\left\{\left|\hat{Q}_k^b-\frac{\hat{v}_k b_k}{2}\right|,\left|\bar{Q}_k^b-\frac{v_k b_k}{2}\right|\right\}\right)^2}{v_k} \leq \bar{f}_k \tag{2.54}$$

combining with (2.29)-(2.32) it comes that:

$$\hat{S}_k^t \leq S_k^t \leq \bar{S}_k^t \tag{2.55}$$

this show item 1 of *Lemma I*.

b) Based on the induction assumption and equation (2.15.e) we have $\left(\bar{S}_l^b\right)'' \leq \left(\bar{S}_l^b\right)'$ for all buses l that are downstream of l and also $v' \leq v$. Thus one can choose $\bar{f}_k''$ as follows so that $\bar{f}_k'' \leq \bar{f}_k'$ and $\bar{f}_k''$ satisfies (2.15.g), and (2.15.h):

$$\bar{f}_k^{'} \geq \bar{f}_k^{''} \geq \max\left\{\begin{array}{l}\left(\begin{array}{l}\dfrac{\left|\max\left\{\left|\hat{P}_k^b\right|,\left|\left(\bar{P}_k^b\right)^{'}\right|\right\}\right|^2}{v_k^{'}}+\\ \dfrac{\left(\max\left\{\left|\hat{Q}_k^b-\dfrac{\hat{v}_k b_k}{2}\right|,\left|\left(\bar{Q}_k^b\right)^{'}-\dfrac{v_k^{'} b_k}{2}\right|\right\}\right)^2}{v_k^{'}}\end{array}\right),\\ \left(\begin{array}{l}\dfrac{\left|\max\left\{\left|\hat{P}_k^b\right|,\left|\left(\bar{P}_k^b\right)^{'}+r_k\bar{f}_k^{'}\right|\right\}\right|^2}{v_{\mathrm{up}(k)}^{'}}+\\ \dfrac{\left(\max\left\{\left|\hat{Q}_k^b-\dfrac{\hat{v}_k b_k}{2}\right|,\left|\left(\bar{Q}_k^b\right)^{'}+x_k\bar{f}_k^{'}-\dfrac{v_k^{'} b_k}{2}\right|\right\}\right)^2}{v_{\mathrm{up}(k)}^{'}}\end{array}\right)\end{array}\right\} \geq$$

$$\max\left\{\begin{array}{l}\left(\begin{array}{l}\dfrac{\left|\max\left\{\left|\hat{P}_k^b\right|,\left|\left(\bar{P}_k^b\right)^{''}\right|\right\}\right|^2}{v_k}+\\ \dfrac{\left(\max\left\{\left|\hat{Q}_k^b-\dfrac{\hat{v}_k b_k}{2}\right|,\left|\left(\bar{Q}_k^b\right)^{''}-\dfrac{v_k b_k}{2}\right|\right\}\right)^2}{v_k}\end{array}\right),\\ \left(\begin{array}{l}\dfrac{\left|\max\left\{\left|\hat{P}_k^b\right|,\left|\left(\bar{P}_k^b\right)^{''}+r_k\bar{f}_k^{''}\right|\right\}\right|^2}{v_{\mathrm{up}(k)}}+\\ \dfrac{\left(\max\left\{\left|\hat{Q}_k^b-\dfrac{\hat{v}_k b_k}{2}\right|,\left|\left(\bar{Q}_k^b\right)^{''}+x_k\bar{f}_k^{''}-\dfrac{v_k b_k}{2}\right|\right\}\right)^2}{v_{\mathrm{up}(k)}}\end{array}\right)\end{array}\right\} \tag{2.56}$$

thus $\bar{f}_k^{''} \leq \bar{f}_k^{\prime}$ and $\bar{f}_k^{''}$ satisfies (2.15.g) and (2.15.h). Consequently from (2.31) and (2.32) we have $(\bar{S}_k^t)^{''} \leq (\bar{S}_k^t)^{\prime}$

This shows item 2 of *Lemma I.*

Both basis and inductive steps are proved which completes the proof of *Lemma I.*

■

A) Inverse of matrix C

We prove that when C1 holds, $\mathbf{I}-\mathbf{G}^T-\mathbf{M}$ is invertible and has non-negative entries.

We can rewrite $\mathbf{I}-\mathbf{G}^T-\mathbf{M}$ as follows:

$$\mathbf{I}-\mathbf{G}^T-\mathbf{M}=\left(\mathbf{I}-\mathbf{G}^T\right)\left[\mathbf{I}-\left(\mathbf{I}-\mathbf{G}^T\right)^{-1}\mathbf{M}\right]=\left(\mathbf{I}-\mathbf{G}^T\right)\left[\mathbf{I}-\mathbf{H}^{\mathrm{T}}\mathbf{M}\right] \tag{2.57}.$$

We now use the identity:

$$\left(\mathbf{I}-\mathbf{H}^{\mathrm{T}}\mathbf{M}\right)\left[\mathbf{I}+\mathbf{H}^{\mathrm{T}}\mathbf{M}+\left(\mathbf{H}^{\mathrm{T}}\mathbf{M}\right)^{2}+\ldots\right]=\mathbf{I} \tag{2.58}$$

which holds whenever$\|\mathbf{H}^{T}\mathbf{M}\|<1$ (recall that $\|.\|$ means induced l_1-norm).

Now:

$$\begin{aligned}\left(\mathbf{H}^{\mathrm{T}}\mathbf{M}\right)_{k,l}&=\left(\mathbf{H}^{\mathrm{T}}\mathrm{diag}\left(x\right)\mathbf{H}\mathrm{diag}\left(B\right)\right)_{k,l}=\\&\sum_{m}\mathbf{H}_{m,k}x_{k}\mathbf{H}_{k,l}B_{l}\leq\max_{l\in\mathcal{L}}x_{l}\max_{l\in\mathcal{L}}B_{l}\sum_{m}\mathbf{H}_{m,k}\mathbf{H}_{k,l}=\\&\max_{l\in\mathcal{L}}x_{l}\max_{l\in\mathcal{L}}B_{l}\left(\mathbf{H}^{T}\mathbf{H}\right)_{k,l}\end{aligned} \tag{2.59}$$

thus:

$$\mathbf{H}^{\mathrm{T}}\mathbf{M}\leq\max_{l\in\mathcal{L}}x_{l}\max_{l\in\mathcal{L}}B_{l}\,\mathbf{H}^{\mathrm{T}}\mathbf{H} \tag{2.60}$$

note that $\mathbf{H}_{k,l}\in\{0,1\}$ thus:

$$\mathbf{H}^{\mathrm{T}}\mathbf{H}\leq L^{2} \tag{2.61}.$$

It follows that, when *C1* holds, then $\left\|\mathbf{H}^{\mathrm{T}}\mathbf{M}\right\|<1$, which by equation (2.58) proves that $\left(\mathbf{I}-\mathbf{H}^{\mathrm{T}}\mathbf{M}\right)$ is invertible. By transposition of equation (2.1), $\left(\mathbf{I}-\mathbf{G}^{\mathrm{T}}\right)$ is also invertible; together with equation (2.57), this shows that $\mathbf{I}-\mathbf{G}^{T}-\mathbf{M}$ is invertible when *C1* holds. Furthermore, equations (2.1), (2.57), (2.58) imply that:

$$\left(\mathbf{I}-\mathbf{G}^{T}-\mathbf{M}\right)^{-1}=\left(\mathbf{I}+\mathbf{H}^{\mathrm{T}}\mathbf{M}+\left(\mathbf{H}^{\mathrm{T}}\mathbf{M}\right)^{2}+\ldots\right)\mathbf{H}^{T}\geq 0 \tag{2.62}$$

■

B) Proof of *Theorem I*

Item 1: Let $\omega=\left(s,P+jQ,v,f,\hat{P}+j\hat{Q},\hat{v},\bar{P}+j\bar{Q},\bar{f}\right)$ be a feasible solution of AR-OPF. Let $\mathcal{L}^{\neq}$ be the set of lines where (2.14) holds with strict inequality. If $\mathcal{L}^{\neq}$ is empty, ω is a load flow solution and *Theorem I* is trivially true. Assume now that $\mathcal{L}^{\neq}$ is not empty and only one line (say line m) has strict inequality in (2.14). (Later we show the general case where several lines have strict inequality). We divide the lines into two groups i) those that $\mathbf{H}_{l,m}=1$ and we call them upstream of bus m, ($\mathcal{L}^{m}$) and ii) those that $\mathbf{H}_{l,m}=0$ and we call them non-upstream of bus m ($\mathcal{L}_{m}$). We now create a load flow solution for s. Using *Lemma II* (defined later in this Appendix) first we will show that the created load flow solution is feasible (satisfies the security limits) and then we will show that it has a lower objective function.

Consider the sequence $(P^{(n)},Q^{c(n)},v^{(n)},f^{(n)})$ defined for $n\geq 0$ by means of *Algorithm I*.

We now show that this sequence converges. For $n \geq 1$ let $\Delta f^{(n)} \triangleq f^{(n)} - f^{(n-1)}$. Using *Lemma II* we have:

$$\left\|\Delta f^{(n)}\right\| \leq \left\|\mathbf{E}\right\|^{(n-1)} \left\|\Delta f^{(1)}\right\| \tag{2.63}$$

when *C2* holds we have:

$$\left\|\mathbf{E}\right\| < 1 \tag{2.64}$$

which ensures the convergence of $\sum_n \left\|\Delta f^{(n)}\right\|$, therefore of $\sum_n \Delta f^{(n)}$ and finally of the sequence $f^{(n)}$. It follows that $(P^{(n)}, Q^{c(n)}, v^{(n)}, f^{(n)})$ converges to some limit, say (P^*, Q^{c*}, v^*, f^*). Since $f^{(n)} \geq 0$ by construction, it follows that $f^* \geq 0$ as well and thus, by *Lemma II* since $\mathbf{D}$ are non-negative thus:

$$v^{\min} \leq v \leq v^* \leq \hat{v} \leq v^{\max} \tag{2.65}.$$

Furthermore, by step 1 we have:

$$f_l^* = \frac{\left(P_l^{t*}\right)^2 + \left(Q_l^{c*}\right)^2}{v^*_{\mathrm{up}(l)}}, \forall\ l \in \mathcal{L} \tag{2.66}.$$

Let $Q^* = Q^{c*} - \frac{1}{2}\mathrm{diag}(b)\mathbf{G}^T v^*$ and $\omega = (s, P^*, jQ^*, v^*, f^*,\ \hat{P} + j\hat{Q}, \hat{v}, \bar{f}^*, \bar{S}^*)$. It follows that ω^* satisfies (2.14) with equality, i.e. it is a load flow solution. From (2.65) we can observe that the voltage security constraints are satisfied. Further item 2) of *Lemma I* guarantees that there exist $\bar{P}^*$ and $\bar{Q}^*$ such that $\bar{P}^* \leq \bar{P} \leq P^{\max}$ and $\bar{Q}^* \leq \bar{Q} \leq Q^{\max}$ thus constraints (2.17.f) and (2.17.g) are satisfied. Further from item 1) of *Lemma I* we have that $P^* \leq \bar{P}^* \leq P^{\max}$ and $Q^* \leq \bar{Q}^* \leq Q^{\max}$ which show that constraints (2.17.h) and (2.17.i) are also satisfied. Thus ω^* is a feasible solution of AR-OPF and of A-OPF.

Algorithm 1: (apexes represent iteration numbers)
Input: $\omega = (s, P, Q, v, f, \hat{P}, \hat{Q}, \hat{v})$
Initialization.

$$f^{(0)} \leftarrow f$$
$$v^{(0)} \leftarrow v$$
$$P^{(0)} \leftarrow P$$
$$Q'^{(0)} \leftarrow Q^c$$
$$n = 1$$

for $n \geq 1$

Step 1: $f_l^{(n)} \leftarrow \frac{\left(P_l^{t(n-1)}\right)^2 + \left(Q_l^{c(n-1)}\right)^2}{v^{(n-1)}_{\mathrm{up}(l)}}$

Step 2: $P^{(n)} \leftarrow \hat{P} + \mathbf{H}\mathrm{diag}(r) f^{(n)}$ (eq. (2.42))

Step 3: $Q^{c(n)} \leftarrow \hat{Q}^c + \mathbf{F} f^{(n)}$ (eq. (2.47))

Step 4: $v^{(n)} \leftarrow \hat{v} - \mathbf{D} f^{(n)}$ (eq. (2.38))

We now show the general case. First, we name the right hand side of (2.11.c) $f^{=}$ and the right hand side of (2.14) $f^{\neq}$ ($f_l^{=} = f_l^{\neq} - \Delta f_l$). Further, having strict inequality for line l is the same case as having equality in (2.14) with nodal consumption of corresponding bus l equal to $s_l = p_l + r_l \Delta f_l + j(q_l + x_l \Delta f_l)$.

Now suppose that there are K lines who have strict inequality in (2.14). Let label these lines $\{l_1, \dots, l_K\} \in \mathcal{L}^{\neq}$ where l_1 has the lowest height in graph (tree) of the network and l_K has the highest height. Now for all the lines belonging to $\mathcal{L}^{\neq}$ except l_1 we replace the $f_{l_k}^{\neq}$ with the corresponding $f_{l_k}^{=}$ and add an artificial load equal to $r_{l_k}\Delta f_{l_k} + jx_{l_k}\Delta f_{l_k}$ to the corresponding nodal consumptions (name the new nodal consumption s^1). Now we have only one line with strict inequality in (2.14). We perform *Algorithm I* and obtain a new load flow solution called $\omega^1 = (s^1, S^1, v^1, f^1, \hat{P}^1 + j\hat{Q}^1, \hat{v}, \bar{f}^1, \bar{S}^1)$. We have already shown that i) $v^1 \geq v$ and ii) $S_l^1 \leq S_l, \forall\, l \in \mathcal{L}^{l_1}$. We also have $s_l^1 = s_l, \forall\ l \in \mathcal{L}_{l_2}$ where l_2 belongs to $\mathcal{L}^{\neq}$ and has the lowest height after l_1. Further from item 2 of *Lemma I* and knowing that $v^1 \geq v$ we have $S_l^1 \leq \bar{S}_l\ \forall\, l \in \mathcal{L}_{l_2}$ ($\mathbf{H}_{ll_2} = 0$)). Finally we have $\hat{S}^1 \geq \hat{S}$.

Now for the next line in $\mathcal{L}^{\neq}$ with lowest height (l_2) we remove its artificial load and make its relaxation inexact (s^2 is the new nodal consumption). Now again perform *Algorithm I*. We obtain a new load flow solution called $\omega^2 = (s^2, S^2, v^2, f^2, \hat{P}^2 + j\hat{Q}^2, \hat{v}, \bar{f}^2, \bar{S}^2)$. Similarly, we have i) $v^2 \geq v^1 \geq v$, ii) $S_l^2 \leq S_l^1 \leq S_l, \forall\, l \in \mathcal{L}^{l_2}$, iii) $s_l^2 = s_l, \forall\ l \in \mathcal{L}_{l_3}$, iv) $S_l^2 \leq \bar{S}_l\ \forall\, l \in \mathcal{L}_{l_3}$), and v) $\hat{S}^2 \geq \hat{S}$.

We can performs this procedure until all the artificial loads are removed and obtain a load flow solution called $\omega^{\text{fin}} = (s, S^{\text{fin}}, v^{\text{fin}}, f^{\text{fin}}, \hat{P} + j\hat{Q}, \hat{v}, \bar{f}^{\text{fin}}, \bar{S}^{\text{fin}})$. This new load flow solution satisfy (2.11.c) and we have $v^{\min} \leq v \leq v^{\text{fin}} \leq \hat{v} \leq v^{\max}$, $Q^{\text{fin}} \leq \bar{Q}^{\text{fin}} \leq \bar{Q} \leq Q^{\max}$, $P^{\text{fin}} \leq \bar{P}^{\text{fin}} \leq \bar{P} \leq P^{\max}$ thus it is a feasible solution of AR-OPF and of A-OPF.

This prove the first item of *Theorem I.*

■

Item 2: Assume that ω is an optimal solution of AR-OPF but not a feasible solution of A-OPF, i.e. $\mathcal{L}^{\neq}$ is non-empty. Assume that only the line m has strict inequality in (2.14) . First note that at the first line ($l = 1$) we always have $\mathbf{H}_{lm} = 1$. Further, for the first line we have:

$$P_1^{t(1)} - P_1^t = \sum_{l \in \mathcal{L}^{\neq}} \mathbf{H}_{1,l} \left(f_l^{(1)} - f_l \right) = \sum_{l \in \mathcal{L}^{\neq}} \left(f_l^{(1)} - f_l \right) < 0 \tag{2.67}$$

thus $P_1^{t(1)} < P_1^t$. Define $\bar{\bar{P}}_1^t = P_1^t - \frac{\eta}{1-\eta}\left(P_1^t - P_1^{t(1)}\right)$ where η is as in *Lemma II*. Since $0 < \eta < 0.5$ it follows that $\bar{\bar{P}}_1^t < P_1^t$. Furthermore, by *Lemma II*,

$$\left|P_1^{t(n)} - P_1^{t(1)}\right| \leq \left|\Delta P_1^{t(n)}\right| + \dots + \left|\Delta P_1^{t(2)}\right| \leq \left(\eta^{n-1} + \dots + \eta\right)\left|\Delta P_1^{t(1)}\right| \leq \frac{\eta}{1-\eta}\left|\Delta P_1^{t(1)}\right| = \frac{\eta}{1-\eta}\left(P_1^t - P_l^{t(1)}\right) \tag{2.68}$$

thus for every $n \geq 1$:

$$P_1^{t(n)} \leq P_1^{t(1)} + \frac{\eta}{1-\eta}\left(P_1^t - P_1^{t(1)}\right) = \overline{\overline{P}}_1^t \tag{2.69}$$

and therefore $(P_1^t)^* \leq \bar{\bar{P}}_1^t < P_1^t$. Now P_1 [resp. $(P_1^t)^*$] is the net active power import from the external grid for the solution ω, [resp. ω^*]. Since the power injections s are identical for ω and ω^*, it follows that the objective function of ω^* is strictly less than that of ω, which contradicts the optimality of ω. Using the similar approach used for item one, one can show that ω^* has lower objective function than ω when $\mathcal{L}^{\neq}$ has more than one member. This proves the second item of *Theorem I.*

■

Lemma II: Under conditions *C1-C7*, let $\eta = \max(\eta_1, \eta_2, \eta_3, \eta_4, \eta_5)$. For $n \geq 1$:

$$\left|\Delta f^{(n)}\right| \leq \mathbf{E}^{n-1}\left|\Delta f^{(1)}\right| \tag{2.70.a}$$

$$\left|\Delta v^{(n)}\right| \leq \eta^{n-1}\left|\Delta v^{(1)}\right| \tag{2.70.b}$$

$$v \leq v^{(n)} \tag{2.70.c}$$

$$\left|\Delta P_l^{t(n)}\right| \leq \eta^{n-1}\left|\Delta P_l^{t(1)}\right|, \forall\, l \in \mathcal{L}^m \tag{2.70.d}$$

$$P_l^{t(n)} \leq P_1^t, \forall\, l \in \mathcal{L}^m \tag{2.70.e}$$

$$\left|\Delta Q_l^{c(n)}\right| \leq \eta^{n-1}\left|\Delta Q_l^{c(1)}\right|, \forall\, l \in \mathcal{L}^m \tag{2.70.f}$$

$$Q_l^{c(n)} \leq Q_l^c, \forall\, l \in \mathcal{L}^m \tag{2.70.g}$$

$$f_l^{(n)} \leq \overline{f}, \ \forall\, l \in \mathcal{L}_m \tag{2.70.h}$$

$$P_l^{t(n)} \leq \bar{P}_l^t, \forall\, l \in \mathcal{L}_m \tag{2.70.i}$$

$$Q_l^{c(n)} \leq \bar{Q}_l^t, \forall\, l \in \mathcal{L}_m \tag{2.70.j}$$

where $\Delta f^{(n)} = f^{(n)} - f^{(n-1)}$ for $n \geq 1$ and similarly with P, Q^c and v.

Proof of Lemma II: The proof is by mathematical induction on $n \geq 1$.

1- Base case ($n = 1$):

(2.70.a),(2.70.b),(2.70.d), and (2.70.f) are trivially true.

We have $f_l^{(1)} \leq f_l^{(0)}$ for every l because $f^{(1)}$ is the right hand side of (2.14) in the original formulation of the constraints and ω is feasible. By equations (2.42) and since $\mathbf{H}\mathrm{diag}(r) \geq 0$, it follows that $P^{(1)} \leq P$. This shows (2.70.e). Similarly, since **F** and **D** are non-negative matrices, from (2.47) and (2.38) it follows that $Q^{(1)} \leq Q$, $Q'^{(1)} \leq Q'$ and $v^{(1)} \geq v$. This shows equations (2.70.g), and (2.70.c).

The relaxation shown in (2.14) is tight for the downstream lines of bus m ($l \in \mathcal{L}_m$) Thus, from *Lemma I* we have that $\bar{f}_l \geq f_l^1 = f_l^0, \forall\, l \in \mathcal{L}_m$, $P_1^{t(1)} \leq \overline{P}_l^t,\ \forall\, l \in \mathcal{L}_m$ and $Q_l^{c(1)} \leq Q_l^t \leq \overline{Q}_l^t,\ \forall\, l \in \mathcal{L}_m$. . This shows equations (2.70.h), (2.70.i) and (2.70.j).

2- Induction step

Assume the statements in *Lemma II* are true for some $n \geq 1$. We now want to show that is also holds for $n+1$.

a) Consider first some fixed $l \in \mathcal{L}$. Define Φ_l by $f_l \triangleq \phi_l(P_l, Q_l^c, v_k)$, from equation (2.11.c) we have:

$$\mathrm{grad}\left(\phi_l\right) = \begin{pmatrix} \dfrac{2P_l^t}{v_{\mathrm{up}(l)}} \\ \dfrac{2\left(Q_l^c\right)}{v_{\mathrm{up}(l)}} \\ -\dfrac{\left(\left(P_l^t\right)^2 + \left(Q_l^c\right)^2\right)}{\left(v_{\mathrm{up}(l)}\right)^2} \end{pmatrix} \tag{2.71}$$

Define $M(t)$ for $t \in [0,1]$ as:

$$M\left(t\right) = t\begin{pmatrix} P_l^{t(n)} \\ Q_l^{c(n)} \\ v_{\mathrm{up}(l)}^{(n)} \end{pmatrix} + \left(1-t\right)\begin{pmatrix} P_l^{t(n-1)} \\ Q_l^{c(n-1)} \\ v_{\mathrm{up}(l)}^{(n-1)} \end{pmatrix} \tag{2.72}$$

then by equation (2.11.c) and by the fundamental law of calculus we have:

$$f_l^{(n+1)} - f_l^{(n)} = \Phi_l\left(M\left(1\right)\right) - \Phi_l\left(M\left(0\right)\right) = \begin{pmatrix} \Delta P_l^{t(n)} \\ \Delta Q_l^{c(n)} \\ \Delta v_{\mathrm{up}(l)}^{(n)} \end{pmatrix} . \int_0^1 \mathrm{grad}\Phi_l\left(M\left(t\right)\right)dt \tag{2.73}$$

We first bound each component of the gradient. For $0 \leq t \leq 1$, by the induction property (2.70.e), (2.70.i), (2.70.g), (2.70.j) and (2.70.c) at $n-1$ and n (note that ω is a feasible

solution thus $P_l^t \le P_l^{\max}, \overline{P}_l^t \le P_l^{\max}, Q_l^c = Q_l^t - \frac{b_l}{2} v_{\mathrm{up}(l)} \le Q_l^t \le Q_l^{\max}$, and $\overline{Q}_l^t - \frac{b_l}{2} v_{\mathrm{up}(l)} \le \overline{Q}_l^t \le Q_l^{\max}$):

$$(1-t)P_l^{t(n)} + tP_l^{t(n-1)} \le P_l^{\max} \tag{2.74}$$

$$(1-t)Q_l^{c(n)} + tQ_l^{c(n-1)} \le Q_l^{\max} \tag{2.75}$$

$$v_{min} \le (1-t)v_l^{(n)} + tv_l^{(n-1)} \tag{2.76}.$$

Furthermore, $f^n \ge 0$ for any $n \ge 0$ and the matrices in equations and are non-negative, therefore, for all $n \ge 0$:

$$\hat{P}_l^t \le P_l^{t(n)} \tag{2.77}$$

$$\hat{Q}_l^c \le Q_l^{c(n)} \tag{2.78}$$

and thus:

$$(1-t)P_l^{t(n)} + tP_l^{t(n-1)} \ge \hat{P}_l^t \tag{2.79}$$

$$(1-t)Q_l^{c(n)} + tQ_l^{c(n-1)} \ge \hat{Q}_l^c \tag{2.80}.$$

By equation (2.71) it follows that (entry-wise)($\pi_l, \vartheta_l, \varrho_l$ are defined in (2.4)-(2.6)):

$$\left|\mathrm{grad}\left(\Phi_l(M(t))\right)\right| \le \begin{pmatrix} 2\pi_l \\ 2\varrho_l \\ \vartheta_l \end{pmatrix} \tag{2.81}$$

thus, we have:

$$\left|\Delta f_l^{(n+1)}\right| \le 2\pi_l \left|\Delta P_l^{t(n)}\right| + 2\varrho_l \left|\Delta Q_l^{c(n)}\right| + \vartheta_l \left|\Delta v_{\mathrm{up}(l)}^{(n)}\right|. \tag{2.82}.$$

Now this is true for some l, so in matrix form we have:

$$\left|\Delta f^{(n+1)}\right| \le 2\mathrm{diag}(\pi)\left|\Delta P^{(n)}\right| + 2\mathrm{diag}(\varrho)\left|\Delta Q^{c(n)}\right| + \mathrm{diag}(\vartheta)\left|\Delta v^{(n)}\right| \tag{2.83}.$$

Further by the construction of $P^{(n)}$, $Q^{,(n)}$, and $v^{(n)}$ we have:

$$\left|\Delta P^{(n)}\right| \le \mathbf{H}\mathrm{diag}(\mathrm{r})\left|\Delta f^{(n)}\right| \tag{2.84}$$

$$\left|\Delta Q^{c(n)}\right| \le (\mathbf{F})\left|\Delta f^{n}\right| \tag{2.85}$$

$$\left|\Delta v^{(n)}\right| \le \mathbf{D}\left|\Delta f^{(n)}\right| \tag{2.86}$$

combined with (2.8) and (2.83) this gives

$$\left|\Delta f^{(n+1)}\right| \le \mathbf{E}\left|\Delta f^{(n)}\right| \tag{2.87}$$

Applying the induction property (2.70.a) for n; it comes:

$$\left|\Delta f^{(n+1)}\right| \le \mathbf{E}^{n}\left|\Delta f^{(1)}\right| \tag{2.88}$$

which shows that he induction property (2.70.a) also holds for $n+1$.

b) From (2.38) we have:

$$\Delta v^{(1)} = \left(-\mathbf{D}\right)\Delta f^{(1)} \tag{2.89}$$

and we have already noted that $\Delta f^{1} \le 0$ thus:

$$\left|\Delta v^{(1)}\right| = \Delta v^{(1)} = \left(-\mathbf{D}\right)\left|\Delta f^{(1)}\right|. \tag{2.90}.$$

Using (2.38) we have:

$$\left|\Delta v^{(n+1)}\right| \le \mathbf{D}\left|\Delta f^{(n+1)}\right| \tag{2.91}$$

apply (2.88)and *C7*:

$$\left|\Delta v^{(n+1)}\right| \le \eta^{n}\mathbf{D}\left|\Delta f^{(1)}\right| \tag{2.92}$$

apply (2.90) it comes:

$$\left|\Delta v^{(n+1)}\right| \le \eta^{n}\left|\Delta v^{(1)}\right| \tag{2.93}.$$

It follows that (2.70.b) also holds for $n+1$.

■

Further we have:

$$\left|v^{(n+1)} - v^{(1)}\right| \le \left|\Delta v^{(n+1)}\right| + \ldots + \left|\Delta v^{(2)}\right| \le \left(\eta^{n-1} + \ldots + \eta\right)\left|\Delta v^{(1)}\right| \le \frac{\eta}{1-\eta}\left|\Delta v^{(1)}\right| \le \left|v^{(1)} - v\right| \tag{2.94}$$

(noting that $v^{(1)} \ge v$) if $v^{(n+1)} \ge v^{(1)}$ thus $v^{(n+1)} \ge v^{(1)} \ge v$ otherwise:

$$v^{(1)} - v^{(n+1)} \le \left| v^{(n+1)} - v^{(1)} \right| \le \left| v^{(1)} - v \right| = v^{(1)} - v \tag{2.95}$$

thus $v^{(n+1)} \ge v$. It follows that (2.70.c) also holds for $n + 1$.

■

c) We have:

$$\Delta P^{(1)} = \mathbf{H}\mathrm{diag}(r)\Delta f^{(1)} \tag{2.96}$$

and we have already noted that $\Delta f^{(1)} \le 0$ thus:

$$\left|\Delta P^{(1)}\right| = -\Delta P^{(1)} = -\mathbf{H}\mathrm{diag}(r)\Delta f^{(1)} = \mathbf{H}\mathrm{diag}(r)\left|\Delta f^{(1)}\right| \tag{2.97}.$$

Since only entry m of $\Delta f^{(1)}$ is non-zero $(\Delta f_m^{(1)} < 0)$ thus:

$$\left|\Delta P_l^{t(1)}\right| = -\Delta P_l^{t(1)} = -\left(\mathbf{H}\mathrm{diag}(r)\right)_{lm} \Delta f_m^{t(1)} = \left(\mathbf{H}\mathrm{diag}(r)\right)_{lm}\left|\Delta f_m^{t(1)}\right| \tag{2.98}.$$

Using (2.29) we have:

$$\left|\Delta P^{(n+1)}\right| \le \mathbf{H}\mathrm{diag}(r)\left|\Delta f^{(n+1)}\right| \tag{2.99}$$

thus:

$$\left|\Delta P_l^{t(n+1)}\right| \le \left(\mathbf{H}\mathrm{diag}(r)\right)_l \left|\Delta f^{(n+1)}\right| \le \left(\mathbf{H}\mathrm{diag}(r)\mathbf{E}^n \left|\Delta f^{(1)}\right|\right)_l = \left(\mathbf{H}\mathrm{diag}(r)\mathbf{E}^n\right)_{lm}\left|\Delta f_m^{(1)}\right| \tag{2.100}.$$

From *C4* we have (recall that $\eta = \{\eta_1, \eta_2, \eta_3, \eta_4, \eta_5\}$:

$$\mathbf{H}\mathrm{diag}(r)\mathbf{E}^{\mathbf{n}+1} \le \eta^{n-1}\mathbf{H}\mathrm{diag}(r)\mathbf{E}, \forall\ \mathrm{n} \ge 1 \tag{2.101}$$

thus:

$$\left(\mathbf{H}\mathrm{diag}(r)\mathbf{E}^{\mathbf{n}}\right)_{lm} \le (\eta)^{\mathbf{n}-1}\left(\mathbf{H}\mathrm{diag}(r)\mathbf{E}\right)_{lm}, \forall\ \mathrm{n} \ge 1 \tag{2.102}.$$

Further from *C3* for the lines that are upstream of line m $(\mathbf{H}_{lm} = 1 \ne 0), l \in \mathcal{L}^m$ we have:

$$\left(\mathbf{H}\mathrm{diag}(r)\mathbf{E}\right)_{lm} \le \eta\left(\mathbf{H}\mathrm{diag}(r)\right)_{lm}, \forall\, l \in \mathcal{L}^m \tag{2.103}$$

combining with (2.102):

$$\left(\mathbf{H}\mathrm{diag}(r)\mathbf{E}^{\mathbf{n}}\right)_{lm} \le (\eta)^{\mathrm{n}}\left(\mathbf{H}\mathrm{diag}(r)\right)_{lm} \forall\, l \in \mathcal{L}^m \tag{2.104}$$

combining with (2.100):

$$\left|\Delta P_l^{t(n+1)}\right| \le \mathbf{H}\text{diag}(r)\left|\Delta f^{n+1}\right| \le \left(\mathbf{H}\text{diag}(r)\mathbf{E}^n\right)_{lm} \Delta f_m^{(1)} \le \eta^n \left(\mathbf{H}\text{diag}(r)\right)_{lm} \left|\Delta f_m^{(1)}\right|, \ \forall l \in \mathcal{L}^m \tag{2.105}$$

apply (2.98)

$$\left|\Delta P_l^{t(n+1)}\right| \le \eta^n \left|\Delta P_l^{t(1)}\right|, \ \forall l \in \mathcal{L}^m \tag{2.106}$$

it follows that (2.70.d) also holds for $n+1$.

■

Further for $l \in \mathcal{L}^m$ we have (noting that $\eta < 0.5$)

$$\left|P_l^{t(n+1)} - P_l^{t(1)}\right| \le \left|\Delta P_l^{t(n+1)}\right| + \ldots + \left|\Delta P_l^{t(2)}\right| \le \left(\eta^{n-1} + \ldots + \eta\right)\left|\Delta P_1^{t(1)}\right| \le \frac{\eta}{1-\eta}\left|\Delta P_l^{t(1)}\right| \le \left|P_l^{t(1)} - P_l^{t}\right|, \forall l \in \mathcal{L}^m \tag{2.107}$$

thus (noting that $P^{(1)} \le P$)

$$P_l^{t(n+1)} - P_l^{t(1)} \le \left|P_l^{t(n+1)} - P_l^{t(1)}\right| \le \left|P_l^{t(1)} - P_l^{t}\right| = P_l^{t} - P_l^{t(1)}, \forall l \in \mathcal{L}^m \tag{2.108}$$

It comes that $P_l^{t(n+1)} \le P_l^t, \forall\, l \in \mathcal{L}^m$ which shows that he induction property (2.70.e) also holds for $n+1$.

■

d) Note that *C5*, *C6* and *C7* imply that

$$\begin{aligned} &\left(\mathbf{FE}\right) \circ \mathbf{H} \le \eta\left(\mathbf{F}\right) \\ &\left(\mathbf{FE}^2\right) \le \eta\left(\mathbf{FE}\right) \end{aligned} \tag{2.109}$$

applying the similar approach used for P_l^t, one can show that:

$$\begin{aligned} &\left|\Delta Q_l^{c(n+1)}\right| \le \eta^n \left|\Delta Q_l^{c(1)}\right|, \forall l \in \mathcal{L}^m \\ &Q_l^{c(n+1)} \le Q_l^c, \forall l \in \mathcal{L}^m \end{aligned} \tag{2.110}$$

which shows that he induction properties (2.70.f) and (2.70.g) also hold for $n+1$.

■

e) We have:

$$f_l^{(n)} \le \overline{f_l}, \forall l \in \mathcal{L}_m \tag{2.111}$$

thus from (2.42), (2.47),(2.31) and (2.32) and knowing that $v^{(n)} \le v$ we have:

$$\hat{P}_l^t \le P_l^{t(n)} \le \bar{P}_l^t \ , \forall l \in \mathcal{L}_m \tag{2.112}$$

$$\hat{Q}_l^c \le Q_l^{c(n)} = Q_l^{t(n)} - \frac{b_l v_{up(l)}^{(n)}}{2} \le \bar{Q}_l^t - \frac{b_l v_{up(l)}}{2}, \forall l \in \mathcal{L}_m \tag{2.113}$$

consequently from step 1 of algorithm 1 we have:

$$f_l^{(n+1)} \le \bar{f}, \ \forall l \in \mathcal{L}_m \tag{2.114}$$

this shows that (2.70.h) holds for $n+1$.

f) From (2.42), (2.47), (2.31), (2.32) and (2.114) we have:

$$P_l^{(n+1)} \le \bar{P}_l, \forall l \in \mathcal{L}_m \tag{2.115}$$

$$Q_l^{'(n+1)} \le \bar{Q}_l^{'}, \forall l \in \mathcal{L}_m \tag{2.116}$$

these show that (2.70.i) and (2.70.j) hold for $n+1$.

Both basis and inductive steps are proved which completes the proof of *Lemma II.*

■

C) Proof of *Theorem II*

Item 1: Similar to the proof of *Theorem I*, let $\omega = \left(s, P + jQ, v, f, \hat{P} + j\hat{Q}, \hat{v}, \bar{P} + j\bar{Q}, \bar{f}\right)$ be a feasible solution of AR-OPF. Let $\mathcal{L}^{\neq}$ be the set of lines where (2.14) holds with strict inequality. If $\mathcal{L}^{\neq}$ is empty, ω is a load flow solution and *Theorem II* is trivially true. Assume now that $\mathcal{L}^{\neq}$ is not empty.

Consider the sequence $(P^{(n)}, Q^{c(n)}, v^{(n)}, f^{(n)})$ defined for $n \ge 0$ by means of *Algorithm I*. For $n \ge 1$ let $\Delta f^{(n)} \triangleq f^{(n)} - f^{(n-1)}$. Using *Lemma III* we have and knowing that $\Delta f^{(1)} \le \Delta f$:

$$\begin{aligned} &\Delta f^{(n)} \le 0, n = 1 \\ &\Delta f^{(n)} < 0, \forall n \ge 2 \end{aligned} \tag{2.117}$$

which ensures the convergence of $\sum_n \left\| \Delta f^{(n)} \right\|$, therefore of $\sum_n \Delta f^{(n)}$ and finally of the sequence $f^{(n)}$. It follows that $(P^{(n)}, Q^{c(n)}, v^{(n)}, f^{(n)})$ converges to some limit, (P^*, Q^{c*}, v^*, f^*) and $f^* \le f$. It follows that ω^* satisfies (2.14) with equality, i.e. it is a load flow solution. Further from (2.38), (2.42), (2.43), and *Lemma I* we have:

$$v^{\min} \le v \le v^* \le v^{\max} \tag{2.118}$$

$$P^* \le P \le P^{\max} \tag{2.119}$$

$$Q^* \le Q \le Q^{\max} \tag{2.120}$$

$$\bar{P}^* \le \bar{P} \le P^{\max} \tag{2.121}$$

$$\overline{Q}^{*} \le \overline{Q} \le Q^{\max} \tag{2.122}$$

We can observe that the security constraints (voltage lower/upper limits and the lines ampacity limits) are satisfied thus ω^* is a feasible solution of AR-OPF *and* of A-OPF. This prove the first item of *Theorem I.*

■

Item 2: Assume that ω is an optimal solution of AR-OPF but not a feasible solution of A-OPF, i.e. $\mathcal{L}^{\neq}$ is non-empty. From *Lemma III* we have for $n \geq 2$ $\Delta f^{(n)} < 0$ and $\Delta f^{(1)} \leq 0$. Consequently we have $f^* < f$ Since $\mathbf{H}_{1l} = 1,\ \forall\, l \in \mathcal{L}$ Thus:

$$P_1^{t(*)} - P_1^{t} = \sum_{l \in \mathcal{L}^{\neq}} \mathbf{H}_{1,l} \left(f_l^{(*)} - f_l \right) = \sum_{l \in \mathcal{L}^{\neq}} \left(f_l^{(*)} - f_l \right) < 0 \tag{2.123}$$

Since the power injections s are identical for ω and ω^*, it follows that the objective function of ω^* is strictly less than that of ω, which contradicts the optimality of ω. This proves the second item of *Theorem I.*

■

Lemma III: When $\mathcal{L}^{\neq}$ is not empty and $\mathbf{H}p^{\min} \geq 0$ and $\mathbf{H}q^{\min} - \frac{1}{2}\mathbf{H}\mathrm{diag}(b)\left(\mathbf{I} + \mathbf{G}^{\mathbf{T}}\right)\left(v^{\max}\right) \geq 0$ under conditions *C1*, for $n \geq 2$:

$$\Delta f^{(n)} < 0 \tag{2.124}$$

where $\Delta f^{(n)} = f^{(n)} - f^{(n-1)}$ for $n \geq 1$ and similarly with P, Q' and v.

Proof of Lemma III: The proof is by mathematical induction on $n \geq 2$.

1- **Base case ($n = 2$):**

We have $f_l^{(1)} \leq f_l^{(0)}$ for every l because $f^{(1)}$ is the right hand side of (2.14) in the original formulation of the constraints and ω is feasible and at least there is one line that $f_l^{(1)} < f_l^{(0)}$because $\mathcal{L}^{\neq}$ is non empty. Since $\mathbf{H}\mathrm{diag}(r)$ is a non-negative matrix and $\mathbf{F}$ is a positive one from (2.42) and (2.47) we have

$$0 \leq \hat{P} \leq P^{(1)} \leq P \tag{2.124}$$

$$0 \leq \hat{Q}^{c} \leq Q^{c(1)} < Q^{c} \tag{2.125}.$$

Consequently from step one of *Algorithm I* we have:

$$\begin{aligned} f^{(2)} &< f^{(1)} \\ \Delta f^{(2)} &< 0 \end{aligned} \tag{2.126}.$$

2- Induction step

Assume the statements in *Lemma III* are true for some $n \geq 2$. We now want to show that is also holds for $n + 1$.

Since $\Delta f^{(n)} \leq 0$ for all n, thus:

$$f^{(n)} < f^{(n-1)}, \forall n \geq 2 \tag{2.127}$$

combining (2.42), (2.43), and (2.38) we have:

$$0 \leq \hat{P} \leq P^{(n)} < P^{(n-1)} \tag{2.128}$$

$$0 \leq \hat{Q}^{c} \leq Q^{c(n)} < Q^{c(n-1)} \tag{2.129}$$

$$v^{\min} \leq v^{(n-1)} < v^{(n)} \tag{2.130}.$$

thus from step I of *Algorithm I* we have:

$$f^{(n+1)} < f^{(n)} \tag{2.131}$$

which means that $\Delta f^{(n+1)} < 0$.

Both basis and inductive steps are proved which completes the proof of *Lemma III.*

■

2.2.6.2 Validity of the conditions as a function of the network electrical parameters and physical extension

It is interesting to note that conditions *C1-C7* are function of the network topology and its electrical parameters. It is of interest to make observations about the validity of *C1-C7* as a function of the grid physical characteristics.

For a power system characterized by a given rated voltage, per-unit length (*pul*) line electrical parameters z_l^{pul} and b_l^{pul} do not vary drastically [26]. Additionally, parameters z_l and b_l are linear with the line lengths $\mathfrak{L}_l$.

By expressing the left hand side of *C1* as a function of the line *pul* parameters and $\mathfrak{L}_\ell$, we note that it is given by $\left(\max_{l\in\mathcal{L}} x_l^{pul}\right)\left(\max_{l\in\mathcal{L}} B_l^{pul}\right)\mathfrak{L}_l^2$. Also for *C2*, it is straightforward to observe that the l_1–norm of matrix **E** has a linear dependence with $\mathfrak{L}_\ell$. Concerning *C3, C5*, and *C7* we can observe that the left hand side of their inequality is propositional to $\mathfrak{L}_l^2$ whilst the right hand side of their inequality is proportional to $\mathfrak{L}_\ell$. Similarly, the left hand side of the *C4* and *C6* is proportional to $\mathfrak{L}_l^3$ while their right hand side is proportional to $\mathfrak{L}_l^2$.

Therefore, for given *pul* parameters z_l^{pul} and b_l^{pul}, it exists a $\mathfrak{L}_\ell$ small enough so that *C1-C7* holds. The consequence of this observation is that *C1-C7* can be verified a-priori for families of networks characterized by given electrical parameters and physical extension. In the following section, we numerically show that the validity of conditions *C1-C7* holds for real distribution networks with large margins.

To summarize, the AR-OPF is a combination of the original load flow equations and the DistFlow models with the inclusion of shunt impedances of the lines. Under the seven conditions provided above, the feasible solution space of the AR-OPF is a subset of the one of the O-OPF whereas the solution of R-OPF could lay outside the feasible solution space of O-OPF. Thus, every feasible solution of the AR-OPF always is in the feasible space of the O-OPF. These concepts are schematically represented in Fig. 2-2.

2.2.7 Numerical analysis of AR-OPF

The IEEE 34 buses network [25] and CIGRE European benchmark medium voltage network [26] are selected to assess the scalability of the provided conditions. The schematic of these networks are shown in Fig. 2-3. The scalability analysis is done by increasing the maximum level of injections into the systems. The choice of these two grids is because, the former network is composed by long overhead lines whereas underground cables with high penetration of distributed energy resources characterize the later one. Both networks are considered to be balanced without coupling between the phases. The minimum and maximum nodal voltage limits are considered to be 0.95 and 1.05 p.u. respectively.

In case of IEEE 34 buses, the line impedances are the positive sequence ones (it is assumed that the gird is a three phase balanced one). The base apparent power and voltage values are chosen to be 5 MVA and 24.9 kV respectively. Since there are no DG in the network, we increased the active and reactive power injection at each bus proportionally to their load share. The first condition that becomes violated when we increase power injections is C5. However, this condition is violated for a total injection

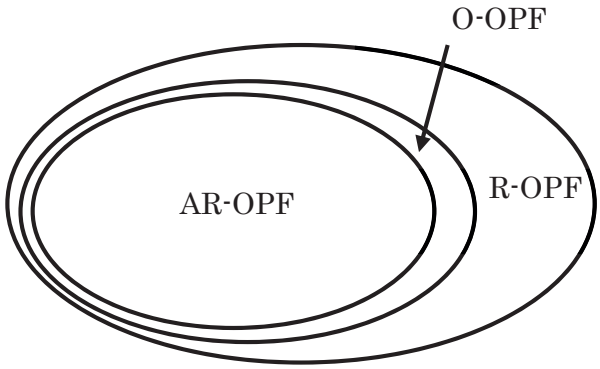

Fig. 2-2: Feasible solution spaces of O-OPF, R-OPF, and AR-OPF under the provided sufficient conditions

equal to 1241.8 kW and 755.35 kVAr respectively. For this operating point, the nodal voltages reach a maximum value of 1.115 p.u., a value far from typical feasible operating conditions.

For the CIGRE network, the positive sequence impedance with base apparent power and voltage base values equal to 25 MVA and 20 kV are selected. The network already has 3.079 MW generation capacity (it is designed for study the penetration of renewable resources). When we increase the generation capacity, the first conditions that are violated are C3 and C5. These violations happen at 570% of DG penetration, corresponding to 17.55 MW of active power production. For this operating point, the maximum value of the nodal voltages reaches 1.105 p.u., again a value far feasible.

The *C1-C7* are sufficient conditions for exactness of the AR-OPF solution. On the other hand we have done simulations well beyond these conditions (with both IEEE 34 buses and European benchmark network) and the solution of the AR-OPF is still exact (it should be noted that these conditions are violated outside the normal operation region of ADNs). Here in Table 2-2 and Table 2-1 we report the solution of AR-OPF and the a-posteriori load flow analysis. As it can be seen, the AR-OPF is still exact even outside the safe operating region of the network where the sufficient conditions do not hold.

Table 2-1: The solution of AR-OPF and a-posteriori load flow analysis in very high loading condition for the IEEE 34 buses network depicted in Fig. 2-3.b

Bus #	Voltage in p.u. (load flow analysis)	Voltage in p.u. (solution of AR-OPF)	Bus #	Voltage in p.u. (load flow analysis)	Voltage in p.u. (solution of AR-OPF)
1	1.000	1.000	17	1.117	1.117
2	1.002	1.002	18	1.117	1.117
3	1.004	1.004	19	1.125	1.125
4	1.031	1.031	20	1.128	1.127
5	1.031	1.031	21	1.120	1.120
6	1.062	1.062	22	1.120	1.120
7	1.087	1.087	23	1.123	1.123
8	1.087	1.087	24	1.123	1.123
9	1.087	1.087	25	1.124	1.124
10	1.094	1.094	26	1.124	1.124
11	1.096	1.096	27	1.124	1.124
12	1.097	1.097	28	1.123	1.124
13	1.097	1.097	29	1.124	1.124
14	1.098	1.098	30	1.124	1.124
15	1.116	1.116	31	1.124	1.124
16	1.117	1.117	32	1.124	1.124

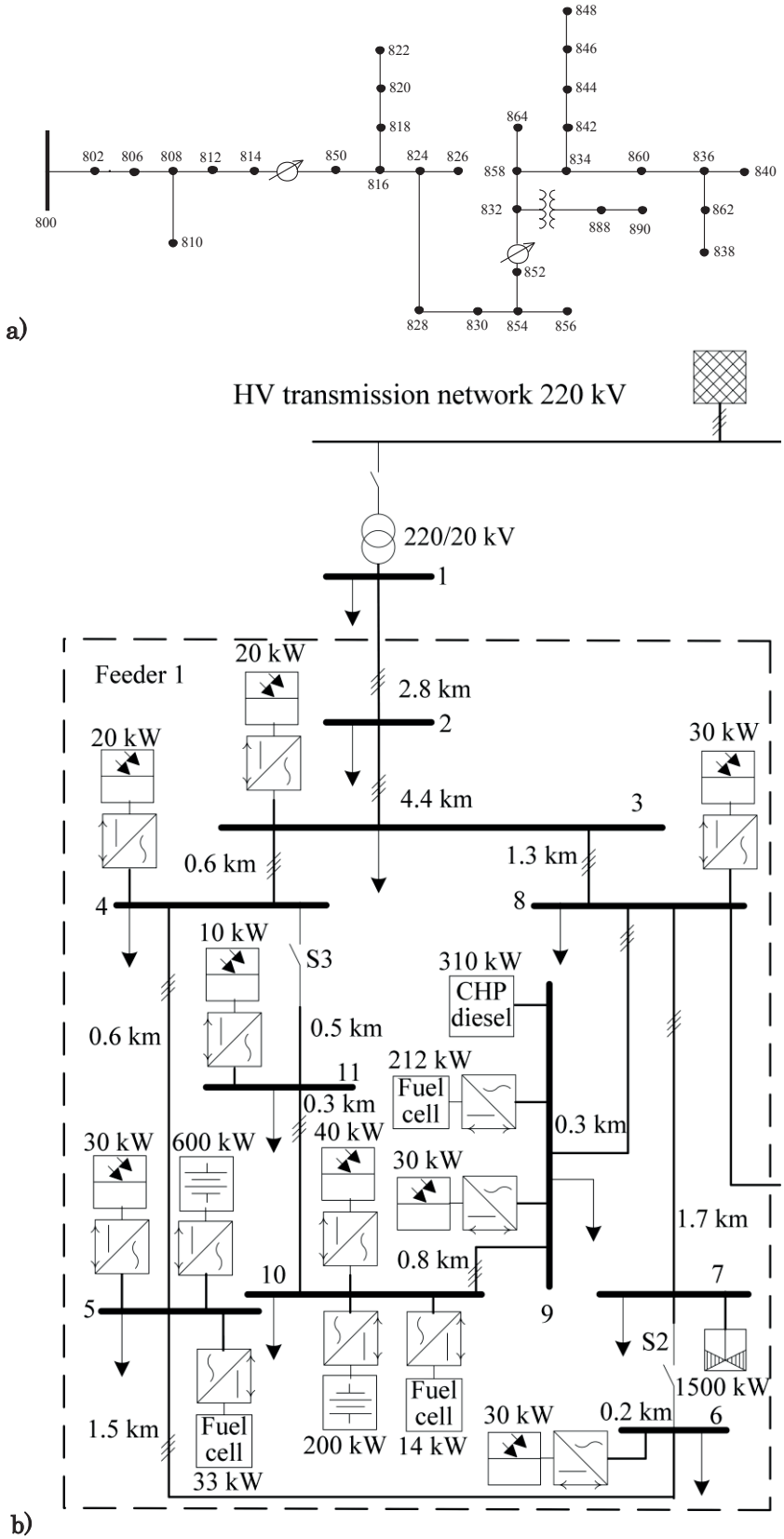

Fig. 2-3: Distribution networks adapted to verify conditions *C1-C7* of AR-OPF. a) IEEE 34 buses distribution test feeder [25], b) CIGRE benchmark distribution grid for integrating distributed energy resources [26]

Table 2-2: The solution of AR-OPF and a-posteriori load flow analysis in very high loading condition for the CIGRE network depicted in Fig. 2-3.b

Bus #	Voltage in p.u. (load flow analysis)	Voltage in p.u. (solution of AR-OPF)
1	1.0000	1.0000
2	1.0232	1.0232
3	1.1348	1.1348
4	1.1391	1.1391
5	1.1438	1.1438
6	1.1416	1.1416
7	1.1743	1.1743
8	1.2163	1.2163
9	1.1773	1.1773
10	1.1786	1.1786
11	1.1782	1.1782

2.2.8 Comparison of AR-OPF with existing OPF formulation

For the sake of reproducibility, the simple network introduced in [24] is chosen to show the infeasible behavior of the R-OPF and the capability of the AR-OPF to provide an optimal/feasible solution. We have slightly modified this network by adding new generation. The network data is presented in Table 2-3 and its topology in Fig. 2-4. It should be noted that the values of the line parameters refer to the typical underground cables, which are in use in distribution networks[1]. It is worth saying that we have intentionally adopted a network in which line transverse parameters cannot be neglected.

In order to show the effectiveness of the AR-OPF we have done a sensitivity analysis with various line lengths and rated voltage values (this sensitivity analysis was done also in [24] to show the shortcomings of the branch flow approximation (R-OPF)). It should be noted that the following results refer to an OPF in which the objective is the minimization of the total energy supply cost (see Table 2-3 for the elements considered in the cost function). Other objective functions that are strictly increasing in the sum of total losses lead to identical conclusions.

Table 2-4 shows the values of the nodal voltages (v) and voltage auxiliary variables ($\hat{v}$) obtained from the solution of the AR-OPF, and the ones calculated by the load-flow analysis using the Newton-Raphson method. We can see that the voltage magnitudes obtained are the same as the a-posteriori load flow analysis showing the correct formulation of the problem and the tightness of the relaxation show in (2.11.c). These

1 They are derived from the page 16 of the following document. http://www.nexans.com/Switzerland/files/NEXANS06_BTMTAcc_F.pdf

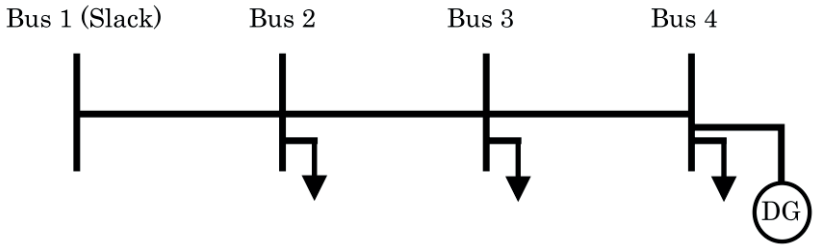

Fig. 2-4: Schematic of the 4 bus case study

Table 2-3: 4 buses test network parameters.

Parameter	Value
Line parameters(positive direct sequence) $R\left(\frac{\text{ohm}}{\text{km}}\right), L\left(\frac{\text{mH}}{\text{km}}\right), C(\frac{\mu\text{F}}{\text{km}})$	(0.193, 0.38, 0.24)
Initial line length (line 1, line 2 line 3) (km)	(3.12, 3.75,4.37)
Network rated voltage and base power (kV, MVA)	(24.9, 5)
P_g^{max}(MVA) (DG on bus 4)	4
(v^{min}, v^{max})	(0.81,1.21)
I_{kl}^m (for all 4 lines)	80 (A)
Complex load on bus 2, and 3 (kW , kVar))	$(50 + j30)$, $(60 - j27)$
Energy cost from external grid, cost of active and reactive production of DG at bus 4 ($/MWh, ($/MWh, ($/MVArh)	(50, 150, 150)

results are for the case with line length factor 3 and nominal voltages equal to 24.9 kV. The same conditions (line length factor equal to 3 and nominal voltage of 24.9 kV) are used to show the inaccuracy of the model when the shunt capacitances are not taken into accounts.

Table 2-5 shows the nodal voltage magnitudes obtained from solution of the AR-OPF formulation without shunt elements vs the ones calculated by the load-flow analysis using the Newton-Raphson method (in the load flow analysis, the shunt capacitances are considered). It is possible to clearly observe the discrepancies between these two sets of results.

Table 2-5 reveals that the transverse parameters have non-negligible effects and they have to be taken into accounts appropriately (especially for the networks characterized by the presence of underground cables).

In section 2.2.1 another drawback has been mentioned concerning the existing literatures regarding the inclusion of the lines ampacity limits in the OPF. In this respect, it is worth underlying that in distribution networks line ampacities represents a more important constraint rather than the voltage one since they are related to a physical constraint capable, if violated, to produce permanent damages to the cables.

Table 2-4: Voltage magnitude obtained with the AR-OPF (line factor: 3, nominal voltage: 24.9 Kv)

	Voltage magnitude (p.u.)		
	Voltage from load flow	$\hat{v}_l$	v_l
bus #1	1	1	1
bus #2	1.0024	1.0025	1.0024
bus #3	1.0046	1.0047	1.0046
bus #4	1.0062	1.0063	1.0062

Table 2-5: Voltage magnitudes obtained using the AR-OPF without the transverse parameters (line factor 3, nominal voltage value 24.9 KV)

	Voltage magnitude (p.u.)	
	Voltage from load flow	v_l
bus #1	1.0000	1.0000
bus #2	1.0024	0.9974
bus #3	1.0046	0.9958
bus #4	1.0062	0.9958

Table 2-6: Voltage magnitude comparison obtained with the R-OPF (line factor 5, nominal voltage value 24.9 kV)

	Voltage magnitude (p.u.)	
	Voltage from load flow	v_l
bus #1	1	1.0000
bus #2	1.0093	1.0067
bus #3	1.0173	1.0116
bus #4	1.0217	1.0142

Table 2-6 shows the voltages obtained from the results of the R-OPF and a-posteriori load flow computations when the transverse parameters are taken into accounts. It can be seen that they are different. It is because the relaxation shown in (2.14) is not tight. The $\sqrt{f_{kl}}$ of the third line has a value equal to 173.97 A, whereas the a-posteriori load flow calculation shows that it is equal to 20.57 A.

The line current magnitudes for three cases (AR-OPF, AR-OPF without considering the shunt capacitances, and the R-OPF for different line lengths are shown in Fig. 2-5. It can be seen that the maximum rating of the lines (dashed line in Fig. 2-5) is satisfied with the AR-OPF whereas they are largely violated in the two other cases.

Another sensitivity analysis with respect to nominal voltage magnitude is shown in Fig. 2-6. This figure also demonstrates the effectiveness and exactness of the AR-OPF, the influences of the transverse parameters as well as the infeasible behavior of R-OPF.

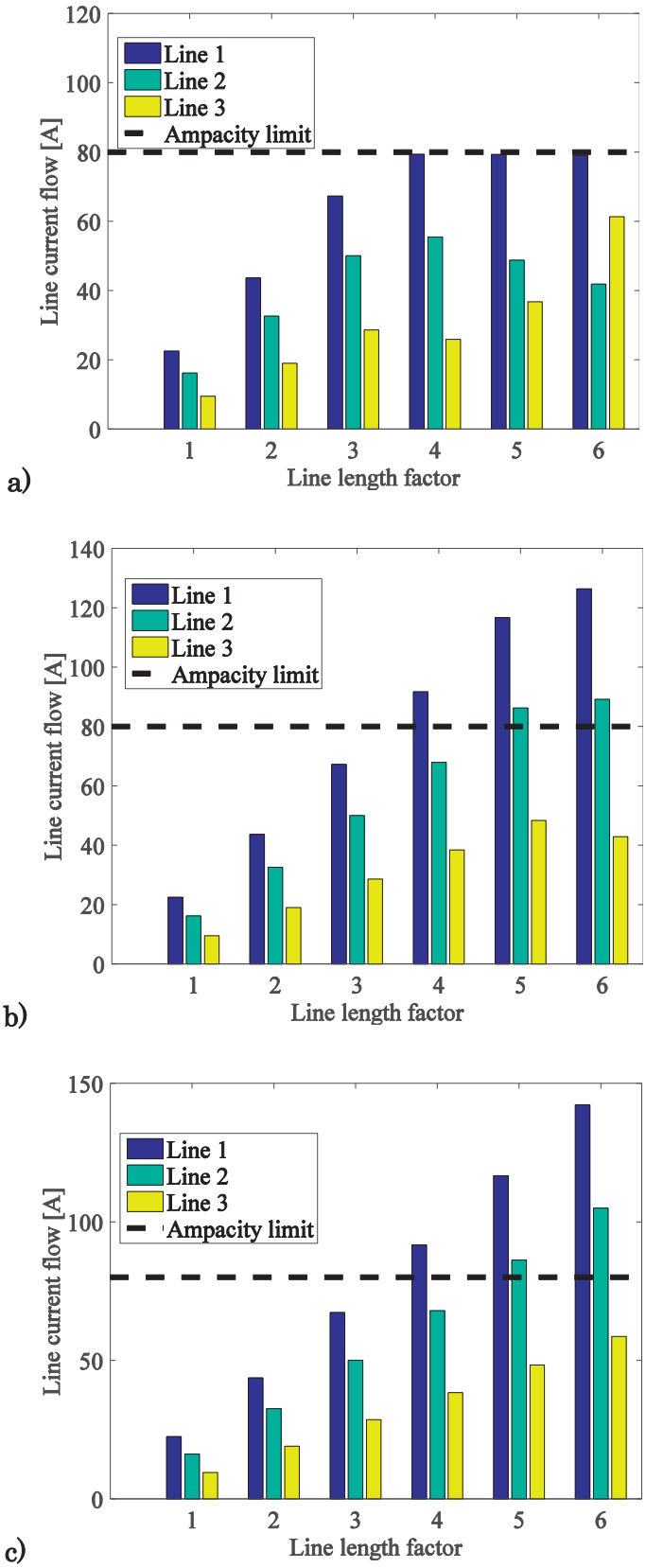

Fig. 2-5: Current flow magnitude of the lines vs. cables length. a) AR-OPF, b) R-OPF, and c) AR-OPF without transverse parameters (nominal voltage 24.9 kV))

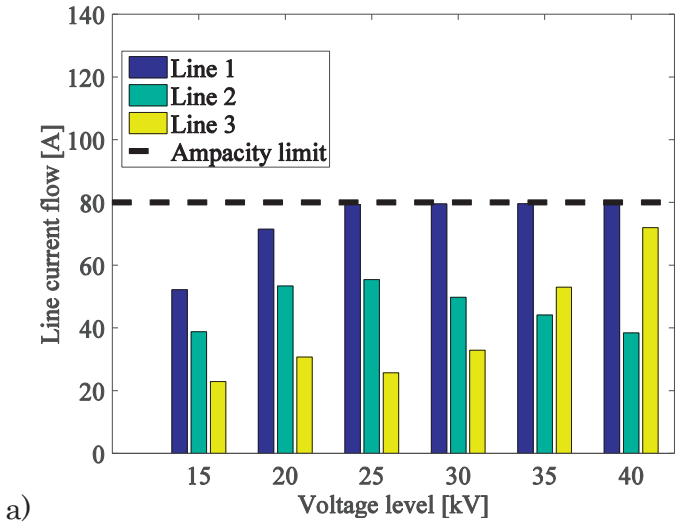

a)

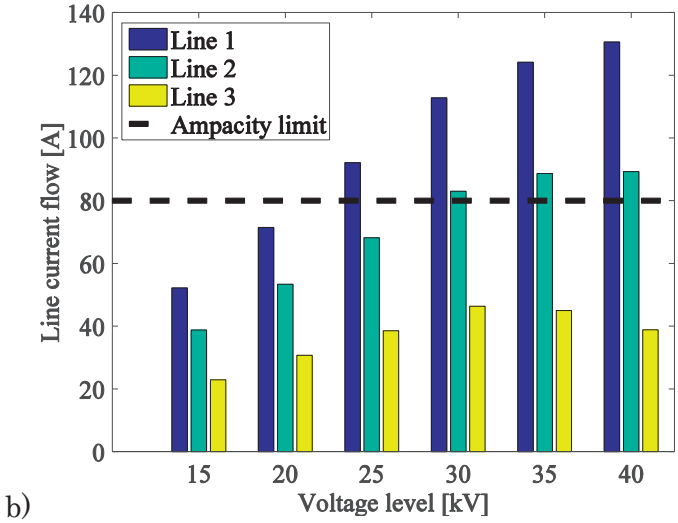

b)

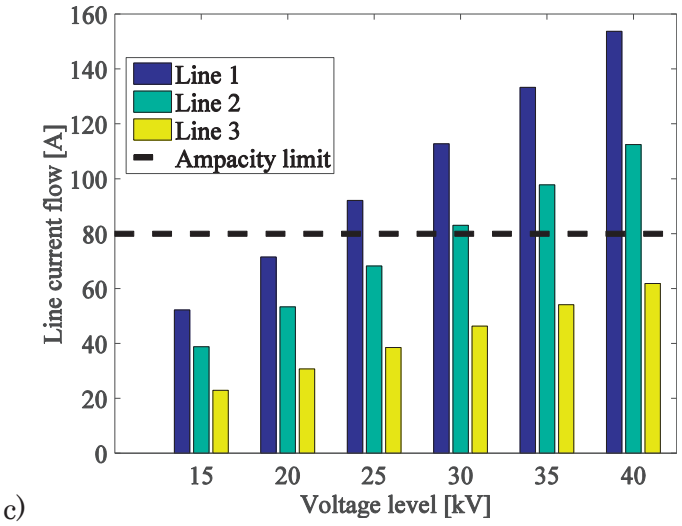

c)

Fig. 2-6: Current flow magnitude of the lines vs. nominal voltage level a) AR-OPF, b) R-OPF, and c) AR-OPF without transverse parameters (line factor 1)

2.3 Topology Changes in Optimal Operation of Radial Power Grids

As known, distribution networks are designed in meshed structure but are normally operated with radial topology. Accordingly, DNOs have several options for their network configuration. The network reconfiguration is mostly done for resistive losses minimization and/or for satisfying the security constraints (nodal voltages and devices loadings limits). The problem of identifying the best configuration of distribution networks has been addressed since many years. This optimization problem involves non-convex constraints as well as binary variables. Since it is a mixed integer non-linear and non-convex problem, is extremely hard to be solved. The topology constraints related to the radial structure of these networks make the solution even more challenging. In this sub-section first, we provide a literature review concerning the existing methods for optimal ADN reconfiguration. Then, we propose a MISOCP model based on the AR-OPF, to solve the network reconfiguration problem.

2.3.1 State-of-the-art of optimal ADN reconfiguration

Several methods have been proposed to solve ADN reconfiguration problem. Heuristic methods have been extensively used for this purpose. The Authors in [27] have used GA to solve the original MINLP problem related to the optimal reconfiguration of distribution networks. The objective is to minimize the voltage sag costs. A multi-objective model has been proposed in [28] to simultaneously select the best network configuration and phase arrangement. The objective function includes minimization of resistive losses, voltage deviations, as well as voltages and currents imbalances. The Authors have used neural network for the network reconfiguration problem and a dedicated heuristic method for the phase balancing/loss minimization problem. Several works have studied the losses minimization in distribution networks using the reconfiguration option [29-37]. The problem of optimal day-ahead scheduling of ADNs, taking into account the network reconfiguration, is addressed in [38]. The objective function tries to minimize the total resistive losses, voltage deviation, feeders' congestion as well as the switching cost. It is solved using discrete GA. The Authors in [39] present a heuristic algorithm for the solution of optimal reconfiguration problem of large-scale distribution networks. The heuristic strategy starts with the initial meshed status, with all switches closed. The status of the switches changes based on the calculation of the minimum value of total resistive losses, using a load-flow analysis. In [40] a heuristic approach based on TABU search algorithm is used to find the optimal configuration of a distribution network. The objective is to have the minimum level of resistive losses.

An exhaustive search algorithm is proposed in [41] for finding the minimal-loss radial configuration of power distribution networks. The Authors have used the graph-theoretic techniques involving semi-sparse transformations of the current sensitivity matrix.

Benders decomposition has been used in [42] and [43] to decompose the original MINLP problem into a MILP master and a non-convex NP subproblem. The state of the switches are defined in the master stage, and the fitness of the solution is evaluated in the subproblems. The subproblems are formulated with non-convex OPF. Therefore, the approach does not guarantee the global optimal solution.

Recently, several works have been done relying on convex formulation of OPF. The convex relaxed formulation of OPF is used in [44] and [45] to formulate a mixed integer convex programming for optimal reconfiguration of distribution networks. In [46] three models i) Mixed-Integer quadratic (MIQP), ii) Mixed-Integer Quadratically Constrained Quadratic Programming (MIQCQP) and iii) Mixed-Integer SOCP programming are proposed for this problem. The Authors have used a convex model of OPF based on the SOCP formulation of OPF. They have provided a new set of constraints to guarantee radial topology of the distribution network where binary variables are only required for the switches. A heuristic algorithm based on the convex relaxation of OPF problem is used in [47] to solve the feeder reconfiguration problem in distribution networks.

As discussed above, most of the works on ADN reconfiguration have used heuristic methods or non-linear solvers to find a local optimum solution for the problem. Additionally, these methods are time consuming. The methods that have used convex formulation of OPF have not modeled the network and the security constraints properly (this aspect has been already discussed in 2.2.1). In this work we have used the radiality constraints proposed in [46] and the proposed AR-OPF. The advantages of the proposed model are i) the voltage and ampacity limits are modeled appropriately ii) the full AC OPF is used without any approximations/simplifications iii) the shunt capacitances related to the transverse parameters of the lines are incorporated into the model and finally iii) similar to [46] binary variables are only required for the switches. The next sub-section provide the mathematical formulation of the proposed model.

2.3.2 Proposed optimization model for distribution network reconfiguration

The radiality constraints are modeled with the set of equations (2.132.a) - (2.132.e). The main idea is to ensure that every single bus is supplied only by one substation through a unique path. In another word, any loop that includes one or more substations is not a feasible solution. The loops without substations cannot supply the loads thus they are not feasible operating solutions. The variable d_{kl} defines the direction between buses k and l ($d_{kl} = 1$ means the direction is from k to l and $d_{lk} = 1$ means the direction is from l to k). $\mathcal{L}$ is the set of the lines. $\mathcal{L}_s$ is the set of the lines with switches whereas $\mathcal{L}\backslash\mathcal{L}_s$ represents the set of the lines without switch. $\mathcal{L}_l$ represents the set of the lines connected to bus l. The set of all buses is represented by N. The buses that are substations are represented by N_G whereas set of rest of the buses is represented by $N\backslash N_G$. The constraint (2.132.a) implies that the lines without switches must have only one direction (either from k to l or from l to k). Every switch has one direction in case its switch (κ_{kl}) is on. This is modeled by equation (2.132.b). The direction of any line connected to a substation is from the substation to its corresponding adjacent bus. It is

shown in the equation (2.132.c). The buses that are not substation can only have one infeed as modeled by (2.132.d).

$$d_{kl} + d_{lk} = 1 \quad (l,k) \in \mathcal{L} \setminus \mathcal{L}_S \tag{2.132.a}$$

$$d_{kl} + d_{lk} = \kappa_{kl} \quad (l,k) \in \mathcal{L}_S \tag{2.132.b}$$

$$d_{kl} = 0 \quad l \in N_G \tag{2.132.c}$$

$$\sum_{k:(k,l)\in\mathcal{L}_l} (d_{kl}) = 1 \quad l \in N \setminus N_G \tag{2.132.d}$$

$$\kappa_{kl} \in \{0,1\} \tag{2.132.e}$$

The AR-OPF is further developed with the above radiality constraints to develop an optimization model for optimal ADN reconfiguration. It should be noted that the notation for power flows is a bit different from the AR-OPF (see Fig. 2-7). In the following formulation the transverse parameters are merged into the nodal loads. It should be noted that the switches do not have transverse parameters. The shunt capacitances are still considered in the lines' ampacity limit constraints and no approximation is introduced in the model.

Resistive losses minimization is the main objective of the network reconfiguration problem. In this work we have formulated the optimization program for resistive losses minimization. It should be noted that other goals (i.e., voltage deviations minimization) can be easily added to the objective function. The objective function is formulated as in (2.133.a). The optimization model is shown in set of equations (2.133.a)-(2.133.ee).

$$\underset{\Xi}{\text{minimize}}: \sum_{(k,l)\in\mathcal{L}} r_{kl}(f_{kl} + f_{lk}) \tag{2.133.a}$$

Subject to:

$$\text{(2.132.a)-(2.132.e)} \tag{2.133.b}$$

$$\begin{aligned} -d_{kl}P_{kl}^{max} \le P_{kl}, \hat{P}_{kl}, \overline{P}_{kl} \le d_{kl}P_{kl}^{max} \\ -d_{lk}P_{lk}^{max} \le P_{lk}, \hat{P}_{lk}, \overline{P}_{lk} \le d_{lk}P_{lk}^{max} \end{aligned}, \quad \forall (k,l) \in \mathcal{L} \tag{2.133.c}$$

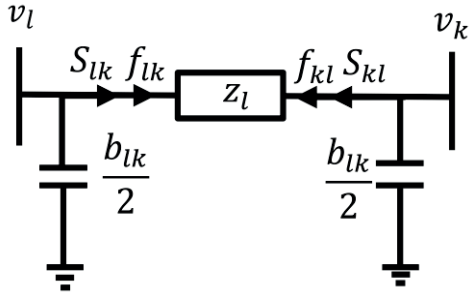

Fig. 2-7: Classical two-port Π model of a transmission line adopted for the formulation of the optimal ADN reconfiguration.

$$\begin{matrix} -d_{kl}Q_{kl}^{max} \le Q_{kl},\hat{Q}_{kl},\overline{Q}_{kl} \le d_{kl}Q_{kl}^{max} \\ -d_{lk}Q_{lk}^{max} \le Q_{lk},\hat{Q}_{lk},\overline{Q}_{lk} \le d_{lk}Q_{lk}^{max} \end{matrix} \quad \forall(k,l) \in \mathcal{L} \tag{2.133.d}$$

$$\begin{matrix} 0 \le f_{kl} \le d_{kl}I_{kl}^{max} \\ 0 \le f_{lk} \le d_{lk}I_{lk}^{max} \end{matrix}, \quad \forall(k,l) \in \mathcal{L} \tag{2.133.e}$$

$$\begin{matrix} 0 \le \overline{f}_{kl} \le d_{kl}I_{kl}^{max} \\ 0 \le \overline{f}_{lk} \le d_{lk}I_{lk}^{max} \end{matrix}, \quad \forall(k,l) \in \mathcal{L} \tag{2.133.f}$$

$$\begin{matrix} v_l^{'} \ge v_l - \mathfrak{B}(1-d_{kl}) \\ v_k^{'} \ge v_k - \mathfrak{B}(1-d_{kl}) \end{matrix} \quad \forall(k,l) \in \mathcal{L} \tag{2.133.g}$$

$$\begin{matrix} v_l^{'} \le v_l + \mathfrak{B}(1-d_{kl}) \\ v_k^{'} \le v_k + \mathfrak{B}(1-d_{kl}) \end{matrix} \quad \forall(k,l) \in \mathcal{L} \tag{2.133.h}$$

$$\begin{matrix} v_l^{''} \ge v_l - \mathfrak{B}(1-d_{lk}) \\ v_k^{''} \ge v_k - \mathfrak{B}(1-d_{lk}) \end{matrix} \quad \forall(k,l) \in \mathcal{L} \tag{2.133.i}$$

$$\begin{matrix} v_l^{''} \le v_l + \mathfrak{B}(1-d_{lk}) \\ v_k^{''} \le v_k + \mathfrak{B}(1-d_{lk}) \end{matrix} \quad \forall(k,l) \in \mathcal{L} \tag{2.133.j}$$

$$\begin{matrix} f_{kl}v_k^{'} \ge \left|(S_{kl})\right|^2 \\ f_{lk}v_l^{''} \ge \left|(S_{lk})\right|^2 \end{matrix}, \quad \forall(k,l) \in \mathcal{L} \tag{2.133.k}$$

$$\begin{matrix} \overline{f}_{kl}v_k^{'} \ge \left|\max\left\{\overline{P}_{kl},\hat{P}_{kl}\right\} + j\max\left\{\left(\overline{Q}_{kl}\right),\left(\hat{Q}_{kl}\right)\right\}\right|^2 \\ \overline{f}_{lk}v_l^{''} \ge \left|\max\left\{\overline{P}_{lk},\hat{P}_{lk}\right\} + j\max\left\{\left(\overline{Q}_{lk}\right),\left(\hat{Q}_{lk}\right)\right\}\right|^2 \end{matrix} \quad \forall(k,l) \in \mathcal{L} \tag{2.133.l}$$

$$\begin{matrix} \overline{f}_{kl}v_l^{'} \ge \left|\max\left\{\overline{P}_{kl} - r_{kl}\overline{f}_{kl},\hat{P}_{kl}\right\} + j\max\left\{\left(\overline{Q}_{kl} - x_{kl}\overline{f}_{kl}\right),\left(\hat{Q}_{kl}\right)\right\}\right|^2 \\ \overline{f}_{lk}v_k^{''} \ge \left|\max\left\{\overline{P}_{lk},-r_{kl}\overline{f}_{lk},\hat{P}_{lk}\right\} + j\max\left\{\left(\overline{Q}_{lk} - x_{kl}\overline{f}_{lk}\right),\left(\hat{Q}_{lk}\right)\right\}\right|^2 \end{matrix}, \forall(k,l) \in \mathcal{L} \tag{2.133.m}$$

$$\begin{matrix} v_k \le v_l^{''} - 2\Re\left(z_{lk}^{*}(S_{lk}\right) + \left|z_{lk}\right|^2 f_{lk} + \mathfrak{B}(1-d_{lk}) \\ v_l \le v_k^{'} - 2\Re\left(z_{kl}^{*}(S_{kl}\right) + \left|z_{kl}\right|^2 f_{kl} + \mathfrak{B}(1-d_{kl}) \end{matrix}, \forall(k,l) \in \mathcal{L} \tag{2.133.n}$$

$$\begin{matrix} v_k \ge v_l^{''} - 2\Re\left(z_{lk}^{*}S_{lk}\right) + \left|z_{lk}\right|^2 f_{lk} - \mathfrak{B}(1-d_{lk}) \\ v_l \ge v_k^{'} - 2\Re\left(z_{kl}^{*}S_{kl}\right) + \left|z_{kl}\right|^2 f_{kl} - \mathfrak{B}(1-d_{kl}) \end{matrix} \quad \forall(k,l) \in \mathcal{L} \tag{2.133.o}$$

$$\begin{matrix} \hat{v}_k \ge \hat{v}_l^{''} - 2\Re\left(z_{lk}^{*}\hat{S}_{lk}\right) - \mathfrak{B}(1-d_{lk}) \\ \hat{v}_l \ge \hat{v}_k^{'} - 2\Re\left(z_{lk}^{*}\hat{S}_{kl}\right) - \mathfrak{B}(1-d_{kl}) \end{matrix}, \forall(k,l) \in \mathcal{L} \tag{2.133.p}$$

$$\begin{aligned}\hat{v}_k &\le \hat{v}_l'' - 2\Re\left(z_{lk}^*\hat{S}_{lk}\right) + \mathfrak{B}\left(1-d_{lk}\right)\\ \hat{v}_l &\le \hat{v}_k' - 2\Re\left(z_{lk}^*\hat{S}_{kl}\right) + \mathfrak{B}\left(1-d_{kl}\right)\end{aligned} \quad \forall(k,l)\in\mathcal{L} \tag{2.133.q}$$

$$\begin{aligned}\hat{v}_l' &\ge \hat{v}_l - \mathfrak{B}\left(1-d_{kl}\right)\\ \hat{v}_k' &\ge \hat{v}_k - \mathfrak{B}\left(1-d_{kl}\right)\end{aligned} \quad \forall(k,l)\in\mathcal{L} \tag{2.133.r}$$

$$\begin{aligned}\hat{v}_l' &\le \hat{v}_l - \mathfrak{B}\left(1-d_{kl}\right)\\ \hat{v}_k' &\le \hat{v}_k - \mathfrak{B}\left(1-d_{kl}\right)\end{aligned} \quad \forall(k,l)\in\mathcal{L} \tag{2.133.s}$$

$$\begin{aligned}\hat{v}_l'' &\ge \hat{v}_l + \mathfrak{B}\left(1-d_{lk}\right)\\ \hat{v}_k'' &\ge \hat{v}_k + \mathfrak{B}\left(1-d_{lk}\right)\end{aligned} \quad \forall(k,l)\in\mathcal{L} \tag{2.133.t}$$

$$\begin{aligned}\hat{v}_l'' &\le \hat{v}_l + \mathfrak{B}\left(1-d_{lk}\right)\\ \hat{v}_k'' &\le \hat{v}_k + \mathfrak{B}\left(1-d_{lk}\right)\end{aligned} \quad \forall(k,l)\in\mathcal{L} \tag{2.133.u}$$

$$\hat{v}_l \le v^{\max} \quad \forall l\in\mathcal{N} \tag{2.133.v}$$

$$v^{\min} \le v_k \quad \forall l\in\mathcal{N} \tag{2.133.w}$$

$$\sum_{k:(l,k)\in\mathcal{L}_l}\left(S_{lk} - S_{kl} - z_{kl}f_{kl}\right) + s_l = jQ_l^{sh} \quad \forall l\in\mathcal{N} \tag{2.133.x}$$

$$\sum_{k:(l,k)\in\mathcal{L}_l}\left(\overline{S}_{lk} - \overline{S}_{kl} - z_{kl}\overline{f}_{kl}\right) + s_l = jQ_l^{sh} \quad \forall l\in\mathcal{N} \tag{2.133.y}$$

$$\sum_{k:(l,k)\in\mathcal{L}_l}\left(\hat{S}_{lk} - \hat{S}_{kl}\right) + s_l = j\hat{Q}_l^{sh} \quad \forall l\in\mathcal{N} \tag{2.133.z}$$

$$Q_l^{sh} = \sum_{(l,k)\in\mathcal{L}_l}\frac{v_l b_{kl}}{2} \quad \forall l\in\mathcal{N} \tag{2.133.aa}$$

$$\hat{Q}_l^{sh} = \sum_{(l,k)\in\mathcal{L}_l}\frac{\hat{v}_l b_{kl}}{2} \quad \forall l\in\mathcal{N} \tag{2.133.bb}$$

$$\frac{\left|\max\left\{\Re\left(\overline{S}_{kl}\right),\Re\left(\hat{S}_{kl}\right)\right\} + j\max\left\{\Im\left(\overline{S}_{kl} - jv_k'\frac{b_{kl}}{2}\right),\Im\left(\hat{S}_{kl} - j\hat{v}_k'\frac{b_{kl}}{2}\right)\right\}\right|^2}{v_k} \le I_{kl}^{\max} \quad \forall(k,l)\in\mathcal{L} \tag{2.133.cc}$$

$$\frac{\left|\max\left\{\Re\left(\overline{S}_{lk}\right),\Re\left(\hat{S}_{lk}\right)\right\} + j\max\left\{\Im\left(\overline{S}_{lk} - jv_l'\frac{b_{lk}}{2}\right),\Im\left(\hat{S}_{lk} - j\hat{v}_l'\frac{b_{lk}}{2}\right)\right\}\right|^2}{v_l} \le I_{lk}^{\max} \quad \forall(k,l)\in\mathcal{L} \tag{2.133.dd}$$

$$v_l^{'} \geq 0, v_l^{''} \geq 0, \hat{v}_l^{'} \geq 0, \hat{v}_l^{''} \geq 0 \qquad (2.133.ee)$$

where $\Xi = \{f, \bar{f}, P, Q, d, v, v', v'', S, \kappa, \hat{v}, \hat{v}', \hat{v}'', \hat{P}, \bar{P}, \hat{Q}, \bar{Q}, \hat{S}, \bar{S}, Q^{sh}, \hat{Q}^{sh}\}$ is the set of optimization variables. Note that a notation without subscript represents the correspond vector. For the lines, it represents the corresponding vector for both directions (e.g., f_{kl} and f_{lk}). The control variables are the status of the switches.

Constraints (2.133.c), (2.133.d), and (2.133.e) impose the flow limit based on the lines' direction variable (d_{kl}). The direction of the line could be either from k to l or vice versa. It should be noted that with any direction, the active and reactive power flows could have both positive and negative values. Equations (2.133.g)-(2.133.m) model the f_{kl} and f_{lk} of the line between buses l and k. $\mathfrak{B}$ is a big number (in per unit system 10 is big enough). These constraints are not activated (d_{kl} and d_{lk} are both zero) when the switch of a line is open. For the closed switches and other lines, this constraint is activated either for $l \to k$ or $k \to l$. The variables $v_l', v_l'', \hat{v}_l''$, and $\hat{v}_l'$ are introduced to put the SOCP constraints in a recognizable form for commercial convex programming solvers. In case of $k \to l$ direction, v is equal to v' and in case of $l \to k$ direction, v for is equal to v''. The voltage and auxiliary voltage equations between two ends of a line are represented by (2.133.n)-(2.133.u). Similar to the case of lines' current flow, these set of constraints are activated either for $l \to k$ or $k \to l$. The nodal voltage magnitudes limits are shown (2.133.w) and (2.133.v). The nodal load balance equations are represented in (2.133.x)-(2.133.z). The reactive power related to the shunt admittance of the lines are modeled by equations (2.133.aa) and (2.133.bb). Finally, the current flow at both ends of the lines is limited by equations (2.133.cc) and (2.133.dd). The reactive power related to the transverse parameters is added to the $S_{kl}(S_{lk})$ to limit the correct current flow of the lines.

In [46] it is shown that any feasible d_{kl} is either one or zero, and it is an edge of a directed tree graph with a root bus. It should be noted that, feasible d_{kl} means that all the buses are connected to one substation.

Let's show how the radiality constraints work by investigating the load balance equation (2.133.x). Fig. 2-8 shows a generic bus (#1) that is connected to three other busses (#2, #3, #4). The equation (2.133.x) represents the nodal power balance at the bus #1. Let suppose that through each of the buses #2, #3, and #4 there could be a path that connects the bus #1 to the external gird. As stated in before, for a feasible solution, there is only one path from the bus #1 to the external grid (any substation). Let suppose that bus#1 is connected to a substation through the path passing from bus #2. Thus, we have that $d_{21} = 1$. Consequently, due to constraint (2.132.d) $d_{31} = 0$ and $d_{41} = 0$. Hence, S_{31}, S_{41},

f_{31} and f_{41} are equal to zero. Therefore, the equation (2.133.x) for the line between buses #1 and #2 becomes (2.134) that is the nodal load balance for bus #1.

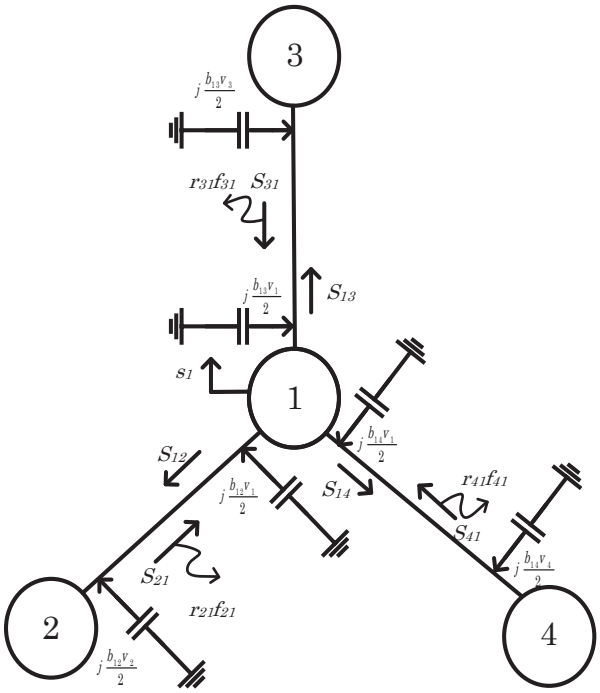

Fig. 2-8: Simple network for verifying radiality constraints

$$S_{13} + S_{14} + s_1 + z_{12}f_{12} - j\left(\frac{b_{12} + b_{13} + b_{14}}{2}\right)v_1 = S_{21} \tag{2.134}$$

It should be noted that for the ampacity limit of the lines (equation (2.133.cc)) we have added the reactive power flow related to the shunt capacitance of the line to the complex power flow resulting from equation (2.133.x).

To summarize, we have incorporated a set of radiality constraints into the AR-OPF to take into account the ADN reconfiguration. In the following sections we provide numerical examples for showing the benefits and effectiveness of the proposed formulation.

2.3.3 Computational Examples

In this section two standard test case systems, 33 buses distribution network [48], and IEEE 123 buses network, are used to evaluate the performances of the proposed formulation. The former case is employed to demonstrate the optimality of the proposed optimization solution, whereas the latter one is used to show the performances of the proposed formulation in terms of feasibility and scalability of the solution.

Case I, standard 33 buses distribution test network:
The single line diagram of this network is shown in Fig. 2-9. It has 33 buses (including the connection bus to the grid, bus #0). It was first introduced in [48]. It is a hypothetical 12.66-kV system with two feeders and five looping branches (tie lines).

The optimum solution for this network is obtained in [41] using a brute-force methodology. The switches s7, s9, s14, s32, and s37 are the open ones. The solution of

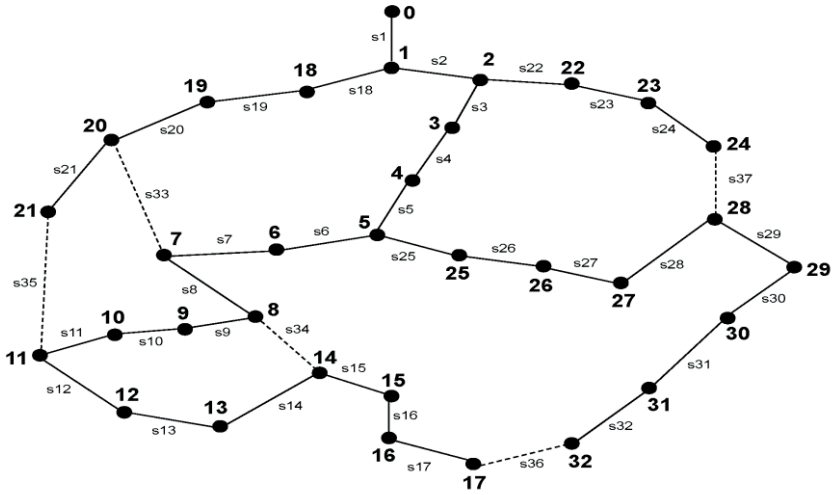

Fig. 2-9: Schematic of the standard 33 buses network [43] (dashed lines are the default open switches).

the proposed model gives the same switching strategy showing the capability of the proposed formulation to find the global optimal solution. The computation time (average of 5 times runs) on a desktop PC with 16 GB RAM and Intel Xenon CPU E5-1650 @ 3.20 GHz is 85 seconds. In this benchmark network every branch has a switch thus the number of binary variables is equal to the number of lines. Consequently, the advantages of the proposed model that use binary variables only for switches cannot be demonstrated with this network. In real networks, all the lines do not have switches. Therefore, models with few binary variables have a big computational advantage with respect to those that have binary variables for all the lines. The following sub-section employ IEEE 123 test buses to demonstrate the accuracy and values of the proposed formulation.

Case 2 IEEE 123 buses test case network

The schematic of this network is shown in Fig. 2-10. It is assumed that there are five sub-stations connected the external gird. They are buses #1, #2, # 3, # 4, and # 5. They have switches to connect a part of the distribution network to the external grid (see Fig. 2-10). There are 6 other switches in the network between buses (#94, #54), (#13, #52), (#18, #35), (#118, #51), (#97, #101), and (#60, #67). It is assumed that there are 10 PV sites in the network (See Fig. 2-10). The PV sites and their respective capacities are shown in Table 2-8 Using the proposed optimization model, the obtained minimum resistive losses is 332.24 kW. The switching statuses obtained from the optimal solution are shown in Table 2-7.

The identified topology of the network is shown in Fig. 2-11. As it can be seen there are three separate radial networks supplied from 3 substations. The nodal voltages obtained from the solution of the optimization problem and the ones calculated a-posteriori using load flow procedure for the network #1 are shown in Table 2-9 (identical feasible results are obtained for the other two grids). It can be seen the obtained nodal

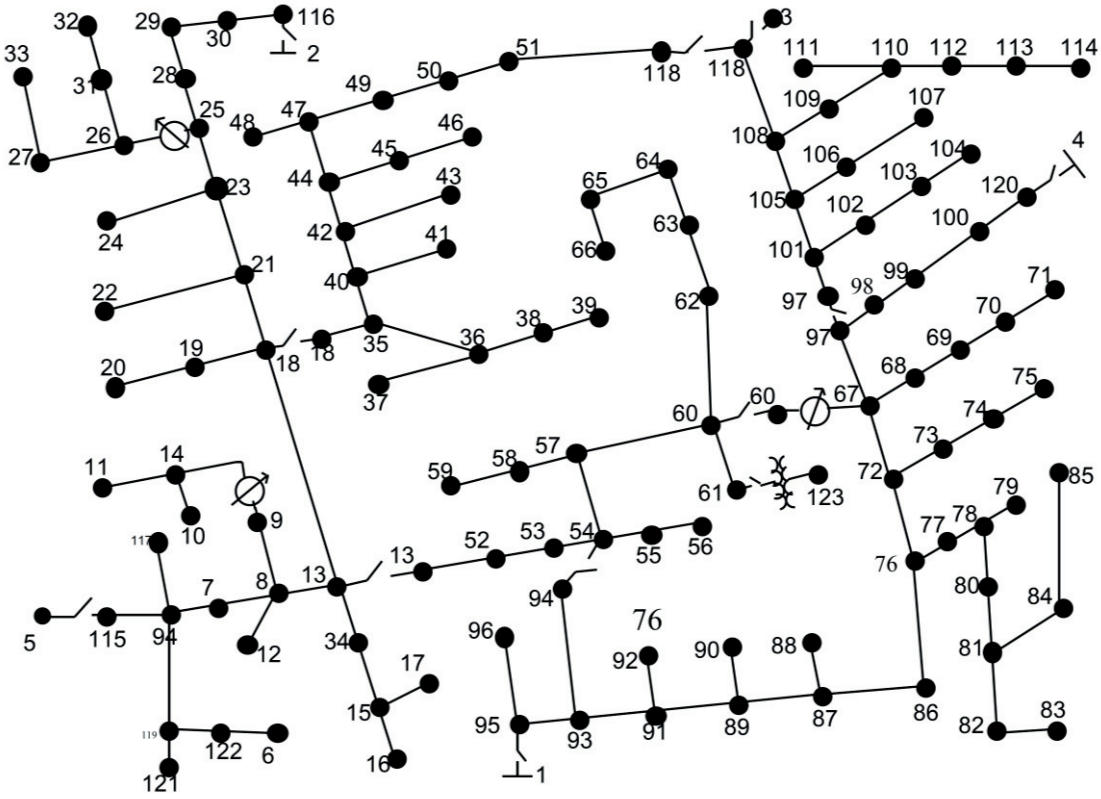

Fig. 2-10: IEEE 123 buses test case network.

voltages from the solution of the optimization problem are identical to those of a-posteriori load flow analysis.

Table 2-7: Identified optimal switches status

Switch	Status	Switch	Status
(#1, #95)	open	(#18, #35)	close
(#2, #116)	open	(#51, #118)	open
(#3, #118)	open	(#54, #93)	open
(#4, #120)	close	(#60, #67)	close
(#5, #115)	close	(#97, #101)	close
(#13, #52)	close		

Table 2-8: PV capacities in the IEEE 123 buses test network

Bus #	10	24	33	58	70	85	87	103	107	114
Capacity (kW)	457.8	320.5	549.4	412.08	686.8	274.7	183.15	503.6	366.3	412.08

In order to quantify the computation time of the targeted problem we report below the computational time. This shows that the proposed model is scalable to real large-scale networks and the solution of the optimization problem could be identified in a reasonable time. The formulated MISOCP problem is performed on a desktop PC with 16 GB RAM and Intel Xenon CPU E5-1650 @ 3.20 GHz and the average computation time for 10 runs is 2.88 seconds.

Table 2-9: Voltage magnitude comparison: load flow vs. optimal solution

Bus#	Voltage: optimal solution	Voltage: load flow solution	Bus#	Voltage: optimal solution	Voltage: load flow solution
1	1	1	77	0.9725	0.9725
95	0.9821	0.9821	64	0.9747	0.9747
93	0.9798	0.9798	67	0.9731	0.9731
96	0.982	0.982	73	0.9725	0.9725
91	0.9788	0.9788	78	0.9725	0.9725
54	0.9789	0.9789	65	0.9744	0.9744
89	0.978	0.978	68	0.9736	0.9736
92	0.9787	0.9787	97	0.9727	0.9727
53	0.9789	0.9789	74	0.9723	0.9723
55	0.9788	0.9788	79	0.9724	0.9724
57	0.9783	0.9783	80	0.9725	0.9725
87	0.977	0.977	66	0.9743	0.9743
90	0.9779	0.9779	69	0.9743	0.9743
52	0.9788	0.9788	98	0.9723	0.9723
56	0.9788	0.9788	75	0.9721	0.9721
58	0.9787	0.9787	81	0.9726	0.9726
60	0.9755	0.9755	70	0.9753	0.9753
86	0.9753	0.9753	99	0.9717	0.9717
88	0.9769	0.9769	82	0.9725	0.9725
59	0.9787	0.9787	84	0.9732	0.9732
61	0.9755	0.9755	71	0.9752	0.9752
62	0.9752	0.9752	100	0.9715	0.9715
76	0.9729	0.9729	83	0.9725	0.9725
123	0.9755	0.9755	85	0.9737	0.9737
63	0.975	0.975	120	0.9712	0.9712

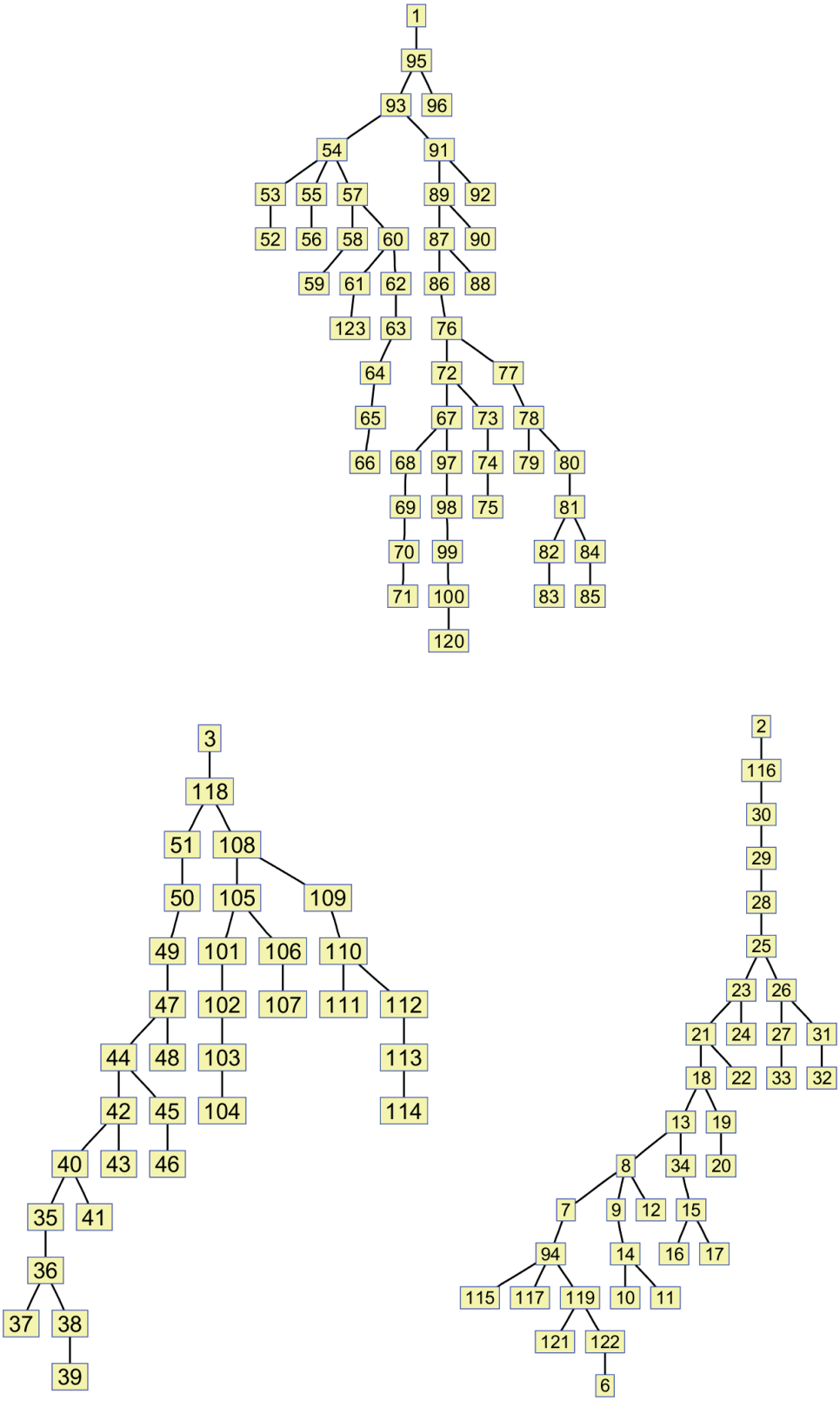

Fig. 2-11: IEEE 123 buses network with obtained switches status

2.4 Voltage Control of Active Distribution Networks Using Sensitivity Coefficients

2.4.1 Introduction and state-of-the-art

A widely used category of control approaches relies on the solution of linear problems by means of sensitivity coefficients. This approach has been also applied to control heterogeneous resources in ADNs by linearizing the dependency between nodal voltages and power flows as a function of the power injections (e.g.,[49] [50], [51], [52]).

In [50] a short-term scheduling procedure is proposed for optimal scheduling and control of ADNs. It is composed by two stages: a day-ahead scheduler for the optimization of distributed resources, an intra-day operator for every 15 minutes. The Authors of [51] proposed a methodology for congestion management in distribution networks. The methodology is based on the quantification of each generators' contribution to the constraints. These contributions are quantified based on voltage-sensitivities coefficients. The Authors of [53] proposed a low-overhead decentralized demand response control mechanism, to provide ancillary services to the ADNs by a seamless control of a large population of elastic appliances. They have linearized the targeted optimization problem using voltage sensitivity coefficients. Further, they have augmented their work in [54] to include the ESSs. In [52] a centralized model predictive control scheme is proposed to regulate distribution network voltages in the presence of high penetration of distributed generation. The Authors have used the voltage sensitivity coefficients to linearize the constraints of the problem.

Since in a subsequent part of this thesis we formulate an ESS planning strategy by relying on the concept of voltage sensitivity coefficients, we briefly illustrate their use in an ADN voltage control process.

In this section, we present a voltage control scheme for ADNs based on the voltage sensitivity coefficients. As known, each coefficient linearizes the dependency between the l_th bus voltage magnitude variation and the k_th bus injected active or reactive power variation. The typical procedure for the computation of these sensitivities is the use of an updated Jacobian matrix derived from the load flow problem (e.g. [55], [50]). An analytical expression of these coefficients, that does not use the load-flow Jacobian matrix, has been recently proposed in [49]. We employ this last method for the sensitivity computation.

2.4.2 Voltage control using sensitivity coefficients

The context of the problem refers to ADNs characterized by the presence of non-dispatchable generations without the possibility to take advantage of demand-side management. We assume to know the phasors of phase-to-ground voltages in all the network busses at a generic time as well as the "per-bus" aggregate power

injections/absorption. This information is assumed to be obtained via a state estimation algorithm (e.g., [56]). Within the context of voltage control in ADNs, it is important to point out that both active and reactive power injections play an important role for the regulation in view of the non-negligible ratio of longitudinal parameters of the medium and low voltage lines.

Knowing the state of the system (nodal voltages and injections) DNO computes the voltage sensitivity coefficients with respect to absorbed/injected power of a bus. The analytical expression of these coefficients as a function of system states and admittance matrix, has been recently proposed in [49] and reported below.

$$A^{P}_{l,k} = \frac{\partial \left|\bar{V}_l\right|}{\partial P_k} = \frac{1}{\left|\bar{V}_l\right|} \Re(\underline{V}_l . \frac{\partial \bar{V}_l}{\partial P_k}) \tag{2.135.a}$$

$$A^{Q}_{l,k} = \frac{\partial \left|\bar{V}_l\right|}{\partial Q_k} = \frac{1}{\left|\bar{V}_l\right|} \Re(\underline{V}_l . \frac{\partial \bar{V}_l}{\partial Q_k}) \tag{2.135.b}$$

where $\bar{V}_l$, and $\underline{V_l}$ are the voltage phasor of bus l, and relevant conjugate. The P_k and Q_k are the active and reactive power injections/absorption at bus k respectively.

It is therefore possible to compute the variation of the voltage magnitude at bus l due to the power absorption/injection at all buses:

$$\Delta\left|\bar{V}_l(t)\right| = \mathrm{A}^{P}_{l}(t)\Delta P(t) + \mathrm{A}^{Q}_{l}(t)\Delta Q(t) \tag{2.136}$$

where $\mathbf{A}^{P}_{l}(t)$ and $\mathbf{A}^{P}_{l}(t)$ are $[A^{P}_{l1}, \dots, A^{P}_{l,L}]$ and $[A^{Q}_{l1}, \dots, A^{Q}_{l,L}]$ respectively and $\boldsymbol{\Delta}\mathbf{P}(t) = [P_1(t), P_2(t), \dots, P_L(t)]$, $\boldsymbol{\Delta}\mathbf{Q}(t) = [Q_1(t), Q_2(t), \dots, Q_L(t)]$.

The optimization problem for the optimal voltage control (minimization of voltage deviation with respect to the rated value) can be formulated as follows (with ESSs as control resources):

$$\underset{\Xi}{\text{minimize}} \sum_{t}\sum_{l}\left(\Delta V_l(t) + V_l(t) - V^{r}\right)^2 \tag{2.137.a}$$

subject to:

$$\Delta V_l(t) = \mathrm{A}^{P}_{l}(t)\Delta P(t) + \mathrm{A}^{Q}_{l}(t)\Delta Q(t) \quad \forall l \in \mathcal{L}, t \in T \tag{2.137.b}$$

$$\Delta P_l(t) = P^{d}_{l}(t) - P^{ch}_{l}(t), \quad \Delta Q_l(t) = Q_l(t), \quad \forall l \in \mathcal{L}_s, t \in T \tag{2.137.c}$$

$$\Delta P_l(t) = 0, \qquad \Delta Q_l(t) = 0 \qquad \forall l \in \mathcal{L} / \mathcal{L}_{ess}, t \in T \tag{2.137.d}$$

$$\left(P^{d}_{l}(t) + P^{ch}_{l}(t)\right)^2 + \left(Q_l(t)\right)^2 \le \left(C_l\right)^2 \quad \forall l \in \mathcal{L}_{ess}, t \in T \tag{2.137.e}$$

$$E_l(t+1) = E_l(t) + \frac{P_l^d}{\eta_l^d} - P_l^{ch}\eta_l^{ch} \quad \forall l \in \mathcal{L}_{ess}, t \in T \tag{2.137.f}$$

$$E_l^{\min} \le E_l(t) \le E_l^{\max} \quad \forall l \in \mathcal{L}_{ess}, t \in T \tag{2.137.g}$$

$$P_i^d(t) \le u_i^d(t) C_l \quad \forall i \in \mathcal{L}_{ess}, t \in T \tag{2.137.h}$$

$$P_l^{ch}(t) \le u_l^{ch}(t) C_l \quad \forall l \in \mathcal{L}_{ess}, t \in T \tag{2.137.i}$$

$$u_l^{ch}(t) + u_l^d(t) \le 1 \quad \forall l \in \mathcal{L}_{ess}, t \in T \tag{2.137.j}$$

$$u_l^{ch}(t), u_l^d(t) \in \{0,1\} \quad \forall l \in \mathcal{L}_{ess}, t \in T \tag{2.137.k}$$

where $\Xi = \{\Delta P, \Delta Q, E, P^{ch}, P^d, Q, u^{ch}, u^d, \Delta V\}$ is the set of variables (recall that the notation without subscript represents the vector of the corresponding variables). l and t are the indices of buses (without slack bus) and the time respectively. $\mathcal{L}, \mathcal{L}_{ess}, \mathcal{L}/\mathcal{L}_{ess}$ are sets of network buses, buses with ESS, and buses without ESS, respectively. The control variables are the ESSs set points.

The objective function formulated in (2.137.a) minimizes the nodal voltage deviations with respect to the reference value (V^r). Equation (2.137.b) represents the total variation of the voltage at bus l due to the power absorption/injection at all buses. For this constraint, we assumed negligible variation of load/generation connected to the same bus l where *l-th* ESS is connected. Constraints (2.137.c) and (2.137.d) show that the nodal active/reactive variations ($\Delta P_l/\Delta Q_l$), result from the ESSs active/reactive (i.e., charging/discharging) productions ($P_l^{ch}(P_l^d)/\ Q_l$)). The ESSs capability curve and *SoC* constraints are modeled by (2.137.e) and (2.137.f) respectively (η_l^d, η_l^{ch} are charging and discharging efficiencies, and E_l represents the energy stored level in ESSs, $E_l^{\max}$ and $E_l^{\min}$ represent the upper and lower limits of ESS l *SoC*). The constraints (2.137.h)-(2.137.k) are added to the problem to ensure the operation of ESSs in only one state (charging or discharging). In the next section the formulated optimization problem is applied to a standard test case network and the results are presented and discussed.

2.4.3 Simulation results

This section presents the use of the proposed method with reference to a modified IEEE 13 buses test feeder. The schematic of this network is shown in Fig. 2-12. It is supposed that the network hosts non-dispatchable DG units composed by photovoltaic panels (PVs). Concerning the representation of the network loads, they are considered as voltage independent PQ absorption. The time series related to active load absorption refer to experimentally recorded data. The power factor of loads is considered constant during the whole time series. The power injections of PVs have been represented by voltage-independent active power injections with null reactive component. It is

assumed that the non-dispatchable PV injections are in correspondence of buses #646, #684, #675, and #633 with a maximum rated power of 400 kW each. The relevant time series make reference to real measured solar irradiation in the central region of Europe. The total load and PV generation curves are shown with reference to a one-day time horizon with 15 minutes' discretization. The available ESSs sites and sizes are shown in Table 2-10. The Cumulative Distribution Function of the nodal voltages are shown in Fig. 2-14 to demonstrate the effectiveness of the voltage control scheme. As it can be seen from this figure, the voltage deviations are significantly decreased (especially the ones that have high deviation magnitudes).

Table 2-10: ESSs sites and sizes

Bus number	#671	#684	#633	#645	#675
ESSs size (kVA/kWh)	310/631	100/290	150/365	100/250	200/464

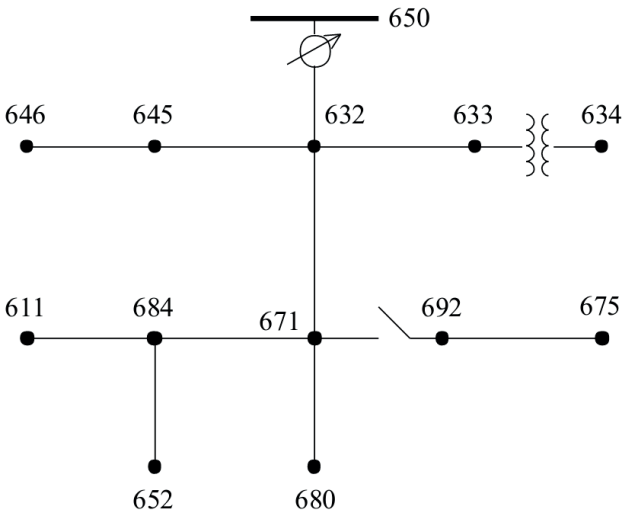

Fig. 2-12: Topology of the IEEE 13 bus test feeder. Adapted from [18].

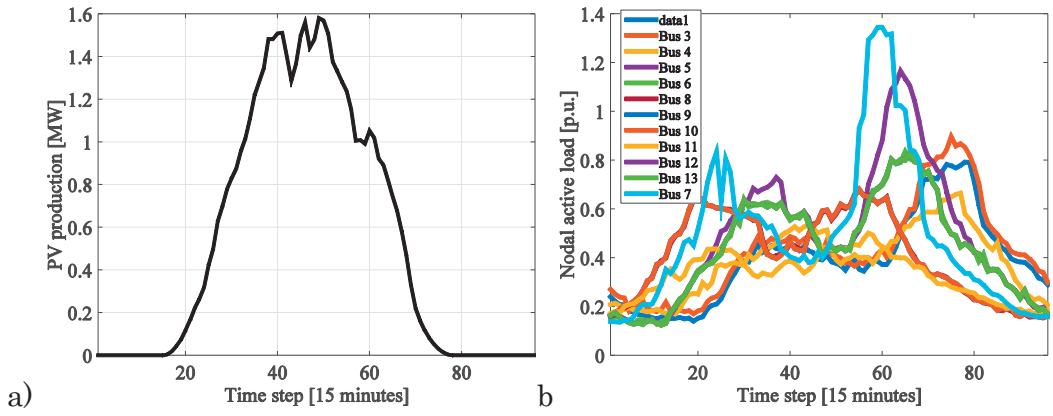

Fig. 2-13: Load and PV time series: a) PV profile b) load profile (base MVA = 2 MW)

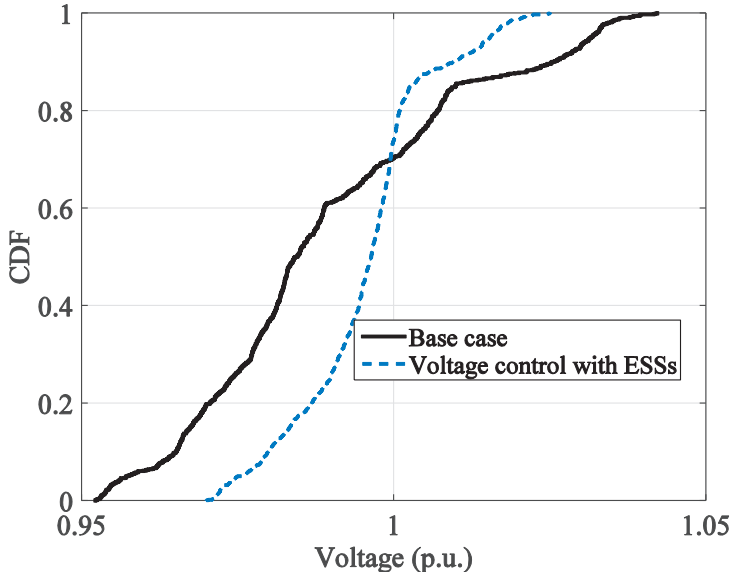

Fig. 2-14: Nodal voltages CDF with and without control action

2.5 Summary and Conclusion

In this chapter, we presented a new convex model for OPF problem (AR-OPF) in ADN. The AR-OPF takes into account the correct electrical model of the lines (classical two-port Π model) in addition to network security constraints (lines ampacity limit and nodal voltage magnitude upper and lower limits). We have derived sufficient condition under which the relaxation used in the AR-OPF is tight (i.e., the solution of the AR-OPF is exact). Further, we showed that the derived conditions holds for real distribution networks with large margins. Using a small benchmark network we presented the effectiveness of the AR-OPF and the shortcomings of the existing models to provide physically feasible solution.

Further in this chapter we made use of the AR-OPF to develop an optimization model for optimal reconfiguration of ADNs. The advantages of the developed model are i) convex model for OPF, ii) proper inclusion of lines ampacity limits, and iii) using the exact electrical model of the lines. We have shown the effectiveness of the proposed optimal ADN reconfiguration model in terms of optimality and feasibility.

Finally in the last part of this chapter, we presented an optimization model for voltage control using a linearized OPF. The linearized OPF is based on the voltage sensitivity coefficients.

3 Optimal Operation and Scheduling of Active Distribution Networks under Uncertainty

Chapter Highlights:

In this chapter, we investigate the inclusion of uncertainties in the optimal day-ahead scheduling of ADNs. In this respect, we first formulate a dedicated two-stage optimization problem for the day-ahead multi period optimal scheduling of ADNs in presence of ESSs. In this optimization problem, the daily forecast curves related to load consumption and PV production are subject to uncertainty. Then, adaptive robust optimization and stochastic optimization techniques are suitably casted to solve the developed optimization problems. The IEEE 34 buses test case network is used to demonstrate the effectiveness of the proposed robust and stochastic methods.

3.1 Chapter Organization

The sources of uncertainties in ADNs are related to the forecast errors of stochastic DG (mainly PV) production, demand and network parameters. In this work, the focus is on the uncertainties of loads and PVs (i.e., in general, on the uncertainties of nodal power absorptions/injections). Intuitively, their day-ahead and intra-day forecasts errors impact the ADN operation, particularly when the PV penetration level is high causing financial and technical problems to DNOs. The focus of this chapter is on the day-ahead forecasting errors. We investigate two general ways to take into account the above uncertainties: i) Adaptive Robust Optimization (ARO) and ii) stochastic optimization. In the following, first the typical Autoregressive Integrated Moving Average (ARIMA) model for PV and load forecasting is briefly introduced. Then, the ADN day-ahead scheduling problem is formulated as a two-stage optimization problem. Later, sections 3.4 and 0 present the use of ARO and stochastic optimization techniques to solve this targeted two-stage optimization problem. A brief comparison between ARO and stochastic optimization techniques is provided in section 3.6. The chapter is concluded with a summary of main findings in section 0.

3.2 Load and PV forecasting methods

The aim of this section is to illustrate a typical approach to forecast daily load and PV profiles. The presence of this section is justified since ARO and stochastic optimization frameworks require the knowledge, to some extent, of the distribution of the uncertain parameters. Therefore, we make reference to the well-known ARIMA forecasting tool. Although in day-ahead scheduling the load is discretized on the hourly basis, the intra-day deviations are quantified on 15 minutes basis. For this reason, we have used the 15 minutes interval to discretize the forecasted time-series. The uncertain parameters have temporal and spatial correlations. In order to consider the spatial correlation, we have considered that the PV profiles have the same variation for all the buses of the system. This is justified since distribution networks are characterized by limited area. Additionally, as we solve the intra-day operation with 15 minutes step, this is sufficient to filter all nodal PV relative variations. For the nodal loads, we assumed spatial correlation only for the same kind of loads (i.e., residential, commercial, and industrial). We use ARIMA time-series forecasting method, trained with experimentally obtained data, to consider the temporal correlation.

Photovoltaics (PV) is the fastest-growing renewable energy production technology since 2002, particularly for the case of distribution networks [57]. However, the forecasting methods for PV are not yet mature enough in contrary to the case of wind power. Recent researches has been concentrated on forecasting solar irradiation, whereas few works focus on prediction of PV production and even less on uncertainty estimation of the predictions [57]. Time series methods are one of the classical PV forecasting tools [58, 59]. However, an appropriate model for day-ahead forecasting of PV requires, to some extent, knowledge of cloud cover and their movements [57].

Nowadays, hybrid models are developed that incorporate the data of the satellite images and weather forecasting tools with statistical methods (like time-series and/or neural network) to effectively predict the day-ahead PV profile [60, 61]. A multiplicative ARMA model to generate instantaneous series of global irradiation is presented in [62]. The developed model is based on removing the annual periodicity and seasonal variation of solar radiation and fitting an AR model to the data. In [63], a two-stage PV forecasting method is proposed where statistical normalization of the solar power is obtained using a clear sky model. The forecasts of the normalized solar power are calculated using an adaptive linear time series model. A medium-term solar irradiance forecasting model is presented in [64] by adopting predicted meteorological variables as inputs to an Artificial Neural Network (ANN) model. A seasonal ARIMA time-series analysis is developed in [65] in order to forecast the power output of a PV site. The developed model is improved by incorporating short-term solar radiation forecasts derived from numerical weather prediction models. In this thesis the basic ARIMA model is used for forecasting the PV data since the data of satellite images and weather parameters are not practically available. A model-free approach for ultra-short-term prediction of solar irradiance is proposed in [66]. It is independent from i) the method used for point-forecast of solar irradiance and ii) the error distribution of the point forecast method.

On the other hand, the existing literature concerning the load forecast is quite rich [67]. There are several methods for short-term (i.e., day-ahead) load forecasting that can effectively forecast the day-ahead load profiles. Neural network [68] and time series methods [69] are the most sophisticated and utilized models. In [70] it is proposed a load forecasting technique based on a nonlinear generalization of Box and Jenkins approach for nonstationary time-series. A self-supervised adaptive neural network for short term load forecasting is presented in [68]. The Authors have used the self-supervised network to extract the correlational features from temperature and load data. The Authors of [71] proposed a forecasting model based on the linear regression analysis of previous load and weather data. The normal load model and the weather-sensitive component of the load are estimated using the parameters of regression analysis. In [72] a two-stage integrated price and load forecasting framework is proposed. The first stage provides initial price and load forecasts separately. The second stage considers load and price interaction with initial forecasts as inputs. At each stage, a hybrid time-series and adaptive wavelet neural network model is used, in which ARIMA model catches the linear dependencies between the price and load time series. In this work we used the standard ARIMA model as a tool for demand forecasting.

3.2.1 The ARIMA forecasting tool

A time series is a sequence of data over a time interval. Under the hypothesis that future values of a time series depend on its previous ones, it is possible to build specific

tools accounting for this correlation. In this respect, a model is first built based on the previous data and, then, the future values are predicted using the developed model. We have used Auto-regressive Integrated Moving Average (ARIMA) to forecast the load and PV profiles since they have been extensively used for these purposes and they also allow a simple quantification of the distribution of the forecasting errors. In the following, the ARIMA process is briefly described for the sake of clarity and introduction of the nomenclature.

The Auto-regressive (AR) models a time series where the future data are a linear combination of its previous values [73]. An AR model of order m (the future data depends on its m previous values) is shown in (3.1).

$$\hat{y}(t) = -\sum_{i=1}^{m} \alpha_{it} y_{t-i} + \psi_t \tag{3.1}$$

where $\hat{y}(t)$ is the forecasted load at time t, ψ_t is the random disturbance and α_{it} represents the random coefficients. Least Mean Square (LMS) method is normally used to tune the random coefficients [74].

The Auto-regressive Moving Average (ARMA) predicts the future values of a time series as a linear function of the previous data and previous values of a white noise $[a(t), a(t-1), ...]$. The ARMA model of order (p, q) is shown in (3.2).

$$y(t) = \phi_1 y(t-1) + ... + \phi_p y(t-p) + a(t) - \theta_1 a(t-1) - ... - \theta_q a(t-q) \tag{3.2}$$

Recursive scheme and maximum-likelihood approaches are mostly used for ARMA parameter identification [73]. The following lag operator is defined to condense the notation and solve linear difference equations:

$$B^i y(t) = y(t-i) \tag{3.3}$$

$$\phi(B) = 1 - \phi_1 B - \phi_2 B^2 - ... - \phi_p B^p \tag{3.4}$$

$$\theta(B) = 1 - \theta_1 B - \theta_2 B^2 - ... - \theta_q B^q \tag{3.5}.$$

The final ARMA formulation is shown in (3.6).

$$\phi(B) y(t) = \theta(B) a(t) \tag{3.6}$$

In case of non-stationary process, it is necessary to transform the series to a stationary form. Let define ∇ operator as: $\nabla y(t) = (1 - B) y(t)$. Then, a series with AR and MA orders equal to p and q, that needs to be differentiated d times, known as Auto-Regressive Integrated Moving-Average (ARIMA(p, q, d)) can be written as (3.7)

$$\phi(B) \nabla^d y(t) = \theta(B) a(t) \tag{3.7}$$

ARIMA is capable of modeling seasonal data. It is possible to include the seasonal terms in the ARIMA model as shown in (3.7). The seasonal ARIMA is written as ARIMA $(p,d,q)(p_s,d_s,q_s)$ where s is the number of periods per season. Finally, the general formulation of ARIMA model, which includes differencing, multiplicative seasonality and seasonal differencing is as follows:

$$\phi(B)\nabla^{d}\Theta(B)\nabla^{d_s}y(t)=\theta(B)\Theta(B)a(t) \tag{3.8.a}$$

$$\phi(\mathrm{B})=1-\phi_1 B^{s}-\ldots-\phi_{p_s}B^{p_s s} \tag{3.8.b}$$

$$\Theta(\mathrm{B})=1-\Theta_1 B^{s}-\ldots-\Theta_{q_s}B^{q_s s} \tag{3.8.c}.$$

In this study, we use the basic ARIMA model as formulated in equation (3.8.a). In this respect, the distribution is considered to be non-stationary (it can be transformed to a stationary one with an initial differencing step) and non-*iid* (independent and identically distributed).

3.2.2 Load and PV forecasting using the ARIMA model

Five days of experimentally recorded data of a region in Southern-east part of Switzerland is used to model the demand profile[1]. The data are categorized based on two types of demand: i) residential ii) commercial/industrial. The recorded data of 4 days is shown in Fig. 3-1.a. These 4 profiles are used to train the ARIMA model and predict the load for 5th day (see Fig. 3-1.b). The average of 15 minutes errors in comparison with the real data over 96 time periods (each 15 minutes) are calculated as (3.9). In this equation s_t^f and s_t^r are the forecasted and actual demands at time step t.

$$MDE_D=\frac{1}{96}\sum_{t=1:96}\left|\frac{\left(s_t^f-s_t^r\right)}{s_t^r}\right| \tag{3.9}$$

The MDE (MDE : Mean Day Error) for the forecasted commercial and residential load profiles shown in Fig. 3-1.b are equal 5% and 9% respectively.

Similar to the load profiles, the recorded PV profiles shown in Fig. 3-2.a are used to create an ARIMA model and forecast the PV profiles shown in Fig. 3-2.b. It should be noted that two categories of PV profiles are taken into account, i) partially cloudy sky (Fig. 3-2.1), and clear sky (Fig. 3-2.2). The MDEs for the forecasted PV profile shown in Fig. 3-2 are equal 20.3% and 2.1% for partially cloudy and clear sky, respectively.

[1] It should be noted that, more available data lead to better prediction. Unfortunately, we had access to only one week of data.

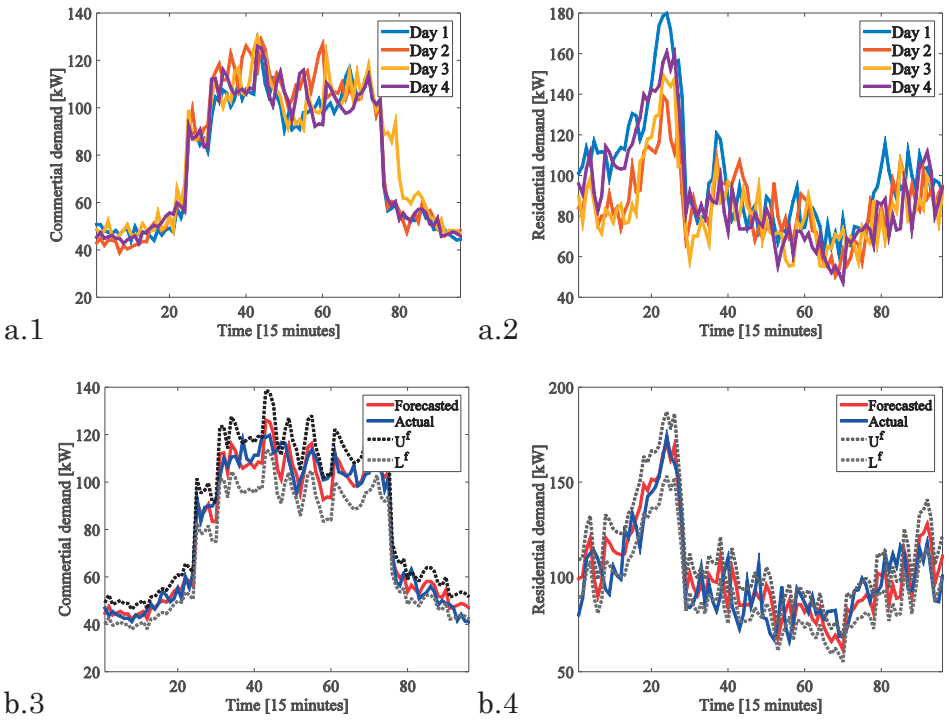

Fig. 3-1: Load forecast using ARIMA a) load profiles used to train the ARIMA , 1. commercial 2. Residential, b) forecasted and actual day-ahead load profiles, 1. commercial 2. Residential (U^f and L^f are upper and lower bounds of confidence interval with $\pm 7\%$ and $\pm$ 10% error intervals for commercial and residential loads, respectively)

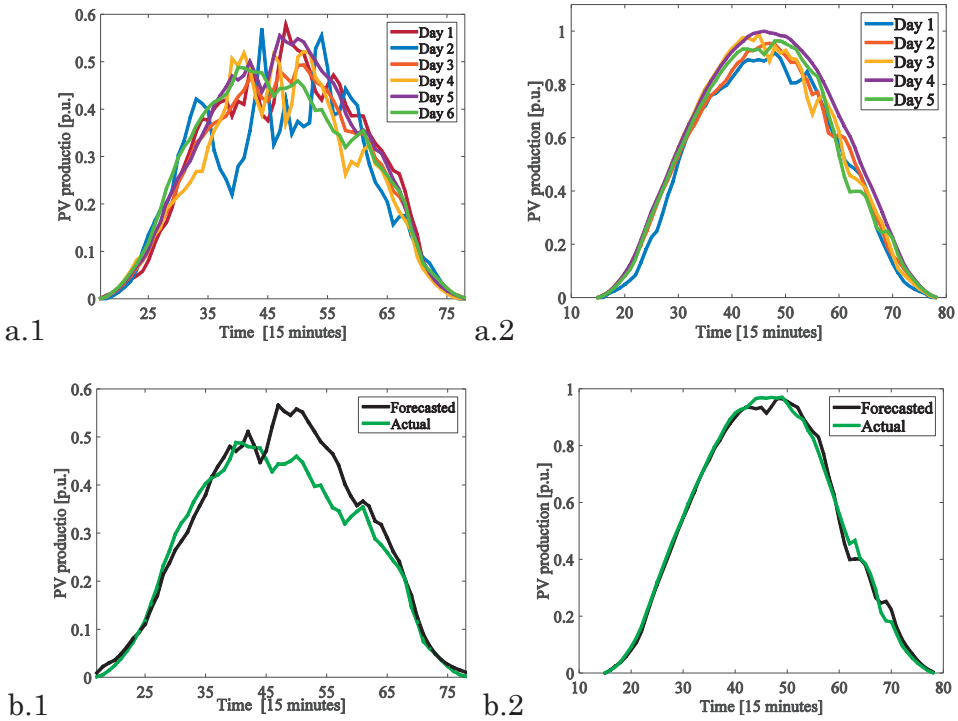

Fig. 3-2: PV forecast using ARIMA in p.u. of total capacity: a. PV profiles used to train the ARIMA (1. partially cloudy sky, 2. clear sky) b. forecasted and actual day-ahead PV profiles (1. partially cloudy sky, 2. clear sky)

3.3 Two-stage Optimization Problem for Day-ahead Scheduling of Active Distribution Networks

The targeted optimization problem is the day-ahead scheduling of an ADN under uncertainty. It is modeled as a two-stage optimization programming.

The decisions of the first stage are made when the random parameters are unknown. In the context of our targeted problem, they deal with the day-ahead decision variables. The first-stage decisions determine the amount of import/export energy from the external grid at each hour and ESSs set points.

The second stage deals with the intra-day decisions variables, given the first stage decisions. The objective function includes cost of deviations from day-ahead energy import/export scheduling, rescheduling cost of ESS units, and deviation cost of nodal voltage magnitudes. The control variables are the ESSs set-points.

3.3.1 First stage formulation

The first stage or the day-ahead scheduling problem is formulated as following.

$$\underset{\tau,\delta,p^{ch},p^{d},q}{\text{minimize:}} \sum_{t}\left(\delta^{DA}(t)\pi(t)+\sum_{l}\left(\Gamma^{\text{ess}}\left(p_l^{ch}(t)+p_l^{d}(t)+\left|q_l(t)\right|\right)\right)\right) \tag{3.10.a}$$

subject to:

$$\Upsilon(\tau(t),\vartheta(t))\geq 0,\quad \forall t\in T \tag{3.10.b}$$

The objective function is to minimize the cost of energy import from the external grid and the ESSs operation one. The operation cost of the ESSs is modeled as in (3.11).

$$C_{ess}=\Gamma^{\text{ess}}\left(p^{ch}+p^{d}+\left|q\right|\right) \tag{3.11}$$

where p_{ch} and p_d are the active power charge and discharge variables, q is the reactive power output of ESS units, and Γ^{ess} is a linear increasing function in $p^{ch}, p^{d}, |q|$.

The energy price and the day-ahead energy import scheduling, are represented by $\pi(t)$, and $\delta^{DA}(t)$, respectively.

For the sake of brevity, the set of load flow, grid security (nodal voltages and lines ampacity limits), and ESSs (capability curve, *SoC*, and energy reservoir capacity) constraints are represented with $\Upsilon(\tau,\vartheta)\geq 0$. τ is the vector of variables (square of nodal voltages, lines complex power flows and current flow, square of current flow producing losses, ESSs active and reactive power outputs, energy level of ESSs) and ϑ is the vector of parameters (nodal load, nodal voltages upper and lower limits, lines ampacity limit,

ESSs power rating and energy reservoir capacities). These constraints are further described in section 3.4.3.1.

The first stage optimization problem is represented in matrix form as following:

$$\overbrace{\underset{x}{\text{minimize}}\left(c_x^T x\right)}^{F(x)} \tag{3.12.a}$$

subject to:

$$Ax = \Psi \tag{3.12.b}$$

$$Gx \le g \tag{3.12.c}$$

3.3.2 Second stage formulation

The second stage optimization problem is formulated as following:

$$\underset{\substack{\tau,d^G,u^G,v,u^{p,ch},u^{p,d},u^{q,p}\\ u^{q,n},d^{p,ch},d^{p,d},d^{q,p},d^{q,n}}}{\text{minimize}} : \sum_t (+\pi^-(t)d^G(t) - \pi^+(t)u^G(t))\Delta t + W_v \sum_l \sum_t \left(\left(v_l(t) - v_{thr}^{\max} : \left(v_l(t) \ge v_{thr}^{\max}\right)\right) + \left(\left(v_{thr}^{\min} - v_l(t)\right) : \left(v_l(t) \le v_{thr}^{\min}\right)\right)\right) + \sum_t \sum_{\mathcal{L}_{ess}} \Gamma^{ess} \left(\left(d_l^{p,ch}(t) + d_l^{p,d}(t) + d_l^{q,p}(t) + d_l^{q,n}(t)\right) - \left(u_l^{p,ch}(t) + u_l^{p,d}(t) + u_l^{q,p}(t) + u_l^{q,n}(t)\right)\right)\Delta t \tag{3.13.a}$$

$$\Upsilon(\tau, \vartheta) \ge 0, \quad \forall t \in T \tag{3.13.b}$$

$$s^r(t) = s^{r,f}(t) + \Delta s^r(t) \quad \forall t \in T \tag{3.13.c}$$

$$s^c(t) = s^{c,f}(t) + \Delta s^c(t) \quad \forall t \in T \tag{3.13.d}$$

$$s^{pv}(t) = s^{pv,f}(t) + \Delta s^{pv}(t) \quad \forall t \in T \tag{3.13.e}$$

The second stage is also a multi-period OPF problem where DistFlow equations with inclusion of transverse parameters are used to model the load flow constraints. The objective function includes minimization of: i) nodal voltages deviations, ii) deviations from day-ahead scheduling and ii) cost of rescheduling of ESSs.

The $u_l^{p,ch}/u_l^{p,d}(d_l^{p,ch}/d_l^{q,d})$ are the charge/discharge upward (downward) variables for the active power outputs of ESSs, respectively. The $u_l^{q,p}/u_l^{q,n}(d_l^{q,p}/d_l^{q,n})$ are the positive/negative upward (downward) variables for the reactive power output of ESSs, respectively. The d^G and u^G represent down and up deviations from day-ahead energy schedule. W_v is the weighting coefficient of voltage deviation cost.

$v_{thr}^{max}, v_{thr}^{min}$ are the square of voltage magnitude thresholds (upper and lower) beyond which the voltage magnitudes deviations with respect to the $v_{thr}^{max}/v_{thr}^{min}$ are minimized.

We have considered three sets of uncertainties, residential load, commercial load, and the PV production as shown in (3.13.c), (3.13.d) and (3.13.e), respectively. The forecasted load and PV profiles and their respective variations are represented by $s^{r,f}(t)/\Delta s^{r}(t)$, $s^{c,f}(t)/\Delta s^{c}(t)$, and $s^{pv,f}(t)/\Delta s^{pv}(t)$, respectively. $s^{r}(t)$, $s^{c}(t)$, and $s^{pv}(t)$ are the aggregated residential, commercial loads and PV production at each time step (t), respectively.

The total load and PV are distributed among the network buses based on their nodal residential/commercial active load, PV production, and residential/commercial reactive load coefficients.

The second stage optimization problem is represented in matrix form as following:

$$\overbrace{\left(\underset{y}{\text{minimize}}\left(c_y^T y\right)\right)}^{H(y)} \tag{3.14.a}$$

subject to:

$$Py = \Delta\Psi + \Psi \tag{3.14.b}$$

$$My + Rx = e \tag{3.14.c}$$

$$Dy \leq d \tag{3.14.d}$$

$\Psi + \Delta\Psi$ is the vector of uncertain parameters (Ψ is the day-ahead forecast and $\Delta\Psi$ represents the corresponding variations), y is the vector of variables in the second stage. The equality constraints of the second stage minimization are divided into two sets i) those that have uncertainty (nodal PV and load) and are shown in (3.14.b), and ii) those that don't have uncertainty (DistFlow, ESSs, and grid security constraints) and are shown in (3.14.d). In the following two techniques are suitably casted to deal with the uncertainties in the equation (3.14.b). In particular, ARO is used to deal with the worst-case realization of the uncertain parameters whereas stochastic optimization is employed to deal with the uncertainties using scenarios sampled from the PDF of uncertain parameters.

3.4 Adaptive Robust Optimization for Day-ahead Scheduling of Active Distribution Networks

Recently, Robust Optimization (RO) methods have gained attention in power systems optimization problems since they allow to deal with the uncertainties and stochasticity of the parameters. The RO needs moderate information (mean value and range of

variation) regarding the stochastic parameters. Additionally, RO provides an immune solution against all realizations of uncertain data within the deterministic uncertainty set. This latter element is the key difference between the RO and stochastic optimization. Indeed, RO provides a solution considering the worst case realization of the uncertain parameters, whereas the stochastic programming provides a solution with respect to probability of the considered scenarios.

In the following, a literature review regarding the application of RO in power system optimization problems is presented. Afterwards, we propose a model to build the uncertainty set for the load and PV profiles. Then, Adaptive Robust Optimization (ARO) applied to the problem of ADN day-ahead scheduling, described in section 3.3, is presented. Finally, the solution approach adapted to solve the proposed ARO model is described.

3.4.1 State-of-the-art of robust optimization in power system optimization problems

The RO has been widely used in power system optimization problems as suitably coupled with planning and operation objectives. The Authors of [75] presented a RO approach for the *transmission network expansion planning*. The presented model is formulated as a tri-level programming problem. The upper level minimizes the investment and operation costs. In the middle level, the contingencies leading to maximum power imbalances are identified. The lower-level problem minimizes the power imbalances following a given contingency. The RO has been also applied to energy storage planning in a transmission network with high level of renewable energy [76]. The Authors used a RO approach to minimize the investment cost of storage units while guaranteeing a feasible system operation, without load or renewable power curtailment.

The RO is also applied to *Security Constrained Unit Commitment* (SCUC) and day-ahead Economic Dispatch (ED) problems. The Authors of [77] have used an ARO for the ED problem with high level of wind penetration. They proposed an ARO model for multi-period economic dispatch problem and also introduced the concept of dynamic uncertainty set to model temporal and spatial correlations of stochastic parameters. In [78] a two-stage adaptive robust unit commitment model for the SCUC problem with uncertain nodal injections (wind power and price responsive demand) is presented. The Authors proposed a solution methodology based on a combination of the Benders decomposition and the Outer approximation techniques. A RO approach is proposed in [79] to accommodate wind power output uncertainties in the *day-ahead market* that tries to minimize the total cost under the worst wind power output scenario. The Authors in [80] have presented a sparse formulation and solution for the affinely adjustable robust counterpart (AARC) of the multi-period OPF problem. The objective of AARC is to operate a storage portfolio via receding horizon control. It provides the

optimal set-points and reserve participation factors of conventional generation and storage units for the forecasted load and renewable generation profiles.

The RO has been also used in context of *offering strategy of energy providers* [81], *demand response management* [82], and *contracting strategies for renewable resources* [83]. It also has been applied to some of the *distribution network optimization problems*. A two-stage RO model is proposed in [84] for distribution network reconfiguration with load uncertainty. The first-stage decision determines the topology of the network whereas the second-stage performs AC-OPF for the worst demand realization. The Authors of [85] proposed a RO planning strategy for siting, sizing, and choosing of dispatchable and intermittent DGs. The costs included in the objective function are investment, operation, maintenance, fuel and emission costs of DGs whereas the revenues come from selling energy. A RO programming for bidirectional dispatch coordination of a large-scale V2G is presented in [86].

In this work we develop an ARO model for day-ahead scheduling of an ADN with presence of PV and ESSs.

3.4.2 Dynamic uncertainty set for ARO

The so-called uncertainty set is the building block of the RO and has a direct impact on its performance. An appropriate uncertainty set has to i) balance between the robustness and the conservativeness of the solution ii) capture the significant aspects of the uncertainties, and iii) be computationally tractable [77]. It should be noted that the DGs are considered to be non-dispatchable and there is no possibility to use demand response.

A simple static uncertainty set applied to robust scheduling of an ADN could be constructed based on the confidence intervals of the total load (commercial and residential) and PV forecasting errors as shown in(3.15).

$$\underline{\zeta}^{c}(t) \le \Delta s^{c}(t) \le \overline{\zeta}^{c}(t) \tag{3.15.a}$$

$$\underline{\zeta}^{r}(t) \le \Delta s^{r}(t) \le \overline{\zeta}^{r}(t) \tag{3.15.2}$$

$$\underline{\zeta}^{pv}(t) \le \Delta s^{pv}(t) \le \overline{\zeta}^{pv}(t) \tag{3.15.c}$$

where $\underline{\zeta}^{c}(\overline{\zeta}^{c}),\underline{\zeta}^{r}(\overline{\zeta}^{r}),\underline{\zeta}^{pv}(\overline{\zeta}^{pv})$ are the forecast confidence intervals lower (upper) bounds for commercial load, residential load, and PV production, respectively. $\Delta s^{c},\Delta s^{r},\Delta s^{pv}$ are the commercial load, residential load and PV production variations with respect to their forecasts. The above uncertainty sets are conservative and, in general, unrealistic since the worst case will not happen for all the forecasted time intervals (it does not consider the temporal correlation between the errors). Demand uncertainty is usually less

dynamic than PV output and a static uncertainty set could be an appropriate model. In this work we used a static uncertainty set for the commercial and residential load profiles. However, an uncertainty budget as in (3.16) is introduced to limit the total deviation of the load profiles (for both commercial and residential). Furthermore, the forecast confidence intervals for the loads are obtained assuming a fixed level of error for each time step.

$$L^c \le \sum_t \Delta s^c(t) \le U^c \tag{3.16.a}$$

$$L^r \le \sum_t \Delta s^r(t) \le U^r \tag{3.16.b}$$

The same approach has been used for PV forecast in case of clear sky, since its uncertainty is not dynamic.

On the other hand, the uncertainty set of PV production, in case of partially cloudy sky, is very dynamic i.e., the uncertainty of each time step depends on its previous values.

The first step in building an appropriate uncertainty set is to determine the forecast confidence interval for each time step $(\overline{\zeta}^{pv}(t), \underline{\zeta}^{pv}(t))$. After fitting a model, it is important to have an index for the variability of what is still unknown. The variances of the error terms could be used to measure these uncertainties. We use the square mean error of the forecast $(\sigma^2(t))$ to estimate the variances. Assuming that the error of the forecast follows a normal distribution, the uncertainty index is defined as $\zeta^{pv}(t) = z\sigma^2(t)$ where $z = \Phi^{-1}(\alpha)$ and α is the level of confidence. The upper and lower bounds of the confidence intervals are calculated as shown in Fig. 3-3.

$$\overline{\zeta}^{pv}(t) = s^{pv,f}(t) + \zeta^{pv}(t) \tag{3.17.a}$$

$$\underline{\zeta}^{pv}(t) = s^{pv,f}(t) - \zeta^{pv}(t) \tag{3.17.b}$$

where $s^{pv,f}(t)$ is the forecasted PV production at time step t.

The upper and lower bounds of the 95% confidence interval $(\alpha = 0.95 \Rightarrow z = 1.64)$ for the forecasted PV of a partially cloudy sky, depicted in Fig. 3-2.b.i, are shown in green and red dashed lines in Fig. 3-3.

As previously observed, a RO with the upper and lower bounds shown in Fig. 3-3 is a conservative model. Fig. 3-4 shows the square mean error of the forecasts with 95% confidence interval. As it can be seen, the cumulative error of the 15 minutes forecasts inside one hour is almost twice as the corresponding hourly forecast. It can be explained by the fact that the per hour variance is 4 times the 15 minutes variance, thus the

standard deviation is doubled. Hence, we have created the following uncertainty budget based on the hourly forecast. In particular, the sum of the variations of the time intervals (each 15 minutes) inside one hour is limited by the corresponding hourly confidence interval.

$$-\underline{\zeta}_h^{pv}(h) \le \sum_{t \in H_t} \Delta s^{pv}(t) \le \overline{\zeta}_h^{pv}(h) \tag{3.18}$$

where h is the index of hours, t is the index of time intervals (15 minutes), and H_t is the set of time intervals inside one hour.

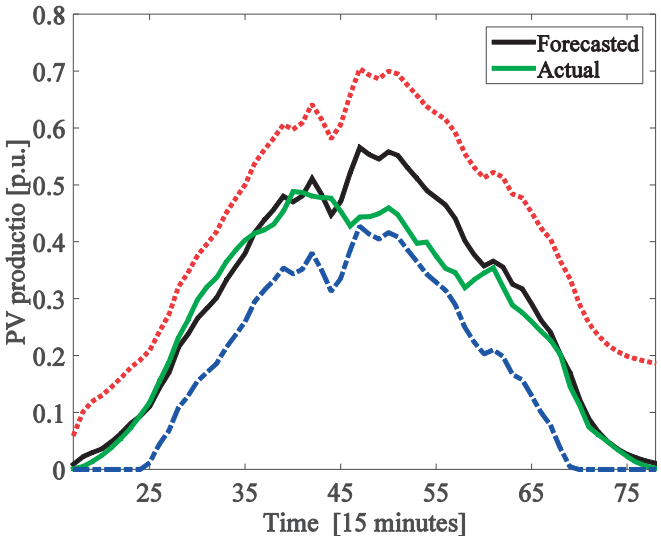

Fig. 3-3: Approximated confidence intervals of PV forecast

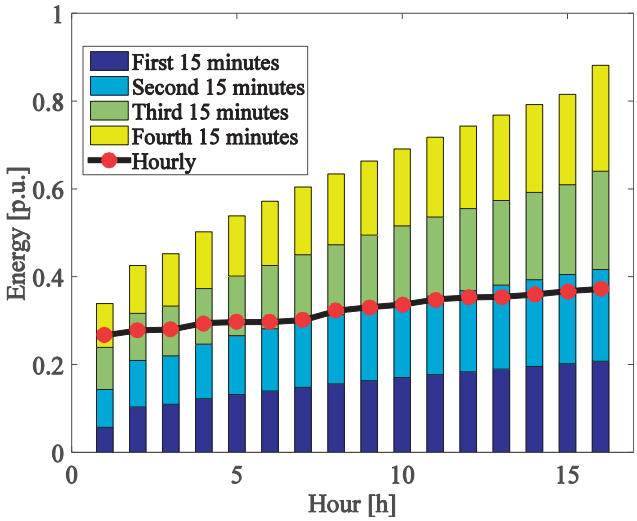

Fig. 3-4: Estimated level of errors for hourly and 15 minutes forecast intervals

Another important observation in Fig. 3-4 is that the estimated level of variations of the PV production is a monotonous increasing function over time. This is due to the fact that the forecasts for the earlier time intervals are relying more on the real data from the day before, whereas the forecasts for the later times are relying more on the forecasts of the earlier time intervals which are less accurate in comparison to the real data. Finally, it is worth to mention that the analysis is on daily basis and it is reset in correspondence of the daily optimization horizon.

3.4.3 ARO problem formulation

The targeted optimization problem is the day-ahead scheduling of an ADN under uncertainty. It is modeled as a two-stage optimization programming, as described in section 3.3.

Given the first stage decisions, the operation cost of the network is minimized for the worst case realization of the stochastic parameters (load and PV).

The DistFlow, with inclusion of transverse parameters, is used here (equations (2.12.a) -(2.12.b)) to model the power flow equations. The optimization problem has the form of $\min_{x}\left(\max_{\Delta\Psi}\left(\min_{y}\mathfrak{X}(x,\Delta\Psi,y)\right)\right)$. In another words, it minimizes the first (day-ahead scheduling) and second stage (intra-day operation) costs while the uncertainties (load and PV forecast errors) are maximally affecting the second stage cost function. The control variables in the first stage are the ESS set points and the hourly energy import/export scheduling, whereas in the second stage, they are the ESSs set points. The general form of the adopted ARO model for the ADN day-ahead scheduling is shown in (3.19) (The ESS model and the linearized DistFlow constraints are described later in 3.4.3.1).

$$\overbrace{\underset{x}{\text{minimize}}\left(c_x^T x\right)}^{F(x)}+\overbrace{\underset{\Delta\Psi}{\text{maximize}}\left(\overbrace{\underset{y}{\text{minimize}}\left(c_y^T y\right)}^{H(y)}\right)}^{G(\Delta\Psi)} \tag{3.19.a}$$

$$\text{s.t.}\quad Py=\Delta\Psi+\Psi \quad :\lambda_1 \tag{3.19.b}$$

$$My+Rx=e \quad :\lambda_2 \tag{3.19.c}$$

$$Dy\le d \quad :\mu \tag{3.19.d}$$

$$\text{s.t.}\quad B\Delta\Psi\le b \tag{3.19.e}$$

$$\text{s.t.}\quad Ax=\Psi' \tag{3.19.f}$$

$$Gx\le g \tag{3.19.g}$$

where x is the vector of variables in first stage, $F(x)$ (day-ahead scheduling), and (3.19.f), (3.19.g) are its set of equality and inequality constraints, respectively. The maximization in the middle, called $G(\Delta\Psi)$, maximizes the minimum of intra-day operation cost over the set of uncertainties. $\Delta\Psi$ is the vector of variables representing the uncertain parameters and the(3.19.e) models the uncertainty sets. Finally, y is the vector of variables in the second stage, $H(y)$(intra-day operation). Equations (3.19.b)-(3.19.d) are the constraints of the second stage minimization. The equality constraints of the second stage minimization are divided into two sets i) those that have uncertainty (nodal PV and load) and are shown in (3.19.b), and ii) those that don't have uncertainties (DistFlow, ESSs, and security (voltage and ampacity limits) constraints) constraints) and are shown in (3.19.c). The Lagrange multipliers associated to the constraints (3.19.b), (3.19.c), and (3.19.d) are represented by λ_1, λ_1, and μ respectively.

The first stage minimization ($F(x)$) is the multi-period OPF problem. The scheduling is done on 15 minutes basis, however the energy import scheduling is determined hourly, since the day-ahead markets are hourly basis. The load flow constraints are modeled using the DistFlow ones (see equations (2.12.a)-(2.12.b)). Other constraints are, nodal voltages limits, feeder ampacity limits, and ESSs ones (the ESSs constraints are formulated later as shown in section 3.4.3.1). The objective function is to minimize the load supply cost as well as the ESSs operation one.

The middle stage programming $G(\Delta\Psi)$, maximize the minimum cost of the ADN operation concerning the worst case realization of the uncertain parameters represented by $\Delta\Psi + \Psi$ (load and PV). The uncertainty sets are modeled as described in section 3.3.2.

The second stage is also a multi-period OPF problem where DistFlow equations with inclusion of transverse parameters are used to model the load flow constraints. Its objective function is to minimize the cost of operation in case of the worst case realization of the uncertain parameters ($\Delta\Psi + \Psi$). It includes minimization of: i) nodal voltages deviation, ii) deviation from day-ahead scheduling and ii) cost of rescheduling of ESS (the expanded formulation is presented in 3.4.3.1).

The min-max-min optimization problem presented in (3.19) cannot be solved in practice by state-of-the-art optimization methods. Thus it is necessary to reformulate the problem. In this respect, the second stage minimization ($H(y)$) is replaced by its dual maximization. Then, the two maximization problems are merged into one as shown in (3.20) [87].

$$\overbrace{\underset{x}{\text{minimize}}\left(c_x^T x\right)}^{F(x)} + \overbrace{\underset{\lambda_1,\lambda_2,\mu,\Delta\Psi}{\text{maximize}}\left(\lambda_1^T(\Delta\Psi+\Psi)+\lambda_2^T(e-Rx)+\mu^T d\right)}^{U(\lambda_1,\lambda_2,\mu,\Delta\Psi)} \tag{3.20.a}$$

$$\text{s.t.} \quad P^T\lambda_1 + M^T\lambda_2 + D^T\mu = c_y \tag{3.20.b}$$

$$\mu \leq 0 \tag{3.20.c}$$

$$B\Delta\Psi \leq b \tag{3.20.d}$$

$$\text{s.t.} \quad Ax = \Psi' \tag{3.20.e}$$

$$Gx \leq g \tag{3.20.f}$$

The right hand side maximization ($\mathcal{U}(\lambda_1, \lambda_2, \mu, \Delta\Psi)$) is a bilinear programming since the cross product of λ_1 and $\Delta\Psi$ appears in the objective function.

The formulated optimization in (3.20) leads to the following two important observations [87]:

1. The maximization on the right hand side ($\mathcal{U}(\lambda_1, \lambda_2, \mu, \Delta\Psi)$) is bilinear and defined over a polyhedral set. Therefore, its optimal solution is one of the vertices of this set.

2. The vector x of day-ahead decision variables only appears in the objective function thus, the feasible polyhedron is independent from the day-ahead decision, and hence it has a finite number of vertices.

The order of the two maximization in the right hand side can be switched (first maximize over $\lambda_1, \lambda_2, \mu$ and then over $\Delta\Psi$). Therefore, (3.20) can be reformulated as (3.21).

$$\overbrace{\underset{x}{\text{minimize}}\left(c_x^T x\right)}^{F(x)} + \overbrace{\underset{\lambda_1,\lambda_2,\mu}{\text{maximize}}\left(\lambda_1^T \Psi + \lambda_2^T (e - Rx) + \mu^T d\right)}^{A(\lambda_1,\lambda_2,\mu)} + \overbrace{\underset{\Delta\Psi}{\text{maximize}}\left(\lambda_1^T \Delta\Psi\right)}^{\Phi(\Delta\Psi)} \tag{3.21.a}$$

$$\text{s.t.} \quad B\Delta\Psi \leq b \quad : \xi \tag{3.21.b}$$

$$\text{s.t.} \quad P^T \lambda_1 + M^T \lambda_2 + D^T \mu = c_y \tag{3.21.c}$$

$$\mu \leq 0 \tag{3.21.d}$$

$$\text{s.t.} \quad Ax = \Psi' \tag{3.21.e}$$

$$Gx \leq g \tag{3.21.f}$$

where ξ is the Lagrange multiplier associated to the constraint (3.21.b).

The right hand side maximization $\left(\Phi(\Delta\Psi)\right)$ is a linear program and the strong duality theorem holds thus at optimality we have [87]:

$$\lambda_1^T \Delta\Psi = b^T \xi \tag{3.22}$$

Due to the Karush-Kuhn-Tucker (KKT) conditions, for a linear program, the complementary slackness conditions together with (3.22) are necessary and sufficient for optimality. Thus one can replace the left hand side of (3.22) with its right hand side. Further, the maximize-maximize optimization problem in the right-hand side can be casted as a Mathematical Program with Equilibrium Constraints (MPEC) [88] and render the following optimization problem.

$$\underset{x}{\text{minimize}}\left(c_x^T x\right) + \underset{\lambda_1,\lambda_2,\mu,\Delta\Psi,\xi}{\text{maximize}}\left(\lambda_1^T \Psi + \lambda_2^T (e - Rx) + \mu^T d + b^T \xi\right) \tag{3.23.a}$$

$$\text{s.t.} \quad 0 \le \xi \perp b - B\Delta\Psi \ge 0 \tag{3.23.b}$$

$$B^T \xi = \lambda_1 \tag{3.23.c}$$

$$P^T \lambda_1 + M^T \lambda_2 + D^T \mu = c_y^T \tag{3.23.d}$$

$$\mu \le 0 \tag{3.23.e}$$

$$\text{s.t.} \quad Ax = \Psi' \tag{3.23.f}$$

$$Gx \le g \tag{3.23.g}$$

The orthogonal condition in (3.23.b) could be replaced with a set of new constraints as shown (3.24).

$$0 \le \xi \le \mathfrak{B} u^{\xi} \tag{3.24.a}$$

$$0 \le b - B\Delta\Psi \le \mathfrak{B} u^{b} \tag{3.24.b}$$

$$u^{\xi} + u^{b} = 1 \tag{3.24.c}$$

$$u^{\xi}, u^{b} \in \{0,1\} \tag{3.24.d}$$

where $\mathfrak{B}$ is a large enough positive number.

It is worth to note that the solution to the inner maximization problem belongs to a set of finite candidates $\mathcal{K}$, which does not depend on the first stage decisions. Therefore, it can be solved effectively using Benders Dual cutting algorithm or Primal cut algorithm. We have employed the Benders dual cut algorithm since the number of vertices of the uncertainty space is very high and primal cut algorithm cannot be easily employed. The Benders dual cut solution algorithm is described in the appendix A.1.

3.4.3.1 Formulation of the second stage minimization

The formulation of the second stage minimization is shown in the following.

$$\begin{aligned}&\underset{y}{\text{minimize:}} \sum_t (+\pi^-(t)d^G(t) - \pi^+(t)u^G(t))\Delta t + \\ &W_v \sum_l \sum_t \left(\left(v_l(t) - v_{thr}^{\max} : \left(v_l(t) \geq v_{thr}^{\max} \right) \right) + \left(\left(v_{thr}^{\min} - v_l(t) \right) : \left(v_l(t) \leq v_{thr}^{\min} \right) \right) \right) \\ &+ \sum_t \sum_{\mathcal{L}_{ess}} \Gamma^{ess} \left(-\left(u_l^{p,ch}(t) + u_l^{p,d}(t) + u_l^{q,p}(t) + u_l^{q,n}(t) \right) + \left(d_l^{p,ch}(t) + d_l^{p,d}(t) + d_l^{q,p}(t) + d_l^{q,n}(t) \right) \right) \Delta t\end{aligned} \tag{3.25.a}$$

$$s^r(t) = s^{r,f}(t) + \Delta s^r(t) \quad \forall t \in T \tag{3.25.b}$$

$$s^c(t) = s^{c,f}(t) + \Delta s^c(t) \quad \forall t \in T \tag{3.25.c}$$

$$s^{pv}(t) = s^{pv,f}(t) + \Delta s^{pv}(t) \quad \forall t \in T \tag{3.25.d}$$

$$\begin{aligned}s_l(t) = &-p_l^d(t) + p_l^{ch}(t) + s^r(t)a_l^{p,r} + s^c(t)a_l^{p,c} + s^{pv}(t)a_l^{pv} + \\ &j\left(-q_l^n(t) + q_l^p(t) + s^r(t)a_l^{q,r} + s^c(t)a_l^{q,c}\right)\end{aligned} \tag{3.25.e}$$

$$S_l(t) = s_l(t) + \sum_{m \in \mathcal{L}} \left(\mathbb{G}_{l,m} S_m(t) \right) - j\left(v_{\text{up}(l)}(t) + v_l(t) \right) \frac{b_l}{2}, \quad \forall l \in \mathcal{L}, \quad \forall t \in T \tag{3.25.f}$$

$$v_l(t) = v_{\text{up}(l)}(t) - 2\Re\left(z_l^* \left(S_l(t) + j\frac{v_{\text{up}(l)}(t) b_l}{2} \right) \right), \quad \forall l \in \mathcal{L}, \quad \forall t \in T \tag{3.25.g}$$

$$v^{\min} \leq v_l(t) \leq v^{\max} \quad \forall l \in \mathcal{L}, \forall t \in T \tag{3.25.h}$$

$$I_l^{P,t}(t) = \Re\left(\frac{S_l(t)}{V^{\min}} \right), \forall l \in \mathcal{L}, \quad \forall t \in T \tag{3.25.i}$$

$$I_l^{Q,t}(t) = \Im\left(\frac{S_l(t)}{V^{\min}} \right), \quad \forall l \in \mathcal{L}, \quad \forall t \in T \tag{3.25.j}$$

$$I_l^{P,b}(t) = \Re\left(\frac{S_l(t) + j\left(v_{\text{up}(l)}(t) + v_l(t) \right) \frac{b_l}{2}}{V^{\min}} \right), \quad \forall l \in \mathcal{L}, \quad \forall t \in T \tag{3.25.k}$$

$$I_l^{Q,b}(t) = \Im\left(\frac{S_l(t) + j\left(v_{\text{up}(l)}(t) + v_l(t) \right) \frac{b_l}{2}}{V^{\min}} \right), \quad \forall l \in \mathcal{L}, \quad \forall t \in T \tag{3.25.l}$$

$$\hat{I}_l^{P,t}(t) \geq F_n\left(I_l^{P,t}(t) \right) \quad \forall n \in \mathcal{N}, \forall l \in \mathcal{L}, \forall t \in T \tag{3.25.m}$$

$$\hat{I}_l^{Q,t}(t) \geq F_n\left(I_l^{Q,t}(t)\right) \quad \forall n \in \mathcal{N}, \forall l \in \mathcal{L}, \forall t \in T \tag{3.25.n}$$

$$\hat{I}_l^{P,b}(t) \geq F_n\left(I_l^{P,b}(t)\right) \quad \forall n \in \mathcal{N}, \forall l \in \mathcal{L}, \forall t \in T \tag{3.25.o}$$

$$\hat{I}_l^{Q,b}(t) \geq F_n\left(I_l^{Q,b}(t)\right) \quad \forall n \in \mathcal{N}, \forall l \in \mathcal{L}, \forall t \in T \tag{3.25.p}$$

$$\hat{I}_l^{P,t}(t) + \hat{I}_l^{Q,t}(t) \leq (I_l^{\max})^2, \ \forall l \in \mathcal{L}, \quad \forall t \in T \tag{3.25.q}$$

$$\hat{I}_l^{P,b}(t) + \hat{I}_l^{Q,b}(t) \leq (I_l^{\max})^2, \ \forall l \in \mathcal{L}, \quad \forall t \in T \tag{3.25.r}$$

$$P_1(t) + u^G(t) - d^G(t) = x^{scd}(t) \quad \forall t \in T \tag{3.25.s}$$

$$p_l^{ch}(t) + u_l^{p,ch}(t) - d_l^{p,ch}(t) = x_l^{p,ch}(t) \quad \forall l \in \mathcal{L}_{\text{ess}}, \forall t \in T \tag{3.25.t}$$

$$q_l^{ch}(t) + u_l^{q,ch}(t) - d_l^{q,ch}(t) = x_l^{q,ch}(t) \quad \forall l \in \mathcal{L}_{\text{ess}}, \forall t \in T \tag{3.25.u}$$

$$p_l^{d}(t) + u_l^{p,d}(t) - d_l^{p,d}(t) = x_l^{p,d}(t) \quad \forall l \in \mathcal{L}_{\text{ess}}, \forall t \in T \tag{3.25.v}$$

$$q_l^{d}(t) + u_l^{q,d}(t) - d_l^{q,d}(t) = x_l^{q,d}(t) \quad \forall l \in \mathcal{L}_{\text{ess}}, \forall t \in T \tag{3.25.w}$$

$$\left(p_l^{d}(t) + p_l^{ch}(t)\right)^2 + \left(q_l^{p}(t) + q_l^{n}(t)\right)^2 \leq C_l \quad \forall l \in \mathcal{L}_{\text{ess}}, \forall t \in T \tag{3.25.x}$$

$$E_l(t+1) = E_l(t) - \frac{p_l^d(t)}{\eta^d} + \eta^{ch} p_l^{ch}(t) \quad \forall l \in \mathcal{L}_{\text{ess}}, \forall t \in T \tag{3.25.y}$$

$$E_l^{\min} \leq E_l(t) \leq E_l^{\max} \quad \forall l \in \mathcal{L}_{\text{ess}}, \forall t \in T \tag{3.25.z}$$

$$\hat{E}_l(t+1) = \hat{E}_l(t) - p_l^d(t) + p_l^{ch}(t) \quad \forall l \in \mathcal{L}_{\text{ess}}, \forall t \in T \tag{3.25.aa}$$

$$E_l^{\min} \leq \hat{E}_l(t) \leq E_l^{\max} \quad \forall l \in \mathcal{L}_{\text{ess}}, \forall t \in T \tag{3.25.bb}$$

$$\begin{aligned} E_l(t^1) &\leq E_l(t^{\text{fin}}) \\ \hat{E}_l(t^1) &\leq \hat{E}_l(t^{\text{fin}}) \end{aligned} \tag{3.25.cc}$$

$$\begin{aligned} &u_l^{p,ch}(t) \geq 0, u_l^{p,d}(t) \geq 0, u_l^{q,p}(t) \geq 0, u_l^{q,n}(t) \geq 0, u^G(t) \geq 0 \\ &d_l^{p,ch}(t) \geq 0, d_l^{p,d}(t) \geq 0, d_l^{q,p}(t) \geq 0, d_l^{q,n}(t) \geq 0, d^G(t) \geq 0 \end{aligned} \tag{3.25.dd}$$

$$p_l^d(t) \geq 0, \quad p_l^{ch}(t) \geq 0, \quad q_l^d(t) \geq 0, \quad q_l^{ch}(t) \geq 0 \tag{3.25.ee}$$

where

$$y = \left\{ \begin{array}{c} E, \hat{E}, u^{p,ch}, u^{p,d}, d^{p,ch}, d^{\text{p,d}}, u^{q,\text{p}}, u^{q,\text{n}}, d^{q,\text{p}}, d^{q,\text{n}} \\ p^{ch}, p^{d}, q^{p}, q^{n}, d^{G}, u^{G}, I^{P,t}, I^{Q,t}, I^{P}, I^{Q,t}, I^{P,\text{b}}, I^{Q,\text{b}}, I^{P,\text{b}}, I^{Q,\text{b}}, v, S \end{array} \right\}$$

is the set of optimization variables (it should be noted that $s^r, s^c, s^{pv}, \Delta s^r, \Delta s^c, \Delta s^{pv}$ are variables of the middle stage maximization and $x_l^{p,ch}, x_l^{q,ch}, x_l^{p,d}, x_l^{q,d}, x^{scd}$ are variables of first stage minimization). The notation without subscript denotes the vector of corresponding variables.

The objective function is represented in (3.25.a) where π_t^- and π_t^+ are the prices for down and up deviations from the day-ahead energy import/export scheduling. As stated previously, it minimizes the cost of deviations from day-ahead scheduling, cost of nodal voltage magnitude deviations, and the ESS rescheduling. We use the nomenclature of chapter 2 and recall it here for reader's convenience. Buses other than the slack bus are denoted with 1, ..., L; $\mathcal{L}$ denotes the set $\mathcal{L} = \{1,2,...,L\}$ and up(l) is the label of the bus that is upstream of bus l. We also label with l the line whose downstream bus is bus l; its upstream bus is therefore up(l). $t \in T$ is the index of time (15 minutes) where T is the set of time steps. The set of buses with ESSs are represented by $\mathcal{L}_{ess}$. The $u_l^{p,ch}/u_l^{p,d}(d_l^{p,ch}/d_l^{q,d})$ are the charge/discharge upward (downward) variables for active power outputs of ESSs, respectively. The $u_l^{q,p}/u_l^{q,n}(d_l^{q,p}/d_l^{q,n})$ are the positive/negative upward (downward) variables for reactive power output of ESSs, respectively. The d^G and u^G represent down and up deviations from day-ahead energy schedule. W_v is the weighting coefficient of voltage deviation cost.

$v_{thr}^{max}, v_{thr}^{min}$ are the square of voltage magnitude thresholds (upper and lower) beyond which the voltage magnitudes deviations with respect to the $v_{thr}^{max}/v_{thr}^{min}$ are minimized.

We have considered three sets of uncertainties, residential load, commercial load, and the PV production as shown in (3.25.b), (3.25.c), and (3.25.d), respectively. The forecasted load and PV profiles and their respective variations are represented by $s^{r,f}(t)/\Delta s^r(t)$, $s^{c,f}(t)/\Delta s^c(t)$, and $s^{pv,f}(t)/\Delta s^{pv}(t)$ respectively. $s^r(t)$, $s^c(t)$, and $s^{pv}(t)$ are the aggregated residential, commercial loads and PV production at each time step (t), respectively.

The total load and PV are distributed among the network buses based on their nodal residential/commercial active load, PV production, and residential/commercial reactive load coefficients ($a_l^{p,r}/a_l^{p,c}, a_l^{pv}$ and $a_l^{q,r}/a_l^{q,c}$), respectively. The equality constraints shown in (3.25.b), (3.25.c), and (3.25.d) are the ones that have uncertainty and are represented by (3.19.b) in the compact form of the optimization problem.

The load and voltage balance equations are modeled by equations (3.25.e) and (3.25.g). Equation (3.25.h) represents the nodal voltage magnitudes limits. Equations (3.25.i)-(3.25.l) model the active and reactive current flows on both ends of line l. These variables are used to model the current flow constraints of line l. It should be noted that V^{min} (the minimum voltage magnitude) is used in the denominator to consider the worst case conditions (Note that v is the square of voltage magnitude whereas V represents voltage magnitude). Constraints (3.25.m)-(3.25.p) provide upper bounds ($\hat{I}_{\mathrm{up}(l)}^P$,

$\hat{I}^{Q}_{\mathrm{up}(l)}, \hat{I}^{P}_{l}, \hat{I}^{Q}_{l}$) for square of $I^{P}_{\mathrm{up}(l)}$, $I^{Q}_{\mathrm{up}(l)}, I^{P}_{l}, I^{Q}_{l}$ using a set of linear constraint, called F_n. These set of linear constraints are shown in Fig. 3-5. The index n corresponds to the line n shown in Fig. 3-5 with dashed red line ($\mathcal{N}$ represents the set of these lines). The current flow at both ends of the lines is limited using constraints (3.25.q) and (3.25.r).

Constraint (3.25.s)-(3.25.w) are the links between the first stage (day-ahead scheduling, $F(x)$) and the second stage ($H(y)$). These equations model the upward and downward deviations from the energy import scheduling and ESSs outputs with respect to their day-ahead scheduling (x). It should be noted that by upward deviation we mean the extra (resp. less) production (resp. consumption) of energy with respect to the day-ahead plan. In contrast, downward deviation means less (resp. extra) production (resp. consumption) of energy with respect to the day-ahead plan. The day-ahead scheduling of energy import/export from the grid is hourly basis whereas the deviations in the second stage are on 15 minutes basis. $P_1, p^{ch}_l/p^{d}_l, q^{p}_l/q^{n}_l$ are actual values of active power imported from the external grid, ESSs active (charge/discharge) and reactive (positive/negative) powers outputs, respectively.

The ESSs constraints (capability curve, State of Charge (SoC), and energy reservoir capacity limit) are shown in (3.25.x)-(3.25.ee). $E_l(t)$ is the energy stored in ESS l at time t and η^{ch} and η^{d} are charging and discharging efficiencies respectively. In order to have a linear formulation, the capability curve constraint (3.25.x) is linearized by merging a-priori defined number of linear boundaries approximating the original curve (see Fig. 3-6). The SoC constraint of ESSs is modeled by (3.25.y). The constraint (3.25.z) models the upper and lower bounds of energy stored in ESS reservoir. Equations (3.25.aa) and (3.25.bb) add auxiliary constraint concerning the SoC of ESSs to avoid ill use of ESSs efficiencies. The constraint (3.25.cc) implies that the energy stored in the ESSs at the end of the day have to be greater than the initial energy level. The last constraint implies that the active (charging and discharging) and reactive (positive and negative) variables of ESSs cannot be negative.

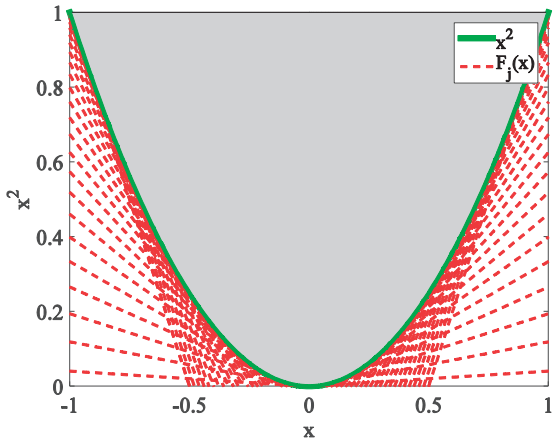

Fig. 3-5: Linearized model of square of active and reactive power flows

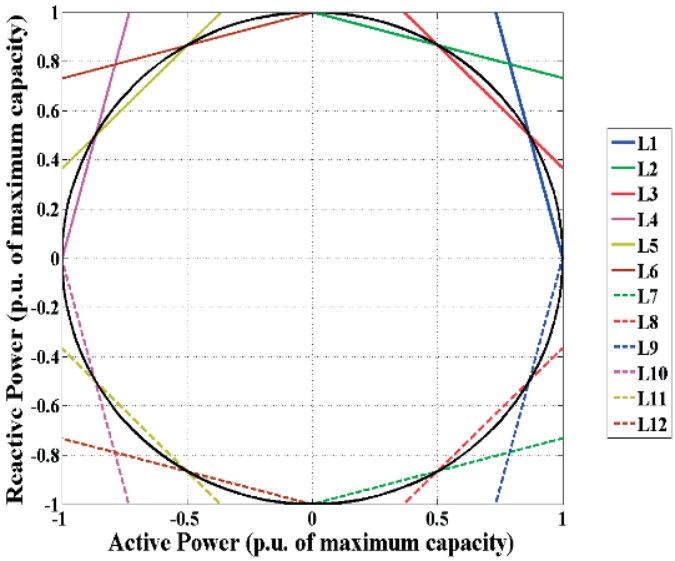

Fig. 3-6: Linearized capability curve of ESS

3.4.4 Numerical analyses

The IEEE 34 buses network is chosen for the test case study (see Fig. 2-3). It is assumed there are two ESS units available in the network. They are located on buses #852 and #860 (see Fig. 2-3). Each ESS has 0.5 MW power rating capacity and 1 MWh energy reservoir capacity. The load and PV profiles modeled and forecasted in section 3.3.2 are used (Fig. 3-1 and Fig. 3-2) as the input to the optimization problem. The partially cloudy sky day (see Fig. 3-2.1) is chosen for PV production (worst case). The PV uncertainty budget is modeled using the method described in section 3.3.2. It is assumed that the forecasts of each time step of residential and commercial loads have ±10% and ±7% errors, respectively. The energy price profile is shown in Fig. 3-7. The downward and upward regulations price are assumed to be 80 and 125 present of the day-ahead energy price, respectively. Finally the voltage deviation (for each 15 minutes) is penalized by 0.03 CHF/volt.

The hourly energy import/export scheduling for two cases, i) base case (without forecast variations) and ARO scheduling are shown in Fig. 3-8. It should be noted that in the former case, the day-ahead decisions are taken without considering the intra-day variations. It can be seen that the biggest differences between the two cases are in the middle of day. It is because of two reasons i) high level of PV production in middle of the day and consequently, high amount of uncertainty ii) high level of commercial load and its relevant uncertainty. Additionally, one can observe that in case of ARO, the scheduling is more conservative when the energy price is high (hours 8, 9, 10 and 19).

The day-ahead scheduling of the two available ESSs are shown in Fig. 3-9. It can be seen that in base case, the ESSs are charged with maximum capacity, when the PV production level is high and the price is low. On the other hand, one can observe that

Table 3-1: Installed PV capacities in the IEEE 34 buses

Bus #	#810	#816	#854	#856	#864	#860	#838	#840
PV capacity (kW)	110	230	450	115	550	800	1000	400

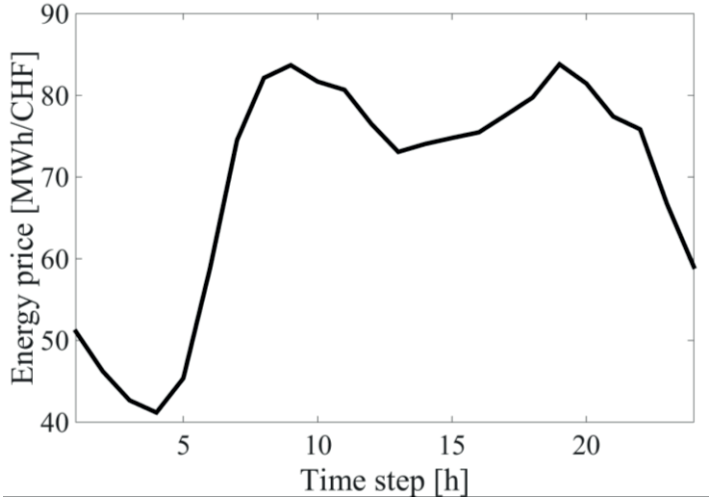

Fig. 3-7: Daily energy price

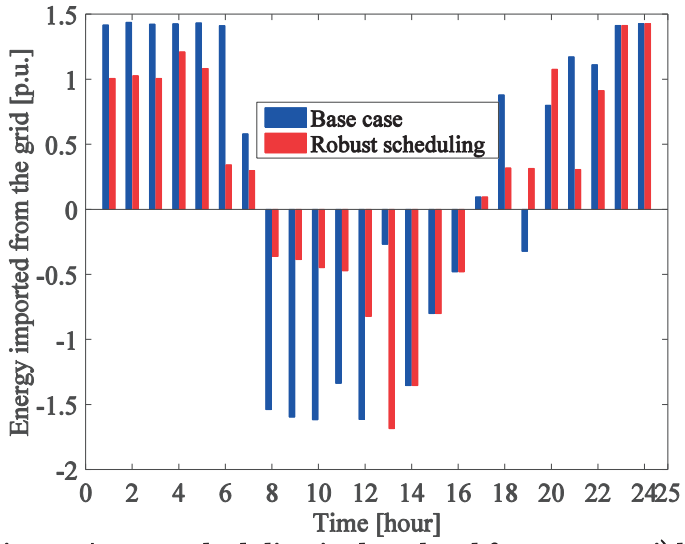

Fig. 3-8: Energy import/export scheduling in day-ahead for two cases i) base case without considering the forecast errors and ii) the ARO scheduling (base value of energy is 2.5 MWh)

the scheduling of ESSs is more conservative in case of ARO. A part of ESSs capacities is preserved to manage the forecast errors. Additionally, one can observe that in base case the ESSs are used to exploit the energy price differences during the day.

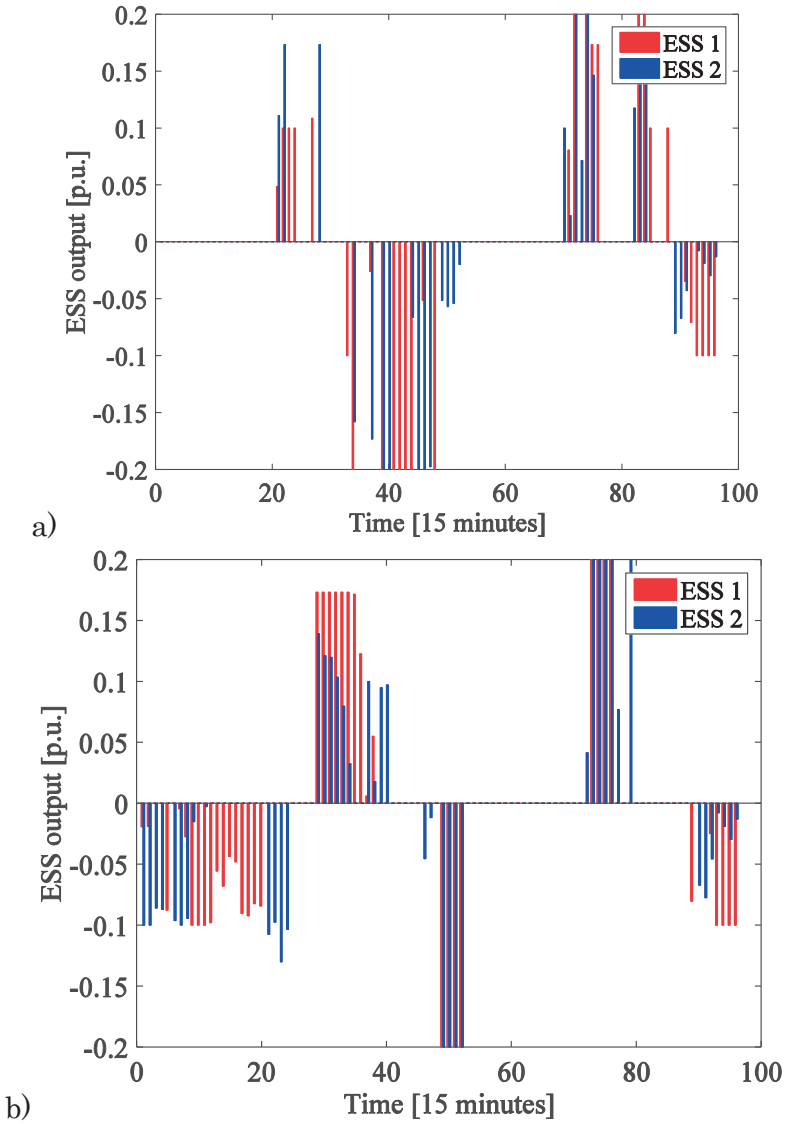

Fig. 3-9: ESSs scheduling in day-ahead a) ARO scheduling, b) base case (base value of power is 2.5 MW)

The day-ahead cost (cost of energy import/export plus the ESSs operation costs) in case of ARO is 182.13 CHF and the worst case intra-day cost is equal 128.16 CHF (the intra-day cost includes the voltage deviations cost as well the unbalance costs and ESSs rescheduling). For the base case, the day-ahead cost is equal 79.36 CHF whereas the worst case intra-day cost is equal 379.62 CHF.

The convergence of the Benders decomposition approach used to solve the ARO is demonstrated in Fig. 3-10. In particular, one can observe the procedure converges after 42 iterations. The stopping criterion is chosen to be 0.1% (the difference between the upper and lower bounds). The details about convergence of Benders decomposition are provided in A.1.

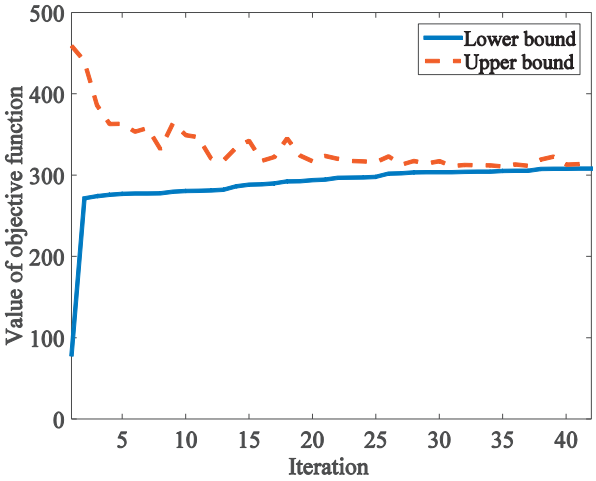

Fig. 3-10: The convergence of Benders decomposition approach used to solve the ARO

3.5 Day-ahead Scheduling of Active Distribution Networks using Scenario-based Stochastic Optimization

As known, stochastic programming is a mathematical framework to deal with the uncertainties of optimization problem parameters. This approach has been extensively used in power system context. It has been used for generation and transmission network expansion planning [89], [90], maintenance scheduling [91], unit commitment and SCUC [92], [93], electricity portfolio optimization [94], optimal bidding strategy [95], and so on. In this section, we develop a two stage stochastic programming to deal with the uncertainties related to the PV and load profiles [96, 97]. In this context, a set of decisions have to be made a priori when the environmental parameters are not completely available. The targeted optimization problem is the day-ahead scheduling of an ADN, as described in section 3.3. In the previous section ARO was presented to deal with the worst-case realization of the uncertain parameters. In contrast, in this section, stochastic optimization is employed to deal with the uncertainties using scenarios sampled from the PDF of uncertain parameters.

The first-stage decisions determine the amount of import/export energy from/to the external grid for each hour, ESSs set points, and the sub-station transformer tap position.

A non-zero cost is considered for the On Load Tap Changer (OLTC) operation. Indeed changing the tap position of OLTC causes arc at the diverter or selector switch contacts producing contact erosion and carbonization of the diverter switch oil. The level of damage depends upon the operating current of the OLTC and number of operations. Thus, an associated cost is considered for changing the tap position of the OLTC [98].

Given the first stage decisions, the second stage or *wait and see decisions* are made based on the realization of the random parameters. In case of our specific problem, the second stage decision variables are the 15 minutes ESSs set points. The random variables of this second stage are the PV production and load consumption.

3.5.1 Stochastic optimization formulation

The general form of the stochastic optimization problem is shown in the following.

$$\underset{x,y^{\varphi}}{\text{minimize}}\left(c_x^T x\right)+\sum_{\varphi\in\Phi}\left(\rho^{\varphi}c_y^T y^{\varphi}\right) \tag{3.26.a}$$

$$\text{s.t.}\quad Ay^{\varphi}+Bx=C\varphi \quad \forall\varphi\in\Phi \tag{3.26.b}$$

$$Dy^{\varphi}+Ex\le d^{\varphi} \qquad \forall\varphi\in\Phi \tag{3.26.c}$$

where x and y^{φ} are the vectors of the first and second decision variables and c_x^T and c_y^T are their corresponding cost coefficients. The objective function includes the first stage cost $c_x^T x$ plus the expectation of the second stage costs with respect to probability (ρ^{φ}) of each scenario.

The control variables in the first stage are ESS set points, OLTC tap position and the amount of hourly energy import/export from the grid. The 15 minutes set point of ESSs are the control variables in the second stage.

The objective function (as it is shown in (3.27.a)) accounts for the minimization of different goals: (i) energy cost from the external grid, (ii) deviation costs from the day-ahead energy import/export scheduling, (iii) nodal voltage deviations, and (iv) OLTC tap-changing cost.

The mathematical formulation of the optimization problem is as follow:

$$\left.\begin{aligned}&\underset{\Xi}{\text{minimize}}\sum_t \delta^{\text{DA}}(t)\pi(t)\Delta t+\\&\rho_{\varphi}\sum_{\varphi}\sum_t\left\{\begin{aligned}&\left(\pi^{-}(t)d_{\varphi}^{G}(t)-\pi^{+}(t)u_{\varphi}^{G}(t)\right)\Delta t+\alpha(t)\\&W_v\sum_t\left(\left(v_{1,\varphi}(t)-v_{thr}^{\max}:\left(v_{1,\varphi}(t)\ge v_{thr}^{\max}\right)\right)+\left(\left(v_{thr}^{\min}-v_{1,\varphi}(t)\right):\left(v_{1,\varphi}(t)\le v_{thr}^{\min}\right)\right)\right)\end{aligned}\right\}\end{aligned}\right\}\begin{aligned}&\text{First stage}\\&\text{Second stage}\end{aligned} \tag{3.27.a}$$

$$\Upsilon(\tau_{\varphi}(t),\vartheta_{\varphi}(t))\ge 0,\quad \forall t\in T,\forall\varphi\in\Phi \tag{3.27.b}$$

$$\delta^{\text{DA}}(t)+u_{\varphi}^{G}(t)-d_{\varphi}^{G}(t)=P_{1,\varphi}(t),\quad \forall t\in T,\forall\varphi\in\Phi \tag{3.27.c}$$

$$u_{\varphi}^{G}(t)\ge 0,\ d_{\varphi}^{G}(t)\ge 0,\quad \forall t\in T,\forall\varphi\in\Phi \tag{3.27.d}$$

$$v_0 = 0.9 + \Delta v^c T^c(t) \quad \forall t \in T \tag{3.27.e}$$

$$0 \le T^c(t) \le T^{\max} \quad \forall t \in T \tag{3.27.f}$$

$$T^c(t) \in \{1,2,...,\} \quad \forall t \in T \tag{3.27.g}$$

$$\alpha(t) \ge 0 \quad \forall t \in T \tag{3.27.h}$$

$$\alpha(t) \ge T^c(t) - T^c(t-1) \quad \forall t \in T \tag{3.27.i}$$

$$\alpha(t) \ge -T^c(t) + T^c(t-1) \quad \forall t \in T \tag{3.27.j}$$

where $\Xi = \{v_{l,\varphi}, \delta^{\mathrm{DA}}, T^c, \tau_\varphi, \alpha, d_\varphi^G, u_\varphi^G\}$ is the set of optimization variables.

v_0 is the voltage magnitude of the slack bus (sub-station) φ is the index of scenarios (load and PV) and ρ_φ is the probability of each scenario. The upper and lower voltage magnitudes thresholds, beyond which the voltage magnitude deviations are minimized, are represented by $v_{thr}^{\max}$, and $v_{thr}^{\min}$, respectively. The energy price, upward and downward prices, day-ahead energy import scheduling, and the cost of transformer tap-changer are represented by $\pi(t)$, $\pi^+(t), \pi^-(t), \delta^{DA}(t)$ and $\alpha(t)$, respectively. The OLTC tap position variable is represented by T^c. W_v is the weighting coefficient of voltage deviation cost. u_φ^G and d_φ^G are upward and downward deviations' variables with respect to day-ahead scheduling (δ^{DA}). $P_{1,\varphi}(t)$ is the amount of active power imported from the external grid at time step t and scenario φ.

Constraint (3.27.e) models the voltage magnitude level at the substation supplying the ADN (slack bus). The numbers of OLTC steps is limited in constraint (normally it is 36 steps) (3.27.f) and its discrete nature is modeled by constraint (3.27.g).

The cost of moving the tap of the OLTC is modeled using (3.27.h)-(3.27.j). T^c is the OLTC position. It is between the minimum position 0, and the maximum position that produce the maximum voltage $T^{\max}$ and is an integer variable. α models the cost of moving OLTC tap.

3.5.2 Uncertainty modeling

The aim of this section is to illustrate a typical approach to generate appropriate scenarios for daily load and PV profiles. It is required since stochastic optimization frameworks require the knowledge of the distribution of the uncertain parameters.

3.5.2.1 Scenario generation

In order to statistically characterize the network loads and PVs, we assume that the aggregate load/PV at the $k-th$ time interval of the day denoted hereafter by L_k is a random variable. In order to generate appropriate scenarios, we take into account temporal correlation of the random variables. In this respect, we assume that the random vector $L-\bar{L}=(L_1-\bar{L}_1,\dots,L_{96}-\bar{L}_{96})$ follows a multivariate Gaussian distribution, $L-\bar{L}\sim N(0,\Omega)$ where Ω is the covariance matrix that contains the whole information about the variance and covariance of the random variables. It should be noted that Ω is a full matrix and its rank corresponds to the number of considered time steps (i.e., 96). Similar to the case of ARO, in order to consider the spatial correlation, we have considered that the PV profiles have the same variation on all buses of the system[1]. For the nodal loads, we assumed spatial correlation only for the same kind of load (i.e., residential, commercial/ industrial).

3.5.2.2 Scenario reduction

Accounting for all possible scenarios may results in a large-scale and computationally expensive simulation. Due to this computationally complexity, often the number of scenarios is reduced to a reasonable one characterized by the same degree of volatility/stochasticity of the original scenarios.

The first step for scenario reduction is to determine an appropriate criterion for comparing the resemblances of the scenarios. It is a case-dependent problem, one method may fit well one application whereas it cannot appropriately model the resemblances of two time-series in another application. Two widely used methods for time series clustering are based on i) Euclidean distance ii) Dynamic Time Warping (DTW).

Dynamic Time Wrapping (DTW) is a well-known algorithm for measuring the similarities between two temporal time series. It can detect the similarities of two time series even with different phases by allowing elastic transformation [99]. On the other hand, Euclidean distance criteria measure the point to point distance. Fig. 3-11 shows the different criteria used by each method for measuring the similarity of two time series. In power systems studies the time shifts in the load or PV curves are important and thus the two curves shown in Fig. 3-11 are different resulting in different scheduling of flexible resources. Consequently, in this study we have employed Euclidean distance algorithm to determine the similarities between each pair of daily profiles.

[1] Remind that this hypothesis is justified in the view of the relatively small geographical extension of ADNs.

Once the similarities between every pair of the daily time series are determined, using an appropriate algorithm (i.e., Euclidean distance), they are grouped into a binary, hierarchical cluster tree. In this respect the pairs of the objects are linked based on their proximity. The new formed clusters are again grouped into larger clusters and this continues until a hierarchical tree is formed. The distance between the newly formed clusters can be defined using several algorithms. In what follows, we have used the furthest distance of the two grouped scenarios.

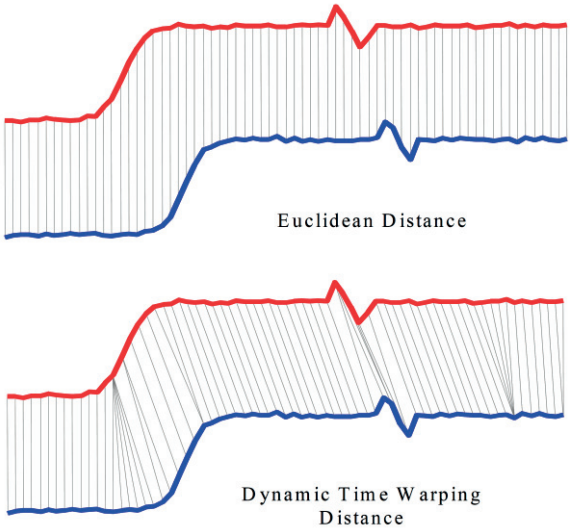

Fig. 3-11: Euclidean distance aligns the *i*th point in one sequence with the *i*th point in the other, DTW alignment allows a more intuitive distance measure to be calculated [100].

The next step is to partition the data into the clusters using the created hierarchical tree of binary clusters. This can be done using several approaches. The simplest one is to determine the number of clusters by the user based on his intuition about the scenarios. It can be done also based on the clusters' inconsistency criteria or distances. Here we have chosen the final number of clusters based on a predefined maximum distance between the clusters.

At the final step, one scenario from each cluster is selected using K-Medoids algorithm [101]. They form the final input scenarios of the optimization problem.

3.5.3 Simulation results

The residential and commercial load profiles shown in Fig. 3-1.a are used as the initial time series for generating the final scenarios. For each category (commercial and residential load, and PV) five time series samples are available. We use these initial time series to obtain the covariance matrix, mean, and standard deviation of data. The final scenarios are shown in Fig. 3-12. The maximum distance of 1.3 p.u. (using Euclidean distance criteria between the time series) is selected as the criteria for

scenario reduction. It should be noted that Euclidean distance corresponds to a vector of 288 elements (96 times steps for PV, commercial load, and residential load). One hundred scenarios are generated using the scenario generation-reduction method presented in section 3.3. The IEEE 34 buses test case network is selected as the case study.

The energy price profile is shown in Fig. 3-7. Similar to the case of ARO, it is assumed that there are two ESS units available in the network. They are located on buses #852 and #860 (See Fig. 2-3). Each ESS units has capacity equal to 0.5 MW and 1 MWh.

In the following the performances of the proposed formulation are demonstrated using two cases, i) with presence of ESSs ii) without ESSs units. The hourly energy import/export schedules for the two cases are shown in Fig. 3-15. One can observe that the amount of imported energy with ESS is less than the case without ESS when the energy cost is high (i.e., between hours 7-9 and 18-20).

The total amount of upward and downward deviations are shown in Table 3-2. The identified value of the objective function for the case with ESS is 10556.5 CHF whereas it is equal 26428.4 CHF when there is no ESS available. The impact of ESSs on decreasing upward and downward deviations are shown in this Table. The upward and downward deviation prices are considered to be 80% and 120% of the corresponding day-ahead price. It should be noted that by upward regulation we mean the extra (resp. less) production (resp. consumption) of energy with respect to the day-ahead plan. In contrast, downward deviation means less (resp. extra) production (resp. consumption) of energy with respect to the day-ahead plan.

The OLTC tap position for each hour is shown in Table 3-3 for two cases. One can observe that with presence of ESSs, the number of changes in OLTC tap-position as well as the corresponding magnitude of change are less than the case without ESS. Particularly, one can observe that in the middle of the day, the changes in the OLTC tap position with presence of ESS is less than the one without ESSs.

Table 3-2: Total upward and downward deviations for two cases i) with ESS ii) without ESS

	Total upward deviation (MWh)	Total downward deviation (MWh)
With ESS	1.126	2.4285
Without ESS	1.6610	4.6250

Finally, the boxplot of nodal voltage magnitudes for each time step for both cases are shown in Fig. 3-17 and Fig. 3-16. The bottom and top of the blue boxes indicate the first and third quartiles (25th and 75th percentiles of the data) of the nodal voltage magnitudes at each time step. The red lines indicate the median while the whiskers show the maximum and minimum of nodal voltage magnitudes. The green lines show

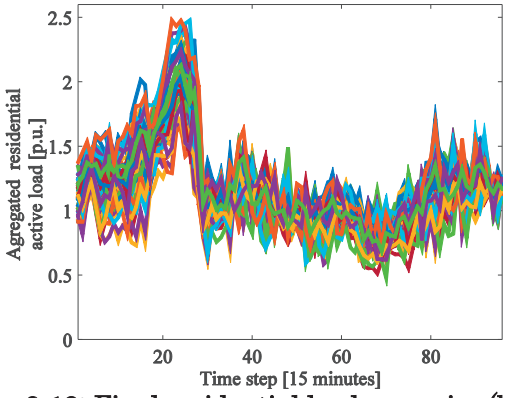

Fig. 3-12: Final residential load scenarios (base value of active power is 2.5 MW)

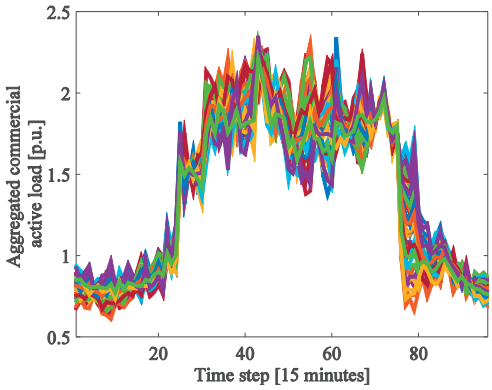

Fig. 3-13: Final commercial load scenarios (base value of active power is 2.5 MW)

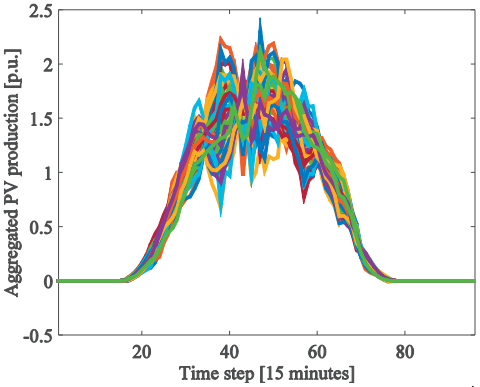

Fig. 3-14: Final PV production scenarios (base value of power is 2.5 MW)

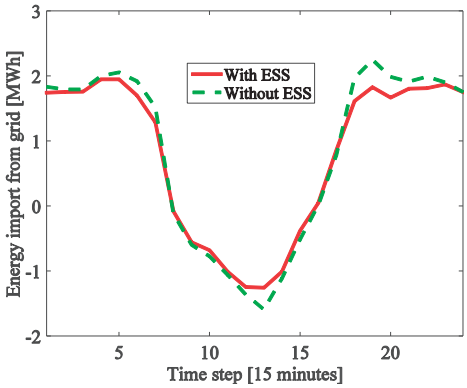

Fig. 3-15: Hourly scheduling of energy import/export from the external grid

the desired voltage region. It can be observed that, for the case without ESSs the voltage deviations outside the desired interval (the range is chosen to be between 0.97 p.u. to 1.03 p.u.) are worse than the case with ESSs. These figures show that the voltage profile of the network has been improved (i.e., the voltage magnitude deviations are minimized) by using ESSs. Particularly one can observe that in presence of ESSs the over-voltages are almost eliminated and under-voltages below 0.93 p.u. are completely removed.

Table 3-3: Hourly OLTC tap position

Time [hour]	1	2	3	4	5	6	7	8	9	10	11	12	13	14	15	16	17	18	19	20	21	22	23	24
OLTC Position without ESS	29	29	29	30	30	30	29	18	16	11	10	8	7	8	15	24	29	32	33	31	30	30	29	29
OLTC position with ESS	29	29	29	29	29	29	29	22	19	18	16	16	16	16	19	24	29	29	29	29	29	29	29	29

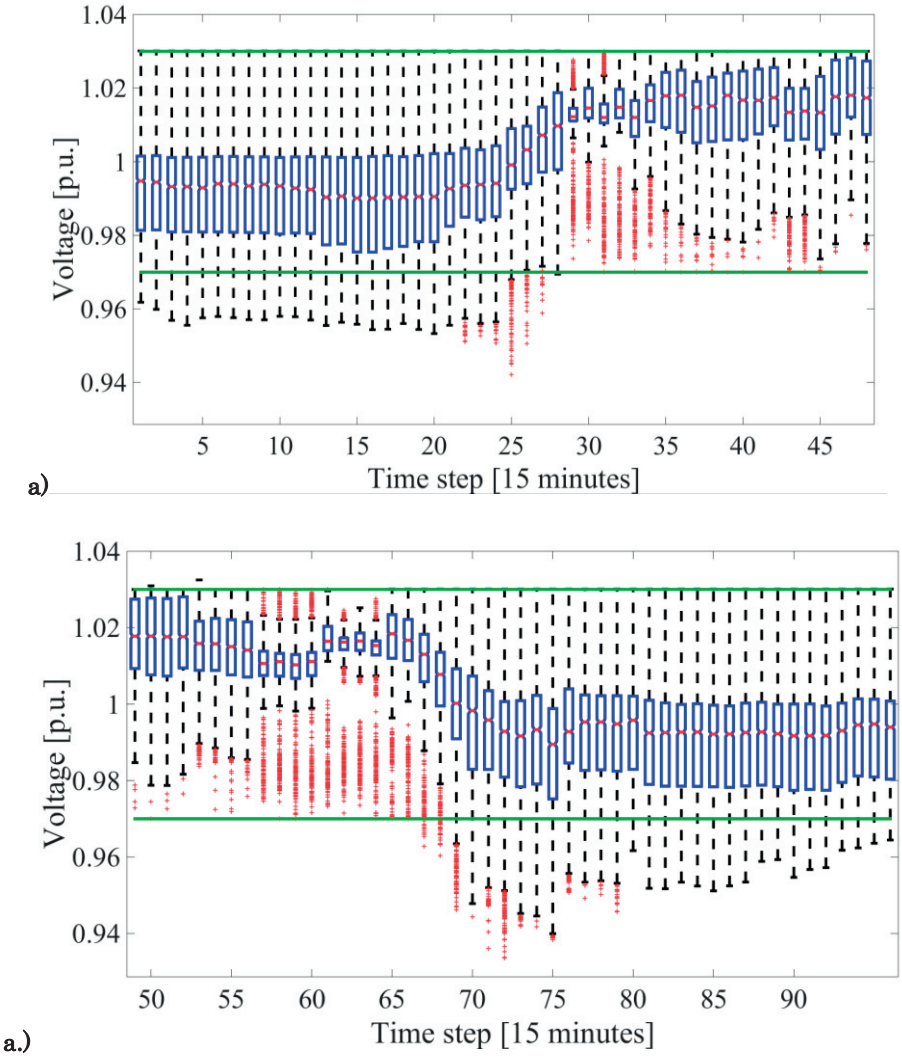

Fig. 3-16: The nodal voltage magnitudes boxplot with presence of ESSs (a). First half of the day, b). Second half of the day)

3.6 Adaptive Robust Approach vs. Stochastic Approach

In this chapter we presented two optimization techniques to deal with uncertainties of the parameters in ADN scheduling and operation. In section 3.40 ARO approach was presented to solve the ADN day-ahead scheduling and the two-stage stochastic optimization was presented in 3.5 to solve almost the same problem (with transformer tap-changer). The question may raise about the advantages and disadvantages of each method and, generally, their comparisons. In general, these two methods do not have same goals thus their solution comparison does not make sense (ARO considers the worst case scenario whereas stochastic programming takes into account the probability of each scenario). However, their advantages, disadvantages and characteristics are summarized and compared in this section.

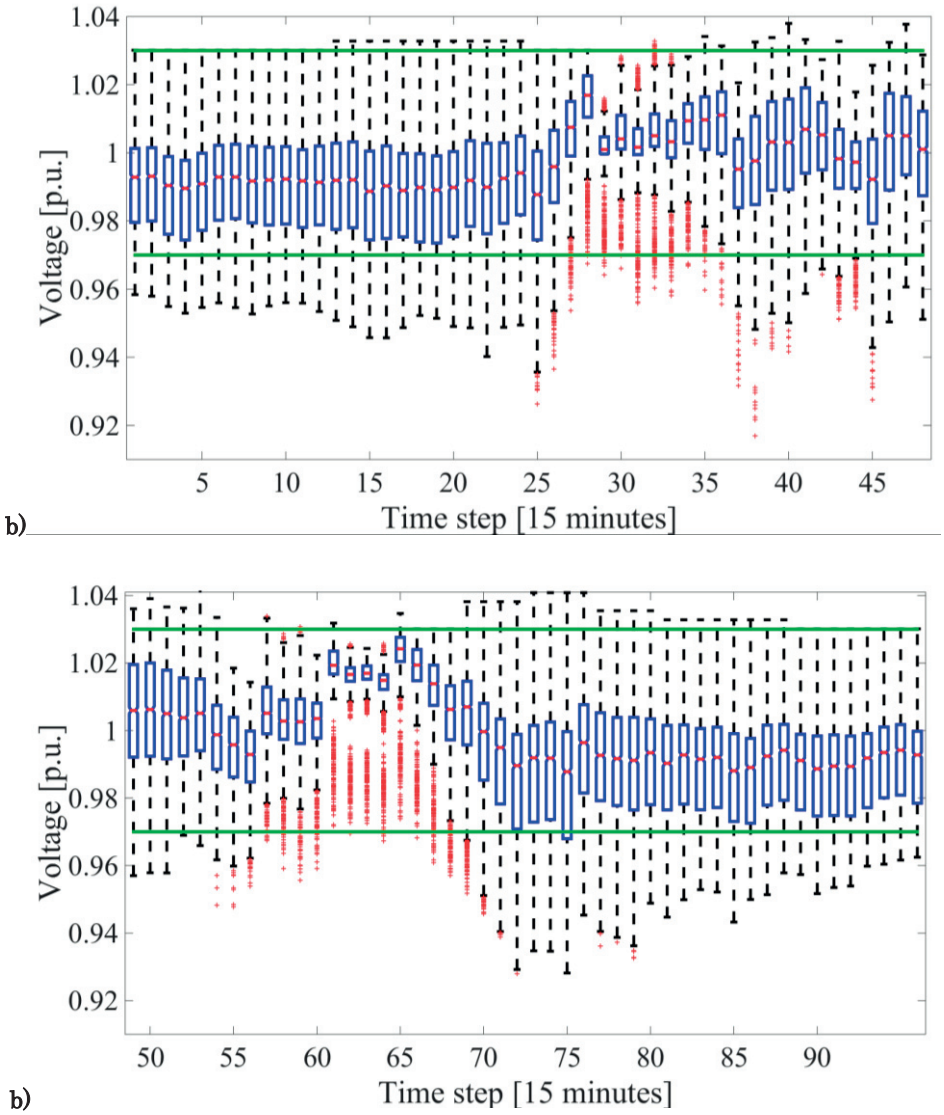

Fig. 3-17: The nodal voltage magnitudes boxplot without presence of ESSs (a). First half of the day, b). Second half of the day)

The stochastic optimization is more straightforward to be modeled. It can have discrete variables (binary and integer ones) as well as non-convex equations. On the other hand, ARO has to be convex (at least the second stage minimization). Due to this fact, we easily modeled the OLTC in the stochastic programming however, it was not included in the ARO approach.

The ARO approach tries to minimize cost of the worst case realization of uncertain parameters whereas the stochastic one minimizes the cost of each scenario concerning its probability. Therefore, the ARO is more conservative but more risk averse. Thus, it depends on the DNO priorities to choose one of the methods.

The stochastic approach requires an accurate estimation of the probability distribution function (pdf) of the uncertain parameters (load, and PV). In contrast, the ARO needs

moderate information concerning the uncertain parameters i.e., the mean and the range of variations. Thus, it is easier and straightforward to model the uncertainty of the parameters in ARO with respect to stochastic approach.

The solution computation time of the ARO depends on the chosen solution strategy. For example, in case of Benders dual cut algorithm, it depends on the number of iterations required for convergence of the algorithm. The solution computation time in case of stochastic programming depends on the number of scenarios. Generally, for small-scale problems stochastic programming is faster than ARO whereas ARO is faster in case of large-scale problems.

A quantitative analysis is provided for comparing ARO and stochastic optimization solutions. In this respect, the solutions of two approaches are compared using the simulation data of section 3.3.4 (test case study of ARO) (uncertainty budget constraints are not considered for load forecasts). The presence of OLTC is not considered in stochastic optimization. The simulation for the case of stochastic optimization is done with 60 scenarios. Afterwards, 1000 scenarios are generated using Multivariate normal random numbers technique. The solutions of ARO and stochastic optimizations are compare using these 1000 scenarios.

Table 3-4: Comparison between ARO and stochastic optimization

	ARO	Stochastic optimization
Computation time [sec]	4098 (average computation time of second stage: 97) Number of Benders iterations : 42	70
Total cost (first and second stages) [CHF]	164.4	128.2
Second stage worst case cost [CHF]	117.6	268

3.7 Summary and Conclusion

In this chapter, the problem of ADN operation and scheduling under uncertainty have been addressed. The sources of uncertainties are load (commercial/industrial and residential ones) and PV productions. A short term forecast method based on ARIMA is developed to model the characteristics of the uncertain parameters and create the uncertainty set for the ARO. The Multivariate Gaussian distribution is used to generate scenarios for stochastic optimization.

The ADN day-ahead scheduling problem is formulated as a two stage optimization programming where the first stage determines the day-ahead decision (hourly schedule

of energy import/export, OLTC tap position and ESSs set points). The second stage deals with intra-day operation of ADN with presence of ESSs.

The results show that the ARO approach is conservative and takes into account the worst case realization of the uncertain parameters. In fact, the day-ahead decision guarantees that the system is feasible for any realization of stochastic parameters and optimal for their worst case realization.

The stochastic programming is more flexible in terms of modeling. Binary variables and non-convex equations could be easily incorporated into the model. Due to this aspect, the OLTC is appropriately modeled and incorporated into the optimization problem.

4 Optimal Planning of Energy Storage Systems in Active Distribution Networks

Chapter highlights:

It is first proposed and discussed a dedicated optimization problem, using voltage sensitivity coefficients, for siting ESSs with the aim of providing voltage support functions.

Then, the AR-OPF proposed in chapter 2, is used to formulate the problem of ESSs optimal siting and sizing in ADNs with a multi-objective approach dealing with energy balance and local grid ancillary services support. Further, the topology changes of ADNs are incorporated in the optimization problem.

In order to account for the stochasticity of different parameters (load, PV and energy price profiles), during the life-time of ESS units, an appropriate scenario generation-reduction procedure is developed. The resulting scenarios are then incorporated into the targeted optimization problems.

In the last part of this chapter, different solutions approach adapted to solve the targeted problems are presented. In particular, the Alternative Direction Method of Multipliers (ADMM) and Benders decomposition are suitably casted to decompose the targeted large-scale problems.

The owner and operator of the ESSs are considered to be the DNO.

4.1 Chapter Organization

In the previous chapters, we assumed to know the sites and sizes of the ESS units. The main goal of this chapter is to propose methodologies for the optimal siting and sizing of ESSs in ADNs. In the followings, a literature review is first presented for the state-of-the-art of the optimal ESS planning in ADNs. Next, the scenario generation and reduction methods, developed to take into account the uncertainties of the parameters, are presented in section 4.4. Then, the proposed model for optimal siting of ESSs aiming to decrease the nodal voltage magnitudes' deviation is described in 4.5. In this model, we use the linear OPF based on the voltage sensitivity coefficients already presented in section 2.4. After that, the proposed optimization models for ESSs siting and sizing in ADNs for network support and energy purposes are then presented in section 4.6. In particular, two models are discussed, i) without considering network reconfiguration ii) with network reconfiguration. The adapted solution approaches are described and compared in section 4.7. Finally, the chapter is concluded in section 4.8 summarizing the main findings.

4.2 State-of-the-art of the optimal ESSs planning in ADNs

In this section, we briefly present the state-of-the-art of optimal resource planning in ADNs including the DGs and ESSs. The subject of DG siting and sizing have been largely addressed in the literature. A comprehensive survey of this subject is presented in [102]. In particular, optimal siting and sizing of DGs in ADNs has been addressed with the following goals: i) minimizing network losses [103, 104], ii) improving reliability criterion [105], iii) performing energy arbitrage [106], and iv) reducing harmonics [107]. In [108], the problem of optimal DG placement is investigated within the specific context of deregulated electricity markets aiming at maximizing the social welfare and profit of DG owners. A multi-objective model for optimal DG siting and sizing in ADNs is presented in [109] and [110]. In particular, the proposed approach takes into account the minimization of investment and maintenance costs of DGs, network operation and capacity adequacy costs, and the total resistive losses. In [111] a methodology based on GA is proposed to determine the sites and sizes of DGs in a distribution network. It takes into account a realistic load model (the power factor of the load is not constant). The objective of the optimization problem includes the minimization of resistive losses, nodal voltage magnitudes' deviations and lines' congestion.

The literature related to ESSs optimal siting and sizing has treated the following aspects. In [112] a methodology for sizing energy storage devices within the context of microgrids is presented. The targeted problem is solved using GA-based approach. In [113] a methodology for allocating energy storage systems in medium voltage distribution networks is proposed with the aim of decreasing wind energy curtailment and minimizing annual cost of the electricity. The Authors in [114] used a hybrid GA, combined with a sequential quadratic programming algorithm, to size and site DGs,

energy storage and reactive power compensation systems. The objective function accounts for the minimization of i) total resistive losses, ii) the costs associated with the network upgrades, and iii) energy cost from the external grid. A hybrid method of dynamic programming with GA has been presented in [115] for optimal integration of energy storage systems in distribution networks. The objective is to find the optimal sites, sizes and control strategy of storage systems in order to minimize the overall investments and network costs (network upgrade and Joule losses). The Authors in [116] presented a model for sizing the ESS systems for providing balancing power in a non-interconnected power network with large penetration of renewables. The peculiarity of the proposed approach is the use of the Discrete Fourier Transform (DFT) to determine the required balancing power in different time-spans. For each time-span (i.e., intra-day, intra-hour and real-time), the proposed approach identifies, by using the DFT-components, the total amount of power/energy required from energy storage systems. A cost-benefit approach is presented in [117] to find the optimal sites and sizes of ESSs in distribution networks. The goal of the optimization is to maximize the DNO profits from energy transactions, as well as investment and operation costs savings. The Authors in [118] presented a methodology for improving the system reliability through the allocation of ESSs in ADNs. The costs of ESS installation are minimized with respect to a dedicated reliability index expressed as customers' willingness to pay to avoid power interruptions. A model for calculating the optimal size of an ESS unit in a microgrid considering a reliability criterion is presented in [119]. The proposed MILP model minimizes the investment cost of the ESS, as well as the expected microgrid operating cost. In [120], the Authors proposed an optimal planning programming for siting and sizing the battery energy storage systems in ADNs. The objective function is to minimize the investment and operation costs (cost of energy purchase, resources maintenance and operation costs). A hybrid Tabu search/particle swarm optimization (TS/PSO) algorithm is used to solve the optimization problem. The planning of ESSs connected to transmission networks has been also investigated in the literature (e.g., [121], [122]). In [121] the optimal planning of ESSs in a network with renewable and uncertain energy production resources is presented. The objective of the optimization is to minimize the operation and investment costs of energy storage devices. The application of ESSs in optimal allocation of wind capacity related to distant wind farms is investigated in [122]. The methodology simultaneously optimizes the wind farm capacity of each site, its ESS and the required transmission connection capacity.

A common technical drawback of the above-listed papers is that they did not account for the capability of ESSs to provide local ancillary services (by supplying both active and reactive powers) with particular reference to voltage control and line congestion management.

Another drawback is related to the proper formulation of the OPF in relation to the correct treatment of its non-linearities and non-convexities. The above-mentioned papers either use non-convex formulation of the OPF or only address the economic aspects without considering the technical constraints of the networks (e.g., network

power flows and bus voltage constraints). In this respect, we propose to make use of AR-OPF (proposed in section 2.2.4) in order to obtain a convex and exact OPF model.

Another contribution of this chapter is related to the inclusion of topology changes in the targeted planning problem. In particular, the ADN optimal reconfiguration model proposed in section 2.3.2 is employed.

Additionally, we appropriately, formulate the objective function as a multi-objective linear one. We have accounted for the minimization of the following elements: a) lines' congestion, b) nodal voltages' deviations c) load curtailment, d) dispatchable DG and ESS units' operation costs as well as energy supply cost, and f) ESSs investment and maintenance costs.

Finally, we incorporate the scenarios related to the variations of PV, load, and energy prices in different time spans (weekly, seasonal, and yearly variations). This inclusion might drastically increase the size of the optimization problem. In order to deal with this issue, we have proposed to use the decomposition techniques relying on the ADMM and Benders procedure.

It should be noted that the owner and operator of the ESSs is considered to be the DNO.

4.3 Energy Storage Modeling

ESSs could cover a wide spectrum of applications into electrical networks ranging from fast power quality problems to energy management. ESS technologies that fit the ADN applications are essentially the following: batteries, super/ultra-capacitors, compressed air systems, power-to-gas, pumped-hydro storage, and flywheels. In this study, the most important characteristics of ESSs in terms of charge/discharge dynamics, the availability of State-of-Charge (SoC) models, power rating capabilities, and internal losses are taken into account for integrating ESSs into the targeted problem. The generic ESS model used in this study is described in the followings.

ESS State-of-Charge (SoC):

The state-of-charge of an energy storage system depends on its power production/consumption, and its losses. The SoC of the ESS is formulated as[1]:

$$E(t) = E(t-1) - \frac{P^d(t)\Delta t}{\eta^d} + P^c(t)\Delta t\eta^c - \Lambda(t)\Delta t \qquad (4.1.a)$$

[1] In the rest of the manuscript, the term "SoC" is used to quantify the energy content of the ESS reservoir. This aspect is specified to avoid confusion with the SoC concept used in electro-chemical storage systems to quantify the charge level (expressed in Coulombs).

$$CE^{l} \le E(t) \le CE^{u} \tag{4.1.b}$$

where $E(t)$ is the energy level in the reservoir at time t, $P^{d}(t)$ and $P^{c}(t)$ are the discharging and charging powers of ESS at time t, η^{d} and η^{c} are the discharging and charging efficiencies, Δt is the time step, C is the capacity of the ESS reservoir, Λ models the resistive losses and is described later (see equation (4.2)), E^{l} and E^{u} are the maximum and minimum allowed SoC levels. Finally C is the capacity of ESS reservoir.

Equation (4.1.a) is the general form of SoC and, based on the type of the ESS can be modified. It implies that the amount of stored energy in the ESS reservoir at time t depends on its state in the previous time step, the net energy injected/extracted from it, and the internal losses. The internal losses may depend on the level of power production/consumption and/or it could be fixed regardless of the ESS output. In case of resistive losses, we have relaxed the original equality constraint to an inequality one (see (4.2)). This allows to have a convex constraint.

$$\Lambda(t) \ge r^{ess}\left(\left(Q^{e}(t)\right)^{2} + \left(P^{d}(t)\right)^{2} + \left(P^{c}(t)\right)^{2}\right) \tag{4.2}$$

where r^{ess} is the internal equivalent resistance of the ESS and $Q^{e}(t)$ is the reactive power production/consumption of the ESS at time t.

We have added an auxiliary SOC constraint, in addition to the original one, assuming an ideal efficiency (100%) for this specific auxiliary variable. This auxiliary constraint is necessary to avoid ill use of relaxed ESS efficiencies in order to create an unreal load (this could happen in case of high amount of injections into the grid). The presence of this auxiliary variable is justified by the relaxation used in (4.2).

$$\hat{E}(t) = \hat{E}(t-1) - P^{d}(t)\Delta t + P^{c}(t)\Delta t \tag{4.2.b}$$

$$CE^{l} \le \hat{E}(t) \le CE^{u} \tag{4.2.c}$$

ESS capability curve:

ESSs are normally interfaced with the grid using a power electronic converter. In this respect, their capability curve is governed by the ampacity limit of the power converter that, in case of an operation under constant AC grid voltage, can be translated into a constraint on the apparent power delivered by the ESS as shown in (4.3).

$$\left(Q^{e}(t)\right)^{2} + \left(P^{d}(t)\right)^{2} + \left(P^{c}(t)\right)^{2} \le \left(\mathcal{R}\right)^{2} \tag{4.3}$$

where $\mathcal{R}$ is the power rating of the ESS.

In case of optimal ESS siting and sizing, $\mathcal{R}$ (ESS power rating) on the right hand side of equation (4.3) is a decision variable. Therefore, this constraint is non-convex. In order to have convex formulation, this constraints is linearized as shown in Fig. 3-6.

ESS Ramping limit:

The ESSs ramp-up and ramp-down constraints are modeled as below:

$$P^d(t+1) - P^d(t) \leq R^{up} \tag{4.4.a}$$

$$P^c(t+1) - P^c(t) \leq R^{dn} \tag{4.4.b}$$

where R^{up} and R^{dn} are obviously the ramp-up and ramp-down of the ESS.

Finally, the energy stored in the ESS at the end of the day have to be greater than or equal to its initial value at the beginning of the day.

$$\begin{aligned} E(t^{\text{fin}}) &\geq E(t^1) \\ \hat{E}(t^{\text{fin}}) &\geq \hat{E}(t^1) \end{aligned} \tag{4.4.c}$$

For the sake of brevity, hereinafter in this document, the above set of equations used for modeling the ESSs are represented as following:

$$\Psi(\alpha, \beta) \geq 0 \tag{4.5}$$

where α is the vector of variables (active and reactive power production/consumption (P^d, P^c, Q^e), energy level of ESS reservoir (E) and its auxiliary variable ($\hat{E}$), power rating and energy reservoir capacities ($C, \mathcal{R}$), and the resistive losses of ESSs (Λ). β is the vector of parameters (charging and discharging efficiencies (η^c, η^d), ramp rates (R^{up}, R^{dn}), and time step (Δt).

4.4 Treatment of Uncertainties for Long-term Planning

The aim of this section is to illustrate an approach to generate appropriate scenarios for load and PV profiles. The presence of this section is needed since the long-term planning problems require the knowledge, to some extent, of the distribution of the parameters' variations. Some of the parameters (load, PV, and energy price) have variations and consequent uncertainties. These variations are characterized by stochastic behaviors over different time spans. The PV profiles have variations across the seasons and, also, they exhibit dissimilar characteristics for the cloudy and clear sky conditions. The load and energy prices have seasonal variations in addition to dissimilarities in weekdays and weekends. Additionally, their profile can have variations with respect to the external parameters like temperature and/or holidays and they also have variations from year to year. These variations need to be taken into account in the planning.

4.4.1 Scenario generation for load consumption, photovoltaic production and energy price

The historical data of the load, solar irradiation (PV production), and energy price are assumed to be available. These data are grouped with different criteria. In case of the load and energy price, they are first divided into 3 bins representing the seasonal

variations (winter/spring-fall/summer). The grouped data for each season is again divided into two categories: weekdays, weekends. Finally, the data in the weekends and weekdays bins are divided into two groups. This last step is necessary since there may exist a big variation in the weekend/weekdays load/energy price profiles of each season with respect to temperature or other external factors. Similar to the load data, the PV data is distributed among three group representing the seasonal variations. The data

of each season is again divided with the irradiation profiles for clear or cloudy sky. Finally, the data in the partially cloudy sky bins are divided into three groups. These data clustering are shown in Fig. 4-1.

In order to statistically characterize these uncertain parameters (load and PV), we assume that the aggregate load/PV at the k_th time interval of the day denoted hereafter by $\mathcal{S}_k$ is a random variable. For each time interval, we observe the available samples and the mean $(\mathcal{S}_k - \bar{\mathcal{S}}_k)$. The QQ-plot of the zero-mean data of load for a specific time interval in each specific season is shown in Fig. 4-2. Similarly, the QQ-plot of PV production for one specific time interval in a clear day and one specific time interval in a partially cloudy sky day are shown in Fig. 4-3. The data for the rest 95 time intervals are not shown here for the sake of brevity as they exhibit almost similar characteristics. As it can be observed the data are approximately Gaussian.

In order to generate scenarios, we have accounted for the temporal correlation of the parameters during the day. We assumed that the daily vector of each input parameter (load, and PV) has a multivariate Gaussian distribution with mean μ and covariance Ω ($\mathcal{N}(\mu, \Omega)$). The mean and covariance matrix of the parameters are obtained empirically using the historical data in each bin. The obtained distributions are used to generate

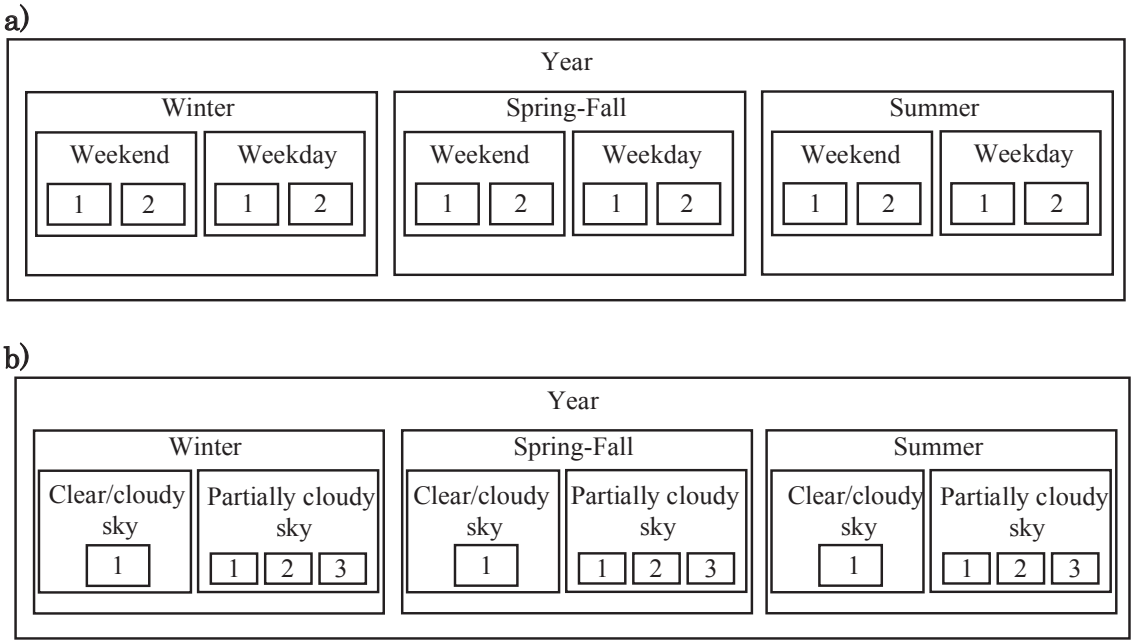

Fig. 4-1: Load, energy price and PV data clustering a) load and energy price b) PV data

appropriate scenarios using multivariate normal random numbers for each bin. Once the scenarios for load and PV are generated, they are used to generate the final scenario tree.

The obtained scenarios for the PV production are distributed among the PV sites in proportion to their nominal power. In this way, we achieve their spatial correlation. In order to account for the spatial correlation of the load data, the generated scenarios for the load are distributed among the buses of the system based on their seasonal/daily load level. It should be noted that the best approach is to treat the load of the system based on their type (i.e., commercial, industrial, and residential). However, we have considered the spatial correlations based on the rating of the low voltage transformers since we did not have the load profiles based on their types.

The annual increase rates of the load and PV are considered to be constant.

In case of energy price scenarios, the historical energy price data for one year are used as the initial scenarios. The energy and fuel prices' growth over the years are modeled by using the Geometric Brownian Motion (GBM) [123].

4.4.2 Scenario reduction technique

Accounting for all possible scenarios may results in computationally expensive simulations. Thus, often the number of scenarios is reduced to a reasonable one characterized by the same degree of volatility/stochasticity of the original scenarios.

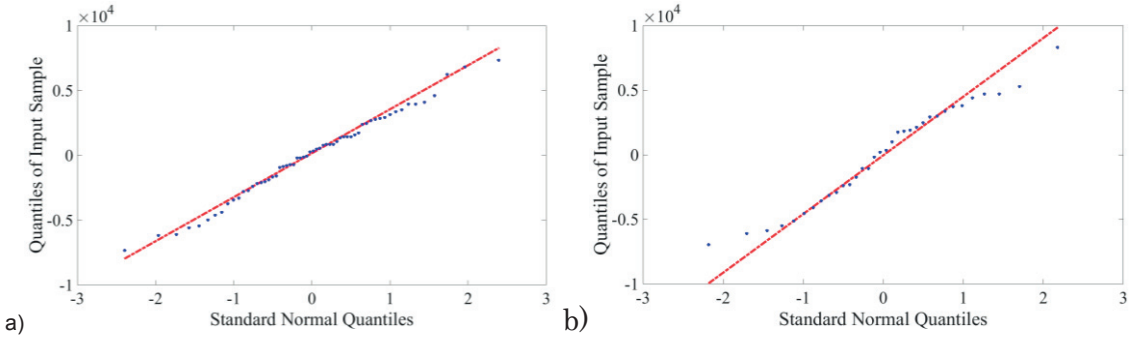

Fig. 4-2: QQ-plots of zero-mean load data (recorded data in the southern east part of Switzerland) for a specific time interval during a) fall-spring b) summer

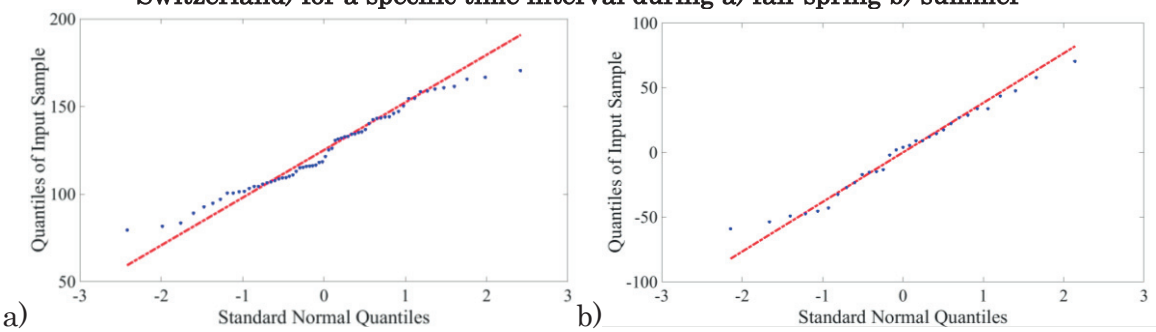

Fig. 4-3: QQ-plots of zero-mean PV data (recorded data in the southern east part of Switzerland) for a specific time interval during a) partially cloudy sky b) clear sky

The scenarios for our targeted problems are the daily load/PV/price ones. In other words, we have scenarios in the form of time series with $T_L + T_{PV} + T_{Pr}$ dimension. T_L, T_{PV} and , T_{pr} are the length of the daily load, PV, and price profiles respectively. The first step for scenario reduction is to determine an appropriate criterion for comparing the resemblances of the scenarios. In this study we have employed Euclidian distance to determine the similarities between each pair of daily profiles. Afterwards, the scenario reduction procedure explained in 3.5.2.2 is employed to reduce the generated scenarios.

4.5 Optimal Siting of ESSs in ADNs to Achieve Voltage Control Using a Linearized OPF Model

The context of the problem refers to active distribution networks characterized by the presence of non-dispatchable generation. The possibility to take advantage of demand-side management is not considered. We assume to know the phasors of phase-to-ground voltages at all the network busses at a generic time t. The objective of the problem is to find the best locations of ESSs that contribute to minimize the voltage deviations at all the network busses. For this reason the problem can be formulated as a planning one with classical time step discretization of 15 minutes. The investment costs are not taken into account. It is assumed that the maximum number of total ESSs units is given. Additionally, it is assumed that the various ESSs locations have equal installation and operation costs. This hypothesis relies on the fact that ESSs used for ADNs are typically composed by electrochemical storage systems whose installation costs is site independent.

In view of the above, the optimization problem is formulated as follows using linearized power flow equations introduced in section 2.4:

$$\underset{\Xi}{\text{minimize:}}\ \theta_{\varphi} \sum_{\varphi\in\Phi}\sum_{t\in T}\sum_{l\in\mathcal{L}}\left(\left(\Delta V_{l,\varphi}(t) + V_{l,\varphi}(t)\right) - V^{r}\right)^{2} \tag{4.6.a}$$

Subject to:

$$\Delta V_{l,\varphi}(t) = \mathbf{A}^{P}_{l,\varphi}(t)\Delta P_{\varphi}(t) + \mathbf{A}^{Q}_{l,\varphi}(t)\Delta Q_{\varphi}(t) \quad \forall l \in \mathcal{L}, t \in T, \varphi \in \Phi \tag{4.6.b}$$

$$\Psi(\alpha_{l,\varphi}(\mathrm{t}), \beta_{l,\varphi}(\mathrm{t})) \geq 0 \quad \forall l \in \mathcal{L}_{ess}, \forall t \in T, \forall \varphi \in \Phi \tag{4.6.c}$$

$$\Delta P_{l,\varphi}(t) = P^{d}_{l,\varphi}(t) - P^{ch}_{l,\varphi}(t), \quad \Delta Q_{l,\varphi}(t) = Q^{e}_{l,\varphi}(t), \quad \forall l \in \mathcal{L}_{ess}, t \in T \tag{4.6.d}$$

$$\mathcal{R}_{l} \leq a\mathrm{u}_{l} \quad \forall\, l \in \mathcal{L} \tag{4.6.e}$$

$$C_{l} \leq b\mathrm{u}_{l} \quad \forall\, l \in \mathcal{L} \tag{4.6.f}$$

$$\sum_{l\in\mathcal{L}} \mathrm{u}_{l} \leq \mathcal{U} \tag{4.6.g}$$

$$\mathrm{u}_l \in \{0,1,\ldots,\} \quad \forall\, l \in \mathcal{L} \tag{4.6.h}$$

where $\Xi = \{\mathrm{u}, \alpha, \Delta V, \mathcal{R}, C, \Delta P, \Delta Q\}$ and $\alpha_\varphi(t) = \{P^d(t), P^c(t), Q^e(t),\ E(t),\ \mathcal{R}, C, \hat{E}(t)\}$ represent the optimization variables (recall that a notation without subscripts represents the vector of corresponding variables/parameters and $\Psi(\alpha, \beta)$ represents the ESS constraints). $\varphi \in \Phi$ is the index of scenarios and $t \in T$ is the index of time step discretization of each scenario. $l \in \mathcal{L}$ is the index of the network buses other than the slack bus, θ_φ represents the probability of scenario φ, and $\mathcal{L}_{ess}$ is the set of busses with ESSs (the candidate buses for installing ESSs).

The objective function shown in (4.6.a) minimizes the differences between the reference voltage magnitude (V^r) and the voltage magnitude of the network buses over a given period of time[1]. For the sake of brevity, the set of constraints of ESSs introduced in section 4.3 are represented as $\Psi(\alpha_{l,\varphi}(t), \beta_{l,\varphi}(t))$ for all buses, scenarios and time steps. It should be noted that the resistive losses, ramp-up and ramp-down limits of the ESSs are not considered here. $\mathcal{R}_l$ and C_l are the maximum power rating and energy reservoir capacity of ESS units which are bounded by the number of ESSs units (u_l) allocated at bus l, $\mathcal{L}_{ess}$ is the set of the buses with ESS. a and b are the power rating and energy reservoir capacity of one ESS unit, respectively. The total number of ESS units is limited to $\mathcal{U}$.

4.5.1 Solution methodologies

The formulated problem is a Mixed Integer Quadratically Constrained Quadratic Programming (MIQCQP). This type of optimization problems can be solved using state-of-the-art commercial software. In case of large-scale distribution networks with high number of scenarios, decomposition methods could be used to decompose the original problem. In what follows we present the Benders decomposition approach applied to our targeted problem. In this respect, the optimization problem is decomposed into a master one, which determines the site and number of ESSs unit for each bus of the system, and a set of subproblems, which quantify the fitness of the master problem solution. The ESSs capacities obtained in the master problem are fixed and imposed on the subproblems. The solution of each sub-problem allows defining a set of dual values indicating the changes in the subproblem objective functions resulting from marginal variations in the ESS capacities. These duals are returned to the master problem as a feedback in order to setup an iterative procedure. In particular, Benders cuts are generated from these dual values governing the determination of the master problem solution. This process is iterated between the master problem and the sub-problems until it converges to the optimal solution. Since the subproblems are independent from each other, they can be processed simultaneously in parallel. Fig. 4-4 demonstrates the

[1] Note that the slack-bus voltage is not considered in the objective function.

proposed procedure. More details about Benders decomposition are given in Appendix A.4.

4.5.1.1 Master problem

The initial master problem determines the number of ESS units at each bus of the grid regardless of the sub-problems. Afterwards, at each iteration, a cut from each sub-problem is added to the master problem representing the changes in the subproblems objective function resulting from marginal variations in the ESS capacities. The master problem is formulated as shown in (4.7.a)-(4.7.d).

$$\underset{\mathcal{Z},\mathcal{I},\mathrm{u}}{\text{minimize:}} \sum_{\varphi\in\Phi} \mathcal{Z}_{\varphi} + \mathcal{I} \tag{4.7.a}$$

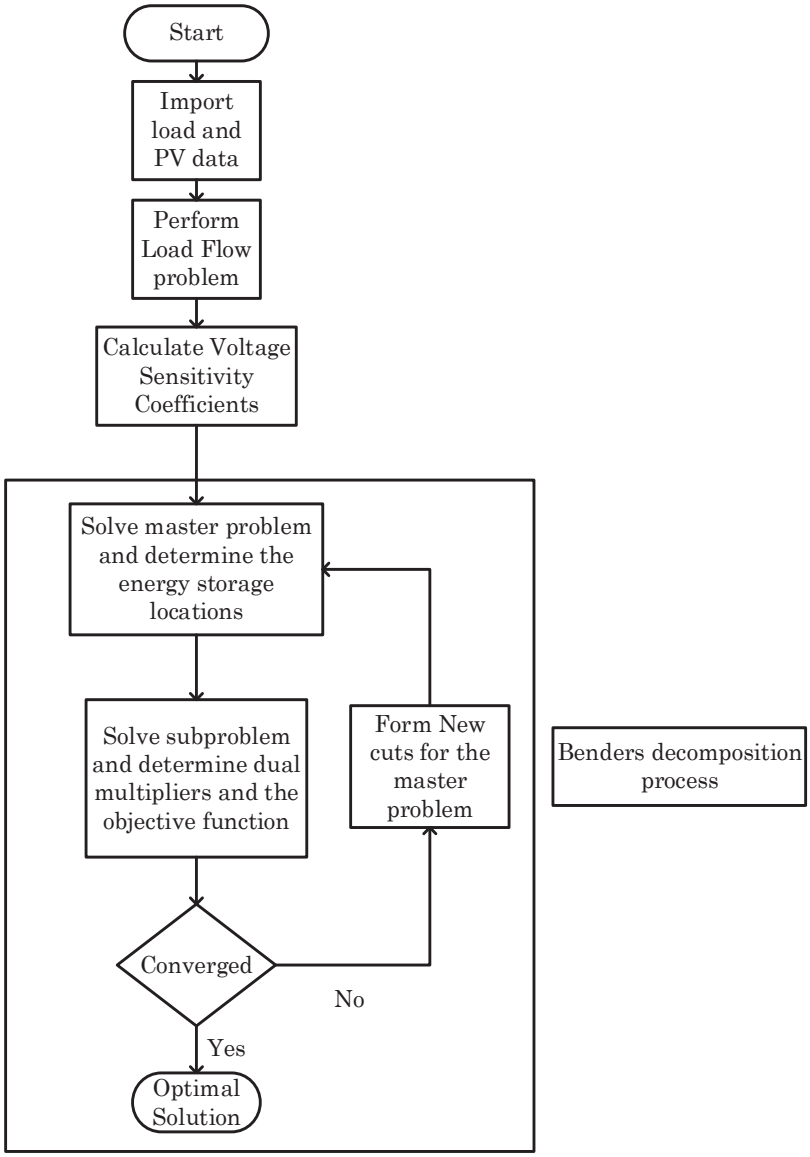

Fig. 4-4: Flowchart of the proposed methodology using Benders decomposition

subject to:

$$\mathcal{Z}_{\varphi} \geq 0, \forall \varphi \in \Phi \tag{4.7.b}$$

$$(4.6.g), (4.6.h) \tag{4.7.c}$$

$$\mathcal{Z}_{\varphi} \geq \Upsilon_{\varphi}^{(n)} \quad \forall \varphi \in \Phi, \forall\, n \in \mathcal{N} \tag{4.7.d}$$

where $\mathcal{I}$ represents the investment and $\mathcal{Z}_{\varphi}$ represents the cost related to each subproblem ($\varphi \in \Phi$) (using dual variables). The other constraints are related to the maximum number of ESS units that can be installed and the discrete nature of ESS units. The constraint (4.7.d) represents the generated cuts from the subproblems. n is the index of Benders iteration. The cuts' formulation is described in the next sub-section.

4.5.1.2 Sub-problem

The sub-problems objective is to minimize the voltage magnitude deviations using the identified ESS units in the master problem. The formulation of the subproblem for each scenario (φ) is shown in (4.8.a)-(4.8.c).

$$\underset{\Xi}{\text{minimize:}}\ \mathrm{A}_{\varphi} = \sum_{t \in T} \sum_{l \in \mathcal{L}} \left(\left(\Delta V_{l,\varphi}(t) + V_{l,\varphi}(t) \right) - V^{r} \right)^{2} \tag{4.8.a}$$

Subject to:

$$(4.6.b)\text{-}(4.6.f) \tag{4.8.b}$$

$$\mathrm{u}_{l} = \hat{\mathrm{u}}_{l} : \quad \lambda_{l,\varphi} \quad \forall\, l \in \mathcal{L} \tag{4.8.c}$$

where $\Xi = \{\mathrm{u}, \alpha_{\varphi}, \Delta V_{\varphi}, \mathcal{R}, C_{l}, \Delta P_{\varphi}, \Delta Q_{\varphi}\}$ and $\alpha_{\varphi} = \{P_{\varphi}^{d}, P_{\varphi}^{c}, Q_{\varphi}, E_{\varphi}, \mathcal{R}, C, \hat{E}_{\varphi}\}$ (α_{φ} is the set of variables for modeling ESSs constraints) represent optimization variables.

The $\lambda_{l,\varphi}$ represents the Lagrange multipliers associated o the constraint (4.8.c). Note that $\widehat{\square}$ indicates that $\hat{\mathrm{u}}_{l}$ is a parameter that is obtained in the master problem.

After solving the subproblems, the following set of cuts is generated and added to the next iteration of the master problem.

$$\Upsilon_{\varphi}^{(n)} = \hat{\mathrm{A}}_{\varphi}^{(n)} - \sum_{l \in \mathcal{L}} \lambda_{l,\varphi} \left(\mathrm{u}_{l} - \hat{\mathrm{u}}_{l}^{n} \right), \forall \varphi \in \Phi \tag{4.9.a}$$

where $\widehat{\mathrm{A}}^{n}$ is the identified value of objective function in the subproblem φ and is a parameter. $\hat{\mathrm{u}}_{l}^{n}$ is the number of ESS units on bus l, in iteration n of the Benders decomposition and is a parameter.

The proposed procedure iterates between the master problem and subproblems until it converges to the optimal solution.

4.5.2 Simulation results

This section presents the use of the proposed method with reference to the IEEE 13 buses test network. We also provide a comparison between solving the original problem and the decomposed one regarding their solutions and computational performances. The schematic of this network is shown in Fig. 2-12. It is supposed to have non-dispatchable DG units composed by photovoltaic panels (PVs). Concerning the representation of the network loads, they are considered as voltage independent PQ absorptions. The time series related to active load absorption and PV production make reference to experimentally measured data in a region located in the southern-east part of Switzerland. The power factor of loads is considered constant during the whole time series.

The power injections of PVs have been represented by voltage-independent active power injections with null reactive component. It is assumed that the non-dispatchable PV injections are installed on buses #646, #684, #675, and #633 with a maximum rated power of 400 kW each. The relevant time series make reference to real measured solar irradiation in the central region of Europe. It is assumed that DNO can allocate a maximum of 10 ESS units with 10 kW power rating capacity and 100 kWh energy capacity each. The maximum number of ESSs units that can be installed on each buses of the system is considered to be 5. The scenario generation/reduction method presented in section 4.4 is used to create 1000 scenarios and then reduced to 100 ones (the Euclidean distance for scenario reduction is considered to be of 0.9 p.u.). The final scenarios for load and PV are shown in Fig. 4-5.

Making reference to a simulation window of 100[1] days discretized in 15 minutes time-intervals, i.e. 96 time intervals per day, Table I shows the results related to the optimal allocated ESSs capacities at each bus of the network. Further a comparison is provided regarding the solutions of the decomposed problem and the original one[2]. As it can be seen from this Table, both approaches give the same solution, however, the computational performance of the case with Benders decomposition outperforms largely the one of original optimization problem[3].

The probability distribution density of the nodal voltage magnitudes corresponding to all buses for the whole simulated period is shown in Fig. 4-6. In particular, Fig. 4-6.a

[1] It should be noted that number of scenarios obtained from scenario generation and reduction method presented in section 4.4 is equal 97. We added three more scenarios to have 100 scenarios.

[2] The simulations are done on a desktop PC with 16 GB RAM memory and Intel Xenon CPU E5-1650@3.20 GHz. Gurobi version 6.0.5 is used to solve the optimization problems. The optimality Gap for MIQCP is chosen to be 0.01 %.

[3] The Gurobi solver benefits from the state of the art in solving MIQCP problems like Presolve, Cutting Planes, Heuristics, and Parallelism for solving MIQCP [124] J. T. Linderoth and A. Lodi, "MILP software," *Wiley encyclopedia of operations research and management science,* 2011..

refers to the case without ESSs whilst Fig. 4-6.b refers to the case in which ESSs are installed in agreement with the optimal location reported in Table I. As it can be observed, this last case results into voltages densities closer to the value of 1 p.u.. In particular, the under-voltages below 0.94 and over-voltages above 1.04 are completely removed.

4.5.2.1 Convergence of Benders decomposition

In case of using Benders decomposition, the value of the objective function for upper and lower bounds (see Appendix A.4), that represents the total nodal voltage magnitudes' deviation for all the considered time intervals and for all the buses, is shown in Fig. 4-7. As it can be seen, the procedure converges after 22 iterations and results into minimum identified total nodal voltage magnitudes' deviations.

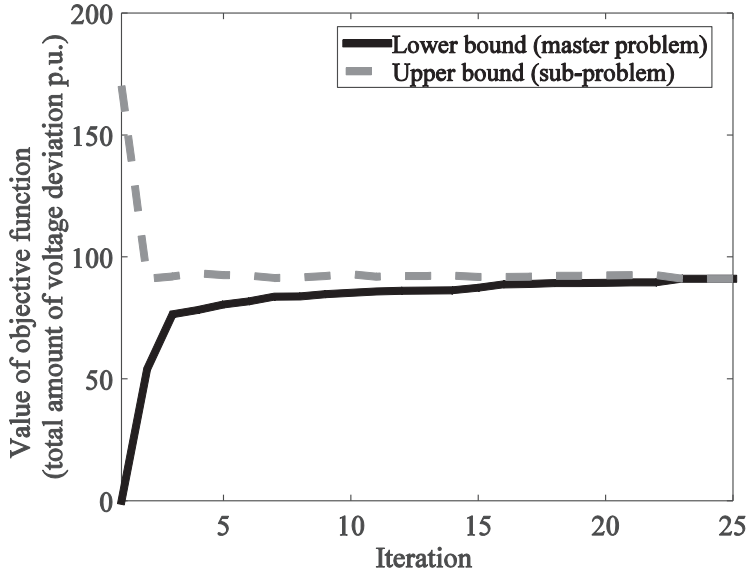

Fig. 4-7: Bender decomposition convergence

4.6 Optimal Planning of ESSs in ADNs for energy balance and local grid support

In the previous section, we proposed a model for optimal siting and sizing of ESSs aiming at minimizing the nodal voltage magnitudes' deviations. We used the voltage sensitivity coefficients to linearize the problem. In order to improve our approach and avoid the approximation related to the linearization, in this section we present two optimization models for optimal siting and sizing of ESSs in ADNs with the AR-OPF model presented in 2.2.4 and the proposed ADN optimal reconfiguration model

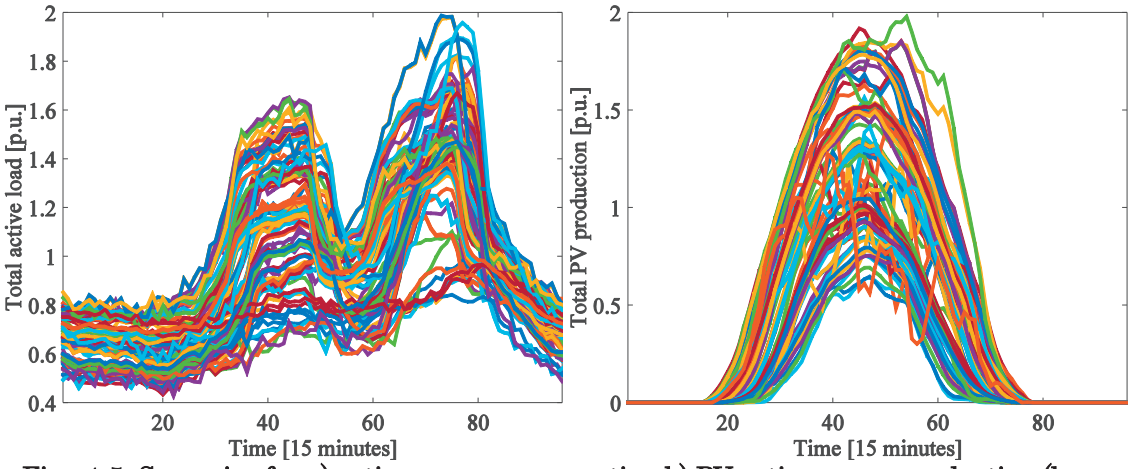

Fig. 4-5: Scenarios for a) active power consumption b) PV active power production (base value is 5 MW)

Table 4-1: Identified ESSs sites and numbers (each unit of ESS has 10kW power rating capacity and 100kWh energy reservoir capacity)

	Bus #	Number of units	Computation time [sec]
Using Benders decomposition	# 684	5	69
	# 652	5	
Without Benders decomposition	# 684	5	685
	# 652	5	

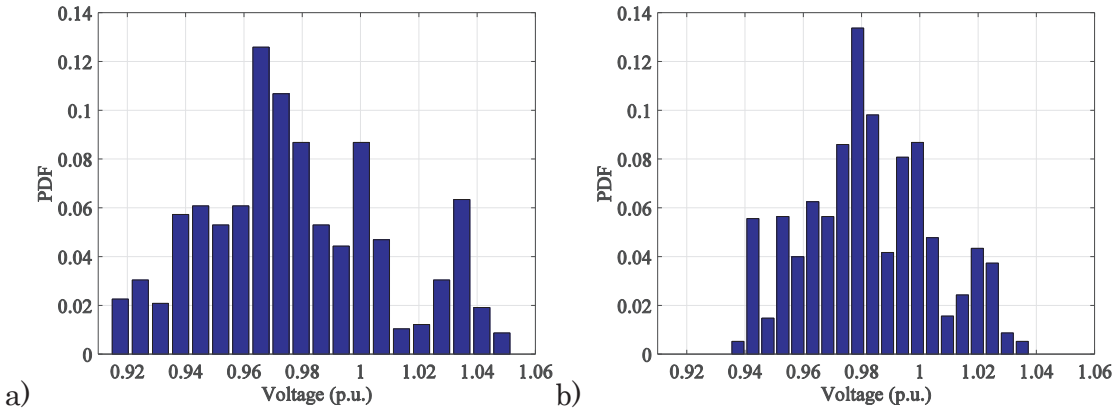

a) b)

Fig. 4-6: Distribution of nodal voltage magnitudes in the network (for 100 days with 15 minutes discretization; a) without ESSs b) with optimally placed ESSs

proposed in 2.3. Further, we augment the objective function to take into account for various goals related to ESS planning.

As introduced in the previous section, the context refers to ADNs with the presence of non-dispatchable generation. It is supposed that the ADN is connected to an external sub-transmission grid characterized by a given day-ahead hourly cost of the energy exchange known for a time window of 24 hours. The goal is to optimally site and size ESSs in the given radial ADN. The objective function includes two main parts (i) the investment and maintenance costs of ESSs ($\mathcal{C}^e$) and (ii) the operation cost of the targeted grid during the ESSs lifetime ($\mathcal{C}^g$) (brought to the year of investment).

The former cost is composed of a fixed investment cost for each ESS and the cost related to its relevant power and energy capacities. The maintenance cost (brought to the year of the investment) is also accounted.

The operation objective aims at minimizing a virtual cost associated with the system operation conditions. This virtual cost includes: (i) nodal voltage magnitude deviations, (ii) line congestions, (iii) total network losses, (iv) cost of energy from the external grid, and (v) load curtailment. Each term in the objective function has a suitable weighting coefficient that might be selected by the DNO as a function of his needs/priorities, or using a dedicated weighting coefficient technique. The virtual cost is minimized for the whole simulated time period considering a set of scenarios.

The weighting coefficient of each term is determined by using the Analytic Hierarchy Process (AHP) proposed by Thomas L. Satty in [125]. In AHP method, first a pairwise comparison is done between the objectives. The decision-maker (i.e. the DNO) defines the importance of each factor in comparison with all the other ones. This pairwise comparison depends on the needs of the decision maker and it can vary from network to network and operator to operator. Then a matrix is built based on these pairwise comparisons and the final weights are calculated based on this metric. The AHP process is described in Appendix A.2.

For the sake of brevity, hereinafter in this chapter, the set of equations for modeling the AR-OPF (see section 2.2.4.2) are represented as follows:

$$\Theta(\gamma, \tau) \geq 0 \tag{4.10}$$

where γ is the vector of variables that includes i) square of nodal voltages' magnitude (v), ii) dispatchable nodal injections (ESS production and consumption), iii) square of current producing losses in the network (f), and its relevant auxiliary variable ($\bar{f}$) iv) complex power flow of the lines ($S = P + jQ$), v) auxiliary variable associated with the square of nodal voltages' magnitude ($\hat{v}$), vi) upper bounds associated with the square of current flows at both ends of the lines (I^t, I^b) and vii) auxiliary variables for the complex power flow of the lines ($\bar{S} = \bar{P} + j\bar{Q}, \hat{S} = \hat{P} + j\hat{Q}$). τ is the vector of parameters that includes i) lines parameters (r, x, b), nodal load and non-dispatchable

generations (PV), square of lines' ampacity limit ($I^{\max}$), and upper and lower limits of the square of nodal voltage magnitudes ($v^{\max}$ and $v^{\min}$).

The upper bounds for the square of current flows at both ends of the lines are formulated as shown in the following (see the constraints of AR-OPF (section 2.2.4)).

$$\left|\max\left\{\left|\hat{P}_l^t\right|,\left|\bar{P}_l^t\right|\right\}+j\left(\max\left\{\left|\hat{Q}_l^t\right|,\left|\bar{Q}_l^t\right|\right\}\right)\right|^2 \le I_l^{\mathrm{t}} V_{\mathrm{up}(l)} \qquad (4.11.a)$$
$$I_l^{\mathrm{t}} \ge 0$$

$$\left\|\max\left\{\left|\hat{P}_l^b\right|,\left|\bar{P}_l^b\right|\right\}+j\max\left\{\left|\hat{Q}_l^b\right|,\left|\bar{Q}_l^b\right|\right\}\right\|^2 \le I_l^{\mathrm{b}} V_l \qquad (4.11.b)$$
$$I_l^{\mathrm{b}} \ge 0$$

Similarly the corresponding set of equations for the proposed optimal ADN reconfiguration model (proposed in section 2.3.2) are represented as following:

$$\mathrm{B}(\sigma,\varsigma) \ge 0 \qquad (4.12)$$

where σ is the vector of variables that includes i) square of nodal voltages magnitude (v), ii) auxiliary variables for the square of nodal voltage magnitudes ($\bar{v}, \hat{v}', v', \hat{v}'', v''$), iii) complex power flow of the lines in both directions ($S_{kl} = P_{kl} + jQ_{kl}, S_{lk} = P_{lk} + jQ_{lk}$), vi) auxiliary variables for the complex power flow of the lines in both directions ($\bar{S}_{kl} = \bar{P}_{kl} + j\bar{Q}_{kl}, \hat{S}_{kl} = \hat{P}_{kl} + j\hat{Q}_{kl}, \bar{S}_{lk} = \bar{P}_{lk} + j\bar{Q}_{lk}, \hat{S}_{lk} = \hat{P}_{lk} + j\hat{Q}_{lk}$), v) lines direction variables (d_{lk}, d_{kl}), vi) binary variables associated with the switches (κ_{kl}), vii) reactive power associated with the shunt capacitances (Q^{sh}), viii) auxiliary variable for reactive power associated with the shunt capacitances ($\hat{Q}^{sh}$), ix) dispatchable nodal injections (ESSs production and consumption), x) square of currents producing losses in the network (f_{kl}, f_{lk}) and their relevant auxiliary variables ($\bar{f}_{kl}, \bar{f}_{lk}$) in both directions, finally upper bounds for the square of current flows at both ends of the lines (I_{kl}, I_{lk}). ς is the vector of parameters that includes i) lines parameters (r, x, b), ii) nodal load and non-dispatchable generations (PV), iii) square of the lines ampacity limit ($I^{\max}$), iv) upper and lower limits of the square of nodal voltage magnitudes ($v^{\max}$ and $v^{\min}$).

The corresponding set of equations for the proposed optimal ADN reconfiguration model using DistFlow equations are represented with $\mathrm{B}'(\sigma',\varsigma') \ge 0$.

In this thesis two models are developed for optimal planning of ESSs in ADNs. The first one, called $\mathcal{P}_1$, is formulated using the AR-OPF formulation (see section 2.2.4.2) and does not take into account ADN reconfiguration (i.e., a fixed topology is considered for the network). The second one, called $\mathcal{P}_2$, is developed using the proposed ADN optimal reconfiguration model (see section 2.3.2). $\mathcal{P}_1$ and $\mathcal{P}_2$ are described in the followings.

$\mathcal{P}_1$:

$$\underset{\Xi}{\text{minimize:}}\ \mathcal{C}^e + \mathcal{C}^g \tag{4.13.a}$$

$$\mathcal{C}^e = \mathcal{W}_E \left(\begin{array}{l} \left\{ \sum_{l\in\mathcal{L}} \left(\mathcal{I}_c \mathfrak{u}_l + \mathcal{I}_p \mathcal{R}_l + \mathcal{I}_e C_l \right) \right\} \text{ Investment cost} \\ + \frac{1}{(1+\omega)^{(y)}} \left\{ \sum_{l\in\mathcal{L}} \mathcal{M}_{l,y} \right\} \text{ Maintenance cost} \end{array} \right) \tag{4.13.b}$$

$$\mathcal{C}^g = \frac{1}{(1+\omega)^{(y)}} \sum_{y\in\mathcal{Y}} \sum_{\varphi\in\Phi} \sum_{t\in T} \theta_{y,\varphi} \Bigg(\left(\begin{array}{l} \mathcal{W}_v \sum_{l\in\mathcal{L}} \left(\left(v^- - v_{l,y,\varphi,t} \right) : \left(v_{l,y,\varphi,t} \le v^- \right) + \left(\hat{v}_{l,y,\varphi,t} - v^+ \right) : \left(\hat{v}_{l,y,\varphi,t} \ge v^+ \right) \right) + \\ \mathcal{W}_I \left(\sum_{l\in\mathcal{L}} \left(I^t_{l,y,\varphi,t} : \left(I^t_{l,y,\varphi,t} \ge I^+ \right) + I^b_{l,y,\varphi,t} : \left(I^b_{l,y,\varphi,t} \ge I^+ \right) \right) \right) + \\ \mathcal{W}_l \sum_{l\in\mathcal{L}} \left(r_l f_{l,y,\varphi,t} \right) + \\ \mathcal{W}_E \left(\xi^E_{y,\varphi,t} P_{1,y,\varphi,t} \right) + \\ \mathcal{W}_s \sum_{l\in\mathcal{L}} \left(\zeta_{l,y,\varphi,t} \right) \end{array} \right) \begin{array}{l} \text{voltage deviation} \\ \text{lines congestion} \\ \text{resistive losses} \\ \text{energy supply cost} \\ \text{load curtailment} \end{array} \Bigg) \tag{4.13.c}$$

$$\Psi(\alpha_{l,y,\varphi,t}, \beta_{l,y,\varphi,t}) \ge 0 \quad \forall l \in \mathcal{L}_{ess}, \forall y \in \mathrm{Y}, \forall \varphi \in \Phi, \forall t \in \mathrm{T} \tag{4.13.d}$$

$$\Theta(\gamma_{y,\varphi,t}, \tau_{y,\varphi,t}) \ge 0 \quad \forall y \in \mathrm{Y}, \forall \varphi \in \Phi, \forall t \in \mathrm{T} \tag{4.13.e}$$

$$s_{l,y,\varphi,t} = P^c_{l,y,\varphi,t} - P^d_{l,y,\varphi,t} - \zeta_{l,y,\varphi,t} - p^{pv}_{l,y,\varphi,t} + p^l_{l,y,\varphi,t} + j\left(Q^e_{l,y,\varphi,t} + q^l_{l,y,\varphi,t} - a\zeta_{l,y,\varphi,t} \right), \quad \forall l \in \mathcal{L}, y \in \mathrm{Y}, \forall \varphi \in \Phi, \forall t \in \mathrm{T} \tag{4.13.f}$$

$$\mathcal{R}_l^{\min} \mathfrak{u}_l \le \mathcal{R}_l \le \mathfrak{u}_l \mathcal{R}_l^{\max}, \quad \forall\, l \in \mathcal{L} \tag{4.13.g}$$

$$\mathfrak{u}_l C_l^{\min} \le C_l \le \mathfrak{u}_l C_l^{\max}, \quad \forall\, l \in \mathcal{L} \tag{4.13.h}$$

$$\sum_{l\in\mathcal{L}} \left(\mathcal{I}_c \mathfrak{u}_l + \mathcal{I}_p \mathcal{R}_l + \mathcal{I}_e C_l \right) \le \mathcal{B}^T \tag{4.13.i}$$

$$\mathfrak{u}_l \in \{0,1\}, \quad \forall\, l \in \mathcal{L} \tag{4.13.j}$$

where $\Xi = \{\mathfrak{u}, \mathcal{M}, \zeta, \alpha, \gamma, \mathcal{R}, C\}$ is the set of the optimization variables. $\gamma = \{s, P, Q, \hat{P}, \hat{Q}, \bar{P}, \bar{Q}, v, \hat{v}, f, \bar{f}, I^t, I^b\}$ and $\alpha = \{P^d, P^c, Q^e, \Lambda, E, \mathcal{R}, C, \hat{E}\}$ are the vectors of variables for AR-OPF and ESSs (recall that the notation without sub-script represents the vector of corresponding variable for all time steps in all scenarios).

l, y, φ and t are, index of the buses other than slack one, index of the years, index of the scenarios in each year, and index of time steps, respectively. $\mathfrak{u}_l$ is the binary variable associated with the presence of an ESS at bus l, $\mathcal{R}_l$ and C_l are the variables representing ESS power rating and energy reservoir capacities, $\mathcal{B}^T$ is the total budget for installing ESS units, $\mathcal{I}_c$, $\mathcal{I}_p$, and $\mathcal{I}_e$ are the unit costs associated with ESSs fixed installation, power rating capacity, and energy reservoir capacity costs, respectively (in per unit). $\mathcal{M}$ is the ESS maintenance cost and is a linear and strictly increasing function of $\mathcal{R}$ and C. s is the net nodal consumption at bus l and the relevant time (year, scenario, and time step), ζ is the load curtailment variable, ξ^E is the per unit energy price, ω is the annual interest rate, p^{pv} and p^l/q^l are the PV active power production and active/reactive demands, a is a constant representing the fixed power factor in case of load curtailment, v^+ and v^- are the upper and lower bounds for the square of nodal voltage magnitudes beyond which the nodal voltage deviations are minimized, I_l^t and I_l^bs represent upper bounds for the square of current flow at both ends of line l, $\mathcal{R}_l^{\max}/\mathcal{R}_l^{\min}$ and $C_l^{\max}/C_l^{\min}$ represent the maximum/minimum power rating and energy reservoir capacities that could be installed on bus l, and finally I^+ is the square of lines current magnitude beyond which the lines current flow is minimized.

$\mathcal{P}_2$:

$$\underset{\Xi}{\text{minimize}}: \mathcal{C}^e + \mathcal{C}^g \tag{4.14.a}$$

$$\mathcal{C}^e = \mathcal{W}_E \left(\begin{array}{l} \left\{ \sum_{l\in\mathcal{L}} \left(\mathcal{I}_c \mathfrak{u}_l + \mathcal{I}_p \mathcal{R}_l + \mathcal{I}_e C_l \right) \right\} \text{ Investment cost} \\ + \frac{1}{(1+\omega)^{(y)}} \sum_{l\in\mathcal{L}} \mathcal{M}_{l,y} \Big\} \text{ Maintenance cost} \end{array} \right) \tag{4.14.b}$$

$$\mathcal{C}^g = \frac{1}{(1+\sigma)^{(y)}} \sum_{y\in\mathcal{Y}} \sum_{\varphi\in\Phi} \sum_{t\in T} \theta_{y,\varphi} \Big(\left(\begin{array}{ll} \mathcal{W}_v \sum_{l\in N} \left(\left(v^- - v_{l,y,\varphi,t} \right) : \left(v_{l,y,\varphi,t} \le v^- \right) + \left(\hat{v}_{l,y,\varphi,t} - v^+ \right) : \left(\hat{v}_{l,y,\varphi,t} \ge v^+ \right) \right) + & \text{voltage deviations} \\ \mathcal{W}_I \left(\sum_{(k,l)\in\mathcal{L}} \left(I_{kl,y,\varphi,t} : \left(I_{kl,y,\varphi,t} \ge I^+ \right) \right) + \left(I_{lk,y,\varphi,t} : \left(I_{lk,y,\varphi,t} \ge I^+ \right) \right) \right) + & \text{lines congestion} \\ \mathcal{W}_l \sum_{(k,l)\in\mathcal{L}} \left(r_{kl} \left(f_{kl,y,\varphi,t} + f_{lk,y,\varphi,t} \right) \right) + & \text{resistive losses} \\ \mathcal{W}_E \sum_{l\in_{N_G}} \left(\xi^E_{y,\varphi,t} P_{lk,y,\varphi,t} \right) + & \text{energy supply cost} \\ \mathcal{W}_s \sum_{l\in N} \left(\zeta_{l,y,\varphi,t} \right) & \text{load curtailment} \end{array} \right) \Big) \tag{4.14.c}$$

$$\Psi(\alpha_{l,y,\varphi,t}, \beta_{l,y,\varphi,t}) \ge 0 \quad \forall l \in \mathcal{N}_{ess}, \forall y \in \mathrm{Y}, \forall \varphi \in \Phi, \forall t \in \mathrm{T} \tag{4.14.d}$$

$$\mathrm{B}(\sigma_{y,\varphi,t},\varsigma_{y,\varphi,t}) \geq 0 \quad \forall y \in \mathrm{Y},\ \forall \varphi \in \Phi, \forall t \in \mathrm{T} \tag{4.14.e}$$

$$s_{l,y,\varphi,t} = P^{c}_{l,y,\varphi,t} - P^{d}_{l,y,\varphi,t} - \zeta_{l,y,\varphi,t} - p^{pv}_{l,y,\varphi,t} + p^{l}_{l,y,\varphi,t} + j\left(Q^{e}_{l,y,\varphi,t} + q^{l}_{l,y,\varphi,t} - a\zeta_{l,y,\varphi,t}\right), \quad \forall l \in N, y \in \mathrm{Y},\ \forall \varphi \in \Phi, \forall t \in \mathrm{T} \tag{4.14.f}$$

$$\mathcal{R}_l^{\min} \mathfrak{u}_l \leq \mathcal{R}_l \leq \mathfrak{u}_l \mathcal{R}_l^{\max}, \quad \forall\, l \in N \tag{4.14.g}$$

$$C_l^{\min} \mathfrak{u}_l \leq C_l \leq \mathfrak{u}_l C_l^{\max} \quad \forall\, l \in N \tag{4.14.h}$$

$$\sum_{l \in \mathcal{L}} \left(\mathcal{I}_c \mathfrak{u}_l + \mathcal{I}_p \mathcal{R}_l + \mathcal{I}_e C_l\right) \leq \mathcal{B}^T \tag{4.14.i}$$

$$\mathfrak{u}_l \in \{0,1\} \quad \forall\, l \in N \tag{4.14.j}$$

where $\Xi = \{\mathfrak{u}, \mathcal{R}, C, \mathcal{M}, \alpha, \sigma\}$ is the set of the optimization variables. $\alpha = \left\{P^d, P^c, Q^e, \Lambda, E, \mathcal{R}, \mathcal{E}, \hat{E}\right\}$ is the vector of variables for energy storage systems and σ represents the vector of ADN reconfiguration model. N is the set of network buses, $\mathcal{L}$ is the set of the lines, N_G is the set of the buses that are substations. $\vec{\alpha}$ for one time step is as follows:

$$\sigma_{y,\varphi,t} = \begin{Bmatrix} s_{y,\varphi,t}, f_{y,\varphi,t}, \bar{f}_{y,\varphi,t}, P_{y,\varphi,t}, \bar{P}_{y,\varphi,t}, \hat{P}_{y,\varphi,t}, Q^{sh}, \hat{Q}^{sh}, \kappa^{kl}, I_{y,\varphi,t} \\ Q_{y,\varphi,t}, \bar{Q}_{y,\varphi,t}, \hat{Q}_{y,\varphi,t}, f_{y,\varphi,t}, v_{y,\varphi,t}, v'_{y,\varphi,t}, v^{"}_{y,\varphi,t}, \hat{v}_{y,\varphi,t}, \hat{v}'_{y,\varphi,t}, \hat{v}^{"}_{y,\varphi,t} \end{Bmatrix}$$

where $f, P, Q, etc.$ represent the vector of corresponding variable associated with the lines of the network in both directions $(k \to l, l \to k)$. Similarly, v, v', etc. shows the vector of corresponding variables associate with the buses of the grid.

4.7 Solution Approaches

The formulated problems, $\mathcal{P}_1$ and $\mathcal{P}_2$, are MISOCP. As it was mentioned in 4.5.1, this type of optimization problems can be solved using state-of-the-art commercial software. However, their solution could be computationally expensive due to the large-scale size of the targeted problems and/or presence of discrete variables. The inherent large-scale nature of the problem lays in the fact that it should cover a reasonable number of scenarios in order to obtain a solution accounting for a sufficiently large set of variations of the considered parameters. Consequently, the solution of the targeted problems, especially $\mathcal{P}_2$, could be computationally challenging for real large-scale networks with high number of scenarios. Further, they may also require a large amount of physical memory. One of the most common approaches used in the literature to treat this kind of problems is to use decomposition methods. In what follows we present the Alternative Direction Method of Multipliers (ADMM) and Benders decomposition approaches suitably applied to the targeted problems.

4.7.1 Alternative Direction Method of Multipliers (ADMM) applied to ESSs optimal planning

The ADMM is a powerful and well-suited method for decentralized convex optimization. The peculiarity of the ADMM is that it uses a decomposition-coordination procedure in order to find the solution to a large global problem by solving small local sub-problems in parallel. It uses the benefits of dual decomposition and augmented Lagrangian methods [126, 127]. In the following, the ADMM is briefly described.

The ADMM is used here to decompose the installation-cost minimization problem from the one of operation-cost minimization enabling a parallel formulation. The two optimization problems are linked by a set of linear constraints. These constraints imply that the ESS capacities obtained in the first stage (investment cost minimization) are identical to the ESSs capacities in the second stage (operation cost minimization). The application of the ADMM for the ESS optimal planning problem is described in what follows.

It should be noted that the convergence of the ADMM process is not guaranteed for the optimization problems with non-convex constraints (e.g., with discrete variables). In this respect, we have considered that the ESS capacities are continuous variables.

First stage optimization

The first stage problem is related to the ESS investment and maintenance costs; its formulation is shown in (4.15.a)-(4.15.c).

$$\underset{\Xi}{\text{minimize:}}\ \mathcal{C}^{e} = \mathcal{W}_{E}\left(\sum_{l\in\mathcal{L}}\left(\mathcal{I}_{p}\mathcal{R}_{l}^{i}+\mathcal{I}_{e}C_{l}^{i}\right)+\frac{1}{(1+\omega)^{(y)}}\sum_{l\in\mathcal{L}}\mathcal{M}_{l,y}\right)+ \sum_{y\in\mathcal{Y}}\sum_{\varphi\in\Phi}\left\{\left(\lambda_{y,\varphi}^{(n-1)}\right)^{\mathrm{T}}\left(\begin{bmatrix}\hat{\mathcal{R}}_{y,\varphi}^{o(n-1)}\\ \hat{C}_{y,\varphi}^{o(n-1)}\end{bmatrix}-\begin{bmatrix}\mathcal{R}^{i}\\ C^{i}\end{bmatrix}\right)+\left(\rho/2\right)\left\|\left(\begin{bmatrix}\hat{\mathcal{R}}_{y,\varphi}^{o(n-1)}\\ \hat{C}_{y,\varphi}^{o(n-1)}\end{bmatrix}-\begin{bmatrix}\mathcal{R}^{i}\\ C^{i}\end{bmatrix}\right)\right\|_{2}^{2}\right\} \quad (4.15.a)$$

subject to:

$$0\le\mathcal{R}_{l}\le\mathcal{R}_{l}^{\max},\quad\forall\, l\in\mathcal{L} \quad (4.15.b)$$

$$0\le C_{l}\le C_{l}^{\max},\quad\forall\, l\in\mathcal{L} \quad (4.15.c)$$

$$\sum_{l\in\mathcal{L}}\left(\mathcal{I}_{p}\mathcal{R}_{l}^{i}+\mathcal{I}_{e}C_{l}^{i}\right)\le\mathcal{B}^{T} \quad (4.15.d)$$

where $\Xi=\left\{\mathcal{R}^{i},\mathcal{C}^{i},\mathcal{M}\right\}$ is the set of optimization variables, n is the index of ADMM iteration, $\lambda_{y,\varphi}^{(n)}$ is the dual multiplier of the constraint that links the first and second stages and is obtained in the dual update stage $(n-1)$ (see Appendix A.3), $\mathcal{R}_{l}^{i}$ and $\mathcal{C}_{l}^{i}$ are the ESS power rating and energy reservoir capacities of ESS located at bus l in first stage problem (investment cost minimization). $\hat{\mathcal{R}}_{l}^{o(n-1)}$ and $\hat{\mathcal{C}}_{l}^{o(n-1)}$ represent the ESS

power rating and energy reservoir capacities in the previous iteration of second stage (they are parameters here). ρ is the penalty parameters.

Second stage optimization

The second step is represented by the operation-cost minimization for all the possible scenarios. In this stage, each scenario is processed separately since they can be evaluated in parallel. The objective function of the problem for every single scenario ($y \in \mathcal{Y}, \varphi \in \Phi$) is formulated as (4.16.a). The constraints of the problem are (4.16.b)-(4.16.d).

$$\underset{\Xi}{\text{minimize:}}\ \mathcal{C}^{g}_{y,\varphi} = \frac{1}{(1+\omega)^{(y)}} \sum_{t \in T} \theta_{y,\varphi} \left(\begin{array}{l} \mathcal{W}_v \sum_{l \in \mathcal{L}} \left(\left(v^{-} - v_{l,y,\varphi,t} \right) : \left(v_{l,y,\varphi,t} \le v^{-} \right) + \left(v_{l,y,\varphi,t} - v^{+} \right) : \left(v_{l,y,\varphi,t} \ge v^{+} \right) \right) + \\ \mathcal{W}_I \sum_{l \in \mathcal{L}} \left(I^{t}_{l,y,\varphi,t} : \left(I^{t}_{l,y,\varphi,t} \ge I^{+} \right) + I^{b}_{l,y,\varphi,t} : \left(I^{b}_{l,y,\varphi,t} \ge I^{+} \right) \right) + \\ \mathcal{W}_l \sum_{l \in \mathcal{L}} \left(r_l f_{l,y,\varphi,t} \right) + \\ \mathcal{W}_E \left(\xi^{E}_{y,\varphi,t} P_{1,y,\varphi,t} \right) + \\ \mathcal{W}_s \sum_{l \in \mathcal{L}} \left(\zeta_{l,y,\varphi,t} \right) \end{array} \right)$$

$$+ \mathcal{W}_E \left\{ \left(\lambda^{(n-1)}_{y,\varphi} \right)^{\mathrm{T}} \left(\begin{bmatrix} \mathcal{R}^{\mathrm{o}}_{y,\varphi} \\ C^{\mathrm{o}}_{y,\varphi} \end{bmatrix} - \begin{bmatrix} \hat{\mathcal{R}}^{i(n)} \\ \hat{C}^{i(n)} \end{bmatrix} \right) + \left(\rho / 2 \right) \left\| \left(\begin{bmatrix} \mathcal{R}^{\mathrm{o}}_{y,\varphi} \\ C^{\mathrm{o}}_{y,\varphi} \end{bmatrix} - \begin{bmatrix} \hat{\mathcal{R}}^{i(n)} \\ \hat{C}^{i(n)} \end{bmatrix} \right) \right\|_2^2 \right\} \tag{4.16.a}$$

subject to:

$$\Psi(\alpha_{l,y,\varphi,t}, \beta_{l,y,\varphi,t}) \ge 0, \quad \forall t \in \mathrm{T}, \forall l \in \mathcal{L}_{ess} \tag{4.16.b}$$

$$\Theta(\gamma_{y,\varphi,t}, \tau_{y,\varphi,t}) \ge 0 \quad \forall t \in \mathrm{T} \tag{4.16.c}$$

$$s_{l,y,\varphi,t} = P^{c}_{l,y,\varphi,t} - P^{d}_{l,y,\varphi,t} - \zeta_{l,y,\varphi,t} - p^{pv}_{l,y,\varphi,t} + p^{l}_{l,y,\varphi,t} + j\left(Q^{e}_{l,y,\varphi,t} + q^{l}_{l,y,\varphi,t} - a\zeta_{l,y,\varphi,t} \right), \quad \forall l \in \mathcal{L}, \forall t \in \mathrm{T} \tag{4.16.d}$$

where $\Xi = \{\alpha, \gamma, \zeta, \mathcal{R}^{o}_{y,\varphi}, \mathcal{C}^{o}_{y,\varphi}\}$ is the set of optimization variables. $\hat{\mathcal{R}}^{i(n)}$ and $\hat{\mathcal{C}}^{i(n)}$ represent the ESS power rating and energy reservoir capacities obtained in the first stage (they are parameters here).

Dual Update:

The last step in ADMM procedure is the dual update as shown in (4.17.a).

$$\lambda^{(n)}_{y,\varphi} = \lambda^{(n-1)}_{y,\varphi} + (\rho) \left(\begin{bmatrix} \hat{\mathcal{R}}^{\mathrm{o}(n)}_{y,\varphi} \\ \hat{C}^{\mathrm{o}(n)}_{y,\varphi} \end{bmatrix} - \begin{bmatrix} \hat{\mathcal{R}}^{i(n)} \\ \hat{C}^{i(n)} \end{bmatrix} \right) \quad \forall y \in \mathrm{Y}, \forall \varphi \in \Phi \tag{4.17.a}$$

These steps are iterated until the solver converges to an optimal solution. The scheme of the proposed ADMM-based procedure is shown in Fig. 4-8. Further details are provided in Appendix A.3 and [126].

4.7.2 Bender decomposition approach applied to the optimal siting and sizing of ESSs in ADNs

Including ADN reconfiguration adds new binary variables and constraints (radiality ones)) to the ESS optimal siting and sizing problem. This could further complicate the solution of the optimization problem. We have employed the Benders decomposition to deal with this difficulty and solve $\mathcal{P}_2$.

Benders decomposition is used to break down the optimization problem into a master problem and a set of subproblems. The Master problem determines the ESSs site and size as well as the state of the switches for each category of load /PV profiles. The constraints are geographical and budget constraints for ESSs installation, the radiality ones, and the linearized DistFlow constraints. Once the solution of the master problem is determined and the configuration of network is defined, the ESSs capacities are fixed and used in the subproblems. For each network configuration, a set of scenarios characterized by load, PV, and energy price profiles are used for assessing the operational benefits of the ESSs. The duals of these constraints are used to form appropriate cuts for the next iteration of the master problem. The procedure iterates between the master problem and subproblems until it converges and the difference

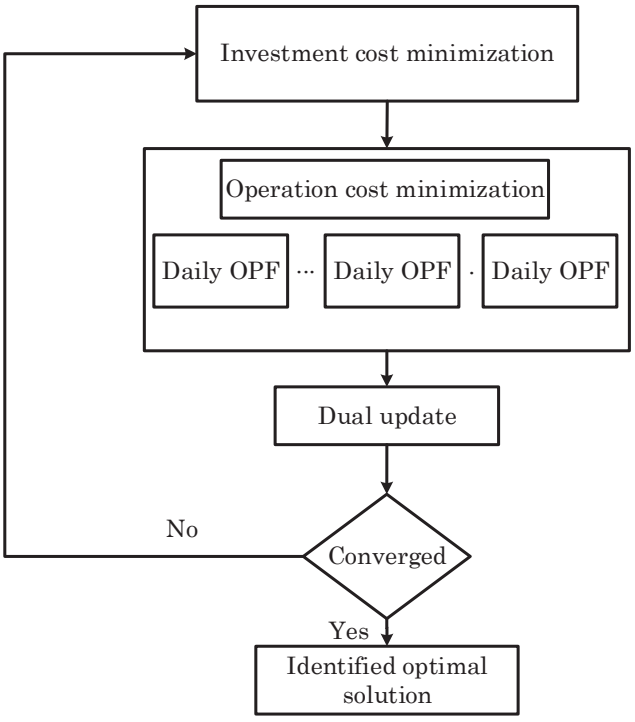

Fig. 4-8: ADMM procedure applied to the problem of ESS optimal planning

between the upper bound and lower bound is less than the predefined tolerance (see Appendix A.4).

4.7.2.1 Master Problem

The Master problem determines the ESSs site and size as well as the state of the switches for each category of load /PV profiles. In this step, the daily time step discretization is considered to be 2 hours (the time step discretization is 15 minutes in the subproblems). This choice of time step is justified because the short term variations of load and PV do not impact the optimal switching strategy. Additionally, the price scenarios are not considered here, since they have no effect on the switching strategies. Taking into account the above mentioned points, the final scenarios for ESS siting and sizing generated as explained in section 4.4 are further clustered into categorizes of load and PV profiles. The state of the switches for each category is determined in master problems aiming at minimizing the total resistive losses (one configuration for each category).

The constraints of the optimization problem are i) geographical and budget constraints for ESSs installation ii) the radiality ones, and iii) the constraints related to the DistFlow equations with inclusion of transverse parameters. The Master problem is formulated as shown in following:

$$\underset{\Xi}{\text{minimize:}}\ \mathcal{W}_E\left(\begin{array}{l}\left(\sum_{l\in\mathcal{L}}\left(\mathcal{I}_c \mathrm{u}_l+\mathcal{I}_p\mathcal{R}_l+\mathcal{I}_e C_l\right)+\frac{1}{(1+\omega)^{(y)}}\sum_{l\in\mathcal{L}}\mathcal{M}_{l,y}\right)+\\ \sum_{\varphi_m\in\Phi_m}\sum_{t\in T}\sum_{(l,k)\in\mathcal{L}}\left(r_{kl}\left(\left(P_{kl,\varphi_m,t}\right)^2+\left(Q_{kl,\varphi_m,t}\right)^2+\left(P_{lk,\varphi_m,t}\right)^2+\left(Q_{lk,\varphi_m,t}\right)^2\right)\right)+\end{array}\right)+ \sum_{y\in\mathrm{Y}}\sum_{\varphi\in\Phi}\mathcal{Z}_{y,\varphi} \tag{4.18.a}$$

subject to:

$$\mathcal{Z}_{y,\varphi}\geq 0,\quad \forall y\in\mathrm{Y},\varphi\in\Phi \tag{4.18.b}$$

$$\mathcal{Z}_{y,\varphi}\geq \Upsilon^{(n)}_{y,\varphi},\ \forall y\in\mathrm{Y},\varphi\in\Phi,\forall\ n\in\mathcal{N}^b \tag{4.18.c}$$

(4.14.g),(4.14.h),(4.14.i)(4.14.j)

$$\Psi(\alpha_{l,\varphi,t},\beta_{l,\varphi,t})\geq 0,\quad \forall l\in\mathcal{L}_{ess},\forall\varphi_m\in\Phi_m,\forall t\in\mathrm{T} \tag{4.18.d}$$

$$\mathrm{B}'(\sigma'_{\varphi_m,t},\varsigma'_{y,\varphi_m,t})\geq 0\quad \forall\varphi_m\in\Phi_m,\forall t\in\mathrm{T} \tag{4.18}$$

where $\Xi=\{\mathrm{u},\mathcal{R},\mathcal{C},\mathcal{M},\mathcal{Z},P,Q,\alpha,\sigma'\}$ is the set of optimization variables. u_l is the binary variable associated with the presence of an ESS at bus l, $\mathcal{R}$ and $\mathcal{C}$ are the ESS power rating and energy reservoir capacities, $\mathcal{M}$ is the maintenance cost of ESSs, $P_{kl,\varphi_m,t}(P_{lk,\varphi_m,t})/\ Q_{kl,\varphi_m,t}(Q_{lk,\varphi_m,t})$ represent the active and reactive power flows in the central part of the lines, α is the set of variables for modeling ESSs, σ' is the set of

variables for modeling ADN reconfiguration constraints with DistFLow equations, n is the index of Benders iteration, and φ_m is the index of master problem scenarios. Constraints (4.18.b) and (4.18.c) model the Benders cuts from the subproblems. The ESSs constraints are presented by equation (4.18.d). Once the solution of the master problem is determined, the ESSs site and size as well as the switching states are fixed and sent to the subproblems.

4.7.2.2 Subproblem (Optimal Day-ahead scheduling)

The fitness of the master problem solution is determined in the subproblems. For each network configuration, a set of scenarios characterized by load, PV, and price variations are used for assessing the operational benefits of the ESSs. The time step discretization is 15 minutes. The formulation of the subproblems is shown in (4.19.a)-(4.19.f).

$$\underset{\Xi}{\text{minimize:}}\ \mathcal{C}^{g}_{y,\varphi} = \frac{1}{(1+\omega)^{(y)}}\sum_{t\in T}\theta_{y,\varphi}\begin{pmatrix}\mathcal{W}_v\sum_{l\in\mathcal{L}}\left(\left(v^{-}-v_{l,y,\varphi,t}\right):\left(v_{l,y,\varphi,t}\le v^{-}\right)+\left(\hat{v}_{l,y,\varphi,t}-v^{+}\right):\left(\hat{v}_{l,y,\varphi,t}\ge v^{+}\right)\right)+\\ \mathcal{W}_I\left(\sum_{l\in\mathcal{L}}\left(I^{t}_{l,y,\varphi,t}:\left(I^{t}_{l,y,\varphi,t}\ge I^{+}\right)+I^{b}_{l,y,\varphi,t}:\left(I^{b}_{l,y,\varphi,t}\ge I^{+}\right)\right)\right)+\\ \mathcal{W}_l\sum_{l\in\mathcal{L}}\left(r_l f_{l,y,\varphi,t}\right)+\\ \mathcal{W}_E\left(\xi^{E}_{y,\varphi,t}P_{1,y,\varphi,t}\right)+\\ \mathcal{W}_s\sum_{l\in\mathcal{L}}\left(\zeta_{l,y,\varphi,t}\right)\end{pmatrix} \tag{4.19.a}$$

subject to:

$$\Psi(\alpha_{y,\varphi,t},\beta_{y,\varphi,t})\ge 0 \quad \forall t\in \mathrm{T},\forall l\in\mathcal{N}_{ess} \tag{4.19.b}$$

$$\Theta(\gamma_{y,\varphi,t},\tau_{y,\varphi,t})\ge 0 \quad \forall t\in \mathrm{T} \tag{4.19.c}$$

$$s_{l,y,\varphi,t} = P^{c}_{l,y,\varphi,t}-P^{d}_{l,y,\varphi,t}-\zeta_{l,y,\varphi,t}-p^{pv}_{l,y,\varphi,t}+p^{l}_{l,y,\varphi,t}+j\left(Q^{e}_{l,y,\varphi,t}+q^{l}_{l,y,\varphi,t}-a\zeta_{l,y,\varphi,t}\right),\quad \forall l\in\mathcal{N},\forall t\in\mathrm{T} \tag{4.19.d}$$

$$\mathcal{R}_l = \hat{\mathcal{R}}_l:\mu_{l,y,\varphi},\quad \forall l\in\mathcal{N} \tag{4.19.e}$$

$$C_l = \hat{C}_l:\vartheta_{l,y,\varphi},\quad \forall l\in\mathcal{N} \tag{4.19.f}$$

where $\Xi=\{\alpha_{y,\varphi},\gamma_{\varphi},s_{\varphi},\zeta_{\varphi},\mathcal{R},\mathcal{C}\}$ is the set of optimization variables. $\hat{\mathcal{R}}$ and $\hat{C}$ are the ESS power rating and energy reservoir capacities obtained in the master problem. They are parameters here.

The capacity of the ESSs power rating and energy reservoirs are fixed to the values obtained from the master problem in equations (4.19.e) and (4.19.f). The Lagrange

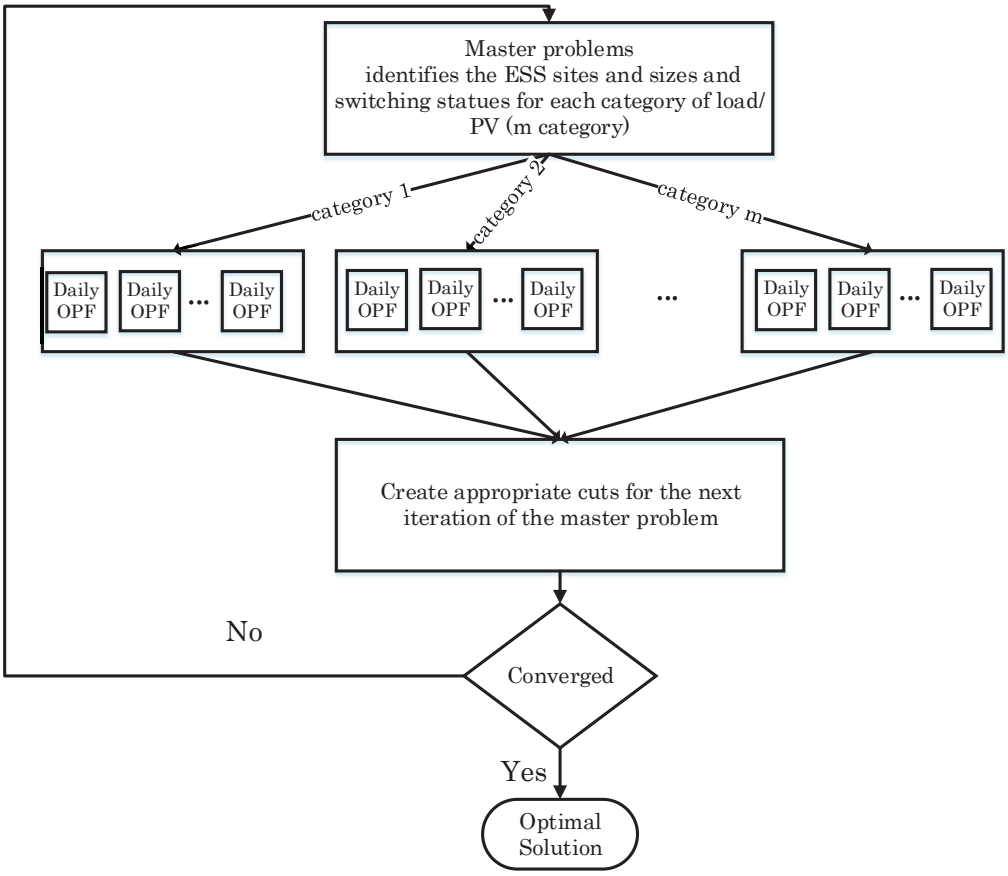

Fig. 4-9: The Benders decomposition procedure adapted for optimal siting and sizing of ESSs considering network reconfiguration

multipliers associated with these constraints are used to form the appropriate cuts as shown in (4.20.a) for the master problem.

$$\Upsilon_{y,\varphi}^{(n)} = \hat{C}_{y,\varphi}^{g} - \sum_{l \in N} \left(\mu_{l,y,\varphi} \left(\mathcal{R}_l - \hat{\mathcal{R}}_l \right) - \vartheta_{l,y,\varphi} \left(C_l - \hat{C}_l \right) \right), \forall y \in \mathrm{Y}, \forall \varphi \in \Phi \qquad (4.20.a)$$

where $\hat{C}_{y,\varphi}^{g}$ represents the identified value of the objective function and $\mu_{l,y,\varphi}/\vartheta_{l,y,\varphi}$ represent the dual of constraints related to the fixed ESS capacities.

The proposed Benders decomposition procedure is depicted in Fig. 4-9.

4.7.3 Comparisons of solution approaches

In this section we compare the three solution approaches discussed above with respect to $\mathcal{P}_1$. The IEEE 34 buses network is used to compare the solution of the three approaches; i) the original problem without making use of a decomposition method [128], ii) decomposed problem using ADMM, and iii) decomposed problem using Benders decomposition. As previously stated, the convergence of the ADMM process is not guaranteed for optimization problems with non-convex constraints (e.g., with discrete variables). In this respect, in the following we provide two analyses, i) a comparison between the solution of the decomposed problem using Benders

decomposition with the solution of the original problem, in presence of discrete variables for ESSs capacities and ii) a comparison between the solution of the decomposed problem using ADMM with the solution of the original problem using continuous variable for ESSs capacities.

4.7.3.1 Comparison between the solutions of the original problem and the decomposed one using Benders decomposition

As mentioned above, IEEE 34 buses network is selected as the test case study. It is assumed that at most 20 ESS units, with 125 kVA power rating and 125 kWh energy reservoir each, could be installed in the grid. The simulations are done with respect to 45 scenarios. The load and PV data are obtained from experimentally measured data in a region in southern-east part of Switzerland. The total aggregated load and energy profiles are shown in Fig. 4-10. Ten buses, # 9, #13, #19, #24, #25, #27, #29, #31, #32, and #34, are considered as the candidates for installing ESS units.

With reference to 45 scenarios with 15 minutes time discretization (96 time step per scenario), the identified optimal solution using the two approaches, are reported in Table 4-2. The simulations are done on a desktop PC with 16 GB RAM memory and Intel Xenon CPU E5-1650@3.20 GHz. Gurobi version 6.0.5 is used to solve the optimization problems. The Gurobi solver benefits from the state-of-the-art methods in solving MIQCP problems like Presolve, Cutting Planes, Heuristics, and Parallelism for solving MIQCP [124]. The optimality gap is chosen to be 0.01%. Similarly, the stopping criterion for Benders decomposition is chosen to be 0.01% (see Appendix A.4). As it can be observed from Table 4-2, the two approaches lead to the same identified optimal solution (the same ESS sites and capacities). Further one can observe that the computation time for the case using Benders decomposition is much smaller than the computation time of the original problem solution.

4.7.3.2 Comparison between the solution of the original problem and the decomposed one using ADMM

The same test case study as the previous section is used here. The capacities (power rating and energy reservoir) of the ESS units are considered to be continuous variables. The same desktop PC and solver as the previous section are used for solving the optimization problems. The identified optimal solution and the corresponding computational time for two cases i) solving the original problem, ii) solving the decomposed problem using ADMM) are demonstrated in Table 4-3. It can be seen that both approaches lead to the same optimal solution. Further it can be observed that solving ADMM in parallel could decrease the total computation time significantly. It should be noted that the advantage of using decomposition methods is not only limited to the computation time. They also decrease the amount of required physical memory since several small scale problems are treated instead of a large-scale one. Finally, it should be noted that the convergence of ADMM largely depends on the selection of penalty parameter, ρ. Here, we used the approach proposed in [126].

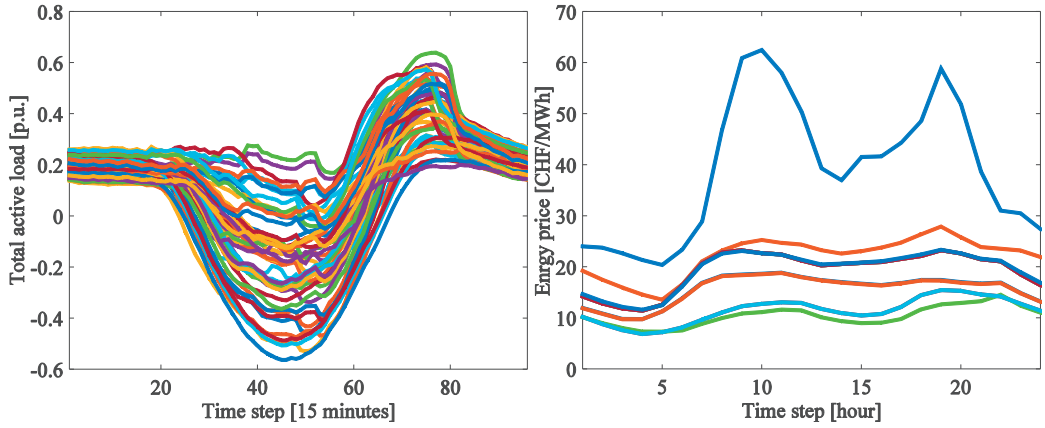

Fig. 4-10: a) the aggregated active power load scenarios (base vale for power is 2.5 MW), b) the energy price scenarios

Table 4-2: Comparison between the solutions of the original problem and the decomposed one using Benders decomposition (each unit of ESS has 125 kVA and 125 kWh capacity)

	Bus #	Number of units	Computation time
Using Benders decomposition	#19	1	# iterations: 17 Average computation time of subproblems (total time for solving original problem and Karush–Kuhn–Tucker (KKT) conditions to obtain dual variables): 4.01 [sec] Average computation time of master problem: 0.022 [sec] Total computation time: 3068 [sec]
	#25	1	
	#34	4	
Without Benders decomposition	#19	1	64822.5 [sec]
	#25	1	
	#34	4	

Table 4-3: Comparison between the solutions of the original problem and the decomposed one using ADMM

	Bus #	Power rating (kVA)	Energy reservoir (kWh)	Computation time
Using ADMM	#34	124	124	# iterations: 30 Average computation time of subproblems: 2.71 [sec] Average computation time of master problem: 0.002 [sec] Total computation time in parallel: 85.33 [sec] Total computation time in series: 3839.1 [sec]
Without ADMM	#34	124	124	1340.7 [sec]

4.8 Summary and Conclusion

In this chapter, the problem of optimal siting and sizing of ESSs in ADNs is studied. First, the linearized OPF, based on voltage sensitivity coefficients, is used to develop a model for optimal siting of ESSs aiming at minimizing the total nodal voltage magnitudes' deviations. Further, Benders decomposition approach is suitably adopted for the solution of this MIQCQP problem. It is shown that the computation time of solving the decomposed problem largely outperforms the one of original problem. Further, the AR-OPF and the proposed ADN reconfiguration models are employed for optimal siting and sizing of ESSs in ADNs with a multi-objective goal including energy balance and network services. Additionally, using the proposed ADN reconfiguration, the topology changes are also incorporated into the problem. Variations of different parameters (load, PV and energy price) during the life-time of ESS units are taken into account using an appropriate scenario generation/reduction method.

In the last part of this chapter, two solution approaches, based on Benders decomposition and ADMM, are adapted to solve the targeted large-scale Mixed Integer Second Cone Programming (MISOCP) problems. In particular, it was shown that the Benders decomposition is potentially the best approach for solving the targeted planning problems because i) it can efficiently handle the discrete variables, ii) it breaks down the problem enabling solving several smaller problems in parallel instead of one single large-scale one. Further, the use of ADMM for solving the problem with continuous variables is investigated. It is shown that this approach also enables reducing the computation time through the decomposition of problem and solving it in parallel.

5 Application Examples of the developed methodologies for ESS siting and sizing using benchmark and real power grids

Chapter highlights:

In this chapter, the developed methodologies related to the optimal ESSs siting and sizing are applied to real and benchmark networks. In particular, IEEE 34 and 123 buses networks and a real distribution network located in southwest Switzerland are used as the test cases. The objective function of the optimization problems includes: i) ESS investment and maintenance costs, ii) nodal voltage magnitudes' deviation, iii) resistive losses, iv) lines congestion v) cost of energy imported from external grid and operation of DGs.

5.1 Chapter Organization

In section 5.2 the modified IEEE 34 buses network is used to apply the process illustrated in section 4.5 without using a decomposition method[1]. The objective function refers to the minimization of: i) ESS investment and maintenance costs, ii) nodal voltage deviations, iii) resistive losses, iv) lines congestion v) cost of energy imported from external grid and operation cost of dispatchable DGs. In section 5.3 a real large-scale network located in southwest of Switzerland is used, as a case study, to apply the developed optimal planning technique based on ADMM. In particular, the problem is decomposed using the ADMM technique. Finally, in section 5.4, the IEEE 123 buses network is employed as a test case to validate the developed methodology taking into account the network reconfiguration. The solution of the optimization problems relies on the use of Benders decomposition technique.

5.2 Optimal ESS Siting and Sizing

The simulation results presented here make reference to the optimization model presented in $\mathcal{P}_1$ (equations (4.13.a)-(4.13.j)). The modified IEEE 34 buses system is used as the test case (see Fig. 5-1) [25]. The two voltage regulators are removed in order to obtain a weaker grid with respect to nodal voltage magnitudes. It is supposed to have both non-dispatchable DGs composed by PV panels and wind turbines, and dispatchable DGs. The yearly profile of active power loads for the entire network is shown in Fig. 5-3. The load profiles are considered to be voltage-independent PQ absorptions. Even for PV and wind units, it is also considered that they are voltage-independent active power injections with null reactive power component. Their yearly power production profiles are shown in Fig. 5-3 and Fig. 5-4. The load data corresponds to real measurements recorded into a primary high-to-medium voltage substation located in north of Italy. The PV and wind profiles are obtained from [129] and [130] respectively.

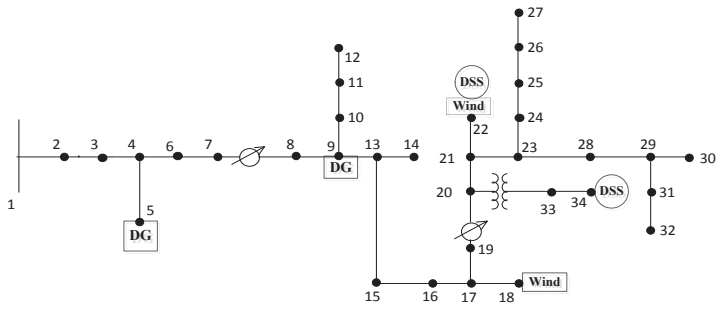

Fig. 5-1: The modified IEEE 34 bus test feeder.

[1] It should be noted that the quadratic term in the voltage equation (equation (2.11.b)) as well as the transverse parameters are neglected in this case study.

As mentioned above, in this study we have also considered the presence of some dispatchable DGs, owned and operated by the DNO. They are molded as follow:

$$u_I^{DG} P_I^{\mathrm{DG,min}} \le P_I^{DG} \le u_I^{DG} P_I^{\mathrm{DG,max}} \quad (5.1.a)$$

$$u_I^{DG} Q_I^{\mathrm{DG,min}} \le Q_I^{DG} \le u_I^{DG} Q_I^{\mathrm{DG,max}} \quad (5.1.b)$$

$$(P_I^{DG}, Q_I^{DG}) \in \mathrm{A}_I \quad (5.1.c)$$

where $P_l^{\mathrm{DG}}, Q_l^{\mathrm{DG}}$ are the active and reactive power output of the DG, u_l^{DG} represents the on/off state of the DG unit, $P_l^{\mathrm{DG,max}}/P_l^{\mathrm{DG,min}}, Q_l^{\mathrm{DG,max}}/Q_l^{\mathrm{DG,min}}$ represent the upper and lower bounds of DG active and reactive power outputs, finally A_l is the feasible operating region of DG as shown in Fig. 5-2. Note that $P_l^{\mathrm{DG}}, Q_l^{\mathrm{DG}}$ and u_l^{DG} are optimization variables.

The constraints (5.2.a) and (5.2.b) define the maximum and minimum active and reactive power that can be produced by dispatchable DGs, respectively. The constraint (5.2.c) defines the capability curve of DG generator that is linearized and shown in Fig. 5-2.

A linear formulation is used for DGs operation and start-up costs [131]. The start-up cost is modeled by a constant cost function.

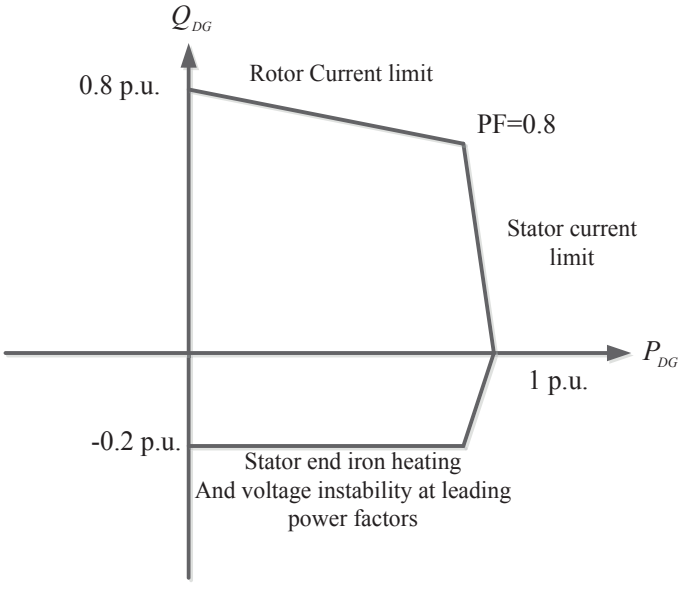

Fig. 5-2: The linearized dispatchable DG capability curve

The simulation parameters are shown in Table 5-1. It is assumed that PV generation units are installed at all load buses where loads are present. The wind turbines are connected to buses #18 and #22 (see Fig. 5-1).

Table 5-1: Simulation parameters

Base power (energy) value	2.5 MW (MWh)	Maximum number of buses where ESSs can be installed	4
Total PV capacity	1 (p.u.)	Total maximum ESS power rating capacity	0.8 (p.u.)
Total wind capacity	0.3 (p.u.)	Total maximum ESS reservoir capacity	2 (p.u.)
Resistive losses of ESSs	0.04 (p.u.)	ESS ramp-up ramp-down limits	0.3 (MW/h)
Max/min voltage-thresholds beyond which voltage deviation is minimized	+/- 3%	Max feeder current-threshold beyond which current feeder flow is minimized	80 %
Annual load growth	2%	Interest rate	3%
Average energy price from external grid in first year	36 ($/MWh)	GBM sigma	0.08
Capital investment cost of ESSs	5000 ($)	Installation cost of ESSs power rating	1200 ($/kW) [39]
Installation cost of ESSs energy reservoir	4000 ($/kWh) [132]	Maintenance cost of ESSs	100 ($/MWh/year)
Dispatchable DGs total maximum capacity	0.2 (p.u.) (2 units)		

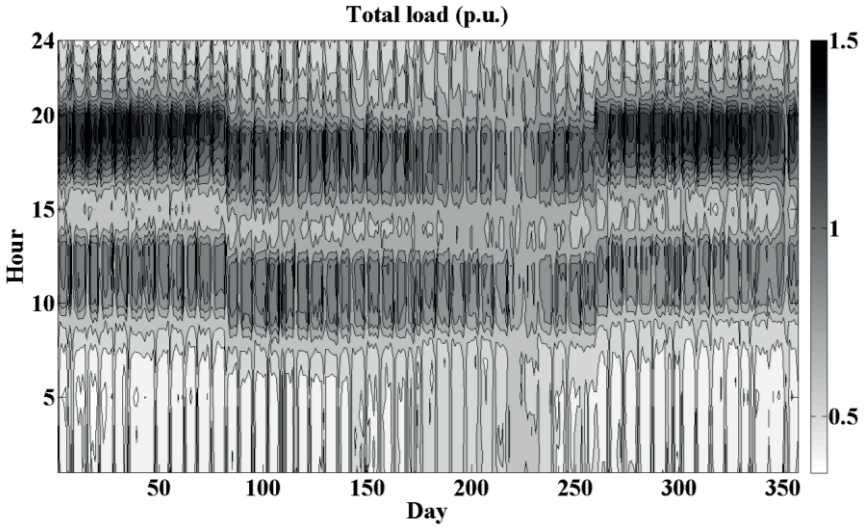

Fig. 5-3: Initial yearly load profile (base power Sb=2.5 MW).

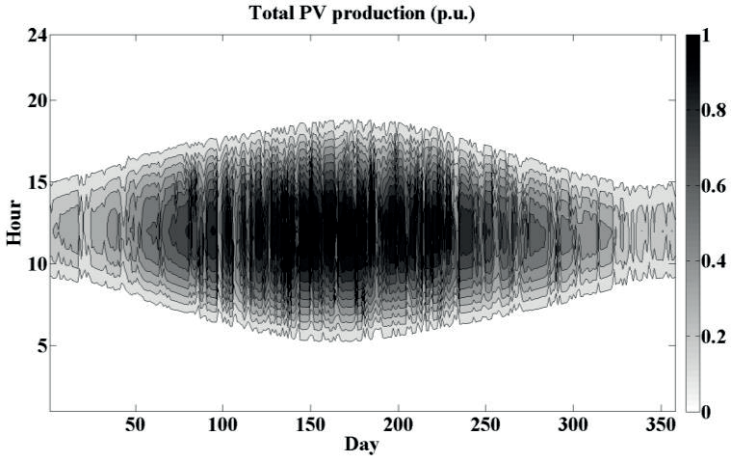

Fig. 5-4: Initial yearly PV production profile (base power Sb=2.5 MW).

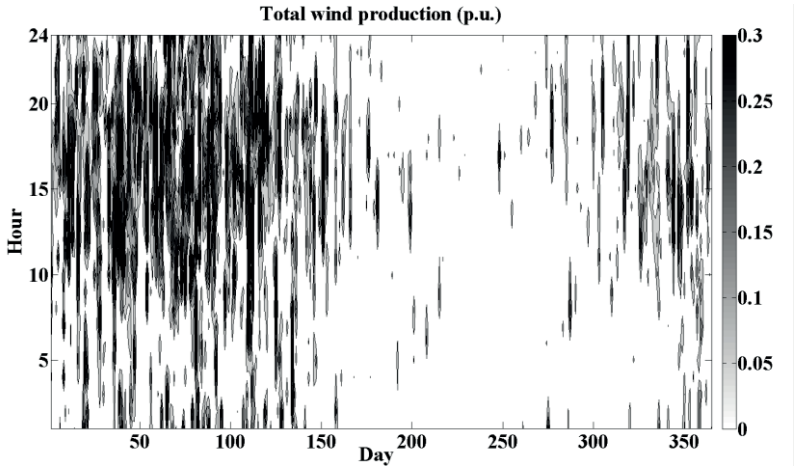

Fig. 5-5: Initial yearly wind production profile (base power Sb=2.5 MW).

Table 5-2: Pairwise comparisons of the objective terms

	Voltage deviation	resistive losses	Energy cost from external grid	Lines' congestion	ESSs losses
Voltage deviation	1	5	7	1/4	12
resistive losses	1/5	1	1/2	1/8	5
Energy cost from external grid	1/7	2	1	1/9	8
Lines' congestion	4	8	9	1	15
ESSs losses	1/12	1/5	1/8	1/15	1

The scenario generation/reduction method presented in section 4.4 is used to generate 150 scenarios for load, PV, wind and energy price profiles. The ESSs lifetime is assumed to be 5 years. The simulation is performed for the considered ESSs lifetime where the parameters' growth/variations are taking into account. The load growth is considered constant during the lifetime. The wind power capacity is considered constant during the lifetime while the PV capacity is considered to have a growth associated with one of the load since these systems are normally installed on the customers' side. The energy and fuel prices' growth over the years are modeled using the GBM [123]. Table 5-2 shows the pairwise comparison of selected relative weights fed into the AHP.

The scaled coefficients of each term in the objective function, obtained using the pairwise comparison reported in Table 5-2 feeding into AHP, are: W_{EP}=0.0562, W_{loss}=0.0396, W_{vol}=0.2535, W_{flow}=0.6421, and $W_{lossESS}$=0.0086. The coefficient of load curtailment is considered to be equal 100. It is equal to the value of unsupplied load. It should be noted that the coefficient of load curtailment is not considered in the AHP method. In this respect, a large weighting coefficient has been considered in order to prevent at most the load curtailment.

Table 5-3 shows the optimal obtained ESS locations and relevant sizes. From the results of Table 5-3, we can see that two buses are selected by the proposed method to host ESSs.

Changes of the other terms of the objective function during the lifetime (i.e., total loss, energy cost, feeders loading and load curtailment) are shown in Table 5-4. These values correspond to the sum of all time periods in 5 years (43800 hours) and the peak value of the load is 3.58 MW. It should be noted that the initial network is heavily loaded and the load curtailment is inevitable. This heavy loading causes relatively high amount of losses and lines over-loading. These results show that all the elements of the objective function, exhibit significant improvements. In addition to the total losses reduction, the total cost of supplied energy, that includes the energy imported from the external grid as well as the energy supplied by local DG units, is significantly reduced.

In order to quantify the benefits related to the optimal ESS placement, in what follows we have reported the results of two cases corresponding to: case 1 with optimal allocated ESSs and case 2 without ESS. In particular, the Cumulative Distribution Functions (CDFs) of the voltages related to both cases 1 and 2 related to the whole time period and for all the network buses are shown in Fig. 5-6. These results show that the optimal solution improves the voltage profiles with reference to the case without ESS. In particular, the voltages exhibit a larger probability of occurrence in correspondence of an interval closer to the desired voltage.

Table 5-3: Obtained optimal ESSs location and size (base power Sb=2.5 MW, base energy Eb=2.5 MWh).

bus	22	34
ESS power rating (p.u.)	0.33	0.39
ESS reservoir capacity (p.u.)	0.88	1.05

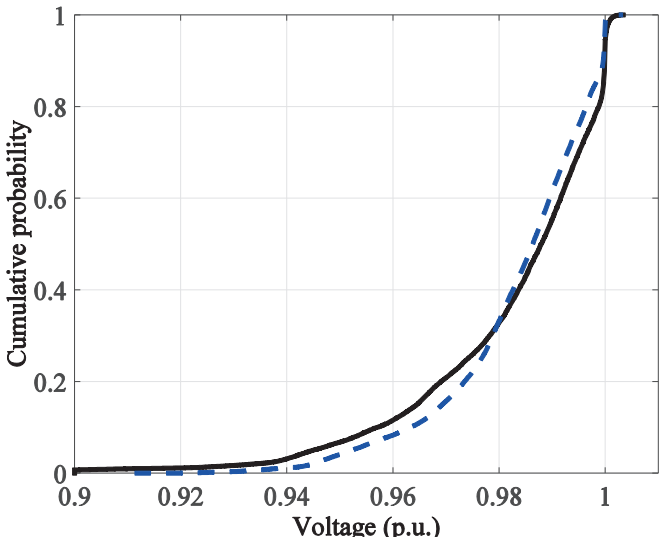

Fig. 5-6: Bus voltage CDFs for the case with and without optimally-planned ESSs.

Furthermore, the presence of load curtailment and feeders over-loading (representing the first and second goals in the objective function) are entirely eliminated with the proposed optimal placement of ESSs.

The daily operation cycle of the two ESSs provided by *case 1* in correspondence of two days (one day in winter and one day in summer of the first year) are shown in Fig. 5-7. In particular, Fig. 5-7a shows the p.u. energy stored in the two ESS units for the summer-day and Fig. 5-7b for the winter-day. Furthermore, in summer days, the ESSs are used to store the power produced by the renewable resources in the mid-hours of the day (essentially the energy produced by PVs) and supply it back to the grid during high peak hours. As it can be also seen from these results, the ESSs state-of-charge constraints are fulfilled.

Table 5-4: Changes in each term of the objective function

	Total network energy losses (MWh)	Total energy cost ($)	Total feeders loading with percentages larger than 80% (MW)	Total load curtailment (MW)
With optimal ESS allocation	1855	2,151,700	0	0
Without ESS	1925	2,609,000	516.06	1729.7

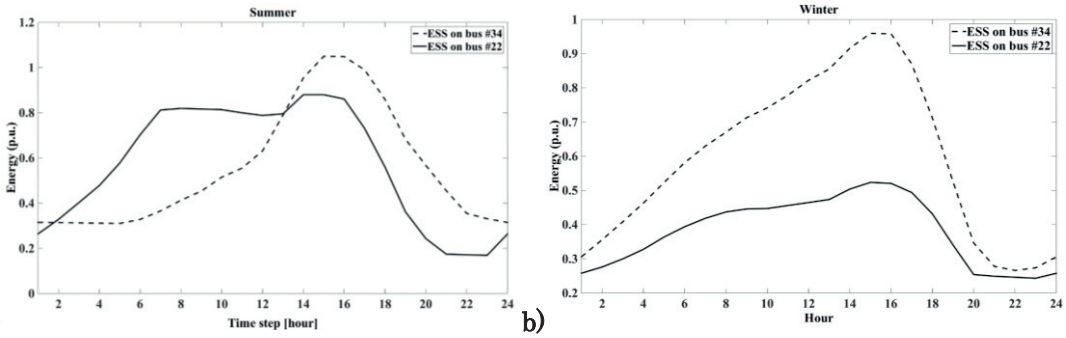

a) b)

Fig. 5-7: ESSs state-of-charge during one summer (a) and one winter (b) day (base energy *Eb*=2.5 MWh).

The total active load, PV, wind and dispatchable DGs power productions are shown in Fig. 5-8. In particular, Fig. 5-8a is related to a generic summer day and Fig. 5-8b to a generic winter day. It can be observed that, in the winter day, the ESS are used to accumulate energy in the first two-third of the day (from both the external grid and, when available, wind and PV supply), in order to support the grid in the peak hours for which high prices appear. Concerning the case of summer days, it can be seen that the ESSs accumulate energy in the central part of the day (essentially from PV). It should be underlined that these objectives are always reached by supporting the quality of the supply (i.e., voltage control, lines congestion and losses minimization).

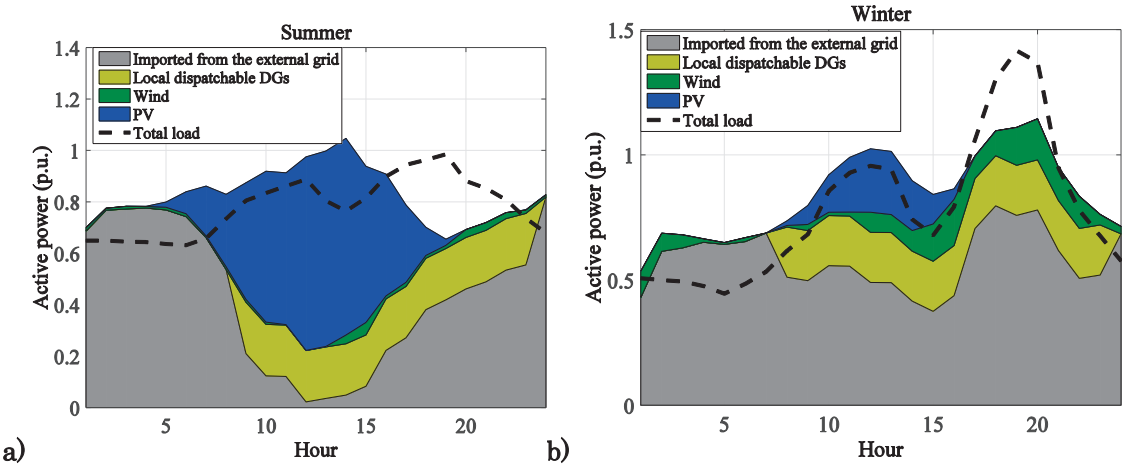

a) b)

Fig. 5-8: Active power profiles of load, PV, wind, and two dispatchable DGs during one summer (a) and one winter (b) day (base power *Sb*=2.5 MW).

5.3 Optimal ESS Planning in a Real Distribution Network Using the ADMM

In this section, we provide numerical analyses with respect to the use of ADMM for solving the ESS optimal planning problem (the model presented in 4.7.1). In this respect, a real distribution network located in the southeast of Switzerland has been used as a case study (see Fig. 5-9). The network contains 287 buses and is characterized by a non-negligible amount of PV installations with a total capacity of 2 MW. Buses where PVs are connected are shown in Fig. 5-9 together with the obtained location of the ESSs inferred from the proposed procedure. The simulation is done for five years (assumed life-time of ESSs) and four weeks in each year: one in spring, one in summer, one in fall, and one in winter. Experimentally measured loads and generation profiles for this specific grid are considered with a discretization time step of 15 minutes. The aggregated load profiles of these four time periods are shown in Fig. 5-10. The load profiles for the other years are considered to have the same profile with 5% increase each year. The load is distributed among the feeders as shown in Table 5-5. The energy price profiles of these weeks (for the first year) are shown in Fig. 5-11. The energy price is assumed to increase by 2% at each year. The load, and PV profiles are obtained from experimentally measured data in a region in south-east part of Switzerland. The energy price profiles make reference to the profile of a specific day. The weight coefficients of the elements composing the objective function are: voltage deviation W_{vol}=0.61, total network loss W_{loss} =0.05, energy cost from the external grid W_{ep}=0.04 and the feeder overloading above 80% of their respective capacities W_{vol}=0.3.

The investment costs for ESSs capacity rating and energy reservoir are assumed to be 1800 CHF/kW and 1000 CHF/kWh respectively. These values are inferred from the report [132] with specific reference to the Li-ion electrochemical batteries.

The annual interest rate is assumed to be 4%. The voltage minimization term in the objective function is activated when the voltage exhibits a deviation from the rated value larger than +/-2%.

The obtained optimal locations and ratings of ESSs are shown in Table 5-6. As it can be seen, 4 buses are selected to install ESSs. All the selected buses are close to the largest loads. Table 5-7 shows the total amount of network losses, feeder over-flow above 80% and energy cost imported from the external grid in both cases, namely: without ESSs and with optimally located ESSs. All these quantities exhibit a clear decrease in case where optimally-allocated ESSs are available in the network (total resistive losses is decreased by 1.6% and he total energy supply cost is decreased by 8.8%).

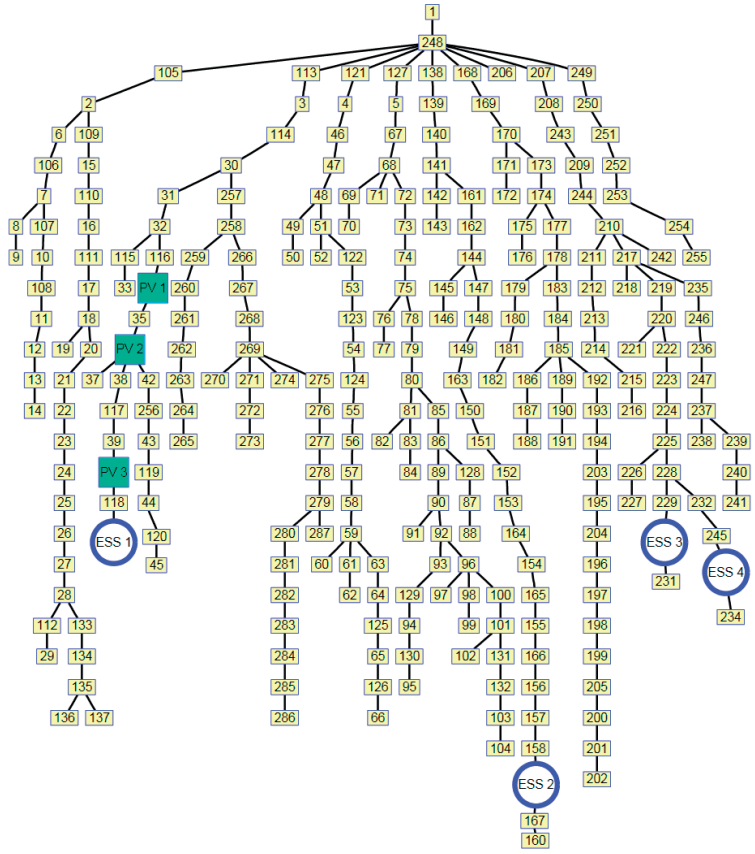

Fig. 5-9: The schematic of the real test case study (total number of buses: 287, number of feeder: 9)

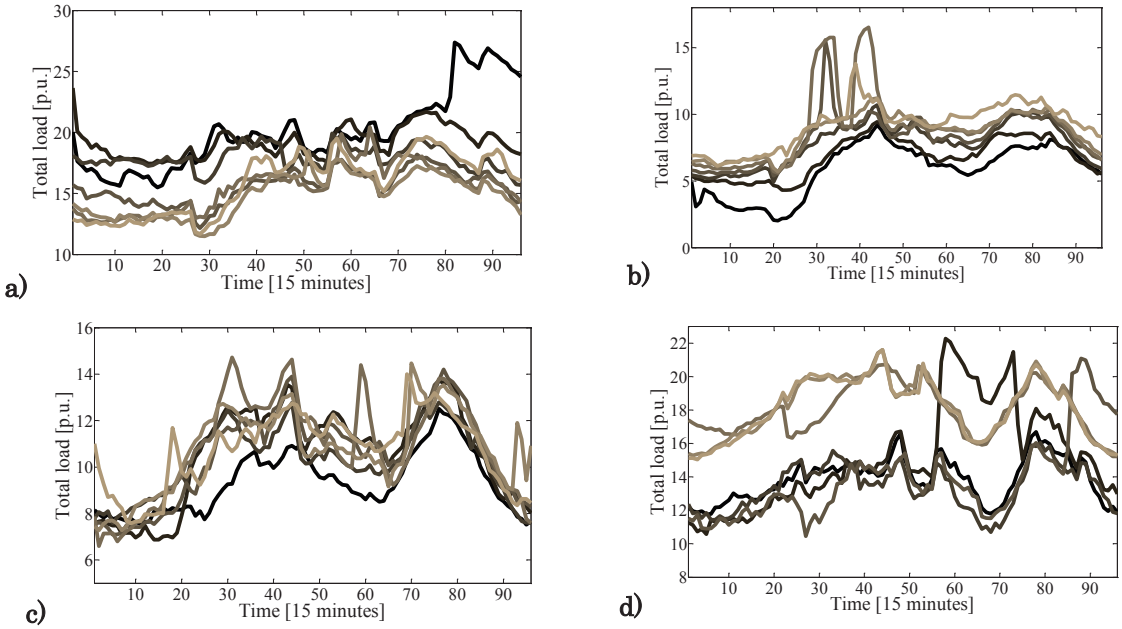

Fig. 5-10: Aggregated network loads: active-power profiles for the four considered weeks. a) winter, b) summer, c) fall, and d) spring (base value of power is 1 MW)

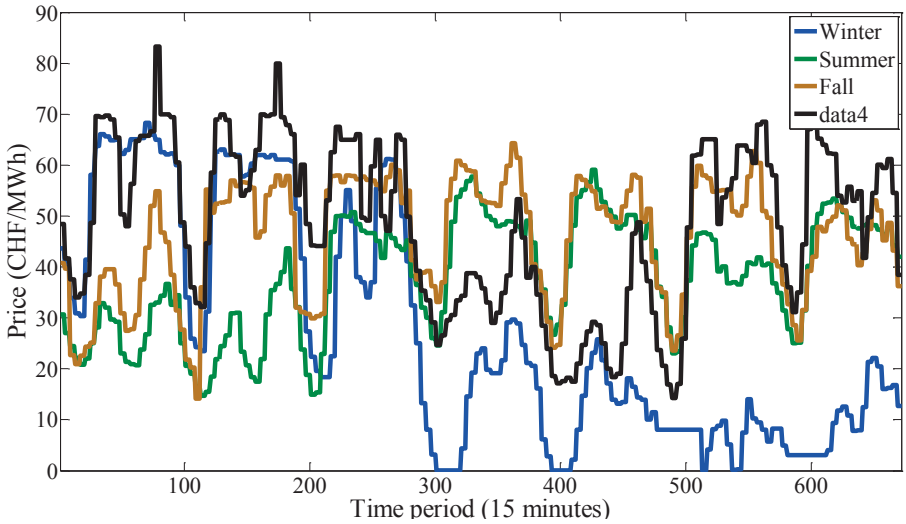

Fig. 5-11: Profiles of the electricity prices in the four considered weeks.

Table 5-5: Average feeder loading with respect to the primary substation aggregated power in the four considered weeks

Feeder #	1	2	3	4	5	6	7	8
Starting bus of the considered feeder (see Fig. 2)	105	113	121	127	138	168	207	249
Load share with respect to total network loading (%)	0.62	25.1	13.2	7	20	5	0.29	28

Table 5-6: Optimal ESS sites and sizes

ESS #	1	2	3	4
Bus number	41	159	230	233
Power rating (MW)	1.1	1.87	0.47	1.12
Reservoir capacity (MWh)	3.4	3.32	0.48	1.15

Table 5-7: Changes in each term of the objective function

	Total network losses in the simulated weeks [MWh]	Total energy cost imported from the external grid in the simulated weeks (CHF)	Total feeders loading with percentages larger than 80% (p.u.)
With optimal ESS siting and sizing	714.7	898,450	0
Without ESS	859.02	985,140	14.7

Fig. 5-12 shows the Cumulative Distribution Function (CDF) of nodal voltages in both analyzed cases (i.e., with and without ESSs). It is evident that the presence of ESSs allows to largely improve the ADN quality-of-service with respect to voltage variations.

The *SoC* of all the ESSs in two days, one day in summer and one day in winter, are shown in Fig. 5-12 and Fig. 5-13, respectively. As it can be observed, the figures show how the constraints on the ESS *SoC* are respected. Fig. 5-12 shows that, in summer period, all the ESSs except the one that is on the feeder with PV production, follow the load profile. The ESS 1, which is located on the feeder with PV production is responding to energy price profile. It stores excess PV production during the day and produce energy during high-peak hours. Fig. 5-13 shows that the ESSs *SoC* in wintertime period is different. In particular, all the ESSs are responding to the load profile. In this respect, it is worth observing that these ESSs are located in the feeders characterized by the highest loading level with associated largest voltage variations. Thus, they tend to minimize the corresponding elements of the multi-objective function since they have a larger priority. In view of the above considerations, it is evident how the proposed process is capable to locate each ESS by distinguishing their influences on: the network quality-of-service, the local energy balance and the network zone of influence.

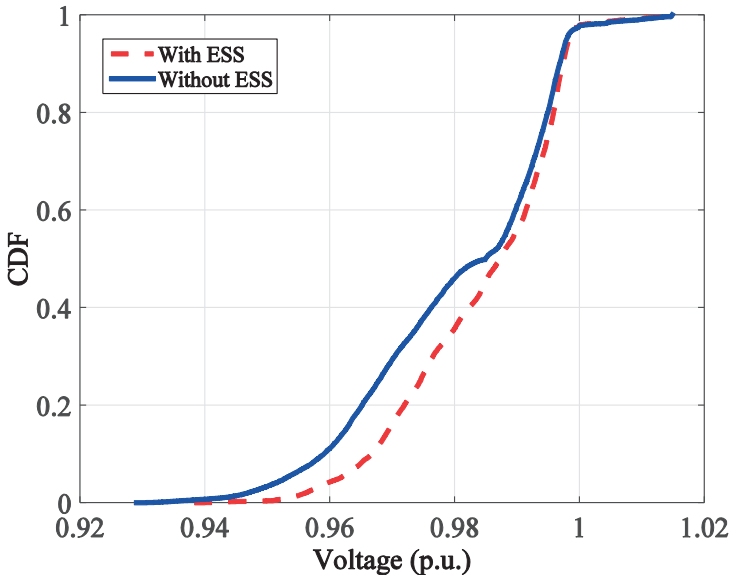

Fig. 5-12: The CDF of nodal voltage magnitudes for the cases with and without optimal ESS siting and sizing

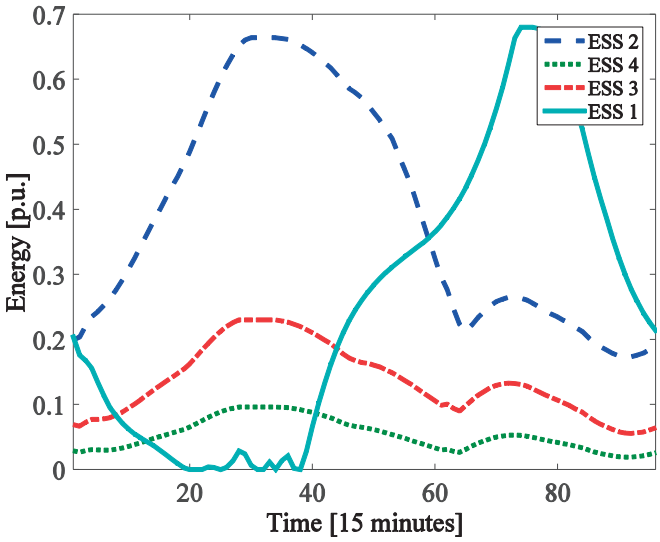

Fig. 5-13: *SoC* profiles of the ESSs in summer period (Base value of energy is 5 MWh).

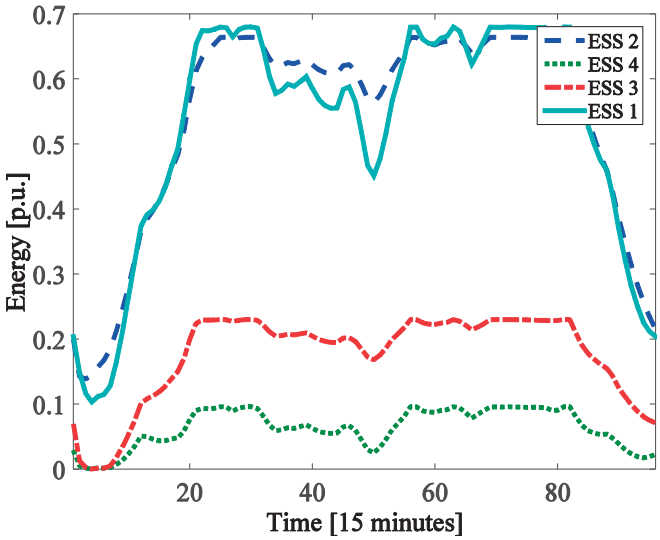

Fig. 5-14: . *SoC* profiles of the ESSs in winter period (Base value of energy is 5 MWh).

It should be noted that the solution provided for the case study in this section does not result in any load curtailment. It is also worth noting that the main objective investigated in this case study is the ESSs contribution to increase the ADN quality-of-service (i.e., compensate the voltage deviations). Therefore, this specific objective is characterized by the highest weight in the objective function. As a result, as it can be noted from Table 5-7, the benefits resulting from the peak shaving cannot justify the ESS high capital cost alone.

Observation about the ADMM convergence

A reasonable stop criterion is that the primal and dual residuals have to be small [126] (see Appendix A.3). The objective sub-optimality is small when these two values are small [126]. The progress of primal and dual residuals as a function of the iteration number is shown in Fig. 5-15 and Fig. 5-16, respectively.

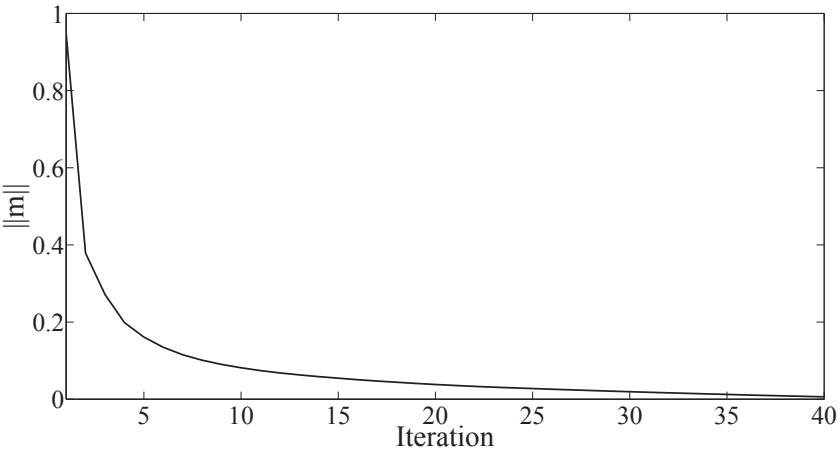

Fig. 5-15: Norm of the primal residual versus iteration

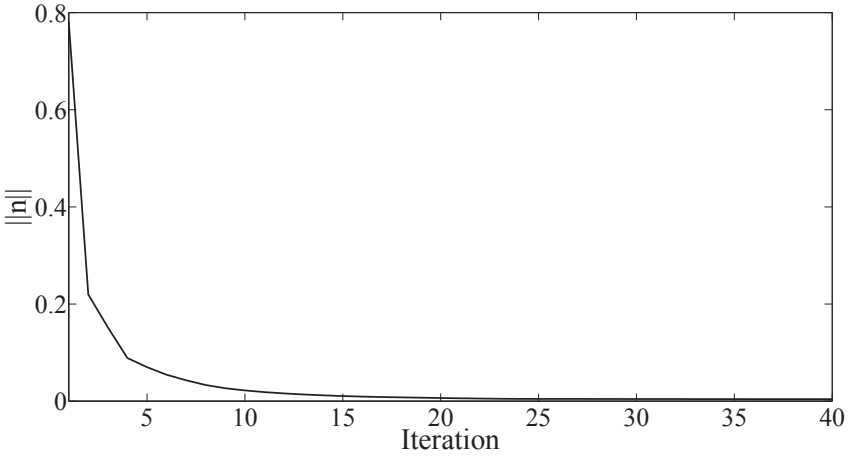

Fig. 5-16: Norm of the dual residual versus iteration

5.4 Optimal ESS Siting and Sizing Taking into Account Network Reconfiguration Using Benders Decomposition

This section provides numerical analysis associated with the solution of optimal ESS siting and sizing taking into account the ADN reconfiguration. Benders decomposition technique is used to decompose the problem into a master problem and several subproblems (see section 4.7.2). The IEEE 123 buses network is selected as the test case. Fifteen scenarios (per year) for the master problem and 300 ones for the

subproblem are created using the scenarios generation/reduction method presented in section 4.4. The master problem scenarios, with time step discretization of two hours, represent the load and PV profiles, whereas the subproblem scenarios, with 15 minutes discretization, are related to the energy price variations in addition to the load and PV ones.

The goal of the reconfiguration in the master problem is to minimize the total resistive losses as well as satisfying the network constraints. The objective function of the subproblems includes minimization of i) energy cost ii) nodal voltage magnitudes deviations, and iii) lines congestion. It should be noted that the load curtailment is not considered here since it is not necessary and can be avoided. Contrary to the other cases, we have assumed that the DNO has pre-selected a list of candidate buses for installing ESSs. They are shown in Table 5-9 (25 buses are selected as the candidate buses). The ESSs installation cost is considered to be 0.6 million CHF per unit of ESS (a typical cost for large-scale Li-On batteries). Each unit of ESS has 0.25 kVA power rating and 0.25 MWh energy reservoir capacity. Other simulation parameters are provided in Table 5-10.

The identified optimal sites and sizes of the ESSs units are provided in Table 5-11. The obtained ADN topology as well as the identified optimal sites of ESSs and PV locatins are shown in Fig. 5-17. In particular, 10 buses are selected for installing 24 ESS units. Note that the configuration obtained for all the 15 cateorizes of the load and PV data is the same (one configuration is obtained for all the 15 categorizes).

The Cumulative Distribution Functions (CDFs) of the nodal voltage magnitudes related to two cases, i) with optimal siting and sizing of ESSs and ii) without ESS, are shown in Fig. 5-18. These results clearly show that the optimal solution improves the voltage profile with reference to the case without ESS. In particular, it can be observed that the voltage magnitudes are well kept in the desired operation region ($\pm$2% deviation). Further, it can be seen that the voltage magnitudes below 0.96 p.u. and larger than 1.02 p.u. are completely removed.

Improvements in the other objectives are presented in Table 5-8. Particularly, it can be observed that the lines congestion is completely removed. Furthermore, the energy supply cost is decreased by 2.4%. It should be noted that the weighting coefficient of each element of the objective function is as follows: i) $W_E = 1$ (ESS investment and maintenance cost as well as the energy supply cost), ii) $W_v = 20$(nodal voltage magnitudes deviations), and iii) $W_l = 40$ (lines congestions).

Table 5-8: Changes in the objective function with optimal planning of ESS units

	Energy cost from external grid [CHF]	Total lines loading over 80% of capacity (sum over all periods) [p.u.]
with optimal ESS placement	25,087,962.30	0
without ESS	25,712,958.15	0.1

Table 5-9: Candidate buses for installing ESSs

Bus #	9	20	22	26	30	34	38	41	49	46	61	63	65
Bus #	66	71	76	78	80	83	88	91	100	102	105	116	

Table 5-10: Simulation parameters

Base power (energy) value	5 MW (MWh)	Maximum number of ESSs that can be installed	30
Resistive losses of ESSs	0.04 (p.u.)	ESS ramp-up ramp-down limits	0.3 (MW/h)
Max/min voltage-thresholds beyond which voltage deviation is minimized	+/- 2%	Max square value of lines current beyond which lines current flow is minimized	80 %
Annual load growth	2%	Interest rate	3%
Total number of buses where ESS can be installed	25	GBM sigma	0.08
Weighting coefficient for Energy supply, investment and maintenance costs [$]	1	Weighting coefficient for voltage deviation [p.u.]	20
Weighting coefficient for lines congestion managements [p.u.]	40		

Table 5-11: Identified optimal ESS sites and sizes

Bus #	26	30	38	41	65	66	76	83	91	105
Number of ESS units	1	1	6	1	5	1	1	2	2	3

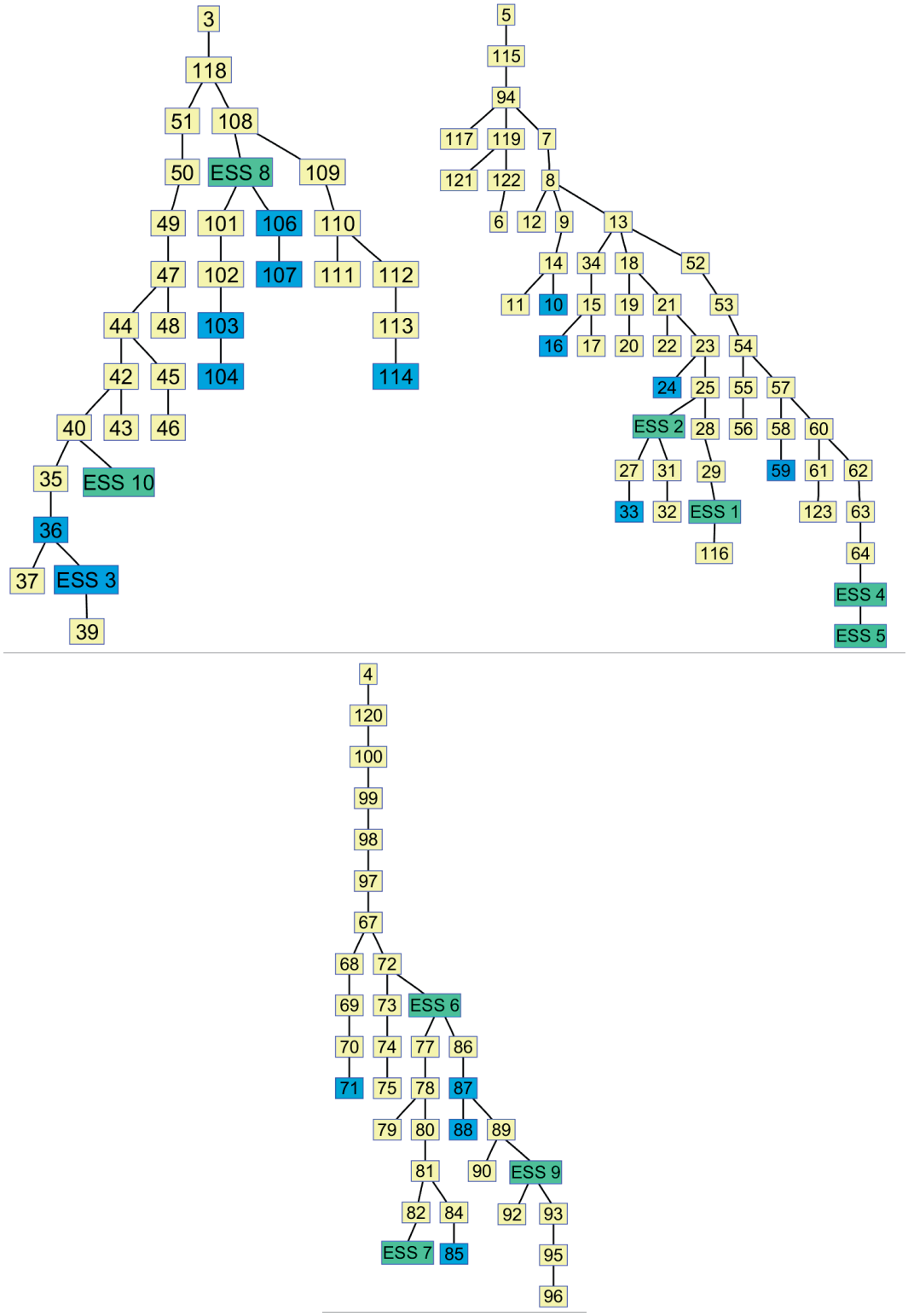

Fig. 5-17: Identified ADN topology and ESS sites (the buses with PV are shown with blue color)

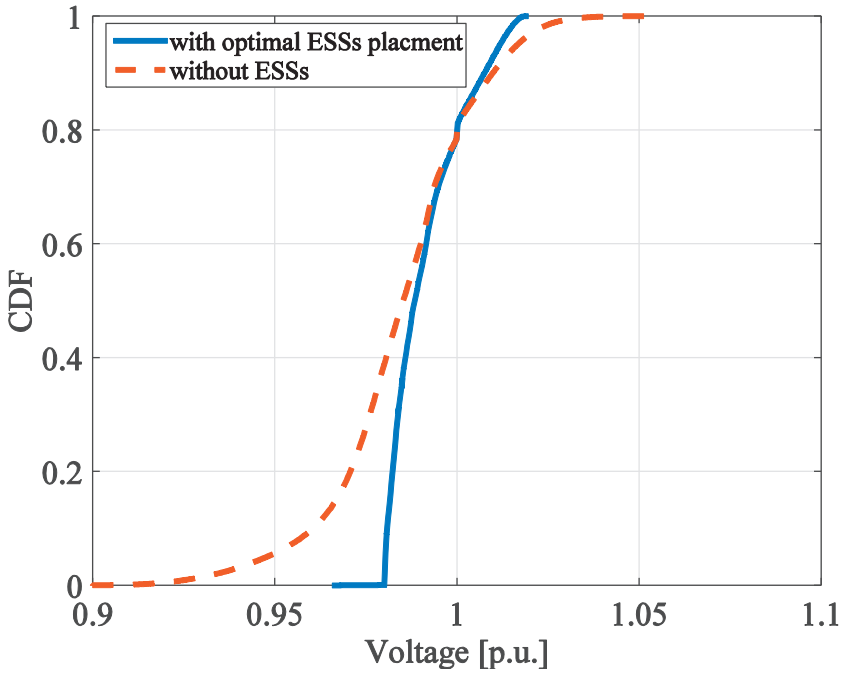

Fig. 5-18: Nodal voltage magnitudes CDF, i) with optimal placement of ESSs ii) without ESSs

Finally in the Fig. 5-19 the convergence of the Benders decomposition is depicted. In particular, the procedure has converged in 11 iterations with stopping criteria equal to 0.01% (see Appendix A.4).

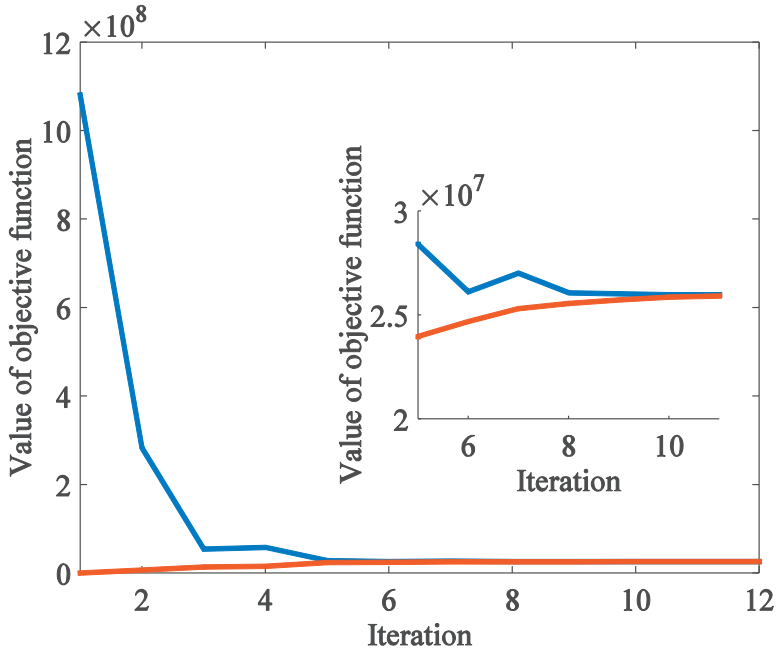

Fig. 5-19: Convergence of the Benders decomposition procedure

5.5 Summary and Conclusion

In this chapter, the developed processes for optimal siting and sizing of ESSs in ADNs are applied to real and standard test case studies. The obtained results have shown the capabilities of the proposed methods to optimally allocate ESSs to: (i) largely improve the quality of supply of the ADNs in terms of mitigating voltage deviations, eliminating line congestions and load curtailment together with (ii) minimizing the total cost of locally-used electricity and investment cost for ESSs installation and maintenance. It is possible to conclude that optimally-allocated ESSs can represent a valid solution for ADN operators that do not want to deploy massive DG controls. This opportunity will potentially postpone large control infrastructure deployment as well as grid infrastructure reinforcement.

6 Conclusion

In this thesis we propose methodologies for optimal control, operation and planning of controllable resources in ADNs with specific reference to ESSs. In this respect, we focus on the following three main problems:

- Optimal control and operation of radial ADNs using an exact convex formulation of the OPF as well as a specific linearized OPF based on voltage sensitivity coefficients;
- Optimal operation of ADNs with uncertainties;
- Optimal planning of ESSs in ADNs aiming at providing local ancillary services and load balance

Optimal operation and control of ADNs

First, an exact convex formulation for OPF in ADNs, called AR-OPF, is proposed. The AR-OPF is capable to include the correct model of transmission lines (two-port Π equivalent) as well as the network security constraints (nodal voltages and lines ampacity limits). In fact, AR-OPF is an augmented-relaxed version of the original OPF (O-OPF). The AR-OPF includes a new set of more conservative constraints, with respect to the original ones in O-OPF, to limit the line current flows as well as the nodal voltage magnitudes. Sufficient conditions are provided to ensure the feasibility and optimality of the proposed OPF solution or, in other words, to ensure the exactness of the SOCP relaxation. We have demonstrated the infeasible behavior of the existing convex OPF formulation using a small benchmark network. Referring to the same network, it is shown that AR-OPF is capable to provide an exact feasible solution. Further, by analysis the exactness conditions, it is revealed that they are mild and hold for real distribution networks operating in feasible region.

Then, the AR-OPF is further augmented with radiality constraints and inclusion of tie-line switches to take into account the topology changes in ADNs. The radiality constraints, are formulated by introducing binary variables only for the tie-line switches. This approach reduces the number of binary variables and, consequently, decreases the computation time. The developed model is Mixed Integer Second Order Cone Programming (MISOCP) and could be solved efficiently by the state-of-the-art commercial solvers for convex optimization. The optimality and the exactness of the proposed ADN reconfiguration, as well as its scalability are demonstrated using standard benchmark networks.

Finally, we have developed an optimal voltage control scheme based on nodal voltage sensitivity coefficients and using ESSs as controllable resources. The developed model is linear and could be used as an alternative to the DistFlow model (with inclusion of transverse parameters) which is also linear or the AR-OPF which is a SOCP model.

Optimal operation of ADNs with uncertainties

First, we have suitably modeled the day-ahead optimal scheduling of ADNs as a two stage optimization programming. The day-ahead decision variables, called first stage decisions, are made when the uncertain parameters are unknown. These decisions correspond to the amount of import/export energy from the external grid at each hour and ESSs set points. The second stage decisions are taken based on the realization of the random parameters and the first stage ones. In case of the targeted problem, the second stage decisions correspond to the 15 minutes ESSs set points.

Further, adaptive robust optimization and stochastic optimization techniques, considering spatial and temporal correlations, are properly casted to solve the above-mentioned two-stage problem.

The simulation results reveal that the ARO approach is feasible for any realization of the uncertain parameters and is optimal for the worst case realization, in other words, it is a conservative and risk averse approach. On the other hand, the stochastic optimization provides a solution taking into account the probability of the considered scenarios. In terms of modeling, stochastic optimization is more flexible and both stages could contain non-convex functions and discrete variables.

Optimal planning of ESSs in ADNs aiming at providing local ancillary services and load balance

First, an optimal ESS siting model based on the concept of voltage sensitivity coefficients is presented. We have also shown the application of Benders decomposition approach for solving the targeted MIQCQP problem. Using standard IEEE 14 buses network, the capability of the proposed methodology to find the best locations for providing local voltage control is demonstrated. Further, it is shown that employing the

Benders decomposition could drastically decrease the computation time (up to 10 times faster than solving the original problem).

Then, the AR-OPF and proposed ADN reconfiguration are suitably employed to develop a multi-objective optimization model for optimal siting and sizing of ESSs. In particular, the proposed methodologies takes into account the following objectives: (i) network voltage deviations, (ii) feeders/lines congestions, (iii) network losses, (iv) cost of supplying loads (from external grid or local producers) together with the cost of ESS investment/maintenance, and (v) load curtailment. Moreover, the stochasticity of loads and renewables productions as well as the possibility of ADN reconfiguration are incorporated into the model. The ESSs are suitably modeled to consider their ability to support the network by both active and reactive powers. Furthermore, two decomposition methods, ADMM and Benders, are appropriately employed to decompose the targeted large-scale problems. Various numerical analysis with respect to the standard and real networks are performed to demonstrate the capabilities of the proposed methodologies for providing optimal and feasible solutions as well as their computational efficiency and scalability. In particular, it was shown that the ESSs could possibly prevent load and generation curtailment, reduce the voltage deviations and lines congestions, and do the peak shaving. Further, it was shown that the Benders decomposition potentially could be the best solution methodology for large-scale problems with presence of binary variables.

Future works

In the continuation of this work, the following topics are suggested for further studies:

- We have developed the optimization models for the balanced power grids. They could be further developed to take into account the unbalanced grids
- We have developed simple schemes for modeling the variations and the uncertainties of the parameters for ARO, stochastic optimization and optimal planning. In future works, more sophisticated statistical models could be developed and incorporated into the proposed models.
- The inclusion of possible contingencies and reliability indices are also interesting aspects that could be developed and incorporated into the optimization models developed for planning of ESSs.
- In this thesis we just considered the planning of ESSs in ADNs. The proposed procedure could be further extended for optimal design of the whole ADN architecture.
- In this thesis it is assumed that the owner of the ESSs is the DNO. The deployment of ESSs owned by other entities could be also the subject of further research.
- We developed simple and static models of ESSs. Their model could be further improved to include their dynamic aspects.

Appendices

A.1. Benders-Dual Cutting-Plane Algorithm for adaptive robust optimization

The solution of the right hand side maximization belongs to a set of finite cardinality K and is independent of the first stage solution. Indicating the elements of this set $(\Delta\Psi_k^T, \lambda_{1,k}, \lambda_{2,k}, \mu_k)$ [87]. The original robust programming can be reformulated as follows [87]:

$$\text{minimize}\left(c_x^T x\right) + \vartheta \tag{7.1.a}$$

$$\text{s.t. } \vartheta \geq \Psi^T \lambda_1 + \Delta\Psi_k^T \lambda_{1,\text{k}} + d^T \mu_k + e^T \lambda_{2,\text{k}} - \lambda_{2,\text{k}} R x, \quad \forall k \tag{7.1.b}$$

$$\vartheta \geq 0 \tag{7.1.c}$$

$$Ax = L \tag{7.1.d}$$

$$Gx \leq g \tag{7.1.e}$$

The term ϑ is bounded from below by pointwise maximum of a finite set of linear functions in the first stage decision variable x. In [133] the following cutting plane algorithm is proposed to solve the above optimization problem. It is guaranteed to converge to the optimal solution in a finite number of iterations. It is called Benders-

dual cutting algorithm since the cut generated are based on the optimal dual solution of the lower level problem [87, 133].

Step 1: set the upper and lower bounds (UB, LB) equal to $+\infty$ and $-\infty$ respectively. Initialize the iteration index $1 \to i$.

Step 2: Define the Master Problem (MP) as the minimization of (7.1.a) and fix a reasonable lower bound for ϑ . Fix a feasible solution (x_1^*, ϑ_1^*) to the MP.

Step 3: solve the Sub-Problem (SP) (right-hand side maximization in (3.17)) while the first stage variables are fixed. Update the upper bound $UB = \min\left\{UB, c_x^T x_i^* + z_i^{SP*}\right\}$ where z_i^{SP*} is the optimal SP objective value. Add the corresponding Benders cut to the MP determined at stage i .

Step 4: Solve the MP. Fix x_{i+1}^* and $z_{i+1}^{\mathrm{MP}*}$ at the solution and the objective function value respectively. Update $LB = z_{i+1}^{\mathrm{MP}*}$.

Step 5: IF $(UB - LB) \le \varepsilon$, where ε is a small value stop, otherwise, update $i+1 \to i$ and go to step 3.

A.2. Analytical Hierarchy Process (AHP)

In AHP method, first a pairwise comparison is done between the objectives. The decision-maker (i.e. the DNO) will define the importance of the each factor in the comparison with all the other factors [125] based on the scale from 1 to 9. A larger scale value indicates that the index associated with is more important.

It depends on the needs of the decision maker and it can vary from network to network and operator to operator. Then a matrix is built based on these pairwise comparisons as shown in (7.2.a).

$$W = \begin{pmatrix} a_{11} & \cdots & a_{1n} \\ \vdots & \ddots & \vdots \\ a_{n1} & \cdots & a_{nn} \end{pmatrix} \tag{7.2.a}$$

where $a_{ij} = 1/a_{ji}$ represents the importance pairwise comparison result between the objective i and j .

The final weighting coefficient for each index is calculated by (7.3.a).

$$W_i = \frac{\sqrt[n]{\prod_i^n a_{ij}}}{\sum_i^n \sqrt[n]{\prod_i^n a_{ij}}} \tag{7.3.a}$$

A.3. Alternative Direction Method of Multipliers

Suppose an optimization problem generically represented by (7.4.a) and (7.4.b)where f, g, ξ, and ζ are convex. The f and g are independent from each other except they are linked by the constraint (7.4.b).

$$\begin{aligned} \underset{x,z}{\text{minimize}} \quad & f(x) + g(z) \\ \text{subject to} \quad & \text{dom } f = \{x \mid x \in \xi\} \\ & \text{dom } g = \{z \mid z \in \zeta\} \end{aligned} \tag{7.4.a}$$

$$Ax + Bz = c \tag{7.4.b}$$

where $A \in \mathbb{R}^{p \times n}$, $B \in \mathbb{R}^{p \times m}$ and $c \in \mathbb{R}^p$ when the variables $x \in \mathbb{R}^n$ and $z \in \mathbb{R}^m$. The augmented lagrangian of this problem with respect to constraint (7.4.b) has the form as shown in (7.5.a).

$$\begin{aligned} L_\rho(x, y, z) = & f(x) + g(z) + y^T(Ax + Bz - c) \\ & + (\rho/2)\|Ax + Bz - c\|_2^2 \\ \text{subject to} \quad & \text{dom } f = \{x \mid x \in \xi\} \\ & \text{dom } g = \{z \mid z \in \zeta\} \end{aligned} \tag{7.5.a}$$

The ADMM procedure is deployed as follows. An iterative process between the three steps shown in equations (7.6.a)-(7.6.c) will results in the optimal solution. First, the augmented Lagrangian problem (7.6.a) is minimized with z and y being fixed. Then the obtained x is then used in the minimization of (7.6.b) with x, and y being fixed. Finally, the dual multipliers are updated as shown in (7.6.c) with the obtained x and z from the previous step. This procedure will be continued until it converges to the global optimal solution.

$$x^{k+1} := \underset{x}{\text{argmin}}\, L_\rho(x, y^k, z^k) \tag{7.6.a}$$

$$z^{k+1} := \underset{z}{\operatorname{argmin}} L_\rho(x^{k+1}, y^k, z) \tag{7.6.b}$$

$$y^{k+1} := y^k + \rho(Ax^{k+1} + Bz^{k+1} - c) \tag{7.6.c}$$

The primal and dual residuals are calculated as (7.7.b) and (7.7.a), respectively and are used as the stopping criteria [126].

$$\left\| m^k \right\| = \left\| Ax^k + Bz^k - c \right\| \tag{7.7.a}$$

$$\left\| n^k \right\| = \left\| z^{k+1} - z^k \right\| \tag{7.7.b}$$

A.4. Benders decomposition

The main idea of using Benders decomposition is to break down the original large-scale problem, having block angular structure with linking variables, into a master problem and several subproblems. The Benders decomposition is briefly described in what follows [134, 135].

Consider the following optimization problem:

$$\underset{x,y}{\text{minimize}} \; c^T x + \sum_{s \in S} q_s^T y_s \tag{7.8.a}$$

subject to:

$$Wy_s = h_s - T_s x, \quad \forall s \in S \tag{7.8.b}$$

$$c(x) \le 0 \tag{7.8.c}$$

$$d(y_s) \le 0, \quad \forall s \in S \tag{7.8.d}$$

The following procedure, called Benders decomposition, decompose the problem at the cost of iteration (the notation with $\widehat{\ }$ implies that the corresponding notation is a parameters).

Step 0: set iteration index $n = 0$

Step 1: Solve the following mater problem:

$$\underset{x}{\text{minimize}} \; \Upsilon^{(0)} = c^T x \tag{7.9.a}$$

$$c(x) \le 0 \tag{7.9.b}$$

The solution of this problem is $\hat{x}^{(n)}$.

Step 2: Set iteration index $n = n + 1$ and solve the following subproblem for each scenario ($s \in S$):

$$\underset{y_s}{\text{minimize}}\ \mathrm{A}_s^{(n)} = q_s^T y_s \tag{7.10.a}$$

$$d(y_s) \le 0 \tag{7.10.b}$$

$$W y_s = h_s - T_s \hat{x}^{(n-1)} \tag{7.10.c}$$

$$x = \hat{x}^{(n-1)} : \quad \pi_s^{(n)} \tag{7.10.d}$$

where π_s represent the dual of constraint (7.10.d). The solution of this problem is $\left(\widehat{y_s}^{(n)}, \widehat{\mathrm{A}}_s^{(n)}\right)$.

Step 3: Solve the master problem (either MP1 or MP2):

MP1:

$$\underset{x,\mathcal{Z}}{\text{minimize}}\ \Upsilon^{(n)} = c^T x + \mathcal{Z} \tag{7.11.a}$$

$$c(x) \le 0 \tag{7.11.b}$$

$$\mathcal{Z} \ge \sum_{s \in S} \hat{\mathrm{A}}_s^{(k)} - \sum_{s \in S} \left(\pi_s^{(k)} \left(x - \hat{x}^{(k)} \right) \right), \quad \forall k = 1, \ldots, n \tag{7.11.c}$$

MP2:

$$\underset{x,\mathcal{Z}}{\text{minimize}}\ \Upsilon^{(n)} = c^T x + \sum_{s \in S} \mathcal{Z}_s \tag{7.12.a}$$

$$c(x) \le 0 \tag{7.12.b}$$

$$\mathcal{Z}_s \ge \hat{\mathrm{A}}_s^{(k)} - \pi_s^{(k)} \left(x - \hat{x}^{(k)} \right), \quad \forall k = 1, \ldots, n, \forall \mathrm{s} \in \mathrm{S} \tag{7.12.c}$$

MP2 is called multi-cut Benders decomposition [135]. The solution of this problem is $\left(\hat{x}^{(n)}, \widehat{\Upsilon}^{(n)}\right)$.

Step 3: Calculate upper bound (UB) and lower bound (LB) as follows:

$$\begin{aligned} \mathrm{UB} &= \Upsilon^{(n)} \\ \mathrm{LB} &= c^T \hat{x}^{(n)} + \sum_{s \in S} \hat{\mathrm{A}}_s^{(n)} \end{aligned} \tag{7.13.a}$$

If $|\mathrm{UB} - \mathrm{LB}| \le \varepsilon$ stop and the optimal solution is $\hat{x}^{(n)}$ and $\hat{y}_s^{(n)}, \forall s \in S$, otherwise go to step 2.

In case that the subproblems are infeasible, first feasibility cuts have to be created and sent to the master problem. For further details we refer the interested reader to [134, 135].

Bibliography

[1] J. A. N. Hataziargyriou, B. Andersen,M. Armstrong, P. Boss, B. Dalle, G. deMontravel, A. Negri, C. Nucci, P. Southwell, "CIGREWG network of the future, electricity supply systems of the future," *Electra,,* vol. 256, pp. 42-49, 2011.

[2] C. W. G. C6.11, "Development and operation of active distribution networks," *Cigre,* April 2011.

[3] J. A. Momoh, M. El-Hawary, and R. Adapa, "A review of selected optimal power flow literature to 1993. Part I: Nonlinear and quadratic programming approaches," *IEEE transactions on power systems,* vol. 14, pp. 96-104, 1999.

[4] J. A. Momoh, M. El-Hawary, and R. Adapa, "A review of selected optimal power flow literature to 1993. Part II: Newton, linear programming and interior point methods," *IEEE Transactions on Power Systems,* vol. 14, pp. 105-111, 1999.

[5] S. Frank, I. Steponavice, and S. Rebennack, "Optimal power flow: a bibliographic survey I," *Energy Systems,* vol. 3, pp. 221-258, 2012.

[6] S. Frank, I. Steponavice, and S. Rebennack, "Optimal power flow: a bibliographic survey II," *Energy Systems,* vol. 3, pp. 259-289, 2012.

[7] B. Stott, J. Jardim, and O. Alsaç, "DC power flow revisited," *IEEE Transactions on Power Systems,* vol. 24, pp. 1290-1300, 2009.

[8] M. E. Baran and F. F. Wu, "Optimal capacitor placement on radial distribution systems," *IEEE Transactions on Power Delivery,* vol. 4, pp. 725-734, 1989.

[9] M. E. Baran and F. F. Wu, "Optimal sizing of capacitors placed on a radial distribution system," *IEEE Transactions on Power Delivery,* vol. 4, pp. 735-743, 1989.

[10] R. A. Jabr, "A primal-dual interior-point method to solve the optimal power flow dispatching problem," *Optimization and Engineering,* vol. 4, pp. 309-336, 2003.

[11] W. Min and L. Shengsong, "A trust region interior point algorithm for optimal power flow problems," *International Journal of Electrical Power & Energy Systems,* vol. 27, pp. 293-300, 2005.

[12] E. C. Baptista, E. A. Belati, and G. R. da Costa, "Logarithmic barrier-augmented Lagrangian function to the optimal power flow problem,"

International journal of electrical power & energy systems, vol. 27, pp. 528-532, 2005.

[13] A. G. Bakirtzis, P. N. Biskas, C. E. Zoumas, and V. Petridis, "Optimal power flow by enhanced genetic algorithm," *IEEE Transactions on Power Systems,* vol. 17, pp. 229-236, 2002.

[14] M. Abido, "Optimal power flow using particle swarm optimization," *International Journal of Electrical Power & Energy Systems,* vol. 24, pp. 563-571, 2002.

[15] P. Panciatici, M. Campi, S. Garatti, S. Low, D. Molzahn, A. Sun*, et al.*, "Advanced optimization methods for power systems," in *Power Systems Computation Conference (PSCC), 2014*, 2014, pp. 1-18.

[16] C. Coffrin and P. Van Hentenryck, "A linear-programming approximation of AC power flows," *INFORMS Journal on Computing,* vol. 26, pp. 718-734, 2014.

[17] J. Lavaei and S. H. Low, "Zero duality gap in optimal power flow problem," *IEEE Transactions on Power Systems,* vol. 27, pp. 92-107, 2012.

[18] E. Dall'Anese, H. Zhu, and G. Giannakis, "Distributed optimal power flow for smart microgrids," *IEEE Transactions on Smart Grid,* vol. 4, pp. 1464-1475, 2013.

[19] D. K. Molzahn and I. Hiskens, "Moment-based relaxation of the optimal power flow problem," in *Power Systems Computation Conference (PSCC), 2014*, 2014, pp. 1-7.

[20] D. K. Molzahn and I. Hiskens, "Sparsity-exploiting moment-based relaxations of the optimal power flow problem," 2014.

[21] M. Farivar, C. R. Clarke, S. H. Low, and K. M. Chandy, "Inverter var control for distribution systems with renewables," in *IEEE International Conference on Smart Grid Communications (SmartGridComm)*, 2011, pp. 457-462.

[22] L. Gan, N. Li, U. Topcu, and S. Low, "On the exactness of convex relaxation for optimal power flow in tree networks," in *IEEE 51st Annual Conference on Decision and Control (CDC)*, 2012, pp. 465-471.

[23] L. Gan, N. Li, U. Topcu, and S. H. Low, "Exact convex relaxation of optimal power flow in radial networks," *IEEE Transactions on Automatic Control,* vol. 60, pp. 72-87, 2015.

[24] K. Christakou, D.-C. Tomozei, J.-Y. L. Boudec, and M. Paolone, "AC OPF in Radial Distribution Networks-Parts I, II," *arXiv preprint arXiv:1503.06809,* 2015.

[25] W. H. Kersting, "Radial distribution test feeders," in *IEEE Power Engineering Society Winter Meeting, 2001*, 2001, pp. 908-912.

[26] K. Strunz, S. Barsali, and Z. Styczynski, "Cigre task force c6. 04.02: Developing benchmark models for integrating distributed energy resources," in *Proceedings of the CIGRE 5th Southern Africa regional conference: study committee C6 colloquium*, 2005.

[27] S. Bahadoorsingh, J. V. Milanovic, Z. Yan, C. P. Gupta, and J. Dragovic, "Minimization of Voltage Sag Costs by Optimal Reconfiguration of Distribution Network Using Genetic Algorithms," *IEEE Transactions on Power Delivery,* vol. 22, pp. 2271-2278, 2007.

[28] M. W. Siti, D. V. Nicolae, A. A. Jimoh, and A. Ukil, "Reconfiguration and Load Balancing in the LV and MV Distribution Networks for Optimal

Performance," *IEEE Transactions on Power Delivery,* vol. 22, pp. 2534-2540, 2007.

[29] W. M. Lin, F. S. Cheng, and M. T. Tsay, "Distribution feeder reconfiguration with refined genetic algorithm," *IEE Generation, Transmission and Distribution,* vol. 147, pp. 349-354, 2000.

[30] R. S. Rao, K. Ravindra, K. Satish, and S. V. L. Narasimham, "Power Loss Minimization in Distribution System Using Network Reconfiguration in the Presence of Distributed Generation," *IEEE Transactions on Power Systems,* vol. 28, pp. 317-325, 2013.

[31] Z. Dong, F. Zhengcai, and Z. Liuchun, "Joint Optimization for Power Loss Reduction in Distribution Systems," *IEEE Transactions on Power Systems,* vol. 23, pp. 161-169, 2008.

[32] A. C. B. Delbem, A. C. P. L. F. de Carvalho, and N. G. Bretas, "Main chain representation for evolutionary algorithms applied to distribution system reconfiguration," *IEEE Transactions on Power Systems,* vol. 20, pp. 425-436, 2005.

[33] V. Borozan and N. Rajakovic, "Application assessments of distribution network minimum loss reconfiguration," *IEEE Transactions on Power Delivery,* vol. 12, pp. 1786-1792, 1997.

[34] C. Hsiao-Dong and R. Jean-Jumeau, "Optimal network reconfigurations in distribution systems. I. A new formulation and a solution methodology," *IEEE Transactions on Power Delivery,* vol. 5, pp. 1902-1909, 1990.

[35] H. D. Chiang and R. Jean-Jumeau, "Optimal network reconfigurations in distribution systems. II. Solution algorithms and numerical results," *IEEE Transactions on Power Delivery,* vol. 5, pp. 1568-1574, 1990.

[36] F. V. Gomes, S. Carneiro Jr, J. L. R. Pereira, M. P. Vinagre, P. A. N. Garcia, and L. R. De Araujo, "A new distribution system reconfiguration approach using optimum power flow and sensitivity analysis for loss reduction," *IEEE Transactions on Power Systems,* vol. 21, pp. 1616-1623, 2006.

[37] A. Bart, R. Cherkaoui, and A. Germond, "Heuristic methods applied to the restoration of distribution networks," in *ISAP" 94. International Conference on Intelligent System Application to Power Systems*, 1994, pp. 279-86.

[38] H. Nafisi, V. Farahani, H. Askarian Abyaneh, and M. Abedi, "Optimal daily scheduling of reconfiguration based on minimisation of the cost of energy losses and switching operations in microgrids," *IET, Generation, Transmission & Distribution,* vol. 9, pp. 513-522, 2015.

[39] F. V. Gomes, S. Carneiro Jr, J. L. R. Pereira, M. P. Vinagre, P. A. N. Garcia, and L. R. Araujo, "A new heuristic reconfiguration algorithm for large distribution systems," *IEEE Transactions on Power Systems,* vol. 20, pp. 1373-1378, 2005.

[40] R. Cherkaoui, A. Bart, and A. Germond, "Optimal configuration of electrical distribution networks using heuristic methods," in *Proceedings of the Eleventh Power Systems Computation Conference (PSCC)*, 1993, pp. 147-54.

[41] A. B. Morton and I. M. Mareels, "An efficient brute-force solution to the network reconfiguration problem," *IEEE Transactions on Power Delivery,* vol. 15, pp. 996-1000, 2000.

[42] H. M. Khodr and J. Martinez-Crespo, "Integral methodology for distribution systems reconfiguration based on optimal power flow using Benders

decomposition technique," *IET Generation, Transmission and Distribution,* vol. 3, pp. 521-534, 2009.

[43] H. M. Khodr, J. Martinez-Crespo, M. A. Matos, and J. Pereira, "Distribution Systems Reconfiguration Based on OPF Using Benders Decomposition," *IEEE Transactions on Power Delivery,,* vol. 24, pp. 2166-2176, 2009.

[44] R. A. Jabr, R. Singh, and B. C. Pal, "Minimum Loss Network Reconfiguration Using Mixed-Integer Convex Programming," *IEEE Transactions on Power Systems,* vol. 27, pp. 1106-1115, 2012.

[45] R. A. Jabr, "Minimum loss operation of distribution networks with photovoltaic generation," *IET Renewable Power Generation,* vol. 8, pp. 33-44, 2014.

[46] J. Taylor and F. S. Hover, "Convex models of distribution system reconfiguration," *IEEE Transactions on Power Systems,* vol. 27, pp. 1407-1413, 2012.

[47] Q. Peng, Y. Tang, and S. H. Low, "Feeder reconfiguration in distribution networks based on convex relaxation of opf," 2014.

[48] M. E. Baran and F. F. Wu, "Network reconfiguration in distribution systems for loss reduction and load balancing," *IEEE Transactions on Power Delivery,* vol. 4, pp. 1401-1407, 1989.

[49] K. Christakou, J. LeBoudec, M. Paolone, and D. C. Tomozei, "Efficient Computation of Sensitivity Coefficients of Node Voltages and Line Currents in Unbalanced Radial Electrical Distribution Networks," *IEEE Transactions on Smart Grid,* vol. 4, pp. 741-750, 2013.

[50] A. Borghetti, M. Bosetti, S. Grillo, S. Massucco, C. A. Nucci, M. Paolone*, et al.*, "Short-Term Scheduling and Control of Active Distribution Systems With High Penetration of Renewable Resources," *IEEE Systems Journal,* vol. 4, pp. 313-322, 2010.

[51] Q. Zhou and J. W. Bialek, "Generation curtailment to manage voltage constraints in distribution networks," *IET Generation, Transmission & Distribution,* vol. 1, pp. 492-498, 2007.

[52] G. Valverde and T. Van Cutsem, "Model Predictive Control of Voltages in Active Distribution Networks," *IEEE Transactions on Smart Grid,* vol. 4, pp. 2152-2161, 2013.

[53] K. Christakou, D. C. Tomozei, J. Y. Le Boudec, and M. Paolone, "GECN: Primary Voltage Control for Active Distribution Networks via Real-Time Demand-Response," *IEEE Transactions on Smart Grid,* vol. 5, pp. 622-631, 2014.

[54] K. Christakou, D. C. Tomozei, M. Bahramipanah, J. Y. Le Boudec, and M. Paolone, "Primary Voltage Control in Active Distribution Networks via Broadcast Signals: The Case of Distributed Storage," *IEEE Transactions on Smart Grid,* vol. 5, pp. 2314-2325, 2014.

[55] D. Shirmohammadi, H. W. Hong, A. Semlyen, and G. X. Luo, "A compensation-based power flow method for weakly meshed distribution and transmission networks," *IEEE transactions on power systems,* vol. 3, pp. 753-762, 1988.

[56] S. Sarri, M. Paolone, R. Cherkaoui, A. Borghetti, F. Napolitano, and C. A. Nucci, "State estimation of Active Distribution Networks: Comparison between WLS and iterated kalman-filter algorithm integrating PMUs," in

Innovative Smart Grid Technologies (ISGT Europe), 2012 3rd IEEE PES International Conference and Exhibition on, 2012, pp. 1-8.

[57] B. Espinar, J.-L. Aznarte, R. Girard, A. M. Moussa, and G. Kariniotakis, "Photovoltaic Forecasting: A state of the art," in *5th European PV-Hybrid and Mini-Grid Conference*, 2010, pp. Pages 250-255-ISBN 978-3-941785-15-1.

[58] T. Bien and H. Musikowski, "Forecasting photovoltaic energy using a fourier series based method," in *23rd European Photovoltaic Solar Energy Conference*, 2008, pp. 3088-3091.

[59] S. Bofinger and G. Heilscher, "Solar electricity forecast-approaches and first results," in *21st PV Conference. Dresden, Germany*, 2006.

[60] D. Mayer, L. Wald, Y. Poissant, and S. Pelland, "Performance prediction of grid-connected photovoltaic systems using remote sensing," International Energy AgencyMarch 2008 2008.

[61] E. Lorenz, J. Remund, S. C. Müller, W. Traunmüller, G. Steinmaurer, D. Pozo*, et al.*, "Benchmarking of different approaches to forecast solar irradiance," in *24th European photovoltaic solar energy conference, Hamburg, Germany*, 2009, p. 25.

[62] A. Moreno-Munoz, J. J. G. De la Rosa, R. Posadillo, Pallare, x, and V. s, "Short term forecasting of solar radiation," in *Industrial Electronics, 2008. ISIE 2008. IEEE International Symposium on*, 2008, pp. 1537-1541.

[63] P. Bacher, H. Madsen, and H. A. Nielsen, "Online short-term solar power forecasting," *Solar Energy,* vol. 83, pp. 1772-1783, 10// 2009.

[64] R. Marquez and C. F. M. Coimbra, "Forecasting of global and direct solar irradiance using stochastic learning methods, ground experiments and the NWS database," *Solar Energy,* vol. 85, pp. 746-756, 5// 2011.

[65] E. G. Kardakos, M. C. Alexiadis, S. I. Vagropoulos, C. K. Simoglou, P. N. Biskas, and A. G. Bakirtzis, "Application of time series and artificial neural network models in short-term forecasting of PV power generation," in *Power Engineering Conference (UPEC), 2013 48th International Universities'*, 2013, pp. 1-6.

[66] D. Torregrossa, J. Y. Le Boudec, and M. Paolone, "Model-free computation of ultra-short-term prediction intervals of solar irradiance," *Solar Energy,* vol. 124, pp. 57-67, 2// 2016.

[67] J. W. Taylor, L. M. de Menezes, and P. E. McSharry, "A comparison of univariate methods for forecasting electricity demand up to a day ahead," *International Journal of Forecasting,* vol. 22, pp. 1-16, 1// 2006.

[68] H. Yoo and R. L. Pimmely, "Short term load forecasting using a self-supervised adaptive neural network," *IEEE Transactions on Power Systems,* vol. 14, pp. 779-784, 1999.

[69] M. T. Hagan and S. M. Behr, "The Time Series Approach to Short Term Load Forecasting," *IEEE Transactions on Power Systems,* vol. 2, pp. 785-791, 1987.

[70] T. W. S. Chow and C. T. Leung, "Neural network based short-term load forecasting using weather compensation," *IEEE Transactions on Power Systems,* vol. 11, pp. 1736-1742, 1996.

[71] O. Hyde and P. F. Hodnett, "An adaptable automated procedure for short-term electricity load forecasting," *IEEE Transactions on Power Systems,* vol. 12, pp. 84-94, 1997.

[72] W. Lei and M. Shahidehpour, "A hybrid model for integrated day-ahead electricity price and load forecasting in smart grid," *IET Generation, Transmission & Distribution,* vol. 8, pp. 1937-1950, 2014.
[73] H. K. Alfares and M. Nazeeruddin, "Electric load forecasting: literature survey and classification of methods," *International Journal of Systems Science,* vol. 33, pp. 23-34, 2002.
[74] G. Mbamalu and M. El-Hawary, "Load forecasting via suboptimal seasonal autoregressive models and iteratively reweighted least squares estimation," *IEEE Transactions on Power Systems,* vol. 8, pp. 343-348, 1993.
[75] A. Moreira, A. Street, and J. M. Arroyo, "An Adjustable Robust Optimization Approach for Contingency-Constrained Transmission Expansion Planning," *IEEE Transactions on Power Systems,* vol. 30, pp. 2013-2022, 2015.
[76] R. A. Jabr, I. Dzafic, and B. C. Pal, "Robust Optimization of Storage Investment on Transmission Networks," *IEEE Transactions on Power Systems,* vol. 30, pp. 531-539, 2015.
[77] A. Lorca and X. A. Sun, "Adaptive robust optimization with dynamic uncertainty sets for multi-period economic dispatch under significant wind," 2014.
[78] D. Bertsimas, E. Litvinov, X. A. Sun, Z. Jinye, and Z. Tongxin, "Adaptive Robust Optimization for the Security Constrained Unit Commitment Problem," *IEEE Transactions on Power Systems,* vol. 28, pp. 52-63, 2013.
[79] J. Ruiwei, W. Jianhui, and G. Yongpei, "Robust Unit Commitment With Wind Power and Pumped Storage Hydro," *IEEE Transactions on Power Systems,* vol. 27, pp. 800-810, 2012.
[80] R. A. Jabr, S. Karaki, and J. A. Korbane, "Robust Multi-Period OPF With Storage and Renewables," *IEEE Transactions on Power Systems,* vol. 30, pp. 2790-2799, 2015.
[81] L. Baringo and A. J. Conejo, "Offering Strategy Via Robust Optimization," *IEEE Transactions on Power Systems,* vol. 26, pp. 1418-1425, 2011.
[82] C. Zhi, W. Lei, and F. Yong, "Real-Time Price-Based Demand Response Management for Residential Appliances via Stochastic Optimization and Robust Optimization," *IEEE Transactions on Smart Grid,* vol. 3, pp. 1822-1831, 2012.
[83] B. Fanzeres, A. Street, and L. A. Barroso, "Contracting Strategies for Renewable Generators: A Hybrid Stochastic and Robust Optimization Approach," *IEEE Transactions on Power Systems,* vol. 30, pp. 1825-1837, 2015.
[84] L. Changhyeok, L. Cong, S. Mehrotra, and B. Zhaohong, "Robust Distribution Network Reconfiguration," *IEEE Transactions on Smart Grid,* vol. 6, pp. 836-842, 2015.
[85] W. Zhaoyu, C. Bokan, W. Jianhui, K. Jinho, and M. M. Begovic, "Robust Optimization Based Optimal DG Placement in Microgrids," *IEEE Transactions on Smart Grid,* vol. 5, pp. 2173-2182, 2014.
[86] B. Xiaoqing and Q. Wei, "Robust Optimization for Bidirectional Dispatch Coordination of Large-Scale V2G," *IEEE Transactions on Smart Grid,* vol. 6, pp. 1944-1954, 2015.

[87] M. Zugno and A. J. Conejo, "A robust optimization approach to energy and reserve dispatch in electricity markets," Technical University of Denmark2013.

[88] S. A. Gabriel, A. J. Conejo, J. D. Fuller, B. F. Hobbs, and C. Ruiz, *Complementarity modeling in energy markets* vol. 180: Springer Science & Business Media, 2012.

[89] x, L. lvarez, x, J. pez, K. Ponnambalam, and V. H. Quintana, "Generation and Transmission Expansion Under Risk Using Stochastic Programming," *IEEE transactions on power systems,* vol. 22, pp. 1369-1378, 2007.

[90] P. Heejung and R. Baldick, "A Stochastic Transmission Planning Model With Dependent Load and Wind Forecasts," *IEEE Transactions on Power Systems,* vol. 30, pp. 1026-1034, 2015.

[91] D. Chattopadhyay, "Life-cycle maintenance management of generating units in a competitive environment," *IEEE Transactions on Power Systems,* vol. 19, pp. 1181-1189, 2004.

[92] P. Carpentier, G. Gohen, J. C. Culioli, and A. Renaud, "Stochastic optimization of unit commitment: a new decomposition framework," *IEEE Transactions on Power Systems,* vol. 11, pp. 1067-1073, 1996.

[93] W. Lei, M. Shahidehpour, and L. Zuyi, "Comparison of Scenario-Based and Interval Optimization Approaches to Stochastic SCUC," *IEEE transactions on power systems,* vol. 27, pp. 913-921, 2012.

[94] A. Hatami, H. Seifi, and M. K. Sheikh-El-Eslami, "A Stochastic-Based Decision-Making Framework for an Electricity Retailer: Time-of-Use Pricing and Electricity Portfolio Optimization," *IEEE transactions on power systems,* vol. 26, pp. 1808-1816, 2011.

[95] S. I. Vagropoulos and A. G. Bakirtzis, "Optimal Bidding Strategy for Electric Vehicle Aggregators in Electricity Markets," *IEEE Transactions on Power Systems,* vol. 28, pp. 4031-4041, 2013.

[96] J. Garcia-Gonzalez, R. M. R. de la Muela, L. M. Santos, and A. M. Gonzalez, "Stochastic Joint Optimization of Wind Generation and Pumped-Storage Units in an Electricity Market," *IEEE Transactions on Power Systems,* vol. 23, pp. 460-468, 2008.

[97] I. G. Moghaddam, M. Nick, F. Fallahi, M. Sanei, and S. Mortazavi, "Risk-averse profit-based optimal operation strategy of a combined wind farm–cascade hydro system in an electricity market," *Renewable Energy,* vol. 55, pp. 252-259, 2013.

[98] C. H. K. W. S. Virayavanich, A. Seiler, C. Hammer, and K. Weck, "Reliability of on-load tap changers with special consideration of experience with delta connected transformer windings and tropical environmental conditions," *Cigré, paper,* pp. 12-103, 1996.

[99] P. Senin, "Dynamic time warping algorithm review," *University of Hawaii,* 2008.

[100] C. A. Ratanamahatana and E. Keogh, "Making time-series classification more accurate using learned constraints," 2004.

[101] H.-S. Park and C.-H. Jun, "A simple and fast algorithm for K-medoids clustering," *Expert Systems with Applications,* vol. 36, pp. 3336-3341, 3// 2009.

[102] P. S. Georgilakis and N. D. Hatziargyriou, "Optimal Distributed Generation Placement in Power Distribution Networks: Models, Methods, and Future Research," *IEEE Transactions on Power Systems,* vol. 28, pp. 3420-3428, 2013.

[103] W. Caisheng and M. H. Nehrir, "Analytical approaches for optimal placement of distributed generation sources in power systems," *IEEE Transactions on Power Systems,* vol. 19, pp. 2068-2076, 2004.

[104] G. Celli and F. Pilo, "Optimal distributed generation allocation in MV distribution networks," in *PICA, 22nd IEEE Power Engineering Society International Conference on Innovative Computing for Power - Electric Energy Meets the Market.* , 2001, pp. 81-86.

[105] J. Mitra, M. R. Vallem, and C. Singh, "Optimal Deployment of Distributed Generation Using a Reliability Criterion," *IEEE Transactions on Industry Applications,* vol. PP, pp. 1-1, 2016.

[106] X. Tan, Y. Wu, and D. H. K. Tsang, "Pareto Optimal Operation of Distributed Battery Energy Storage Systems for Energy Arbitrage under Dynamic Pricing," *IEEE Transactions on Parallel and Distributed Systems,* vol. PP, pp. 1-1, 2015.

[107] V. R. Pandi, H. H. Zeineldin, and X. Weidong, "Determining Optimal Location and Size of Distributed Generation Resources Considering Harmonic and Protection Coordination Limits," *IEEE Transactions on Power Systems,* vol. 28, pp. 1245-1254, 2013.

[108] D. Gautam and N. Mithulananthan, "Optimal DG placement in deregulated electricity market," *Electric Power Systems Research,* vol. 77, pp. 1627-1636, 2007.

[109] G. Celli, E. Ghiani, S. Mocci, and F. Pilo, "A multiobjective evolutionary algorithm for the sizing and siting of distributed generation," *IEEE Transactions on Power Systems,* vol. 20, pp. 750-757, 2005.

[110] Z. Liu, F. Wen, and G. Ledwich, "Optimal siting and sizing of distributed generators in distribution systems considering uncertainties," *IEEE Transactions on Power Delivery,* vol. 26, pp. 2541-2551, 2011.

[111] D. Singh, D. Singh, and K. S. Verma, "Multiobjective Optimization for DG Planning With Load Models," *IEEE Transactions on Power Systems,* vol. 24, pp. 427-436, 2009.

[112] C. Chen, S. Duan, T. Cai, B. Liu, and G. Hu, "Optimal allocation and economic analysis of energy storage system in microgrids," *IEEE Transactions on Power Electronics,* vol. 26, pp. 2762-2773, 2011.

[113] Y. M. Atwa and E. El-Saadany, "Optimal allocation of ESS in distribution systems with a high penetration of wind energy," *IEEE Transactions on Power Systems,* vol. 25, pp. 1815-1822, 2010.

[114] G. Carpinelli, F. Mottola, D. Proto, and A. Russo, "Optimal allocation of dispersed generators, capacitors and distributed energy storage systems in distribution networks," in *Modern Electric Power Systems (MEPS), 2010 Proceedings of the International Symposium*, 2010, pp. 1-6.

[115] G. Celli, S. Mocci, F. Pilo, and M. Loddo, "Optimal integration of energy storage in distribution networks," in *IEEE Bucharest PowerTech*, 2009, pp. 1-7.

[116] Y. V. Makarov, P. Du, M. C. Kintner-Meyer, C. Jin, and H. F. Illian, "Sizing energy storage to accommodate high penetration of variable energy resources," *IEEE Transactions on Sustainable Energy,* vol. 3, pp. 34-40, 2012.
[117] Y. Zheng, Z. Y. Dong, F. J. Luo, K. Meng, J. Qiu, and K. P. Wong, "Optimal allocation of energy storage system for risk mitigation of DISCOs with high renewable penetrations," *IEEE transactions on power systems,* vol. 29, pp. 212-220, 2014.
[118] A. S. A. Awad, T. H. M. El-Fouly, and M. M. A. Salama, "Optimal ESS Allocation and Load Shedding for Improving Distribution System Reliability," *IEEE Transactions on Smart Grid,* vol. 5, pp. 2339-2349, 2014.
[119] S. Bahramirad, W. Reder, and A. Khodaei, "Reliability-Constrained Optimal Sizing of Energy Storage System in a Microgrid," *IEEE Transactions on Smart Grid,* vol. 3, pp. 2056-2062, 2012.
[120] M. Sedghi, A. Ahmadian, and M. Aliakbar-Golkar, "Optimal Storage Planning in Active Distribution Network Considering Uncertainty of Wind Power Distributed Generation," *IEEE Transactions on Power Systems,* vol. 31, pp. 304-316, 2016.
[121] H. Oh, "Optimal planning to include storage devices in power systems," *IEEE transactions on power systems,* vol. 26, pp. 1118-1128, 2011.
[122] F. Fallahi, M. Nick, G. H. Riahy, S. H. Hosseinian, and A. Doroudi, "The value of energy storage in optimal non-firm wind capacity connection to power systems," *Renewable Energy,* vol. 64, pp. 34-42, 2014.
[123] M. T. Barlow, "A diffusion model for electricity prices," *Mathematical Finance,* vol. 12, pp. 287-298, 2002.
[124] J. T. Linderoth and A. Lodi, "MILP software," *Wiley encyclopedia of operations research and management science,* 2011.
[125] T. L. Saaty, "Decision making—the analytic hierarchy and network processes (AHP/ANP)," *Journal of systems science and systems engineering,* vol. 13, pp. 1-35, 2004.
[126] S. Boyd, N. Parikh, E. Chu, B. Peleato, and J. Eckstein, "Distributed optimization and statistical learning via the alternating direction method of multipliers," *Foundations and Trends® in Machine Learning,* vol. 3, pp. 1-122, 2011.
[127] M. Fukushima, "Application of the alternating direction method of multipliers to separable convex programming problems," *Computational Optimization and Applications,* vol. 1, pp. 93-111, 1992.
[128] J. Clausen, "Branch and bound algorithms-principles and examples," *Department of Computer Science, University of Copenhagen,* pp. 1-30, 1999.
[129] S. I. D. (SODA). Available: http://www.soda-is.com/eng/index.html
[130] H. Energy. Available: http://homerenergy.com/
[131] M. Carrión and J. M. Arroyo, "A computationally efficient mixed-integer linear formulation for the thermal unit commitment problem," *IEEE Transactions on Power Systems,* vol. 21, pp. 1371-1378, 2006.
[132] D. Rastler, *Electricity energy storage technology options: a white paper primer on applications, costs and benefits*: Electric Power Research Institute, 2010.
[133] A. Thiele, T. Terry, and M. Epelman, "Robust linear optimization with recourse," *Rapport technique,* pp. 4-37, 2009.

[134] A. J. Conejo, E. Castillo, R. Minguez, and R. Garcia-Bertrand, *Decomposition techniques in mathematical programming: engineering and science applications*: Springer Science & Business Media, 2006.

[135] F. You and I. E. Grossmann, "Multicut Benders decomposition algorithm for process supply chain planning under uncertainty," *Annals of Operations Research,* vol. 210, pp. 191-211, 2013.

Curriculum Vitae

Mostafa NICK

Distributed Electrical Systems Laboratory (DESL)
École Polytechnique Fédérale de Lausanne (EPFL)

Born in 23th January, 1986, Marvdasht, Iran
Email: mostafanick@gmail.com
Linkedin :
https://ch.linkedin.com/in/mostafanick

Education

2012-2016	**Ph.D. in Electrical Engineering**, *Swiss Federal Institute of Technology (EPFL)*, Switzerland. **Thesis:** Exact convex modeling of the optimal power flow for the operation and planning of active distribution networks with energy storage systems.
2008-2011	**Master of Science in Electrical Power Engineering,** *Amirkabir University of Technology (Tehran Polytechnic),* Tehran, Iran **Thesis:** Optimal planning of wind farms considering transmission network security constraints.
2004-2008	**Bachelor of Science in Electrical Engineering,** *Shiraz University*, Iran.

Professional Experience

2012-2016	**Doctoral assistant**, Distributed Electrical Systems Laboratory (DESL)-EPFL, Lausanne, Switzerland.
2008-2011	**Researcher**, Niroo Research Institute, Tehran, Iran.

Research Interests

- Distribute Energy Storage Planning and Control
- Distribution networks operation and planning
- Smart Grid
- Application of Optimization Methods into Power Systems

Language Skills:

- Persian (Native)
- English (Fluent, IBT: 98/120)
- French (Intermediate, B2)

List of Publications

Journals:

[J7]. **M. Nick**, R. Cherkaoui, J.Y, Le Boudec, M. Paolone, "An Exact Convex Formulation of Optimal Power Flow in Radial Distribution Networks Including Transverse Components," under review, *IEEE Transactions on Automatic Control.*

[J6]. M. Nick, O. Alizadeh, R. Cherkaoui, M. Paolone, "Security Constrained Unit Commitment with Dynamic Thermal Line Rating," *IEEE Transactions on Power Systems*, accepted in press, available online.

[J5]. M. Nick, R. Cherkaoui, M. Paolone, "Optimal siting and sizing of distributed energy storage systems via alternating direction method of multipliers," *International Journal of Electrical Power & Energy Systems*, vol. 72, pp. 33–39, Nov. 2015.

[J4]. M. Nick, R. Cherkaoui, and M. Paolone. "Optimal Allocation of Dispersed Energy Storage Systems in Active Distribution Networks for Energy Balance and Grid Support," *IEEE Transactions on Power Systems,* vol. 29, pp. 2300-2310, Sep. 2014.

[J3]. M. Nick, S.G.H.Riahy, S.H.Hosseinian, F.Fallahi "Wind Power Optimal Capacity Allocation to Remote Areas Taking into Account Transmission Connection Requirements," *IET Renewable Power Generation,* vol. 5, pp. 347–355, Sep. 2011.

[J2]. F. Farhad, **M. Nick,** G. H. Riahy, S. H. Hosseinian, and A. Doroudi. "The value of energy storage in optimal non-firm wind capacity connection to power systems," *Renewable Energy*, vol. 64, pp. 34-42, Apr. 2014.

[J1]. I. Gerami, **M.Nick,** F.FAllahi, M. Sanei, S. Mortazavi "Risk-Averse Profit-Based Optimal Operation Strategy of a Combined Wind Farm-Cascade Hydro system in an Electricity Market," *Renewable Energy,* vol. 55, pp. 252–259, Jul. 2013.

Conferences:

[C9]. O. Aliazdeh Mousavi, **M. Nick,** "Stochastic Security Constrained Unit Commitment with Fixed and Variable Speed Pumped-Storage Hydro Units", accepted to be presented in *Power System Computation Conference (PSCC),* Genoa, Italy, 2016.

[C8]. M. Nick, O. Alizadeh Mousavi, R. Cherkaoui and M. Paolone, "Integration of Transmission Lines Dynamic Thermal Rating into Real-Time Optimal Operation of Power Systems", *50th International Universities Power Engineering Conference (UPEC)*, Staffordshire, UK, 2015.

[C7]. M. Nick, R. Cherkaoui, M. Paolone, "Optimal siting and sizing of distributed energy storage systems via alternating direction method of multipliers," *Power System Computation Conference (PSCC),* Wroclaw, Poland, August 2014.

[C6]. M. Nick, R. Cherkaoui, M. Paolone, "Stochastic day-ahead optimal scheduling of Active Distribution Networks with dispersed energy storage and renewable resources," *IEEE Conference on Technologies for Sustainability (SusTech)*, Portland, USA, 2014.

[C5]. M. Bahramipanah, **M. Nick,** R. Cherkaoui, and M. Paolone, “Network Clustering for Voltage Control in Active Distribution Network Including Energy Storage Systems” *International conference on Smart Grid Technologies (ISGT)*, Washington, USA, 2015.

[C4]. M. Nick, M. Hohmann, R. Cherkaoui, and M. Paolone, “On the Optimal Placement of Distributed Storage Systems for Voltage Control in Active Distribution Networks”, *IEEE PES ISGT Europe*, Berlin, Germany, 2012.

[C3]. M. Nick, M. Hohmann, R. Cherkaoui, and M. Paolone, “Optimal Location and Sizing of Distributed Storage Systems in Active Distribution Networks”, *IEEE PowerTech conference,* Grenoble, France, 2013.

[C2]. S.Abedi, H.Gharavi, **M. Nick,** S.H.Hosseinian "Economic and reliable design of a hybrid PV-wind-fuel cell energy system" 19th *ICEE conference*, Tehran, Iran, 2011.

[C1]. M. Hasani , F. Fallahi, **M. Nick**, " Review of Different Capacity Mechanisms in Electricity Markets of the World and Iran Electricity Market" *25th International Power System Conference (PSC)* , Tehran, Iran, 2011.